



Year: 2011

A dissertation submitted in the partial fulfilment of the requirement for the award of

DOCTOR OF PHILOSOPHY (PhD)

in

AUTOMATIQUE, GENIE INFORMATIQUE

from

UNIVERSITY OF SCIENCE AND TECHNOLOGY, LILLE

by

Senem KURŞUN BAHADIR

**WEARABLE OBSTACLE AVOIDANCE
SYSTEM INTEGRATED WITH CONDUCTIVE
YARNS FOR VISUALLY IMPAIRED PEOPLE**

Defended on November 10, 2011

Mrs. Ender YAZGAN BULGUN

Professor, Dokuz Eylul University, Izmir,
Turkey

Rapporteur

Mr. Ahmed RACHID

Professor, Université de Picardie Jules
Verne (UPJV), Amiens, France

Rapporteur

Mrs. Binnaz MERİÇ KAPLANGİRAY

Professor, Uludağ University, Bursa, Turkey

Examineur

Mrs. Fatma KALAOĞLU

Professor, Istanbul Technical University,
Istanbul, Turkey

Co-directeur

Mr. Vladan KONCAR

Professor, ENSAIT, Roubaix, France

Co-directeur

Mr. Sebastien THOMASSEY

Associate Professor ENSAIT, Roubaix,
France

Co-directeur

ACKNOWLEDGEMENTS

This work was accomplished through the collaboration of and **Ecole Nationale Supérieure des Arts et Industries Textiles, Roubaix (France)** and **Istanbul Technical University, Istanbul (Turkey)**.

First of all, I would like to express my deepest gratitude to my supervisors, **Prof. Dr. Vladan KONCAR**, **Prof. Dr. Fatma KALAOĞLU** and **Assoc. Prof. Dr. Sebastien THOMASSEY** for giving me continuous guidance and unconditional support during the entire project work. Their guidance and encouragement, drawn from their profound academic attainments and rich research experience, have been continuously enlightening my study.

Deepest thanks also to **Prof. Dr. Ata MUĞAN** and **Assoc. Prof. Dr. Hale Canbaz KARAKAŞ** for their timely suggestions. My special thanks go to **Prof. Dr. Cevza CANDAN**, who delivered kind guidance during the design of knitting structure of the prototype. Gratefully acknowledge to **Dr. Irina CRISTIAN** for her valuable advices and assistance during design of woven structures.

I would like to express my sincere gratitude to **Assist. Prof. Dr. U. Kıvanç ŞAHİN** for his help during washing tests, strong support and timely suggestions throughout this research not only professionally but also personally.

Many thanks are due to the technical staff of GEMTEX to weaving and knitting departments for their sincere efforts for the completion of this project.

I especially express my sincere gratitude to **French Embassy in Turkey** for providing me financial support through PhD scholarship. Deepest thanks also go to **Istanbul Technical University** (for Postgraduate Research Fellowship), **Tinçel Kültür Vakfı** (for PhD Scholarship) and **Vehbi Koc Vakfı** (for Research Assistant Scholarship) for funding during the entire project work which not only fostered my technical outlook but also contributed manifolds to the development of my multicultural horizon.

I acknowledge to **Sim-Art Tekstil San. Tic. Ltd. Şti.** for giving me an opportunity to produce my final prototype. My special thanks go to **Bahadır Arı** during the production of prototype.

Moreover, my deepest gratitude goes to my friend and my husband **Çağrı BAHADIR** for his strong support, help, encouragement, understanding, and endless love during the past years throughout this research. Without him this study could not have come this far.

Finally, but not the least, from the depth of my heart, deepest gratitude goes to my parents, family and friends for supporting me through all my endeavours for completing this thesis.

September 2011

Senem KURŞUN BAHADIR

TABLE OF CONTENTS

GENERAL INTRODUCTION	1
CHAPTER 1	5
STATE OF THE ART	
1.1. Introduction.....	5
1.2. Literature Review about Visually Impaired People’s Navigation Problem	5
1.2.1 Camera-based systems	6
1.2.2 RFID Tag based systems.....	9
1.2.3 GPS based systems.....	11
1.2.4 Sonar based systems.....	14
1.3. Literature review for electronic textiles	18
1.3.1 Electrically conductive yarn-like materials.....	18
1.3.2 Electrically conductive fabrics	21
1.3.3 Interactive cloths	27
1.4. Summary.....	31
CHAPTER 2.....	33
E-TEXTILE ARCHITECTURE FOR OBSTACLE AVOIDANCE	
2.1 Basis of system architecture	33
2.1.1 Software and hardware components requirements.....	33
2.1.2 Wearability performance requirements.....	34
2.2 Determination of electronic system components using an algorithm based on fuzzy AHP and fuzzy information axiom	35
2.2.1 Criteria and alternatives for visually impaired’s smart clothing electronic components ..	35
2.2.2 Axiomatic design methodology and its axioms	36
2.2.3. Main structure of the proposed methodology.....	38
2.2.3.1 Initial phase	38
2.2.3.2 Definition of criteria phase.....	38
2.2.3.3 Evaluation phase	40
2.2.3.4 Output phase.....	41
2.2.4. Application	41
2.2.4.1 Initial phase	41
2.2.4.2 Definition of criteria phase.....	42
2.2.4.3 Evaluation phase	42
2.2.4.4 Output phase.....	44

2.2.5. Conclusion.....	47
2.3 Adaptation of sensor methodology to textile structure.....	47
2.3.1. Introduction.....	47
2.3.2. Materials.....	47
2.3.2.1 Characteristics of ultrasonic sensor.....	47
2.3.2.2 Characteristics of conductive yarns.....	48
2.3.3. Design of woven fabric structure	50
2.3.4. Integration of ultrasonic sensor	51
2.3.4.1 Integration of single ultrasonic sensor.....	51
2.3.4.2 Integration of multi-connected ultrasonic sensors.....	52
2.3.5. Conclusion.....	54
2.4 Adaptation of actuator methodology to textile structures.....	54
2.4.1. Introduction.....	54
2.4.2. Materials.....	55
2.4.2.1 Characteristics of vibration motor.....	55
2.4.2.2 Characteristics of conductive yarns.....	55
2.4.3. Formation of e-textile structures	55
2.4.4. Integration of vibration motor.....	56
2.4.5. Conclusion.....	57
CHAPTER 3	59
SYSTEM ANALYSIS & RESULTS FOR E-TEXTILE ARCHITECTURE	
3.1 Analysis on signal quality of ultrasonic sensor.....	59
3.1.1 Introduction.....	59
3.1.2 Experimental	59
3.1.2.1 Measurement set up.....	59
3.1.2.2 Measurement procedure	60
3.1.2.3 Noise level identification	61
3.1.3 Results	61
3.1.4 Conclusion.....	67
3.2 Analysis of the Beam Pattern of Ultrasonic Sensor	67
3.2.1 Introduction.....	67
3.2.2 Experimental	67
3.2.2.1 Distance and object direction measurement by ultrasonic sensor	67
3.2.2.2 Measurement set up.....	69
3.2.2.3 Measurement procedure	69
3.2.3 Results	70
3.2.4 Conclusion.....	72

3.3	Analysis of Obstacle Detection with Multi-Connected Ultrasonic Sensors.....	72
3.3.1	Introduction	72
3.3.2	Experimental	72
3.3.2.1	Developed scenarios by using wires	72
3.3.2.2	Developed scenarios in textile structure using conductive yarns.....	74
3.3.2.3	Measurement set up.....	75
3.3.3	Results	76
3.3.3.1	Comparison of scenarios according to position of obstacle	76
3.3.3.2	Comparison of scenarios according to detection success.....	78
3.3.3.3	Comparison of scenarios according to detection error	84
3.3.3.4	Comparison of scenarios according to detection range.....	85
3.3.4	Conclusion.....	88
3.4	Analysis of Vibrotactile Perception via Vibration Motors by using Fuzzy Logic	89
3.4.1	Introduction	89
3.4.1.1	Vibrotactile sensation	89
3.4.1.2	Factors effecting vibrotactile perception.....	89
3.4.2	Experimental	90
3.4.2.1	Measurement set up.....	91
3.4.2.2	Evaluation method.....	92
3.4.3	Results	94
3.4.3.1	Results according to signal alternatives	94
3.4.3.2	Results according to e-textile structure alternatives.....	97
3.4.3.3	Results according to body part alternatives.....	98
3.4.4	Conclusion.....	100
CHAPTER 4	103
DESIGN AND DEVELOPMENT OF SMART CLOTHING PROTOTYPE WITH AN		
ALGORITHM FOR OBSTACLE AVOIDANCE		
4.1.	An algorithm for obstacle avoidance.....	103
4.1.1	Introduction	103
4.1.2	Kinematics analysis of walking person	105
4.1.3	Obstacle avoidance strategy	106
4.1.4	Principals of neural network architecture.....	110
4.1.5	Basis of fuzzy logic	111
4.1.6	Neuro-fuzzy control algorithm for obstacle avoidance.....	115
4.1.6.1.	Data filtration and pre-processing.....	116
4.1.6.2.	Input layer / Fuzzification.....	120
4.1.6.3.	Hidden layer-1 / Fuzzy rule layer.....	123

4.1.6.4. Hidden layer-2/ Consequence layer: Fuzzy Implication - Defuzzification...	124
4.1.6.5. Output Layer/Fuzzy-Neural Approximation and Final Outputs.....	130
4.1.7 Implementation and comparison of multi-layer fuzzy controller with one layer fuzzy controller.....	132
4.1.8 Microcontroller programming.....	135
4.2. Design and Development Concept of Smart Clothing Prototype for Visually Impaired People	137
4.2.1. Circuit design	138
4.2.1.1. Schematic circuit diagram of microcontroller.....	140
4.2.1.2. Schematic circuit diagram of ultrasonic sensors.....	140
4.2.1.3. Schematic circuit diagram of vibration motors.....	142
4.2.2. Design Layout	142
4.2.2.1. Sensor placement.....	143
4.2.2.2. Actuator-vibration motor placement.....	143
4.2.2.3. Microcontroller and power supply placement.....	144
4.2.3. Smart clothing prototype.....	144
4.2.3.1. Base structure of interactive garment.....	144
4.2.3.2. Removable structures of interactive garment.....	145
4.2.3.3. Interactive garment prototype.....	149
4.3. Final Experiments and Performances of Smart Clothing System	150
4.3.1. Detection capability and robustness of the developed system	151
4.3.2. Power consumption.....	154
4.3.3. Heating behavior.....	155
4.3.4. Washability	158
4.4. Summary.....	158
GENERAL CONCLUSION AND FUTURE RESEARCHES WORKS.....	161
REFERENCES.....	167
APPENDICES.....	189
ABBREVIATIONS	201
ABSTRACT.....	202

LIST OF FIGURES

Fig. 1.1: Summary of the image-processing procedure	6
Fig. 1.2: NAVI system	6
Fig. 1.3: SVETA system.....	7
Fig. 1.4: Visually acoustic space prototype.....	7
Fig. 1.5: Camera mounted on the chest system	8
Fig. 1.6: Tyflos prototype.....	8
Fig. 1.7: Tyflos system hardware-modalities overview	8
Fig. 1.8: Camera based robotic travel aids	9
Fig. 1.9: RFID tag	9
Fig. 1.10: On the left hand side of the figure is the iCane overview; on the top right of the figure is RFID antenna; on the bottom right of the figure is RFID reader	10
Fig. 1.11: White cane system overview.....	10
Fig. 1.12: Microstrip antennas can be embedded on the jacket (made of conductive cloth).....	11
Fig. 1.13: Overview of the GPS-based navigation system components.....	12
Fig. 1.14: The functional components for all GPS-based navigation system for visually impaired	12
Fig. 1.15: Personal Guidance System.....	12
Fig. 1.16: ODILIA System	13
Fig. 1.17: Outdoor and indoor mobile user of DRISTHI	13
Fig. 1.18: Principle of active sonar	14
Fig. 1.19: Ultrasonic based cane system	14
Fig. 1.20: The Navbelt system.....	15
Fig. 1.21: a-b) Overview and module of Andha Astra c) another navigation aid worn by blind.....	15
Fig. 1.22: Arm9-based embedded wearable ultrasonic based system	15
Fig. 1.23: Details of EPFL prototype	16
Fig. 1.24: Shoe mounted sensors.....	16
Fig. 1.25: Tactile navigation system	17
Fig. 1.26: Commercial products that uses sonar system	17
Fig. 1.27: Guido Robotic Traveler	18
Fig. 1.28: Various forms of conductive threads	19
Fig. 1.29: The yarn structure of yarn-based sensors: (a) single wrapping and (b)double wrapping	19
Fig. 1.30: a) Cross-sectional and b) longitudinal views of core–sheath c) Developed yarn: Core/Copper filament; Sheath/Cotton fiber.....	19
Fig. 1.31: Overview of coating process.....	20
Fig. 1.32: (a) Prototype of conductive yarns covered with plastic films and (b) LED lighting test.....	20

Fig. 1.33: Schematic diagram of photovoltaic fiber	20
Fig. 1.34: Overview of photovoltaic fibers	21
Fig. 1.35: Schematic of fibre cell	21
Fig. 1.36: Woven fabric with metal fibers and GSSG transmission line on woven e-fabric.....	22
Fig. 1.37: a) Metals in woven structure b) Three-layer woven antenna of a textile RFID tag c) Textile based USB.....	23
Fig. 1.38: Woven prototype containing multiple stainless steel fibres.....	23
Fig. 1.39: Woven specimens connected to halogen lamp OFF and ON, POF in weft direction, white PET fibers in warp direction, Optical fiber core conductive fabric (b)	24
Fig. 1.40: Fabric tactile sensor	24
Fig. 1.41: Production procedure of heating panels.....	24
Fig. 1.42: Conductive fabric electrodes constructed with knitting technology	25
Fig. 1.43: Tubular conductive knitted fabric	25
Fig. 1.44: Electronic modules connected with conductive yarn by embroidery	26
Fig. 1.45: Coated e-fabrics as a heating element.....	26
Fig. 1.46: Screen printed structures.....	26
Fig. 1.47: Solder joints on a fabric PCB.....	27
Fig. 1.48: Wearable Motherboard (early prototype of SmartShirt) and SmartShirt®.....	27
Fig. 1.49: a)WEALTHY system prototype model b) Smart Jacket prototype	28
Fig. 1.50: Lifeshirt developed by Vivometrics Sensor-based Sportswear by Phillips b) Fully Integrated EKG Shirt	28
Fig. 1.51: Philips emotion jacket-outer and inner lining	29
Fig. 1.52: A virtual 3D mobile guidance jacket	29
Fig. 1.53: Prototypes for recognizing body posture	30
Fig. 1.54: Prototype of garment with electrical nerve stimulation (TENS) function	30
Fig. 2.1: Wearability performance requirements of the proposed system.....	34
Fig. 2.2: Design range, system range, common range and probability density function of a FR 36	
Fig. 2.3: Framework of evaluation model	39
Fig. 2.4: Triangular fuzzy numbers for linguistic terms.....	41
Fig. 2.5: Overview of ultrasonic sensor and its dimensions	48
Fig. 2.6: Linear resistance graph of sample 2 (Silver Plated Nylon 66-4 ply)	50
Fig. 2.7: a) The draft for double-woven cloth with weft stuffers and conductive yarn position b) fabric on the loom	50
Fig. 2.8: 3D representation of the double-woven cloth (TexGen software®).....	51
Fig. 2.9: Samples.....	51
Fig. 2.10: a) Sample overview: conductive yarns corresponding to sensor ground, Vcc and analog voltage output points.....	52
Fig. 2.11: Chaining of ultrasonic sensors	53

Fig. 2.12: MATLAB file for sensors constantly looping	53
Fig. 2.13: Sample overview: conductive yarns corresponding to sensor ground, Vcc, TX, RX, analog voltage, and BW output points.....	54
Fig. 2.14: Arduino LilyPad Vibe Board®.....	55
Fig. 2.15: 3D representation of the 1x1 rib fabric	56
Fig. 2.16: Samples	56
Fig. 3.1: Electrical circuit of integrated ultrasonic sensor and experimental set up.....	60
Fig. 3.2: Measurement configurations.....	60
Fig. 3.3: Signal recorded by sample 3 woven with silver-plated nylon 66-2 ply yarn during the sensor measurement with case I (without phone)	62
Fig. 3.4: Comparison of signals during the sensor measurement with case I (without phone)	62
Fig. 3.5: Comparison of SNRs during the sensor measurement with case I (without phone).....	63
Fig. 3.6: Comparison of signals during the sensor measurement with case II (with phone vertical direction during calling).....	63
Fig. 3.7: Comparison of signals during the sensor measurement with case III (with phone horizontal direction during calling).....	64
Fig. 3.8: Comparison of SNRs during the sensor measurement with case II and III (with phone horizontal and vertical direction during calling).....	64
Fig. 3.9: Comparison of signals during the sensor measurement with case II (with phone in horizontal position during standby)	65
Fig. 3.10: Comparison of signals during the sensor measurement with case II (with phone in vertical position during standby)	65
Fig. 3.11: Comparison of SNRs during the sensor measurement with case II and III (with phone in horizontal and vertical position during standby).....	66
Fig. 3.12: Change in SNRs according to situations.....	66
Fig. 3.13: Geometrical relationship in measuring azimuth of objects.....	68
Fig. 3.14: (a) Experiment set-up (b) Block diagram of system	69
Fig. 3.15: Experimental procedure to determine border of sensor working range	70
Fig. 3.16: a) Determined beam pattern of ultrasonic sensor integrated to the woven fabric b) Beam pattern of sensor according to its datasheet	70
Fig. 3.17: Error differentiation between actual and measured distance	71
Fig. 3.18: Various scenarios related to sensor positions	73
Fig. 3.19: Scenarios developed by mounting sensors onto textile surface	74
Fig. 3.20: Distances between sensors	75
Fig. 3.21: Overview of experiment set-up for obstacle detection	75
Fig. 3.22: Comparison of scenarios when object locates at $x=0$, $y=60\text{cm}$	76
Fig. 3.23: Comparison of scenarios when object locates at $x=0$ (from left side), $y=60\text{cm}$	77
Fig. 3.24: Comparison of scenarios when object locates at $x=0$ (from right side), $y=60\text{cm}$	78

Fig. 3.25: Total detection success of scenarios	81
Fig. 3.26: Detection success of each sensor in each scenario.....	81
Fig. 3.27: Total average detection error of each scenario	85
Fig. 3.28: Comparison of detection range of sensors when object at y=80cm.....	86
Fig. 3.29: Detection range of sensor 1 according to scenarios.....	87
Fig. 3.30: Detection range of sensor 2 according to scenarios.....	87
Fig. 3.31: Generated signals: sinwave, square wave, sawtooth wave with 5V amplitude at 0.5Hz.....	91
Fig. 3.32: Stimulated contact areas of human body during the measurements	91
Fig. 3.33: Measurement-set up (a) measurement over outer wrist (b)	92
Fig. 3.34: Framework of the fuzzy evaluation method	93
Fig. 3.35: Triangular fuzzy numbers for linguistic terms.....	94
Fig. 3.36: Hierarchy of the evaluation.....	95
Fig. 3.37: Result of total evaluation of vibrotactile perception according to signal alternatives	96
Fig. 3.38: Result of total evaluation of vibrotactile perception according to e-textile structure alternatives	98
Fig. 3.39: Result of total evaluation of vibrotactile perception according to body parts alternatives ...	99
Fig. 3.40: Result of total evaluation of vibrotactile perception according to body parts alternatives (95% Confidence Interval).....	100
Fig. 4.1: Model of walking person in coordinate system	105
Fig. 4.2: Block diagram of guidance strategy.....	107
Fig. 4.3: Navigation of walking person under multi-obstacles environment	107
Fig. 4.4: Basic flow diagram of obstacle avoidance strategy	109
Fig. 4.5: Simple neuron model.....	110
Fig. 4.6: One-layer neural network	110
Fig. 4.7: Abbreviated notation of one layer neural network.....	111
Fig. 4.8: Examples of membership functions.....	111
Fig. 4.9: Boolean logic ANDs and ORs and NOTs [284]	112
Fig. 4.10: Fuzzy inference with logical operations [284].....	112
Fig. 4.11: Fuzzify inputs [284].....	112
Fig. 4.12: Example of Step:2-Apply fuzzy operator [284].....	113
Fig. 4.13: Example of Step:3-Apply implication method [284].....	113
Fig. 4.14: Example of aggregation method (max) [284]	114
Fig. 4.15: Example of defuzzification method (centroid) [284].....	114
Fig. 4.16: Composition diagram of fuzzy controller	114
Fig. 4.17: Sensor's position on the garment.....	115
Fig. 4.18: Different cases between obstacles and user	115
Fig. 4.19: Framework of control system for proposed smart clothing	116
Fig. 4.20: Data elimination process.....	117

Fig. 4.21: Proposed neuro-fuzzy control system for the smart clothing.....	119
Fig. 4.22: Fuzzy Inference System (FIS) for left obstacle avoidance	120
Fig. 4.23: The membership functions for input variables.....	121
Fig. 4.24: Measurement results when the obstacle at (-10, 60) cm	121
Fig. 4.25: The membership functions for output variables “turn left”	122
Fig. 4.26: The membership functions for output variables “turn right”	122
Fig. 4.27: Implication and defuzzification process of front obstacle avoidance neuron	126
Fig. 4.28: Fuzzification for input 1 (data read by sensor 1) for the 3 rd rule	127
Fig. 4.29: Fuzzification for input 2 (data read by sensor 2) for the 3 rd rule	127
Fig. 4.30: Fuzzification for input 3 (data read by sensor 3) for the 3 rd rule	127
Fig. 4.31: Fuzzification for input 4 (data read by sensor 4) for the 3 rd rule.....	127
Fig. 4.32: Output membership function for 3 rd rule in front obstacle avoidance	128
Fig. 4.33: Implication process for 3 rd rule in front obstacle avoidance	128
Fig. 4.34: Final output function for the front obstacle avoidance neuron for a given example.....	129
Fig. 4.35: Example of control surface for right obstacle avoidance neuron.....	130
Fig. 4.36: Basic diagram of fuzzy neural approximation of proposed controller.....	131
Fig. 4.37: Outputs of the multi-layer FIS and one-layer FIS and target angles when the obstacle is at the right.....	133
Fig. 4.38: Outputs of the multi-layer FIS and one layer FIS and target angles when the obstacle is in the front.....	133
Fig. 4.39: Outputs of the multi-layer FIS and basic FIS and target angles when the obstacle is at the left	134
Fig. 4.40: Flow diagram of microcontroller’s main program.....	135
Fig. 4.41: Smoothing algorithm working principle	136
Fig. 4.42: Timing diagram for microcontroller	137
Fig. 4.43: Schematic diagram of smart clothing system circuit	139
Fig. 4.44: Schematic diagram of LilyPad Mainboard Microcontroller [289].....	140
Fig. 4.45: Schematic circuit diagram of LV-MaxSonar®-EZ3 sensor [204]	141
Fig. 4.46: Arduino LilyPad Button Board® [290]	141
Fig. 4.47: Schematic circuit diagram of Arduinio LilyPad Vibe Board® [291]	142
Fig. 4.48: Circuit layout design on the garment	142
Fig. 4.49: MBS Merz ® single-jersey circular knitting machine	144
Fig. 4.50: Base structure of developed interactive garment	145
Fig. 4.51: The production of removable parts for sensor and vibration motor integration	146
Fig. 4.52: Ultrasonic sensor integrated to woven fabric to attach under the breast zone of garment..	146
Fig. 4.53: Vibration motors integrated to woven fabric to attach over hip bone area of the garment.	147
Fig. 4.54: Vibration motors integrated to woven fabric to attach over wrist area of the garment.....	147
Fig. 4.55: Removable fabrics for sensor and actuator connections to main circuit.....	148

Fig. 4.56: Removable fabrics for microcontroller and pockets for batteries	148
Fig. 4.57: Interactive garment with its removable parts	149
Fig. 4.58: Final smart clothing prototype for visually impaired people	150
Fig. 4.59: Measurements for detection capability of the developed system.....	151
Fig. 4.60: Detection capability of the developed smart clothing.....	152
Fig. 4.61: Layout of environment including obstacles	153
Fig. 4.62: ATmega328: Active Supply Current vs. V_{CC} [286].....	155
Fig. 4.63: Thermal image of the structure at 5V (a) and its temperature distribution along conductive yarn with a distance of $ AP $ (b).....	156
Fig. 4.64: Thermal images of the structure over a sample area at 1V, 4V, 10V,16V	157
Fig. 4.65: Average temperatures over the transmission lines on the garment vs. voltage.....	157

LIST OF TABLES

Table 2.1: Comparison of power generators useful for wearable Microsystems	35
Table 2.2: Linguistic terms.....	42
Table 2.3: Fuzzy pairwise comparisons for importance of the criteria	43
Table 2.4: Experts' preferences.....	45
Table 2.5: Aggregated fuzzy numbers for experts' preferences.....	45
Table 2.6: Information content values.....	46
Table 2.7: Weighted information contents	46
Table 2.8: Comparison of ultrasonic sensor types.....	48
Table 2.9: Characteristics of yarns for integration of ultrasonic sensor	49
Table 2.10: Conductivity calculations for yarn sample 2.....	49
Table 2.11: Characteristics of yarns for integration of vibration motor	55
Table 2.12: Physical characteristic of samples.....	57
Table 3.1: Cases for measurement procedure.....	60
Table 3.2: Results of experiments at the border of working range of sensor in one direction	71
Table 3.3: Average values of measured distance data taken by different sensors in each scenario	79
Table 3.4: Standard deviations of measured distance data taken by different sensors in each scenari	82
Table 3.5: Average detection error for each sensor in each scenario in cm	85
Table 3.6: Vibrotactile perception values of each evaluator according to signal alternatives.....	96
Table 3.7: Perception Level & Signal Type ANOVA Results	96
Table 3.8: Perception Level & Frequency ANOVA Results.....	97
Table 3.9: Vibrotactile perception values of evaluators according to e-textile structure alternatives..	97
Table 3.10: Perception Level & Conductive yarn ANOVA Results.....	98
Table 3.11: Vibrotactile perception values of each evaluator according to body part alternatives	99
Table 3.12: Perception Level & Body parts ANOVA Results.....	100
Table 4.1: Motion state of walking person	106
Table 4.2: The relation between turning angle and detected object position	123
Table 4.3: Resistance variation along transmission line after washing	158

LIST OF PUBLICATIONS

In International Journals

Kursun Bahadir S., Thomassey, S., Koncar, V., Kalaoglu, F., **An Algorithm Based on Neuro-Fuzzy Controller Implemented in A Smart Clothing System For Obstacle Avoidance**, submitted to *Expert Systems with Applications*, June 2011

Kursun Bahadir S., Kalaoglu, F., Koncar, V., **A Comparative Study on Detection Capabilities of Multi-Connected Miniaturized Sonar Sensors Embedded to Textile Structure**, submitted to *Sensors and Actuators A: Physical*, May 2011

Kursun Bahadir S., Koncar V., Kalaoglu, F., **Wearable Obstacle Detection System Fully Integrated to Textile Structures for Visually Impaired People**, submitted to *Sensors and Actuators A: Physical*, May 2011

Kursun Bahadir S., Kalaoglu, F., Koncar, V., **Analysis of Vibrotactile Perception via E-textile Structure By Using Fuzzy Logic**, submitted to *Journal of Experimental Psychology: Applied*, June, 2011

Kursun Bahadir S., Koncar, V., Kalaoglu, F., I. Cristian, Thomassey, S., **Assessing Signal Quality of Ultrasonic Sensor on Different Conductive Yarns Used As Transmission Lines**, *Fibres & Textiles In Eastern Europe*, Vol. 19, No.5 (88), pp.75-81, 2011

Kursun, S. Kalaoglu, F., Thomassey, S. , I.Cristian, Koncar, V. , **A Study on the beam pattern of ultrasonic sensor integrated to textile structure**, *International Journal of Clothing Science and Technology*, Vol. 23, No. 4, pp. 232 – 241, 2011

In International Conference Proceedings

Kursun Bahadir, S., Kalaoglu, F., Koncar, V. **Comparison Of Multi-Connected Miniaturized Sonar Sensors Mounted On Textile Structure In A Different Position Angle For Obstacle Detection**, *ITMC International Conference*, 27- 29 October 2011, Casablanca, Morocco

Kursun Bahadir, S., Koncar, V., Kalaoglu, F., **Multi-Connection Of Miniaturized Sonar Sensors Onto Textile Structure For Obstacle Detection**, *AUTEX 2011*, 8-10 June 2011, Mulhouse, France

Lazareviciute, L. Marcinkute, M., Kursun Bahadir, S., Koncar, V. , Kalaoglu, F., **Crosstalk Effect In A Woven Fabric Circuit Developed For Multi-Connection Of Sonar Sensors**, *1st Smartex-Egypt 2011 World Textiles Conference*, May 23rd–25th 2011, Egypt, accepted.

Kursun, S., Kalaoglu, F., Koncar, V. , Thomassey, S., **Comparison On Perceived Vibrotactile Stimuli Of E-Textile Structures By Using Fuzzy Logic**, *4th International Conference Of Applied Research In Textile- Cirat-4*, December 2-5 2010, Monastir, Tunisia

Kursun, S. Koncar, V. , Kalaoglu, F., Thomassey, S., **Fuzzy Based Evaluation of Vibrotactile Perception By Using Vibration Motor Embedded To Woven Fabric**, *ICIT 2010*, 16-18 June 2010, Pp.49-51, Seoul-Korea

Kursun, S. Kalaoglu, F., Thomassey, S., I.Cristian, Koncar, V., **Integration Of Sonar Sensors To Textile Structures**, *4th International Technical Textiles Congress (ITCC)*, 16-17 May 2010, Istanbul

Awards

System Student Award 2011-1st Prize

Platform for Smart Textiles and Wearable Microsystems/BELGIUM-USA

Théophile Legrand International Award For Textile Innovation 2011- 2nd Prize

Fondation Théophile Legrand – Institut de France/FRANCE

TMMOB Makina Mühendisleri Odası-V. Necdet Eraslan Proje Yarışması 2011- 2nd Prize

TMMOB Makina Mühendisleri Odası İstanbul Şubesi, Innovations For Disabled People Project Competition 2011/TURKEY

GENERAL INTRODUCTION

Motivations

Lacking of visual perception due to the physiological or neurological factors is known as blindness. According to the world health report, about 314 million people are visually impaired and among them 45 million are blind. This means that approximately 45 million people are dependent on others around them for movement, information processing and environmental interpretation [1].

Lack of visual perception is paralleled with a loss of independence. In today's society where the social independence is important, visually impaired people like everyone else want to live without depending on others. They want to travel without any fear of getting crashed or lost. They want to reach information individually as everyone else does. Therefore, those who do not have the benefit of sight require assistive devices to be independent such as for navigation, for reading signs etc.

Navigation is the art and science of determining one's position by directing him to a desired destination in a safe way. In particular, outdoor and indoor navigation has always been a challenging problem for visually impaired people for their mobility since navigation concern restricts the visually impaired right access to many buildings, precludes their use of public transit and makes their integration into local communities difficult.

To overcome navigation concerns of visually impaired people considerable researches have been conducted and thereby several mobility aids like walking stick, electronic travel robot aids etc. were developed. However, as far as overcoming navigation aids is concerned, there are several limitations in such devices. For instance; the most widely used mobility aid today is the long cane. Long cane has some limitations as its detection range is limited due to its length, or it has difficulties in detecting overhanging obstacles and storing in public places etc. Additionally, weight of cane is another critical problem like in those of other mobility aids [2].

Thus, in order to overcome navigation concerns of visually impaired, there is a significant need for a new assisted navigation system to help blind people in the visualization of environment easily.

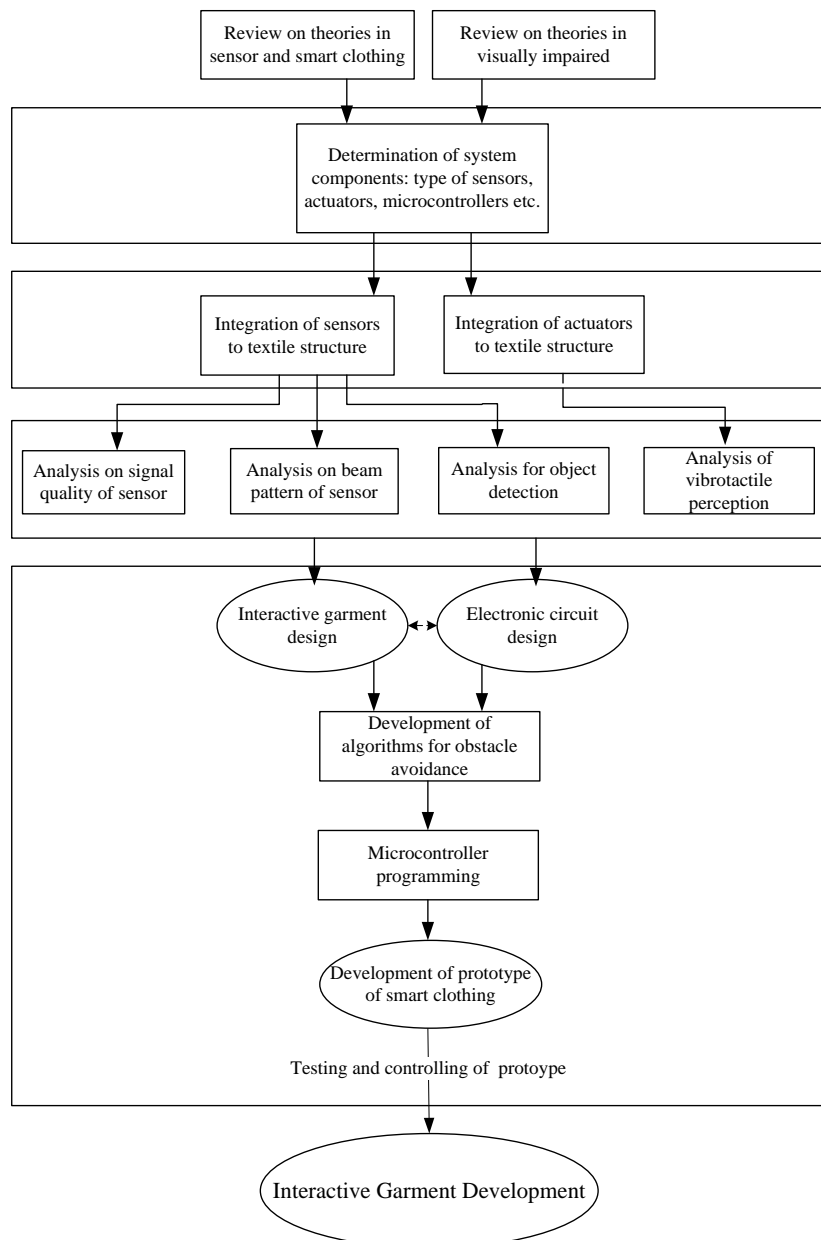
Purpose of the thesis

The main objective of this study is to help blind or visually impaired people to navigate safely and quickly among obstacles and other hazards faced by blind pedestrians in indoor environment. Towards this objective, an innovative approach based on integration of electronic components onto textile structures was realized. By this way, a new wearable obstacle detection system, which can be worn as a garment that is flexible, lightweight and comfortable for the human body has been designed. The proposed smart clothing navigation system would become united part of visually impaired people's

lifestyle, and it would help them overcome navigation concerns seamlessly, without imposing upon them any physical or cognitive load.

Research methodology

The smart clothing navigation system is an initial prototype system that combines garment with sensors, actuators, power supplies and a data processing unit. The working principle of the system is based on two main functions: sensing the surrounding environment as well as detection of obstacles via sensors and guiding the user by actuators through a feedback process interpreted in signal processing unit. Within this approach, the design of the smart clothing prototype navigation system is consisted of the review on theories subjecting both visually impaired and smart clothing. The framework of the study is shown in below figure and the research methodology with respect to specific objective is summarized as:



Flow chart for the study

First of all, electronic components for smart clothing navigation system were determined by using an algorithm based on fuzzy AHP and fuzzy information axiom. Secondly, integration of electronic components to textile structures was performed. Afterwards, working performances of electronic components integrated to textile structure were analyzed. Then, both electronic circuit and smart clothing have been designed simultaneously. Algorithm for obstacle avoidance has been developed and according to developed algorithms microcontroller programming has been done.

Finally, the prototype of smart clothing navigation system has been developed and tested. Herewith, interactive garment development was completed successfully.

Main contributions and originality of research

Although there are numerous researches and developments of mobility aids for visually impaired people, there is no development of any interactive garment, which can help visually impaired people to overcome navigation concerns.

Comprehensive investigation on the developed smart clothing navigation system with respect to sensing performance of the indoor environment and guiding the visually impaired accurately will provide a new scientific understanding of interactive garment design and development. It represents a great challenge and significant contribution to the sensor and actuator integration knowledge to textile structure. In addition, intelligent textiles is a recently developing area and there is still many to be invented, therefore successful implementation and integration of electronics used in our smart clothing system are significantly valuable for smart textiles researches. By this way, within the scope of this research;

- ✓ The first interactive garment for visually impaired people was designed and developed using conductive yarns.
- ✓ An innovative neuro-fuzzy based control algorithm for obstacle avoidance was developed to guide visually impaired with interactive garment.
- ✓ For the first time in the literature, the integration of sonar sensors to textile structure was realized successfully.
- ✓ For the first time in the literature, vibrotactile perception was analyzed via e-textiles within varying parameters such as signal type, frequency, textile structure, different body parts etc.
- ✓ For the first time in the literature, the signal quality of sonars integrated to textile structure was analyzed using different conductive yarns.

These highly value added results should bring benefits not only to textile and clothing industries but also to electronics, military, sports, medical and even rehabilitation fields.

Thesis overview

The thesis comprises four chapters summarized below:

Chapter 1 provides a comprehensive literature review for the recent developments in both visually impaired people's navigation problems and electronic textiles. Various ideas and developments for visually impaired people's navigation concerns were compared. The fabrication processes for electronic textiles were explained.

Chapter 2 presents e-textile architecture for obstacle avoidance. Wearability, and hardware and software system requirements were discussed. Determination of electronic components for smart clothing system using an algorithm based on fuzzy AHP and fuzzy information axiom was presented. Adaptation of sensor and actuator methodology to textile structure was realized.

Chapter 3 brings discussion on system analysis and results for e-textile architecture. Signal quality of ultrasonic sensor by using different conductive yarns were investigated and compared. Beam pattern of ultrasonic sensor was studied and compared. Obstacle detection with multiconnected sensors was analyzed and presented. Vibrotactile perception by using vibration motors integrated to textile structure was investigated in fuzzy relations. Comparisons of vibrotactile perceptions within signal alternatives, e-textile alternatives, and body alternatives were discussed.

Chapter 4 illustrates design and development of interactive garment prototype as well as algorithm for obstacle avoidance. Obstacle avoidance strategy and kinematic analysis of walking person were realized. Neuro-fuzzy control algorithm for obstacle avoidance was developed and explained to navigate visually impaired people through interactive garment. Microcontroller programming according to developed algorithm was presented. Design concept and design layout of interactive garment was demonstrated. Frameworks of the prototype including ultrasonic sensors, vibration motors, microcontroller, circuit design was thoroughly studied. Finally, performances of prototype were tested and discussed.

The thesis ends with a conclusion of the theoretical and practical work presented in the previous parts. A perspective has also been given on the possibilities of further expanding the research presented in this thesis.

Chapter 1

State Of The Art

1.1. Introduction

Towards the objective of the study, a brief summary of what has been done so far to help navigation concerns of visually impaired people was given. Moreover, concerning the objective, in order to transform garment into an interactive-intelligent infrastructure that facilitates information processing around visually impaired's environment, fabrication of electronic textiles from fiber to fabric and garment was investigated. Therefore, literature review about electronic textiles was also given.

1.2. Literature Review about Visually Impaired People's Navigation Problem

During the last decades, several researches have been focused on visually impaired individuals' navigation and reading concerns in their living environment. These researches have concentrated on developing new devices by adapting them new technologies. The development of these devices and application of technologies for orientation and mobility have evolved since 1960's, a long history covering the postwar period.

The devices developed for visually impaired can be categorized as ETA (Electronic Travel Aids) or RTA (Robotic Travel Aids).

These ETAs generally provide feedback to the user through a range of tones and fixed intensity vibrations, and are usually implemented as a portable system. They consist of cameras to capture the image and detect obstacles or find pathways using image processing techniques. Moreover, they include sonar sensors to measure the distances to obstacles, and/or GPS (Global Positioning Systems) - RFID (Radio Frequency Identification) to identify their local position. Besides, in order to guide user, vibrators, earphone, audio etc. are generally used as an actuator in those systems.

When the literature is reviewed, we came across a set of systems that represents the four principal approaches to solve the identification and navigation problems of the visually impaired people: Camera, RFID, GPS, and sonar based systems.

1.2.1. Camera-based systems

In camera-based systems, cameras are used to capture visual information from the surrounding environment. The captured image is processed via image processing methods, and then it is mapped to stereo sound patterns or vibrations. The basic concept of image processing is shown in the Fig. 1.1. Images captured by a camera are enhanced, pixelized, and then converted into stimulation commands [3-9].

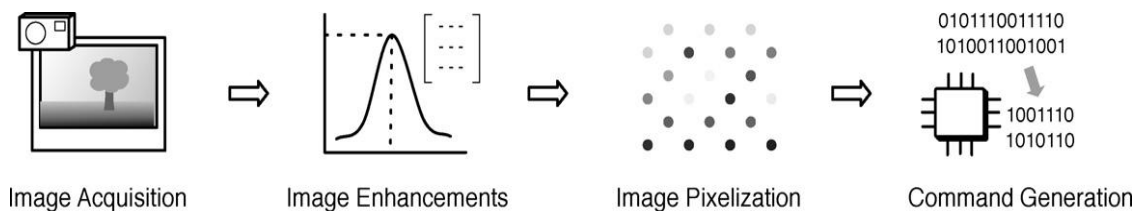


Fig. 1.1: Summary of the image-processing procedure [4].

The earliest camera based system was NAVI (Navigation Assistant for Visually Impaired), which was designed to convert images captured by a vision sensor into verbal messages through stereo earphone. In that system, digital video camera was used as a vision sensor. Furthermore, Single Board Processing System (SBPS) was mounted in a specially designed vest that has to be worn by user (see Fig. 1.2). In those studies fuzzy based image processing was used [10, 11].

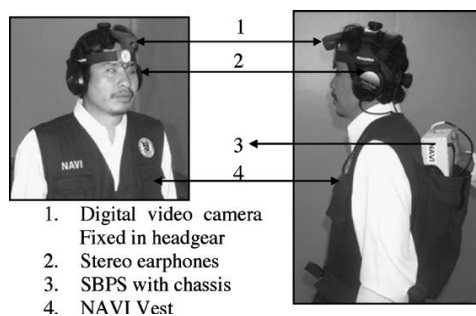


Fig. 1.2: NAVI system [11]

Balakhrihnan et al. developed *SVETA* (Stereo Vision based Electronic Travel Aid) system as shown in the Fig. 1.3. The system was composed of a wearable computer, stereo earphones and a helmet molded with stereo cameras capturing the images. The images were processed via wearable computer based on fuzzy relations and the information was conveyed to the user through a set of earphones in terms of musical tones [12, 13].

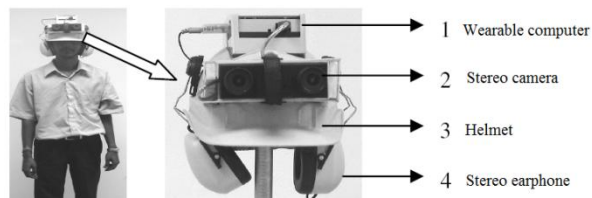


Fig. 1.3: *SVETA* system [12]

Similarly, Gozales et al. developed Virtual acoustic space prototype as seen in Fig. 1.4. This system was consisted of a processor, headphones and two micro cameras attached to the frame of some conventional eyeglasses.

The cameras were used for capturing information of the surroundings. It was reported that in most cases (>75%), individuals could detect objects and their distances, and in small simple experimental rooms, it was possible for them to move freely and extract information for objects like walls, table, window and opened door [14].



Fig. 1.4: *Visually acoustic space* prototype [14]

Unlike the previous studies, in some studies mounting the visual camera on the head was found to be an inconvenient solution for the blind user. Thus, another system in which the camera was mounted on the chest of the user was proposed [15, 16]. As seen in Fig. 1.5 camera is hung over the chest and the system is integrated with earphones, laptop and a wireless communication [17].

Bourbakis et al. developed a various prototypes of *Tyflos* system for visually impaired people. *Tyflos* system consisted of two tiny cameras placed at the dark glasses, a microphone, an ear-speaker, a GPS device, a range sensor, an RFID Reader, 2D vibration vest and a portable computer as seen in the Fig. 1.6. It used laser range sensors to detect the distance and camera to capture the images. In that system, the visual information was converted into either vibrations on the 2D vest for navigation purposes or spoken natural language sentences for reading purpose (see Fig. 1.7).



Fig. 1.5: Camera mounted on the chest system [17]

Furthermore, a verbal description of surroundings was provided to user. For example, for the nominal question where I am? It provides additional information about surroundings using GPS module. Thus, this system gives to the user both navigation and reading information [18-22].



Fig. 1.6: Tyflos prototype [19]

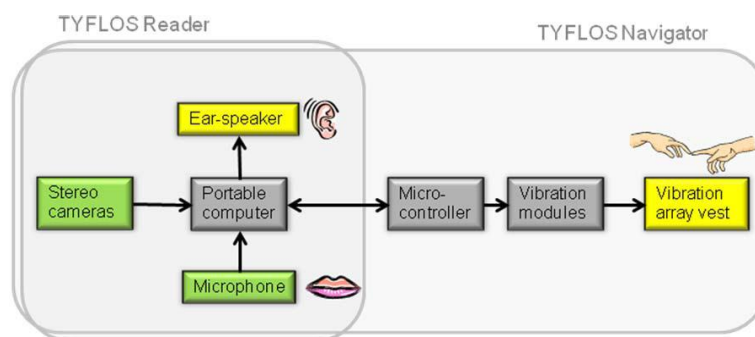


Fig. 1.7: Tyflos system hardware-modalities overview [19]

Apart from portable and wearable camera based navigation systems, there have been also some studies on robotic travel aids [23-24]. At first, RTA (Robotic Travel Aid) HITOMI had been developed as seen in Fig. 1.8a, and then the novel concept of HITOMI was presented (Figure 1.8b-c). As seen in Fig. 1.8, robotic system contains video camera, a stereo camera, sonar sensors and a bumper sensor. Due to image processing information, audio guiding system in which the names of avenues, intersections, and hotels etc. were recorded before, was activated by its digital map guide.

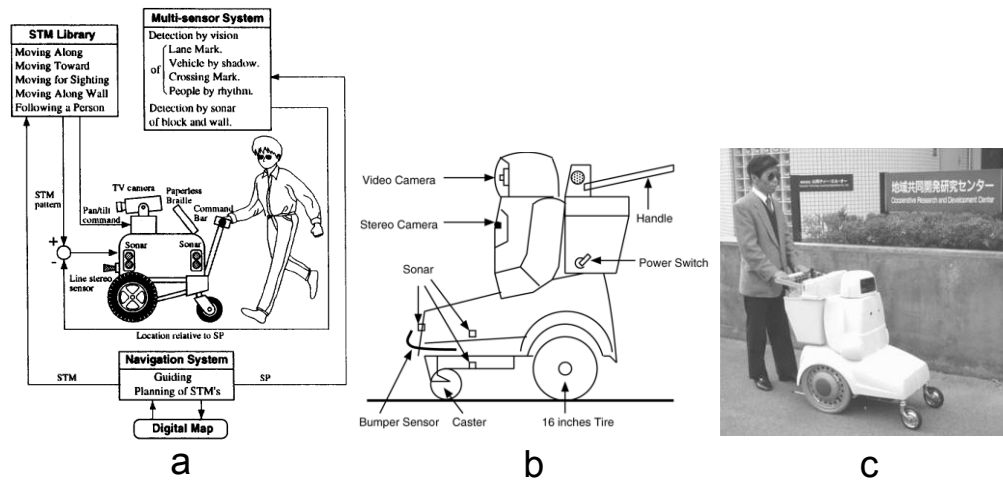


Fig. 1.8: Camera based robotic travel aids [23-24]

The biggest disadvantage of the camera based systems is the processing of captured images. The right image processing and, afterwards conversion of these images into stimulation commands are difficult procedures. Besides, other factors such as lighting conditions, camera angle and the amount of clutter are also other criteria that affect the visual information of the system.

1.2.2. RFID Tag based systems

Radio-frequency identification (RFID) is used for identification and tracking of an object such as car, product or person by using radio waves. An RFID tag is a microchip combined with an antenna, and it contains at least two parts: One is an integrated circuit for storing and processing information, modulating and demodulating a radio-frequency (RF) signal, and other specialized functions and the other is an antenna for receiving and transmitting signals. An example to RFID tag is shown in the Fig. 1.9 [25].

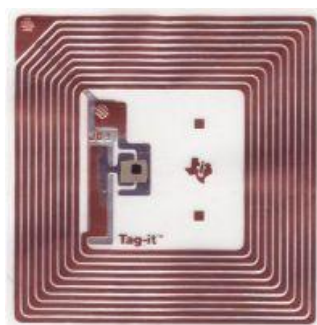


Fig. 1.9: RFID tag [25]

RFID tag based systems can be used for both indoor and outdoor applications. The basic concepts of RFID tags used for visually impaired navigation concerns are such that at first tags are mounted on the objects in the environment that are significant for the user, then the signal sent by the RFID tags is read by the receiver that user carries [27]. In last two decades, a number of research projects have focused on development of suitable guidance system using RFID [2, 27-41].

Chang et al. developed *iCane System* equipped with an RFID reader, Personal Digital Assistant (PDA) and earphones communicating via bluetooth. The overview of the *iCane* system is shown in the Fig. 1.10. RFID tags preloaded with information were used. The RFID reader embedded in *iCane* sends the information gathered from the RFID tags to the PDA to show local points (e.g. crossing points, stairs etc.). By this way, the instructions are transmitted to the user via speech through the Bluetooth earphones [28].



Fig. 1.10: On the left hand side of the figure is the *iCane* overview; on the top right of the figure is RFID antenna; on the bottom right of the figure is RFID reader [28]

Similar to *iCane* system, Shiizu et al. developed *White cane* system by using RFID tags as seen in the Fig. 1.11. Apart from *iCane*, this system was composed of colored navigation lines. Thus, the working principle of the system was based on two concepts: color sensing and RFID tag. RFID tags set on those colored lines are sensed by white cane. Along the navigation line, if the user is oriented to wrong line he/she is informed by vibration of the white cane. Moreover, information is sent to him/her by pre-recorded voice [32-33]. Similar type of RFID-tag systems embedded in the cane for the visually impaired people have also been studied and developed [34-38].

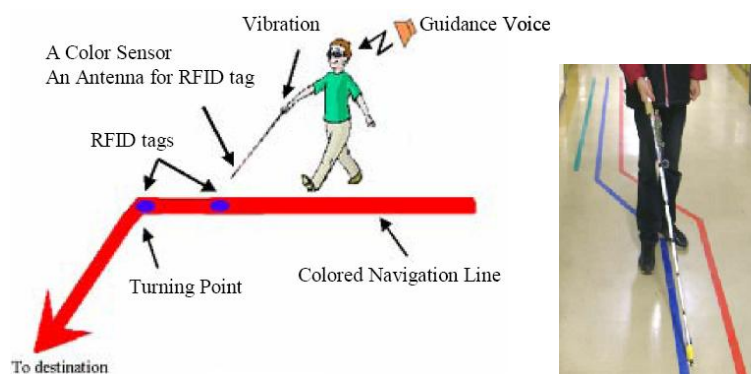


Fig. 1.11: *White cane* system overview [33]

Unlike canes, there have also been some robotic guides using RFID tags. Such as a kind of robot resembling wheel chair was equipped with a vision system, RFID tag, and a laptop [27, 39, 42-43].

Moreover, Liu et al. developed a new self-positioning method that combines RFID, Bluetooth and FLC (Fluorescent light Communication). In their system, unlike other studies, a photo sensor receives a positioning signal from the fluorescent lights in indoor environment, thus information taken by FLC is transmitted to user via PDA [44].

Differently, an interesting approach in the RFID tag systems was suggested by Szeto et al. that was embedding RFID reader antennas on a jacket (see Fig. 1.12). They suggested that microstrip antennas could be etched or sewn on to wearable conducting clothing while the pocket PC and a rechargeable battery are placed in the pocket of the jacket [45].

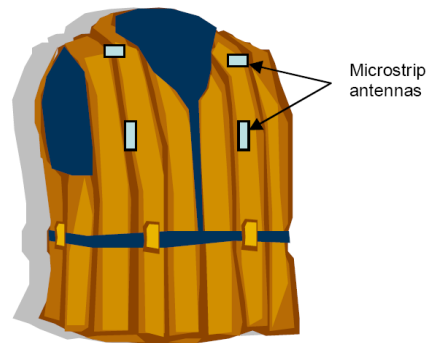


Fig. 1.12: Microstrip antennas can be embedded on the jacket (made of conductive cloth) [45]

To sum up, tag-based systems, as portrayed in the literature, seem to have two disadvantages: First, the system needs to be placed in local places that is significant for the user to get information.

Secondly, tagging devices can fail completely or their power can expire. By means of this, the reliability of the tagging devices is a critical issue. In spite of these disadvantages, tag-based systems seem to be more suitable for identification the location of the user rather than GPS based systems especially for indoor environment.

1.2.3. GPS based systems

GPS (Global Positioning System) is a kind of system that calculates the position information of a user using GPS signals sent from 24-32 GPS satellites high above the earth. This is mainly used by car navigation, airplane etc. [46]. Since the mids 1980s, researchers have focused on the GPS-based systems in order to overcome the visually impaired navigation concerns, maintain orientation, and store and retrieve information about specific location [47-50].

The basic concept of GPS-based system is taking the location of user as reported by GPS device through Geographic Information System (GIS). This information can then provide the user his/her localization such as by identifying which building the user is close to or how far the user is from the desired destination [51-52]. In the Fig. 1.13 and Fig. 1.14, the overview of GPS-based navigation system components and the functional components of GPS-based navigation system for visually impaired are shown respectively.

As seen in Fig. 1.14, the functional components of the system are a GPS module for determining the traveler's position and orientation, a Geographic Information System (GIS) comprising the system software and the spatial database for the traveler's orientation, and a user interface for providing information about surrounding environment [53-55].

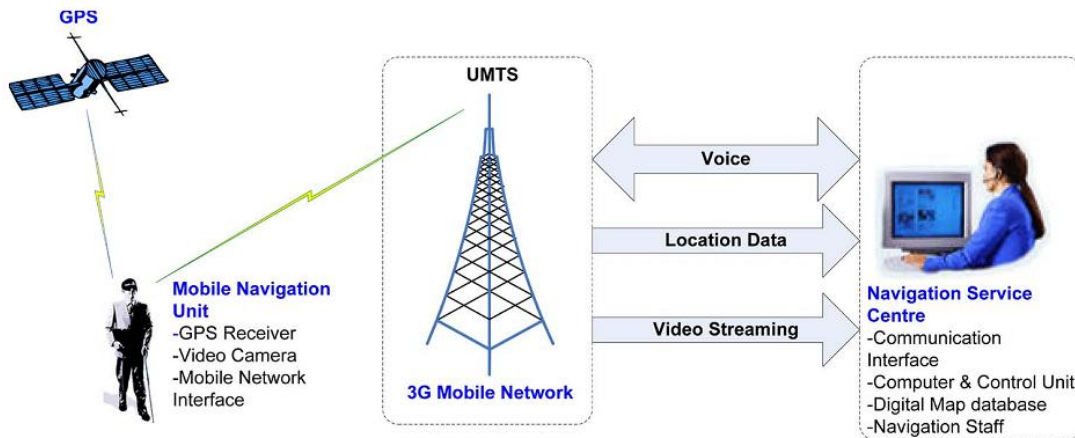


Fig. 1.13: Overview of the GPS-based navigation system components [53]

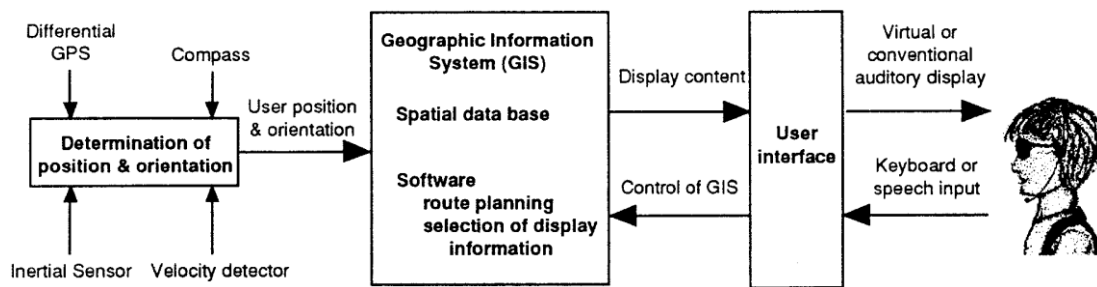


Fig. 1.14: The functional components for all GPS-based navigation system for visually impaired [54]

Loomis et al. developed *Personal Guidance System* including GPS module with stereo head set as seen in Fig. 1.15 [56]. Another portable system including GPS module was the *ODILLA System* with white cane. In that system, the information about the localization of a user was provided by audible text-to-speech information as shown in Fig. 1.16 [57].

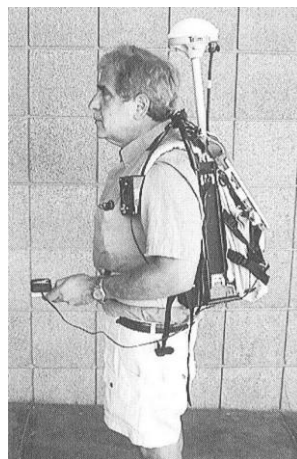


Fig. 1.15: Personal Guidance System [56]



Fig. 1.16: ODILIA System [57]

Ran et al. developed *DRISTHI System* for outdoor and indoor environments. In their system, GPS module was used for outdoor navigation whereas ultrasound-positioning tags were used for indoor environment. System comprised of additionally wireless connection, a wearable computer and a vocal communication interface for guiding the user as shown in Fig. 1.17 [58].



Fig. 1.17: Outdoor and indoor mobile user of DRISTHI [58]

LaPiere and Kargoankar developed a portable navigation system using Global Positioning that would accurately let user know his/her location [58-60]

Hunaiti and et. al studied on the performances of 2G, 2.5G and 3G mobile links. They evaluated the suitability of these GPS mobile communication links for application of a navigation system since these link characteristics such as bandwidth, latency, link outages and packet losses directly influence the navigation system performance [54, 61-62].

As presented above, GPS-based navigation systems are mainly suitable for outdoor applications. Since they provide information about localization, vocal communication interface is generally preferred as a guidance tool. One of the greatest weaknesses of these systems is to get the information from the satellites, which is a problem especially in some points where the system does not work. Moreover, another weakness of the system as deduced from the above is the fact that in order to ensure information, system has to be integrated with a portable computer.

1.2.4. Sonar based systems

Sonar is a kind of instrument used for detecting, locating, determining objects or measuring the distance to an object through reflected sound waves. The working principle in sonar systems is as seen in Fig. 1.18. First, electrical impulse is converted into sound waves by sonar equipment and then, sonar equipment picks up the echoes of reflected sound waves that crash to an object. Thus, the distance to an object is identified by the measurement of the time from transmission of a pulse to reception.

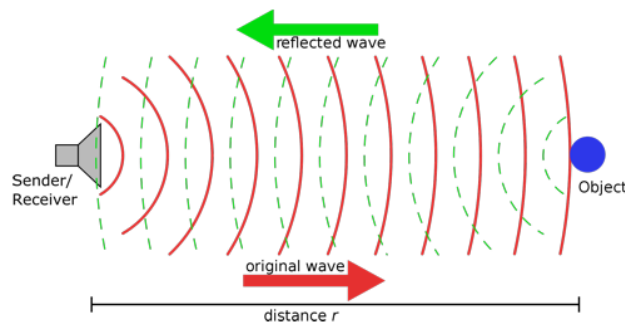


Fig. 1.18: Principle of active sonar [63]

The frequencies used in sonar systems changes from infrasonic to ultrasonic. The term ultrasonic refers to frequencies above audible sounds, which humans could not hear, and it nominally indicates anything over 20000Hz. In nature; bats, dolphins and some other species communicate and navigate in the range of 20-100 KHz.

During the past decades, several researchers have introduced devices that use sonar system to provide mobility to the visually impaired. Cane or stick is the one approach in which the sonar system is integrated (see Fig. 1.19). In the researches, since the number of sensors due to their beam angles affects the detection capability of cane, researchers have concentrated on finding the optimum number of ultrasonic sensors to be used in the cane. In those cane systems, as soon as the information is get by the sensors, the information is processed and by this way, encoder generates control pulses for the servos as a routing system [64-70].

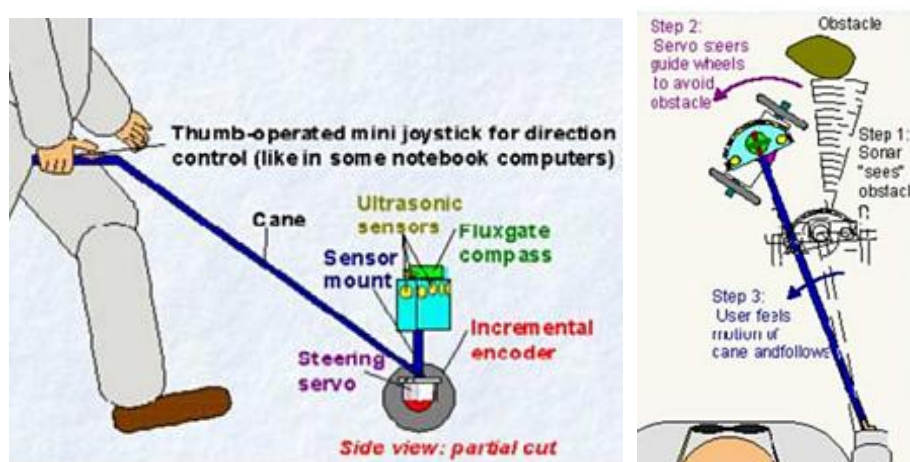


Fig. 1.19: Ultrasonic based cane system [64]

Another approach is to implement sonar system on a wearable concept. Shoval et al. developed Navbelt system that involves ultrasonic sensors mounted on a belt with a computer (see Fig. 1.20). In this system, signals acquired by the sensors were processed in the computer, and then resulted signals were sent to the user by stereophonic headphones using a stereo imaging technique [71-73].

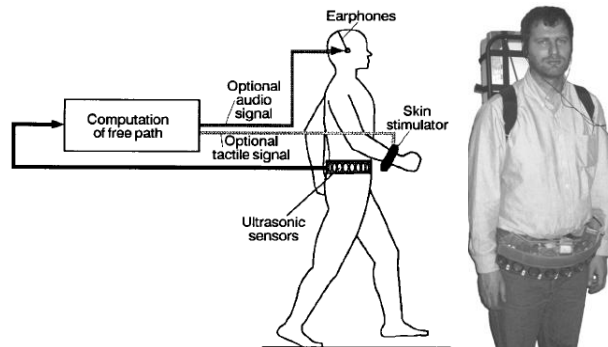


Fig. 1.20: The Navbelt system [71]

Recently, unlike Navbelt, researchers have suggested novel wearable devices in which sonars are attached to textile structures. Fig. 1.21 and 1.22 show examples of suggested systems e.g. Andha Astra, Arm9-based embedded system. The basic working principles of these systems are similar to those mentioned above.

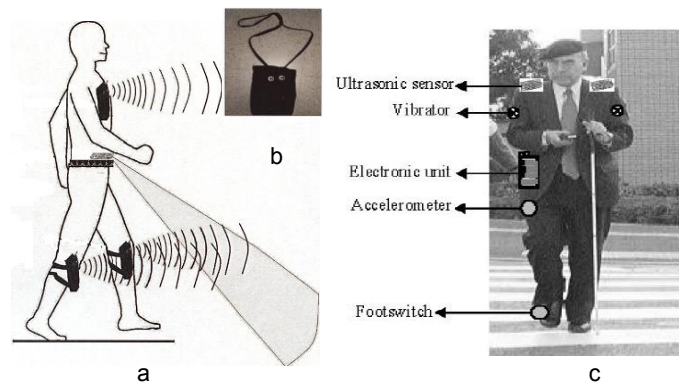


Fig. 1.21: a-b) Overview and module of Andha Astra c) another navigation aid worn by blind [74,75]

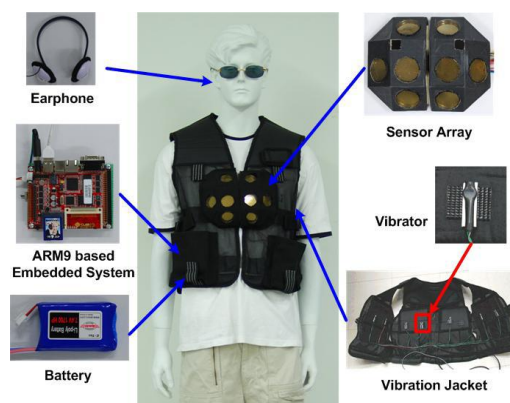


Fig. 1.22: Arm9-based embedded wearable ultrasonic based system [76]

For instance, in a study of Cardin et al. sonars were placed on the shoulder of cloth, and vibrators were mounted on the same cloth. Prototype was composed of sonars, vibration motors, a microcontroller and a PDA as shown in Fig. 1.23. The microcontroller gathers information via sonars, and sends feedback the user through vibration motors. They reported that in an indoor environment the users managed to distinguish (which are on the left or right) and avoid obstacles [77].

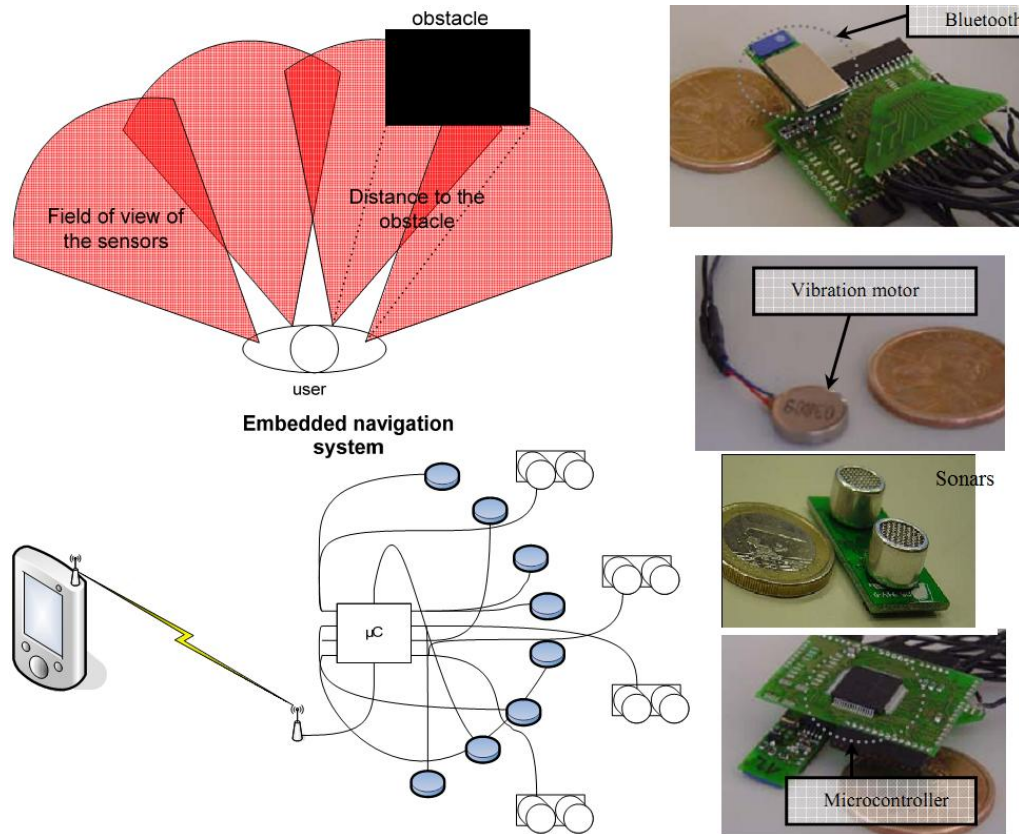


Fig. 1.23: Details of EPFL prototype

However, in those studies, the integration of electronic components to textile structures was not given in detail; this was the missing part. It seems that they only suggested a system, or attached these components by using conductive wires to the garment [74-77].

In some studies, sensors were mounted on shoes as shown in Fig. 1.24, and the performance of the system was analyzed in terms of both direct distance detection and road surface reflectance detection [78-79].

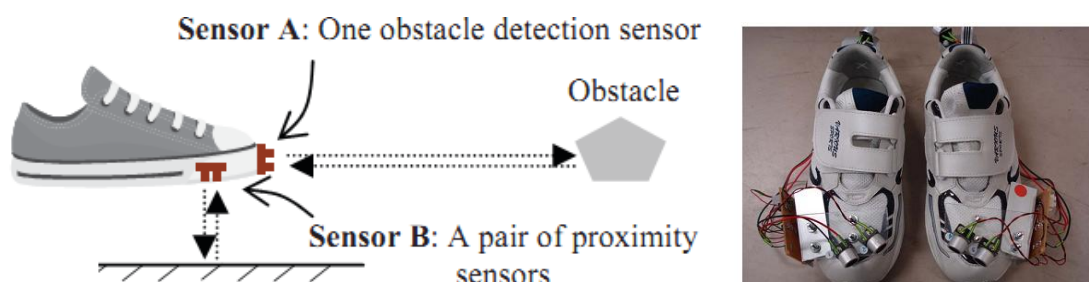


Fig. 1.24: Shoe mounted sensors [78-79]

Shah et al. developed *Tactile* navigation system composed of sonar sensors, a microcontroller, and a tactile array, where each actuator matches with one finger. Signals acquired via ultrasonic sensors were transformed into commands through variable and synchronized vibrations on the user hand. Vibration intensity levels and points of the devices sensed by the hand according to distance are shown in Fig. 1.25. For instance, the corresponding feedback signal according to obstacle distance was provided by vibration levels [66]. However, this system may be difficult for user to sense precise vibration levels and their locations accurately.

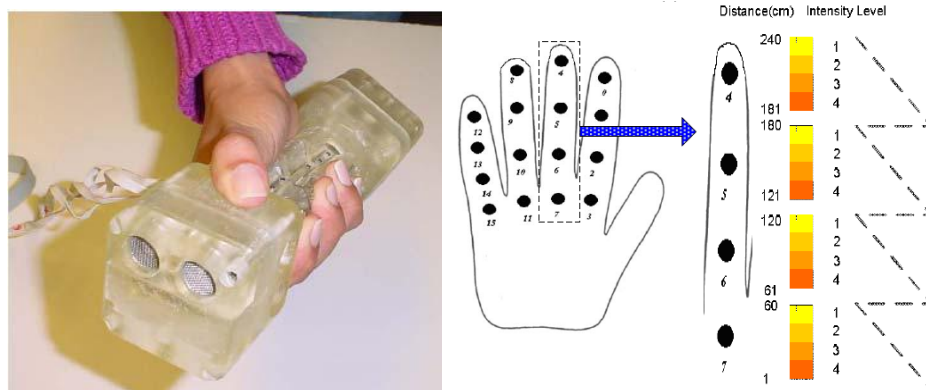


Fig. 1.25: Tactile navigation system [66]

Similarly, there are various commercial products, which can be carried by hand including sonar systems (see Fig. 1.26). Despite their low scientific and technological values, their costs are relatively high [81-84].



Fig. 1.26: Commercial products that use sonar system [81-84]

In addition to above studies, Rentschler et al. have recently developed Guido Robotic Traveler equipped with sonar system (see Fig. 1.27). It consisted of both laser and sonar sensors. Sonar sensors were added to the system in the case where laser sensors cannot detect objects that are out of their viewing capability such as glass or transparent materials. Furthermore, system consisted of two optical encoders to calculate the orientation and position, force sensor to sense the command, and a volume knob to give auditory messages [85]



Fig. 1.27: Guido Robotic Traveler [85]

According to studies, it is clear that ultrasonic based systems have advantages in the detection of objects over lasers and cameras, because they are not affected by light like cameras or lasers. Furthermore, there is no need to use image processing system. Nevertheless, they only detect the presence or absence of an object as well as measure the distance to it. They do not give any information about the user location.

1.3. Literature review for electronic textiles

E-textiles are playing a vital role in many applications such as military, medical, telecommunications, and healthcare. In recent years, the field of e-textiles is more and more extending due to new sensing elements, multifunctional fibers, flexible technologies, MEMS actuators etc.

The research carried out in this area is primarily driven by the motivation of creating yarn-like material assemblies that can sense, act, communicate and compute.

Since the hierarchical nature of textile structures goes from fiber to cloth/garment (fiber-yarn-fabric-garment), the way for the development of fully integrated electronic textiles (or Electotextiles) with transistors, circuits, sensors, batteries, solar cells and other electronic devices were explained starting from yarn-like materials to conductive fabrics and finally interactive cloths.

1.3.1. Electrically conductive yarn-like materials

The explored yarn-like materials are traditional and conventional yarns modified with various functional materials such as conductive yarns, conducting polymers, carbon nanotube fibers, optic fibers, piezoelectric materials etc.

Methods of creating yarn-like conductive materials can be summarized as:

- 1) filling fibers with conductive particles;
- 2) coating fibers with conductive polymer composites or metals;
- 3) use of continuous or short fibers that are completely made of conductive material [86-87].

Conductive threads are made of single or multiple strands of conductive and nonconductive fibers.

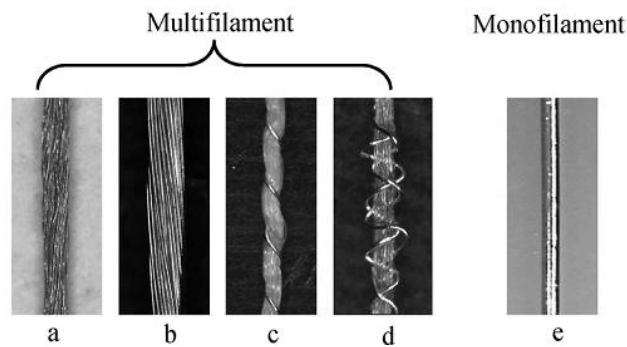


Fig. 1.28: Various forms of conductive threads [88]

As shown in Fig. 1.28, there are two types of conductive threads: multi-filament threads (see Fig. 1.28a–d) and monofilament threads (see Fig. 1.28e) [88].

Huang et al. developed yarn-based sensor for breathing monitoring using piezo-resistive carbon coated fibers (CCF), elastic and regular polyester fibers. To manufacture the yarn structure they utilized single and double wrapping methods (see Fig. 1.29). They concluded that the yarn-based sensor could track breathing signals precisely [89-91].

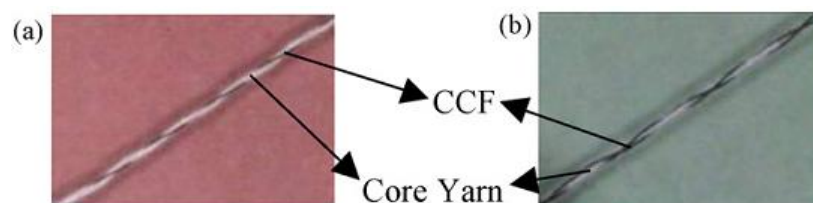


Fig. 1.29: The yarn structure of yarn-based sensors: (a) single wrapping and (b) double wrapping [89]

Kaynak et al. prepared conductive materials from nylon, cotton, and wool yarns by continuous vapour polymerization of pyrrole [92]. Ramachandran and Vignesweran developed core–sheath conductive yarn using copper filament as core and cotton fibers as sheath as seen in Fig. 1.30 and they studied the electro-mechanical characteristics of developed conductive yarns [93].

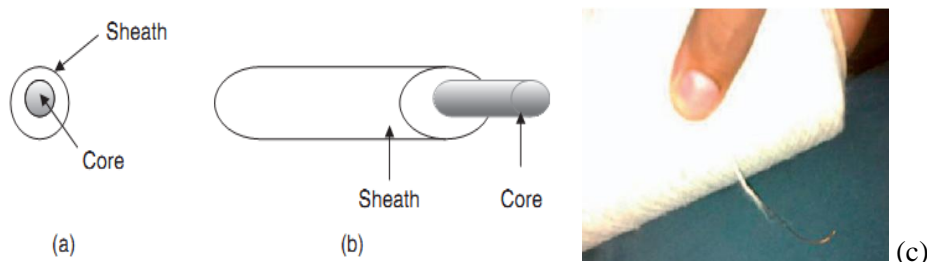


Fig. 1.30: a) Cross-sectional and b) longitudinal views of core–sheath c) Developed yarn: Core/Copper filament; Sheath/Cotton fiber [93]

Kim et al. and Koncar et al. studied electrical and morphological properties of PP and PET conductive polymer fibers. In order to create conductive fibers, melt spinning and coating processes were used. PANI coating on PET yarns was carried out during the impregnation of PET yarns in the PANI solutions as shown in Figure. 1.31 [94-95].

In another study, PANI-coated PE (Dyneema) conductive yarns were obtained by coating process. The effects of time and temperature on electro-mechanical properties of yarns were studied. They reported that conductive yarns showed interesting properties for electrical applications. Moreover, they preserved the original strength and flexibility of the textile in which they were integrated (see Fig. 1.32) [96]. Similarly, Xue et al. developed different electrically conductive yarns based on carbon nanotubes (CNTs) and polyvinyl alcohol (PVA) by using wet-spinning and coating process [97].

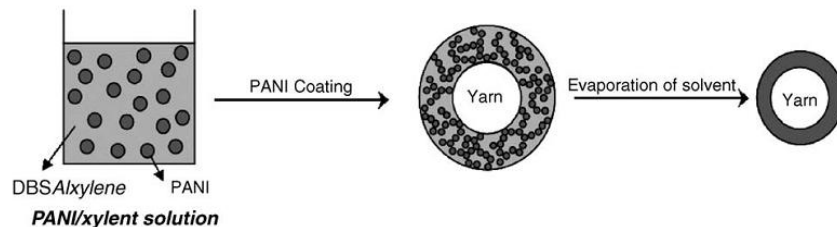


Fig. 1.31: Overview of coating process [95]

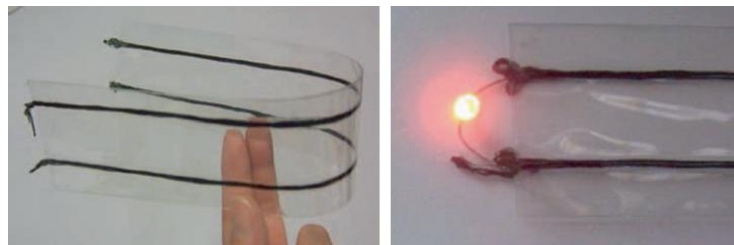


Fig. 1.32: (a) Prototype of conductive yarns covered with plastic films and (b) LED lighting test [96]

Apart from electrically conductive yarns mentioned above, there were also some studies on fiber-based cells. In one of these studies, the structure and properties of the photovoltaic fiber converting sunlight into electricity were described. Photovoltaic fibers were prepared by using flexible polypropylene (PP) monofilament, the PEDOT:PSS layer, the photoactive layer and a metal-based electrode as shown in Fig. 1.33 [98]. Similarly, Toivala et al. developed photovoltaic fiber as shown in Fig. 1.34. They used both optical and silica fibers as substrates [99].

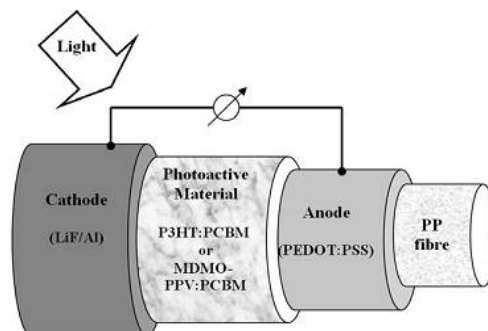


Fig. 1.33: Schematic diagram of photovoltaic fiber [98]

In another study, Wang et al. developed flexible fiber battery based on conducting polymers. Batteries consisting of a PPy/PF6 cathode and a PPy/PSS anode were fabricated as presented in Fig. 1.35 [100].

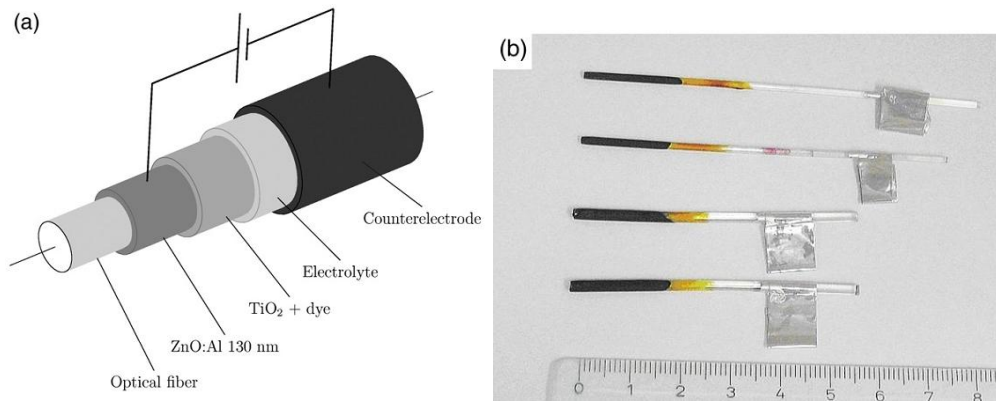


Fig. 1.34: Overview of photovoltaic fibers [99]

Moreover, there were also some attempts to fibrous transistors [101-107]. According to articles published until now, fibre transistors can be divided into two families: wire thin film transistors (WTFTs) [102-104] and wire electrochemical transistors (WECTs) [105-106]. For instance, Tao et al. studied the integration of fibrous transistor into a weaving fabric. In their study, two parallel filaments were twisted together like a thread. One of them was used for the gate electrode and the other was used for drain and source electrodes. The PEDOT:PSS was used as thin-film electrodes in the wire electrochemical transistors (WECTs). This kind of WECT was inserted into a cotton fabric and the numerical and analog circuits were realized [107].

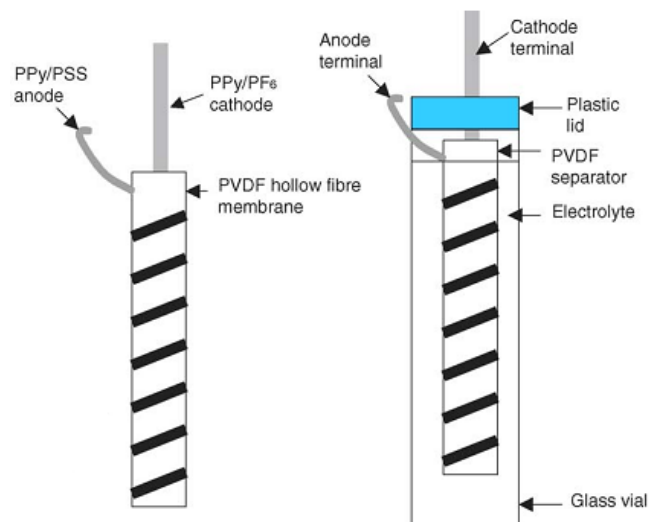


Fig. 1.35: Schematic of fibre cell [100]

1.3.2. Electrically conductive fabrics

In order to realize fabric based circuits or electrically conductive fabrics, several processes could be utilized including embroidery, weaving, knitting, printing, deposition and coating.

In embroidery, conductive threads are exposed to high level of stress and friction during stitch formation. These stresses may lead to yarn breakages or discontinuities in sewn conductor lines.

As a result, undesirable additional impedance can occur in fabric circuit. Similarly, when electrically conductive fabric is formed by printing, deposition or coating, electrical discontinuities at certain points can occur due to non-uniform dissipation of conductive materials e.g inks, films, pastes.

Additionally, these fabrics are stiff and prone to cracking; as a result bending of such a fabric may cause electrical discontinuities. However, woven and knitted fabrics are mainly well suited for the formation of electrically conductive fabrics due to their structural order and flexibility [108].

Dhawan et al. gave information about the formation of fabric-based circuit by weaving of conductive and non-conductive yarns [109]. Moreover, they observed signal crosstalk noise between transmission lines due to the distance. They reported that as the distance between conducting transmission lines increases, the magnitude of crosstalk noise decreases [110]. Additionally, Cottet et al and Locher et al. studied the electrical performance of fabric based signal transmission lines. The conductive yarns (ground-G or signal lines-S) were woven and separated from each other by any number of non-conductive yarns. GS, GSG, GSSG, and GSSSG configurations of signal and ground transmission lines were formed as seen in Fig. 1.36.

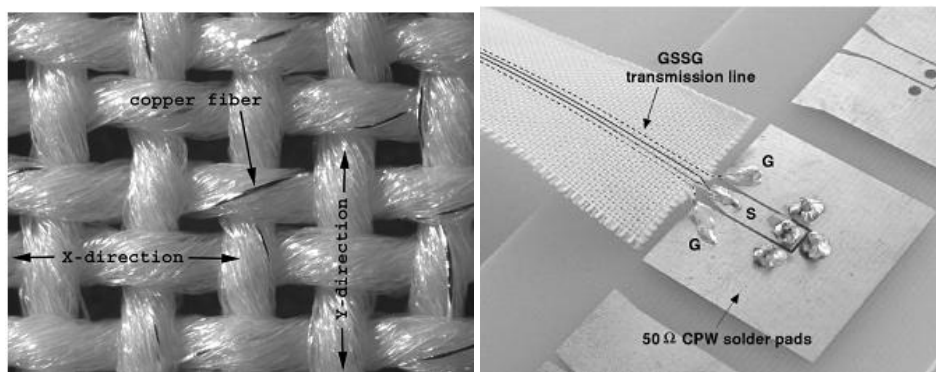


Fig. 1.36: Woven fabric with metal fibers and GSSG transmission line on woven e-fabric[86]

Electrical parameters (e.g., line impedance, insertion loss, far end crosstalk, etc.) for different configurations of woven e-fabrics were investigated using time and frequency domain analysis [86, 111].

In the work being carried out on communication systems, several fabric based antennas operating at 2.45 GHz have been developed [112-118]. Hertleer et al. reported that the efficiency of developed fabric based antennas were over 75%, which was a very promising result since a similar non textile antenna would have an efficiency of 80% [118].

Gimpel et al. developed three-layer woven antenna of a textile RFID tag by using Ag/PA threads as shown in Fig. 1.37 [119]. Winterhalter et al. utilized double plain weave construction to develop textile based USB [120].

Nakad et al. designed an electronic acoustic array in order to detect the location of passing vehicle according to vehicle's acoustics emissions. This acoustic array e-fabric was developed by first weaving of conductive yarns (see Fig. 1.38) and then, by integration of microphones to certain location of fabric [121].

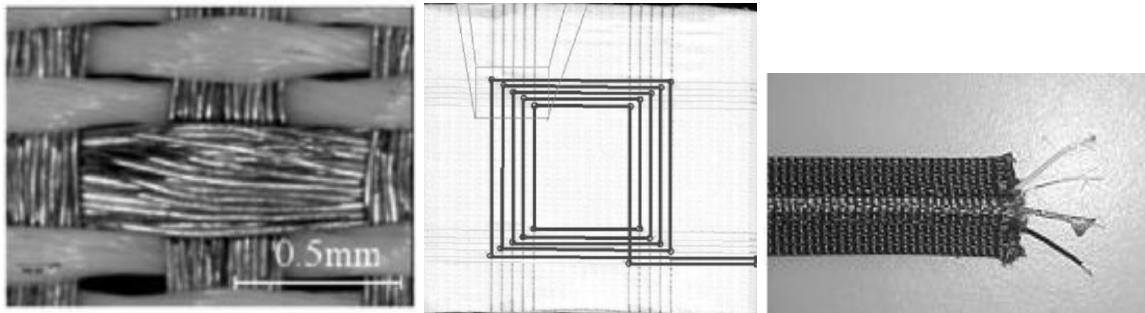


Fig. 1.37: a) Metals in woven structure b) Three-layer woven antenna of a textile RFID tag [119] c) Textile based USB [120]

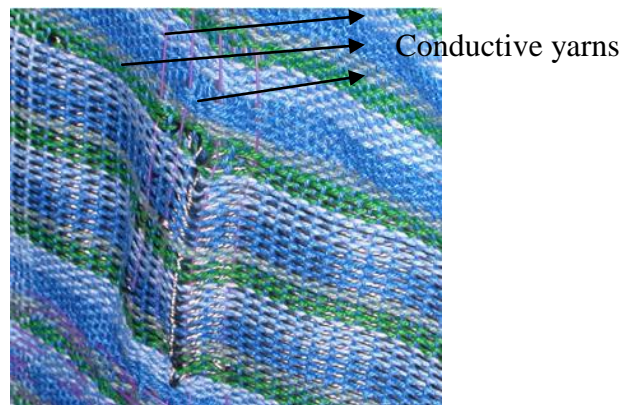


Fig. 1.38: Woven prototype containing multiple stainless steel fibres [121]

Moreover, there are some other studies focusing on electromagnetic shielding effect of woven e-fabrics. In those studies, the effect of varying weft density, warp density, conductive yarn diameter/count, conductive yarn type such as copper, stainless steel, carbon etc. on electromagnetic shielding effectiveness were studied [122-124].

Rothmaier et al. investigated the effect of woven fabric construction on the resulting performance of light emitting and receiving capabilities of plastic optical fibers (POF). They concluded that capability of emitting or receiving light without further conditioning of optical fibers changed due to the structure [125]. Moreover, Kumar et al. studied signal transmission efficiency of woven POF fabrics (see Fig. 1.39) [126].

In a study of Hasegawa et al., fabric tactile sensor formed by artificial hollow fibers and cotton yarns was developed by weaving process as seen in Fig. 1.40. Hollow fibers were silicon rubber tubes coated with gold. They investigated the relationship between applied load and sensor output (capacitance change) [127].

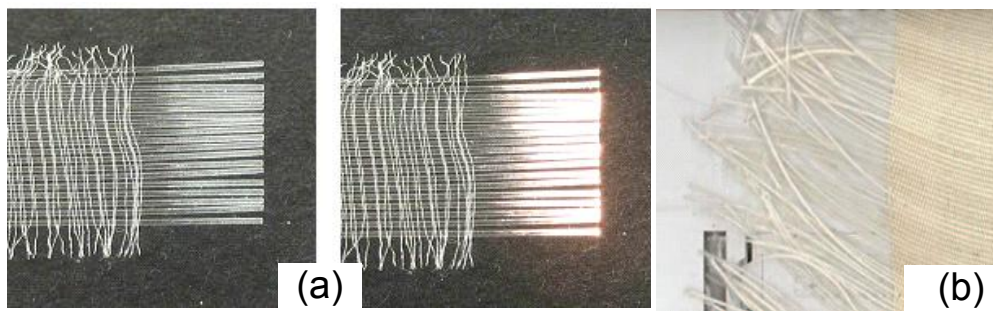


Fig. 1.39: Woven specimens connected to halogen lamp OFF and ON, POF in weft direction, white PET fibers in warp direction, [125] Optical fiber core conductive fabric (b) [126]

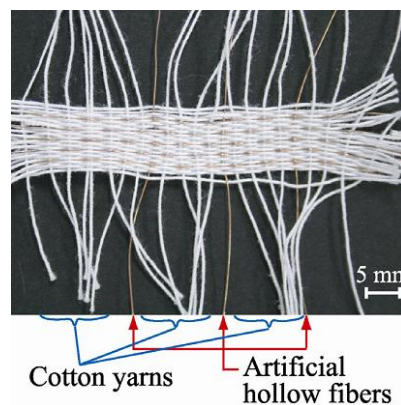


Fig. 1.40: Fabric tactile sensor [127]

Apart from weaving techniques, there are other studies where knitting techniques were used to produce e-fabrics. Kayacan et al. investigated heating behavior of knitted e-fabrics. Heated fabric panels including steel yarns were produced by weft knitting techniques as seen in Fig. 1.41. They observed and analyzed the electrical and temperature characteristics of heated e-fabric panels [128-129].

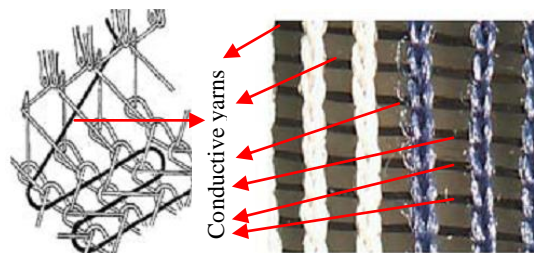


Fig. 1.41: Production procedure of heating panels [129]

Scilingo et al. and Wijesiriwardana et al. developed conductive fabric electrodes with knitting technology to measure respiratory monitoring and ECG as seen in Fig. 1.42. Scilingo et al. used stainless steel yarn twisted around viscose yarn as a conductive yarn whereas Wijesiriwardana et al. used carbon or metal loaded rubber (CLR/MLR), polypyrrole (PPY) coated fibers and copper wire.

Conductive fabric electrodes developed by Wijesiriwardana et al. were called as resistive fibre-meshed transducers or FMTs as seen in Fig. 1.42b [130-132].

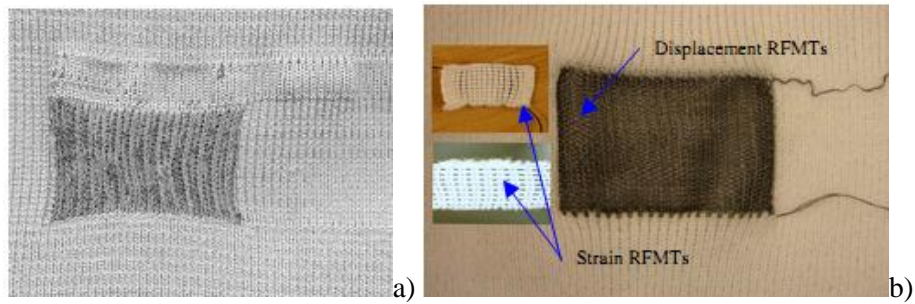


Fig. 1.42: Conductive fabric electrodes constructed with knitting technology [130-131]

Soleimai designed knitted switches based on resistive and capacitive sensing methods [133]. Soleimai et al. and Zhang et al. developed conductive knitted fabrics as strain gauges [134-135]. In a study of Zhang et al., fabric was knitted as tubular weft plain fabric using steel and stabilized carbon fiber as shown in Fig. 1.43. They analyzed the effects of strain-rate and temperature on the sensitivity of the gauge experimentally.

They reported that fabric gauges made from carbon fibers displayed a higher sensitivity, repeatability and accuracy than those made from stainless steel.

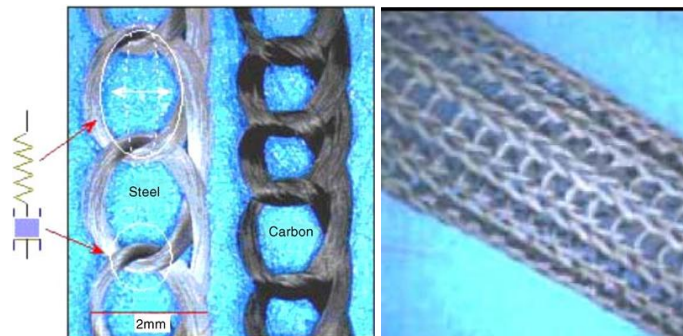


Fig. 1.43: Tubular conductive knitted fabric [135]

Li et al. derived the analytical model of conductive knitted stitch network based on the common intersia knitting technique and jersey knitting techniques [136]. They also studied the pressure effect of different knitting stitches. They found that conductive knitted fabric of specific stitches resulted in a different pressure effect on human skin. By this way, they concluded that knitting technologies as well as garment design skills play an important role in intelligent clothing applications, such as monitoring sensors and heat generators [137].

In order to develop textile-based electronic circuits, researchers also used different manufacturing processes such as embroidery, coating, printing and dyeing. Linz et al. developed a mechanism to embroider through flexible electronic modules using conductive yarns [138-139]. As shown in Fig. 1.44, interconnections of electronic modules with conductive yarns were accomplished by embroidery.

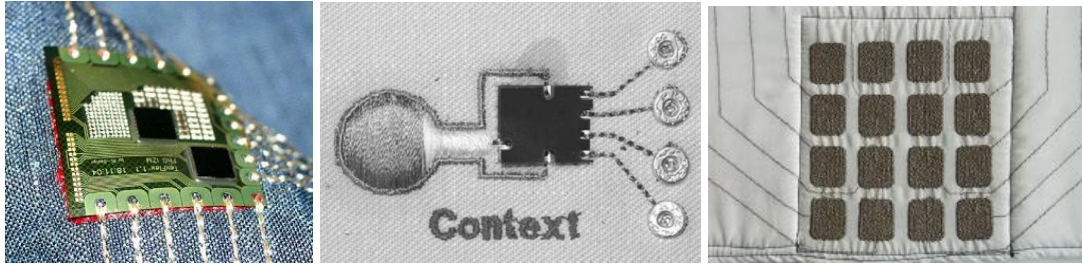


Fig. 1.44: Electronic modules connected with conductive yarn by embroidery [138-140]

Koncar et al. studied on heating performance of e-fabrics which were coated with conductive polymer composites (CPCs). To construct e-fabric, they first produced woven fabric using conductive yarns, and then applied CPC coating including conductive carbon black nanoparticles on fabric surface as seen Fig. 1.45 [141].

In addition, Li et al. also used coating process in order to develop flexible strain fabric sensor [142].

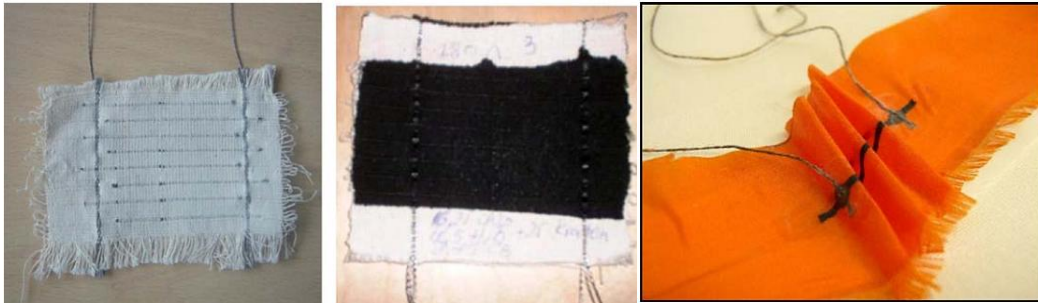


Fig. 1.45: Coated e-fabrics as a heating element [141]

Moreover, screen-printing method has also been tried to form transmission lines in fabrics [143-145]. As a print ink, conductive pastes (e.g silver filled paste) were used. The number of print passes in a different scale was tried in order to find efficiency of transmission lines (see Fig. 1.46). For instance, Locher et al. reported that a higher number of passes resulted in a better penetration of the fabric and therefore, resulted in better conductivity [145].

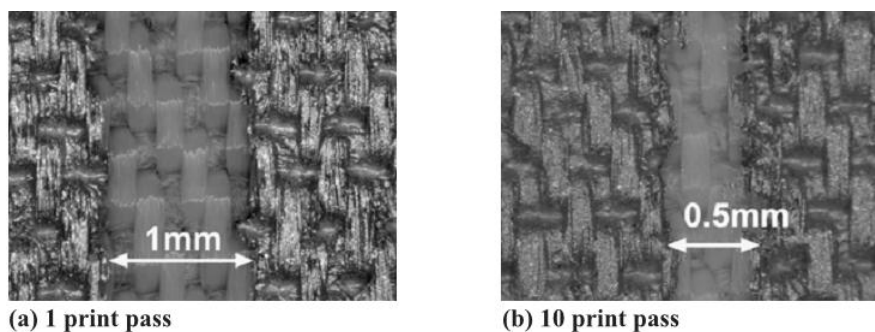


Fig. 1.46: Screen printed structures [145]

Similar to coating and printing techniques, Leah et al. presented fabric printed circuit boards (Fabric PCBs) techniques based on adhesion principles [146]. In their study, at first circuit was designed on conductive fabric, and then this fabric was cut by laser cutters.

As a further step, laser-cut fabric was exposed to heat activated adhesive, and then it was placed on non-conductive fabric. Owing to heating and adhesion principle, conductive fabric having circuit was attached to non-conductive fabric. Finally, soldering was implemented on certain conductive parts to encapsulate joints on epoxy resin (see Fig. 1.47).

In addition to all studies mentioned above, dyeing methods were used to form electrically conductive fabrics. Panhuis et al. investigated the incorporation of carbon nanotubes into textiles through conventional dyeing. They found that suggested dyeing process provided a simple way to fabricate conducting textiles [147].



Fig. 1.47: Solder joints on a fabric PCB [146]

1.3.3. Interactive cloths

This section provides an overview of existing efforts and associated challenges in interactive cloths. Electronic components embedded to textile structures, as well as built into yarns, can gather sensitive information, monitor vital statistics and send information for further processing. The developed interactive cloths mainly take a role in entertainment, safety, communication, military, and medical applications.

One of the earliest accounts of interactive cloths is *Wearable Motherboard/Smart Shirt* developed at the Georgia Institute of Technology as seen in Fig. 1.48, in mid-1990s.

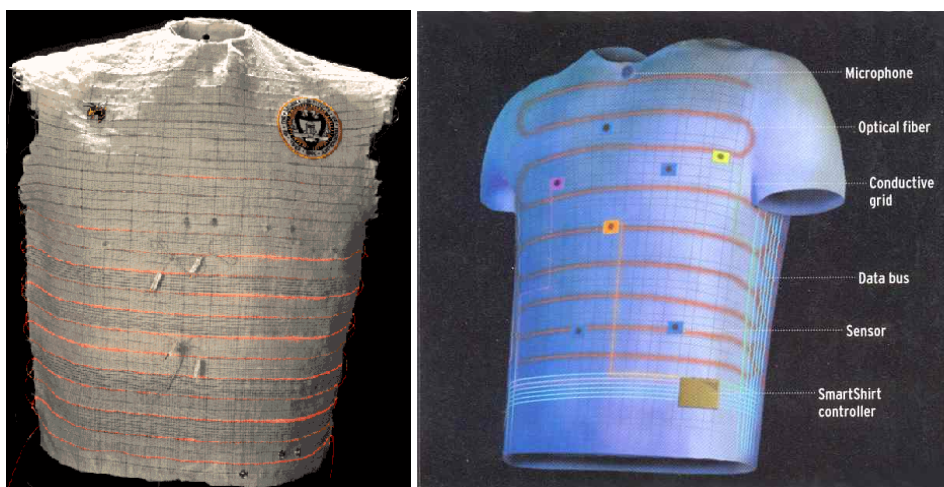


Fig. 1.48: Wearable Motherboard (early prototype of SmartShirt) and SmartShirt® [148]

The aim of the proposed garment was to ensure combat soldiers information about their personal survival. The garment integrated with sensor technology enabled monitoring heart rate, respiration rate, electrocardiograph (ECG), pulse oximetry and temperature [148].

The feasibility of Wearable Motherboard paradigm brought new challenges for numerous application domains especially for medical applications. There have been handful attempts to design and build prototypes for health monitoring systems especially for detection of biosignals such as ECG, respiration [149-171].

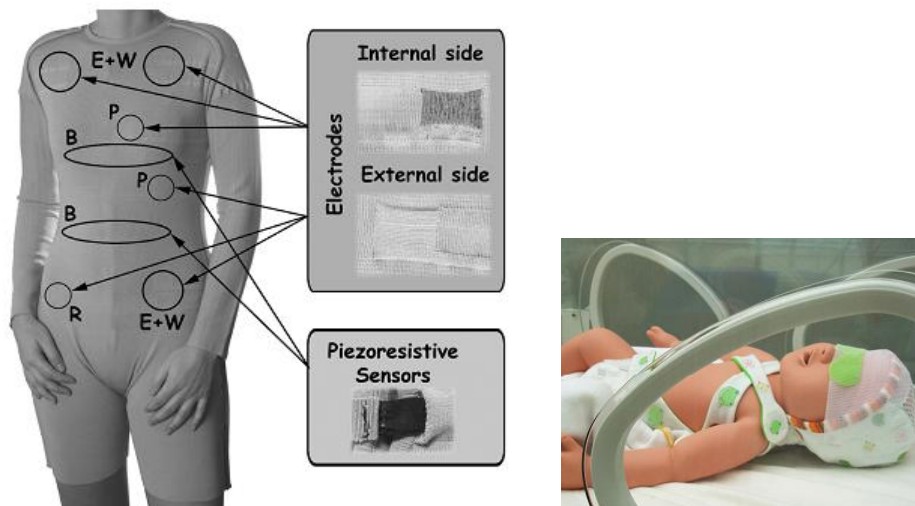


Fig. 1.49: a) WEALTHY system prototype model [153] b) Smart Jacket prototype [168]

Figures 1.49 and 1.50 show some kind of interactive cloths developed for medical applications. For instance in a study of Paradiso et al., sensors, electrodes and connections were realized with conductive and piezoresistive yarns in order to get several biomedical signals (i.e ECG, respiration, activity). The interactive cloth produced by knitting technology combined advanced signal processing and telecommunication techniques as others (Fig. 1.49a) [153].

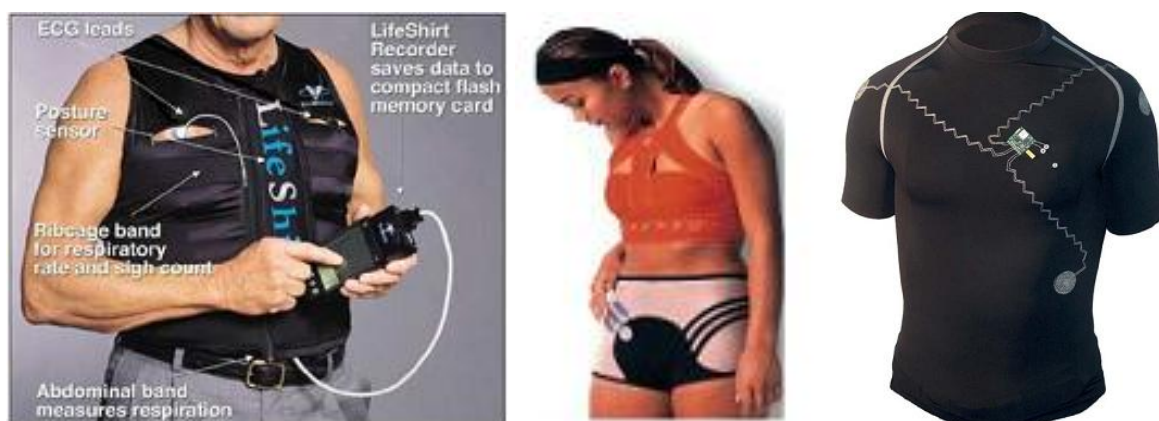


Fig. 1.50: Lifeshirt developed by Vivometrics [158] Sensor-based Sportswear by Phillips [149] b) Fully Integrated EKG Shirt [160]

For entertainment purposes, an interesting study was Emotions Jacket from Philips®. The Emotions Jacket was a tightly fitting garment, which consisted of a series of vibration motors sewn into the arms and torso (see Fig. 1.51). In response to what is happening on screen, these vibration motors are activated by a control unit. Thus, certain feelings being experienced by the characters in the film can be perceived by the user [172].



Fig. 1.51: Philips emotion jacket-outer and inner lining [172]

Thalmann et al. developed a garment to guide user to the required destination in a building environment. Concerning indoor location tracking; WiFi, RFID and sensors were integrated to inside of developed jacket. Target destination in a building, could be selected through input buttons on sleeve as seen in Fig. 1.52 [173].

There have been also some prototypes developed for measuring body postures, [174-179]. In a study of Tognetti et al., fabric was coated by using electrically conductive elastomer composites (CEs) as seen in Fig. 1.53a. Since CEs show piezo resistive properties when deformation is applied, they act as strain sensors.



Fig. 1.52: A virtual 3D mobile guidance jacket [173]

By the help of CE sensors, which were connected to acquisition unit, posture and movement of a user were detected and analyzed [175-176, 180]. Similar to approach of Tognetti et al, to measure the body posture Matmann et al. used a tight-fitting clothing and strain sensors that were composed of thermoplastic elastomer (TPE) filled with 50wt-% carbon black powder (Fig. 1.53b) [177].

Wu et al. and Munra et al. also studied strain sensors placed on a fabric by coating method. They developed intelligent knee sleeve sensing system composed of conducting polypyrrole-coated nylon lycra, which can monitor human motion and provide feedback to the wearer (Fig. 1.53c). Such a system could be useful for injury prevention, rehabilitation, and sports [181-182].

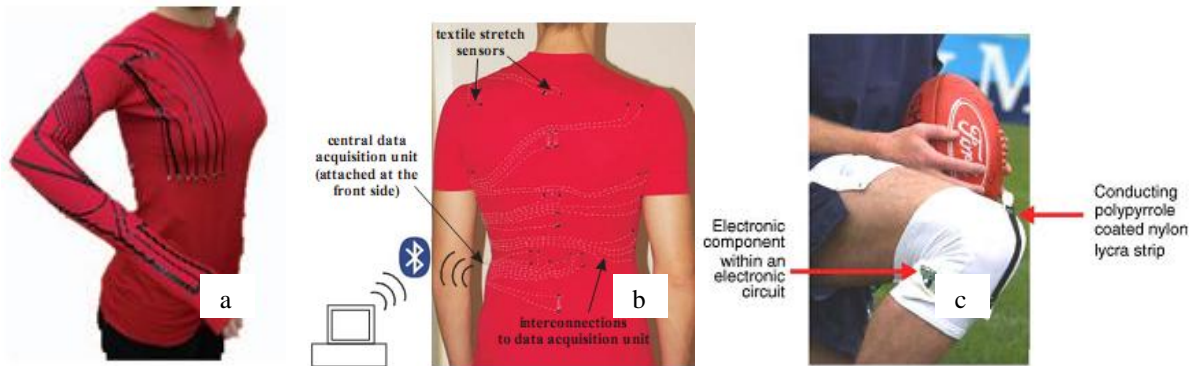


Fig. 1.53: Prototypes for recognizing body posture [176-177,181]

Li et al. developed an interactive cloth with transcutaneous electrical nerve stimulation (TENS) function from a knitwear design. They designed knitwear based on intarsia knitting technique by using conductive yarns. Textile electrodes connected to the end of conductive yarns were activated by energy supply in order to give electrical stimulation to acupuncture points (see Fig. 1.54) [183].



Fig. 1.54: Prototype of garment with electrical nerve stimulation (TENS) function [183]

Stead et al. and Goulev et al. worked on development of emotional garment, which has a capability of understanding user's feelings and thereby, presenting emotional response through the interface technology. The system was configured from under and over garment. The analogue signals taken by physiological sensors embedded to garment was transferred into digital signals through control system. By this way, control system estimates the mood of user and passes display information [184-185].

1.4. Summary

Based on literature review, it is important for a usable electronic travel aid to let the visually impaired be hand free and comfortable during the navigation. The most suitable approach to let the user be hand free is embedding whole system into clothes. In the literature, some of the researchers suggested this idea as explained above. However, in their researches the implementation of electronic components into textile structures was not given in detail, they all considered to attach the components onto clothes [2, 74, 76-77, 186].

To conclude, the design of the textile architecture in this concept is missing part. For example, in order to satisfy the electrical conduction between electronic components in the textile structure of the system, smart clothing approaches mentioned above could be utilized such as integrating electronic circuit by using conductive fibers through woven or knitted structure.

Thus, based on the analysis literature mentioned above, we developed an innovative wearable obstacle avoidance system fully integrated to textile structures for visually impaired people.

Chapter 2

E-Textile architecture for obstacle avoidance

2.1 Basis of system architecture

Designing interactive garment requires exploring the design parameters not only in software and hardware components but also in everyday wearing requirements.

2.1.1. Software and hardware components requirements

Before starting to design proposed smart clothing, many questions related with design variables were considered. In electronic system architecture towards the objective of the study, the questions that were answered are as follows:

- What types of sensors are required?
- What types of actuators can be used?
- How the data will be processed, which types of signal processing units are required?
- What will be the decision parameters in signal processing unit?
- How many sensors of each type are required?
- How many actuators of each type are required?
- What is the optimum placement of sensors and actuators on human body?
- What is the most useful placement for the microcontroller?
- What algorithms are needed to provide accuracy in analyzing data gathered by sensors?
- What is the required power consumption for the system?

- Which types of power supplies are adequate?
- Which types of conductive fibers are suitable for this system architecture?

2.1.2. Wearability performance requirements

When designing smart clothing system, apart from electronic hardware and software concept, the wearability of the system is a also critical issue. In wearability concept, some performance requirements such as lightweight, breathable, comfortable, easy to wear etc. have to be taken into consideration.

In our system, the whole wearability performance requirements were expected as shown in the Fig. 2.1.

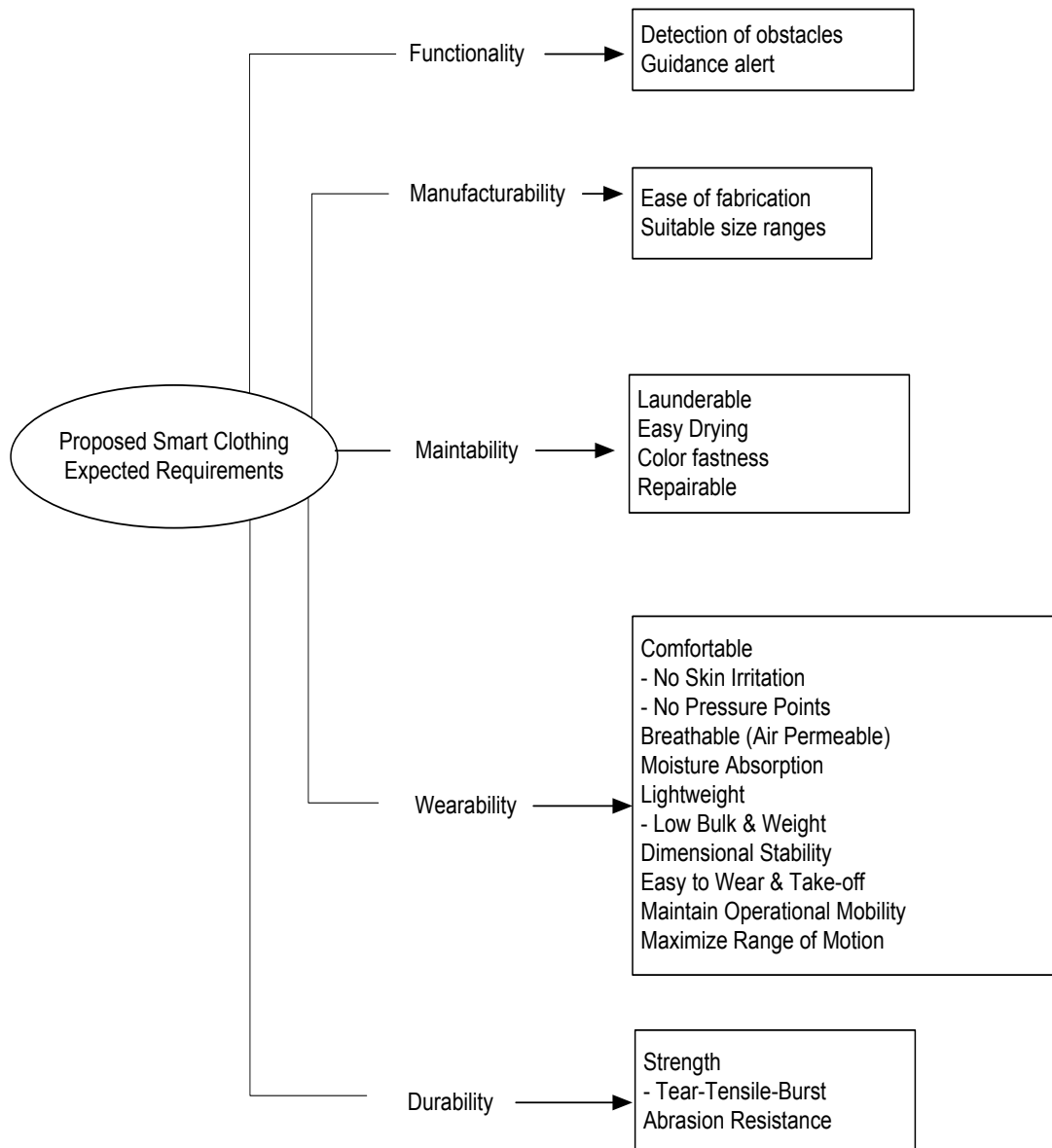


Fig. 2.1: Wearability performance requirements of the proposed system

2.2 Determination of electronic system components using an algorithm based on fuzzy AHP and fuzzy information axiom

A major challenge in smart clothing system is the integration of a multitude of diverse components, which are developed and produced in different technologies and materials. Each component in the system plays an important role in terms of performance and design. Therefore, designing a smart clothing system is a complex problem. In this context, in order to determine the most suitable components related to our objective, information axiom of axiomatic design was used to compose the optimal smart clothing system.

2.2.1. Criteria and alternatives for visually impaired's smart clothing electronic components

In the scope of this study, types of sensors, actuators and power supplies, which are suitable for smart clothing system, were investigated.

The first main critical question in this system design that must be answered was the type of sensor. According to previous studies, it was observed that there are three possible sensor options to measure the distance to an obstacle: ultrasound, laser and infrared (IR). These sensors could be evaluated due to their power consumptions, costs, sizes, weights, accuracies, working ranges and comfort issues.

The second critical question that must be answered was the type of actuator. Actuator is a mechanical device that converts energy into some kind of motion. According to our system design, vibration, audio or artificial muscle could be used as an actuator to ensure the user stimuli through feedback process. As sensors, these actuators could also be evaluated due to power consumption, cost, size, weight, accuracy and comfort issues.

The last criterion that should be considered was the type of power supply. For the power consumption of this smart clothing; solar cells, mechanical, chemical or thermal energy could be used. Unlike the power generators given in Table 2.1, flat battery can also be used because of easy replacement and recharging. These power supplies could be evaluated according to their power generations, costs, sizes, weights, accuracies, working ranges and comfort issues.

Table 2.1: Comparison of power generators useful for wearable Microsystems [187]

Power Generator	Power	Remarks
Solar cell (outdoors)	150 $\mu\text{W}/\text{mm}^2$	Direct sun
	1.5 $\mu\text{W}/\text{mm}^2$	Cloudy day
Solar cell (indoors)	5.7 $\mu\text{W}/\text{mm}^2$	Desk lamp
	0.06 $\mu\text{W}/\text{mm}^2$	Standard desk
Motion (Shoe generator)	1-10mW	Piezoelectric
	50-250mW	Electro-magnetic (rotary)
Motion (Inertial generator)	200 μW	For legs when walking
	50 μW	For torso when walking
Thermoelectric generator	0.2 $\mu\text{W}/(\text{cm}^2\text{K})$	Human body

For example; thin battery presents us some advantages like ease of removal before washing. It could be attached with snap fasteners for easy replacement and recharging.

2.2.2. Axiomatic design methodology and its axioms

Axiomatic Design (AD) was introduced by Suh to provide a scientific basis for design activities by presenting designer theoretical foundation based on logical and rational thought process and tools. The primarily goal of AD is to establish a thinking process to create a new design and/or to improve the existing design [188]. Axiomatic design methodology includes four main concepts; (1) domains (2) hierarchies (3) zigzagging, and (4) design axioms. The domains consist of customer, functional, physical, and process domains. The functional and physical domains are used for generating the design map. The functional domains are the functional requirements of a design solution. A minimum set of independent requirements that completely characterize the functional needs of a design solution in the functional domain are called as functional requirements (FRs). The physical domain shows the design parameters (DPs) of a design solution that are selected to represent the specified FRs [188-190]. The hierarchies are figured out by the decomposition of functional requirements and design parameters. The selected highest level of FR/DP is decomposed into the lower levels of FRs/DPs until the point where design solutions are considered to be reasonable. To decompose FRs and DPs, zigzagging should take place between domains. Zigzagging is the compromise of what a designer wants to achieve and how he/she achieves it. In any design situation, the probability of success is given by what the designer wishes to achieve in terms of tolerance (i.e. design range) and what the system is capable of delivering (i.e. system range) (see Fig. 2.2) [191].

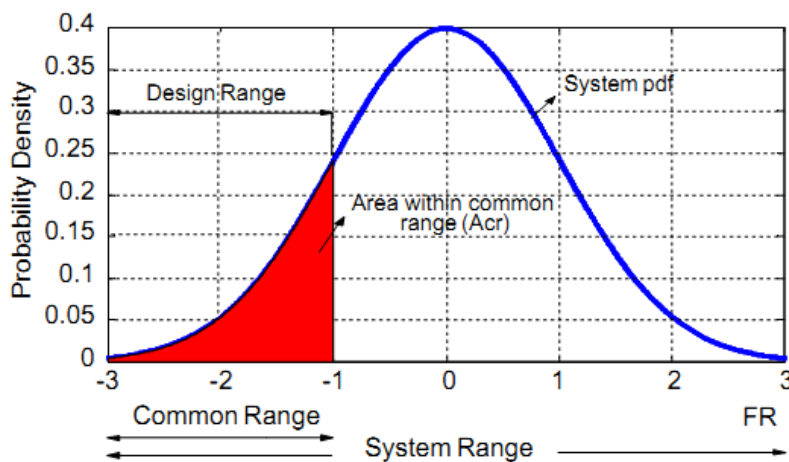


Fig. 2.2: Design range, system range, common range and probability density function of a FR [191]

AD methodology was derived from two axioms: the independence axiom and the information axiom. These axioms are shortly defined below [188-190]:

Axiom 1. Independence axiom: Axiom 1 requires maintaining the independence of FRs

Axiom 2. Information axiom: Axiom 2 requires minimizing the information content

In this study, information axiom was used to determine electronic components of smart clothing design. In this concept, information axiom was used to select the best components with respect to the defined FRs. The information axiom states that the design having the highest probability of success is the best design [189]. Information content (I_j) is defined in terms of probability p_j of satisfying FR_j , where j indicates the number of criteria. The information content is given by Equation 2.1.

$$I_j = \log_2 \frac{1}{p_j} \quad (2.1)$$

The logarithmic function is selected in order to make the information content additive when there are many FRs that must be satisfied simultaneously [188]. In the case of more than one FR, the information content of a system (I_{system}) can be calculated by Equations 2.2.

$$I_{system} = -\sum_{j=1}^m \log_2 p_j = \sum_{j=1}^m \log_2 (1/p_j) \quad (2.2)$$

The probability of success (p_j) is calculated by Equation 2.3,

$$p = \frac{\text{common range}}{\text{system range}} \quad (2.3)$$

where system range and common range are defined by the area of system range and by the intersection area of the system range and design range, which is determined by a functional requirement of the design, respectively.

Kulak and Kahraman used the information axiom under fuzzy environment for the solution of the complex decision making problems [191-192]. Instead of conventional information axiom, they used fuzzy numbers to satisfy the fuzzy information axiom.

Kulak et al. developed unweighted and weighted multi attribute axiomatic design approaches by considering both crisp and fuzzy criteria. Their application as a case study was about an equipment selection problem [193]. Additionally, Kulak developed a decision support system for the selection of a material handling system [194]. Then, Kahraman and Cebi improved the usability of the fuzzy information axiom for different decision-making problems [195]. In the literature, the proposed fuzzy information axiom has been tried in several applications. For instance, Celik et al. used the fuzzy information axiom to search a systematic evaluation model on docking facilities of shipyards [196]. In another study of theirs, they designed a hybrid approach that combines fuzzy information axiom and fuzzy technique in order to rank the performance of competitiveness requirements for container ports by presenting similarity to ideal solution (TOPSIS) [197].

Celik et al. implemented information axiom into quality function deployment method to analyze shipping investment processes [198]. Coelho and Mourão used the information axiom to choose an appropriate technology required for the subsequent detailed design of a mechanical component [199]. Kahraman et al. used information axiom to choose the best alternative for renewable energy investment of Turkey [200]. Moreover, Cebi and Kahraman designed a decision support system based on fuzzy information that can be easily adapted to decision making problems [201].

Herewith, we implemented the information axiom to determine the most suitable electronic components of our proposed smart clothing system.

2.2.3. Main structure of the proposed methodology

The framework of the proposed methodology for smart clothing system design was given in Fig. 2.3.

2.2.3.1 Initial phase

First, expert team was established. Then, the experts' weights were assigned with respect to their experiences.

Assume that the expert team consists of m experts and

$$w_{e1} + w_{e2} + \dots + w_{em} = 1 \quad (2.4)$$

where w_{ei} is the weight of i^{th} expert and $w_{ei} \in [0,1]$. Then, to evaluate alternatives since the linguistic terms are good at representing human logic, fuzzy membership functions were determined.

2.2.3.2 Definition of criteria phase

In this phase, evaluation criteria were determined by expert team after a literature review. Since each criterion may result a different impact on the final decision, it is necessary to identify the importance of each criterion due to our case. The best way to determine the importance of the criteria was the pairwise comparisons of the criteria. In this study, a modified fuzzy analytic hierarch process (AHP) proposed by Zeng et al. was used to define the priorities of the criteria [202]. In the classical AHP method proposed by Saaty, (1-9) scale was generally used for calculation of the priorities of the criteria [203].

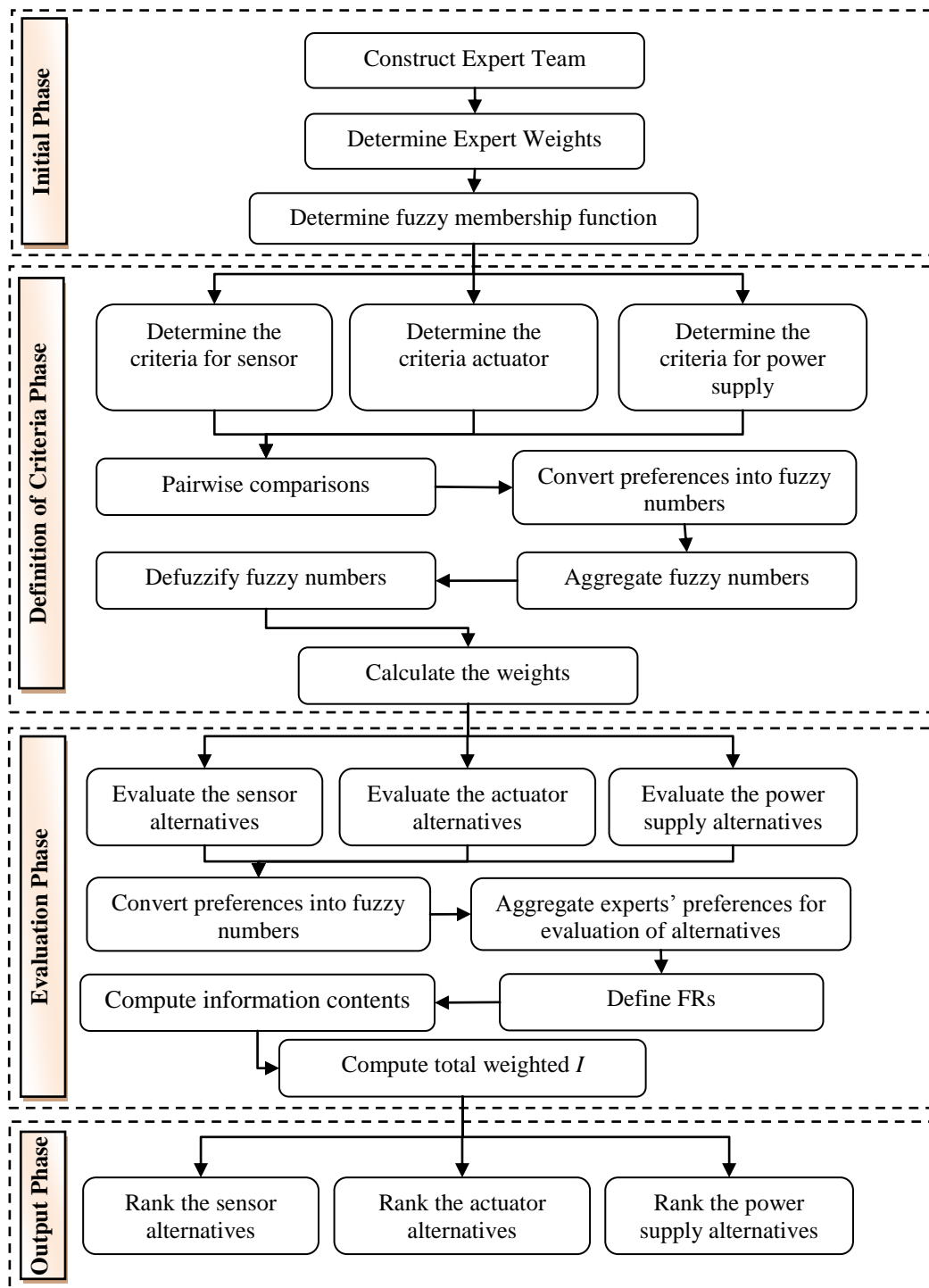


Fig. 2.3: Framework of evaluation model

The odd numbers between (1-9] range correspond the linguistic evaluations; *more important*, *strongly more important*, *very strongly more important*, and *absolutely more important*, respectively. Even numbers were used to express intermediate values. For the reverse comparison, the reciprocals of the corresponding numbers were used such as 1, 1/2, 1/3, ..., 1/9.

However, in the modified fuzzy AHP developed by Zeng et al., experts present their preferences in fuzzy scale such as “about 5”, “between 3 and 5”, etc. In the case that there is no comparison between two factors at all, experts leave absent that means they can’t be compared [202]. In our study, each expert made pairwise comparisons of the criteria using fuzzy numbers defined by Zeng et al. [202]. Then, evaluations were transformed into standard fuzzy numbers. To calculate the priorities of the criteria, experts’ evaluations for pairwise comparisons were aggregated by using Equation 2.5.

$$\tilde{S}_i = \tilde{S}_{i1} \otimes w_{e1} \oplus \tilde{S}_{i2} \otimes w_{e2} \oplus \dots \oplus \tilde{S}_{im} \otimes w_{em} \quad (2.5)$$

where \tilde{S}_i is the fuzzy aggregated score of the i^{th} criterion and \otimes and \oplus denote the fuzzy multiplication and fuzzy addition operators, respectively. Then, defuzzification operation was used to defuzzify the fuzzy numbers. In Equation 2.6, defuzzification operation was given for trapezoidal fuzzy numbers. Let $\tilde{A} = (a_{ij}^l, a_{ij}^m, a_{ij}^n, a_{ij}^u)$ be a trapezoidal fuzzy number, then

$$a_{ij} = \frac{a_{ij}^l + 2(a_{ij}^m + a_{ij}^n) + a_{ij}^u}{6} \quad (2.6)$$

The priority weights of the criteria in the aggregated comparison matrix were calculated by Equation 2.7.

$$w_i = \frac{1}{n} \sum_{j=1}^n \frac{a_{ij}}{\sum_{k=1}^n a_{kj}} \quad i, j = 1, 2, 3, \dots, n \quad (2.7)$$

2.2.3.3 Evaluation phase

In this phase, each alternative was evaluated under defined criteria. Then, experts’ preferences were transformed into fuzzy numbers, and fuzzy numbers were aggregated by using Equation 3.5. Functional requirements for the design were determined to calculate the information contents of the design. Information content values for the problem was calculated as follows [195]:

Case. Exact value problems;

$$I = \begin{cases} \text{infinite,} & \text{if there is not any intersection} \\ \log_2 \frac{\text{TFN of System Range}}{\text{Common Area}}, & \text{otherwise} \end{cases} \quad (2.8)$$

2.2.3.4 Output phase

In this step, weighted total information contents (I^t) were calculated by Eq. 2.9. Then the designs that have the minimum total information content value was selected (Eq. 2.10).

$$\begin{Bmatrix} I_1^t \\ I_1^t \\ \vdots \\ I_m^t \end{Bmatrix} = \begin{Bmatrix} \sum_{i=1}^n w_1 I_{1i} \\ \sum_{i=1}^n w_2 I_{1i} \\ \vdots \\ \sum_{i=1}^n w_m I_{1i} \end{Bmatrix} \quad (2.9)$$

$$I^* = \min \begin{Bmatrix} I_1^t \\ I_1^t \\ \vdots \\ I_m^t \end{Bmatrix} \quad (2.10)$$

2.2.4. Application

In this section, electronic components to be used for smart clothing system were determined. For this purpose, type of sensor, type of actuator and type of power supply were selected. To make the methodology easily understandable, it was given phase by phase.

2.2.4.1 Initial phase

The expert team consisted of three experts. Due to their expertise, weights of the experts were taken as $w_{e1}=0.3$, $w_{e2}=0.4$, and $w_{e3}=0.3$, respectively. Linguistic scale given in Fig. 2.4 was selected for the evaluation of the alternatives under the defined criteria. The explanation of the linguistic terms was presented in the Table 2.2.

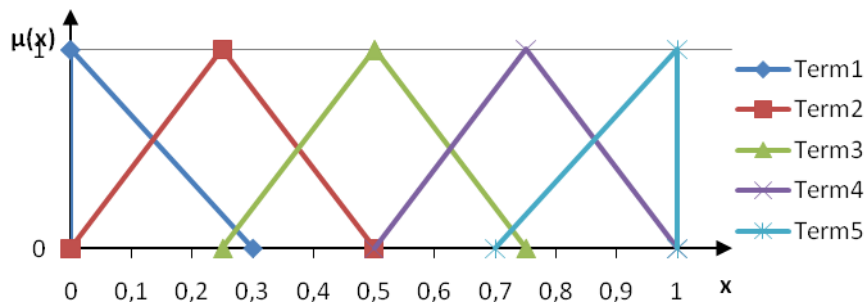


Fig. 2.4: Triangular fuzzy numbers for linguistic terms

2.2.4.2 Definition of criteria phase

Following criteria were determined for the evaluation phase of the electronic components; power consumption/generation, cost, size, weight, accuracy, working range and comfort level. In the evaluation phase, linguistic terms given in Table 2.2 were used.

Table 2.2: Linguistic terms

Criteria	Evaluation Scale	
	Linguistic Term	Label
Power consumption	Very low	VL
Cost	Low	L
Size	Medium	M
Accuracy	High	H
Working range	Very high	VH
Usability	Very light	VLi
Weight	Light	Li
	Medium	JR
	Heavy	Hv
	Very Heavy	VHv
Comfort level	Very uncomfortable	VU
	Uncomfortable	U
	Fair	F
	Comfortable	C
	Very comfortable	VC

To determine the importance of the defined criteria given in Table 2.2, pairwise comparison matrix was constructed by each expert. Table 2.3 represents the pairwise preferences of the experts and fuzzy numbers for experts' preferences. Experts' preferences were aggregated by using Eq. 2.5 and fuzzy numbers were defuzzified by using Eq. 2.6. The aggregated and defuzzified pairwise comparison matrix C is given below.

$$C = \begin{pmatrix} 1 & 2,55 & 0,24 & 0,29 & 0,15 & 1,7 & 0,2 & 0,13 \\ 0,39 & 1 & 0,29 & 0,26 & 0,13 & 0,31 & 0,15 & 0,15 \\ 4,17 & 3,45 & 1 & 3,15 & 0,14 & 0,76 & 0,46 & 0,56 \\ 3,45 & 3,85 & 0,32 & 1 & 0,16 & 1,18 & 0,33 & 0,53 \\ 6,67 & 7,69 & 7,14 & 6,25 & 1 & 5,3 & 0,56 & 5,9 \\ 0,59 & 3,23 & 1,32 & 0,85 & 0,19 & 1 & 4,1 & 4,3 \\ 5,00 & 6,67 & 2,17 & 3,03 & 1,79 & 0,24 & 1 & 0,87 \\ 7,69 & 6,67 & 1,79 & 1,89 & 0,17 & 0,23 & 1,15 & 1 \end{pmatrix}$$

The importance of the criteria is obtained by using Eq. 2.7 as follows 0.05, 0.02, 0.09, 0.07, 0.32, 0.15, 0.17, 0.12 for power consumption/ generation, cost, size, weight, accuracy, working range, usability, and comfort level, respectively.

2.2.4.3 Evaluation phase

Experts evaluated the alternatives by using linguistic-scale given in Table 2.2. Their preferences were given in Table 2.4.

Table 2.3: Fuzzy pairwise comparisons for importance of the criteria

	Power	Cost	Size	Weight	Accuracy	Working Range	Usability	Comfort Level
Power	E1	(1,3)	(1/5)	(0.2,0.2,0.2,0.2)	(1/5,1/3)	(0.2,0.2,0.33,0.33)	(1/9,1/7)	(0.11,0.11,0.14,0.14)
	E2	3	(1/5)	(0.2,0.2,0.2,0.2)	(1/3)	(0.33,0.33,0.33,0.33)	1/7,1/5)	(0.14,0.14,0.2,0.2)
	E3	(2,3)	(1/3)	(0.33,0.33,0.33,0.33)	(1/5,1/3)	(0.2,0.2,0.33,0.33)	(1/7)	(0.14,0.14,0.14,0.14)
	Aggregetion	1	(2.1,2.1,3,3)	(0.24,0.24,0.24,0.24)	(0.252,0.252,0.33,0.33)	(0.13,0.13,0.16,0.16)	(1.6,1.6,1.8,1.8)	(0.2,0.2,0.2,0.2)
Cost	E1		(1/5, 1/3)	(0.2,0.2,0.33,0.33)	(1/5, 1/3)	(0.2,0.2,0.33,0.33)	(1/7)	(0.14,0.14,0.14,0.14)
	E2		(1/3)	(0.33,0.33,0.33,0.33)	(1/5)	(0.2,0.2,0.2,0.2)	(1/7)	(0.14,0.14,0.14,0.14)
	E3		(1/5, 1/3)	(0.2,0.2,0.33,0.33)	(1/3)	(0.33,0.33,0.33,0.33)	(1/7)	(0.14,0.14,0.14,0.14)
	Aggregetion	1		(0.25, 0.25, 0.33,0.33)	(0.24,0.24,0.28,0.28)	(0.12,0.12,0.13,0.13)	(0.29,0.29,0.33,0.33)	(0.14,0.14,0.164,0.164)
Size	E1			3	(3,3,3,3)	(1/7)	(0.14,0.14,0.14,0.14)	(1/5)
	E2			3	(3,3,3,3)	(1/7)	(0.14,0.14,0.14,0.14)	(1/5, 1/3)
	E3			(3, 5)	(3,3,4,4)	(1/7)	(0.14,0.14,0.14,0.14)	(1/5)
	Aggregetion		1		(3,3,3,3,3)	(0.14,0.14,0.14,0.14)	(0.2,0.2,1.32,1.32)	(0.33,0.33,0.6,0.6)
Weight	E1					(1/5)	(0.2,0.2,0.2,0.2)	(1/5, 1/3)
	E2					(1/7)	(0.14,0.14,0.14,0.14)	(1/5, 1/3)
	E3					(1/9, 1/7)	(0.11,0.11,0.14,0.14)	(1/5)
	Aggregetion			1			(0.15,0.15,0.16,0.16)	(0.2,0.2,2.16,2.16)
Accuracy	E1						5.00	(5,5,5,5)
	E2						5.00	(5,5,5,5)
	E3						(5, 7)	(5,5,7,7)
	Aggregetion					1		(5,5,5,6,5,6)
Working Range	E1						(3,5)	(3,3,5,5)
	E2						5	(5,5,5,5)
	E3						3	(3,3,3,3)
	Aggregetion					1		(3,8,3,8,4,4,4,4)
Usability	E1							1
	E2							(1/3, 1)
	E3							1.00
	Aggregetion						1	(0.732,0.732,1,1)
Comfort Level	E1							
	E2							
	E3							
	Aggregetion							1

The experts' preferences were transformed into fuzzy numbers, and fuzzy numbers were aggregated by using Equation 2.5 (see Table 2.5).

To calculate the information content values of the alternatives, functional requirements were defined. For the design of smart clothing system, the functional requirements that must be satisfied and their fuzzy number are given as follows;

- *Power consumption of sensor and actuator alternatives must be at most low; (0, 0, 0.5)*
- *Power generation of power supply alternatives must be at least high; (0.5, 1, 1)*
- *Cost of alternatives must be at most medium; (0, 0, 0.75)*
- *Size of alternatives must be at most low; (0, 0, 0.5)*
- *Weight of alternatives must be at most light; (0, 0, 0.5)*
- *Accuracy of alternatives must be at least medium; (0.25, 1, 1)*
- *Working range of alternatives must be medium; (0.25, 0.5, 0.75)*
- *Usability of alternatives must be at least medium; (0.25, 1, 1)*
- *Comfort level of alternatives must be at least medium; (0.25, 1, 1)*

By using Equation 2.8, information content values were obtained as in Table 2.6. Then, weighted information contents were calculated by using Equation 2.9 (see Table 2.7).

2.2.4.4 Output phase

According to weighted information contents (see Table 2.7), ultrasound, vibration, and chemical cells were selected as sensor, actuator, and power supply, respectively for our smart clothing system design. However, when the importance of the criteria was not taken into account, ultrasound, vibration, and mechanical energy would be the best options as seen in Table 2.6. This showed that mechanical energy was affected by the importance of the criteria. Since, experts emphasized that chemical energy is better than mechanical energy in terms of accuracy criterion, chemical cells became important for our study.

As a result, a chemical cell, which provides continuous and determined energy was selected as a power supply for our smart clothing system. Since ultrasound sensor alternative has more advantages than the other ones in terms of power, cost, size, weight and working range criteria, ultrasonic sensor was selected for our smart clothing system. Additionally, since vibration alternative has more advantages than the other alternatives in terms of cost, size, weight, accuracy and usability criteria, vibration motor was selected as an actuator for our smart clothing system.

Table 2.4: Experts' preferences

Alternatives	Power			Cost			Size			Weight			Accuracy			Range			Usability			Comfort			
	E1	E2	E3	E1	E2	E3	E1	E2	E3	E1	E2	E3	E1	E2	E3	E1	E2	E3	E1	E2	E3	E1	E2	E3	
Sensors	Ultrasound	L	VL	L	VL	VL	L	M	VL	L	VLi	JR	VLi	M	M	M	M	M	M	M	M	M	F	U	U
	Laser	H	M	H	VH	VH	H	VH	M	M	JR	Hv	Hv	H	H	VH	VH	VH	VH	M	M	H	C	F	C
	Infrared	M	L	M	L	L	L	M	L	L	VLi	JR	Li	M	H	H	VL	VL	VL	VL	L	L	U	U	F
Actuator	Vibration	L	M	M	VL	VL	M	VL	VL	L	VLi	VLi	VLi	H	H	M				VH	H	M	U	U	F
	Audio	H	H	M	VL	VL	VL	L	VL	VL	VLi	Li	VLi	M	M	M				H	M	M	F	U	U
	Artificial muscle	VL	VL	VL	H	H	H	M	L	L	Li	VLi	VLi	L	M	L				M	L	L	C	C	F
Powersupply	Solar cells	L	L	L	L	L	M	M	L	L	Li	Li	Li	L	L	L	L	L	L	L	L	M	VC	C	VC
	Mechanical	M	M	M	L	L	L	M	M	M	Li	Li	Li	L	L	M	L	M	L	L	M	L	U	U	U
	Chemical	H	H	H	M	H	M	VH	M	M	Hv	Hv	Li	VH	H	VH	H	VH	H	H	VH	M	U	U	U
	Thermal energy	VL	VL	VL	L	M	H	VL	VL	VL	VLi	VLi	VLi	VL	VL	VL	VL	VL	VL	VL	L	VL	C	F	F

Table 2.5: Aggregated fuzzy numbers for experts' preferences

Alternatives	Power	Cost	Size	Weight	Accuracy	Working Range	Usability	Comfort Level	
	Sensors	Ultrasound	(0,0,15,0,42)	(0,0,075,0,36)	(0,075,0,225,0,495)	(0,1,0,2,0,48)	(0,25,0,5,0,75)	(0,5174,0,5,0,75)	(0,25,0,5,0,75)
Laser		(0,4,0,65,0,9)	(0,64,0,925,1)	(0,385,0,65,0,825)	(0,425,0,675,0,925)	(0,56,0,825,1)	(0,5211,1,1)	(0,325,0,575,0,825)	(0,4,0,65,0,9)
Infrared		(0,15,0,4,0,65)	(0,0,25,0,5)	(0,075,0,325,0,575)	(0,1,0,275,0,54)	(0,425,0,675,0,925)	(0,0,0,3)	(0,0,175,0,44)	(0,075,0,325,0,575)
Actuator	Vibration	(0,175,0,425,0,675)	(0,075,0,15,0,435)	(0,0,075,0,36)	(0,0,0,3)	(0,425,0,675,0,925)		(0,485,0,75,0,925)	(0,075,0,325,0,575)
	Audio	(0,425,0,675,0,925)	(0,0,0,3)	(0,0,075,0,36)	(0,0,1,0,38)	(0,25,0,5,0,75)		(0,325,0,575,0,825)	(0,075,0,325,0,575)
	Artificial muscle	(0,0,0,3)	(0,5,0,75,1)	(0,075,0,325,0,575)	(0,0,075,0,36)	(0,1,0,35,0,6)		(0,075,0,325,0,575)	(0,425,0,675,0,925)
Powersupply	Solar cells	(0,0,25,0,5)	(0,075,0,325,0,575)	(0,075,0,325,0,575)	(0,0,25,0,5)	(0,0,25,0,5)	(0,5396,0,25,0,5)	(0,075,0,325,0,575)	(0,62,0,9,1)
	Mechanical	(0,25,0,5,0,75)	(0,0,25,0,5)	(0,25,0,5,0,75)	(0,0,25,0,5)	(0,075,0,325,0,575)	(0,5433,0,35,0,6)	(0,1,0,35,0,6)	(0,0,25,0,5)
	Chemical	(0,5,0,75,1)	(0,35,0,6,0,85)	(0,385,0,65,0,825)	(0,35,0,6,0,85)	(0,62,0,9,1)	(0,52,0,85,1)	(0,505,0,775,0,925)	(0,0,25,0,5)
	Thermal energy	(0,0,0,3)	(0,25,0,5,0,75)	(0,0,0,3)	(0,0,0,3)	(0,0,0,3)	(0,0,0,3)	(0,0,1,0,38)	(0,325,0,575,0,825)

Table 2.6: Information content values

		Power	Cost	Size	Weight	Accuracy	Working Range	Usability	Comfort Level	Total
Sensors	Ultrasound	0,24	0,02	0,63	0,52	1,00	0,00	1,00	2,20	5,61
	Laser	5,23	4,95	4,79	6,26	0,10	2,73	0,63	0,41	25,09
	Infrared	1,61	0,19	1,09	0,90	0,33	6,04	3,62	2,20	15,99
Actuator	Vibration	1,87	0,09	0,07	0,00	0,33		0,21	2,20	4,78
	Audio	6,26	0,00	0,07	0,11	1,00		0,63	2,20	10,27
	Artificial muscle	0,00	3,00	1,09	0,07	2,03		2,20	0,33	8,72
Powersupply	Solar cells	Inf	0,35	1,09	0,58	3,00	0,38	2,20	0,04	Inf
	Mechanical	2,58	0,19	2,58	0,58	2,20	0,16	2,03	3,00	13,33
	Chemical	0,58	1,64	4,79	4,06	0,04	2,40	0,17	3,00	16,68
	Thermal energy	Inf	1,00	0,00	0,00	6,98	6,04	4,53	0,63	Inf

Table 2.7: Weighted information contents

		Power	Cost	Size	Weight	Accuracy	Working Range	Usability	Comfort Level	Total I
Sensors	Ultrasound	0,01	0,00	0,06	0,04	0,32	0,00	0,17	0,26	0,86
	Laser	0,26	0,10	0,43	0,44	0,03	0,41	0,11	0,05	1,83
	Infrared	0,08	0,00	0,10	0,06	0,11	0,91	0,62	0,26	2,14
Actuator	Vibration	0,09	0,00	0,01	0,00	0,11		0,04	0,26	0,51
	Audio	0,31	0,00	0,01	0,01	0,32		0,11	0,26	1,02
	Artificial muscle	0,00	0,06	0,10	0,01	0,65		0,37	0,04	1,23
Power supply	Solar cells	Inf	0,01	0,10	0,04	0,96	0,06	0,37	0,00	Inf
	Mechanical	0,13	0,00	0,23	0,04	0,70	0,02	0,34	0,36	1,84
	Chemical	0,03	0,03	0,43	0,28	0,01	0,36	0,03	0,36	1,54
	Thermal energy	Inf	0,02	0,00	0,00	2,23	0,91	0,77	0,08	Inf

2.2.5. Conclusion

An algorithm based on fuzzy AHP and fuzzy information axiom was presented to determine electronic components for the design of smart clothing system. In the scope of the study, sensor, actuator and power supply components of the smart clothing system were taken into consideration. First, criteria and the importance of the criteria were determined for the evaluation procedure. In order to obtain importance, fuzzy AHP proposed by Zeng et al. (2007) was used [202]. Then, alternatives of the components in industry and literature were determined and an expert team consisting of three engineers was set up. Then, the functional requirements for the smart clothing system design were defined. The linguistic evaluations of the experts for the alternatives under the defined criteria were processed with fuzzy information axiom methodology with respect to defined functional requirements. According to the results, the accuracy criterion was thought to be the most important among all criteria, while cost was the least. Finally, ultrasonic sensor, vibration motor, and chemical cell were selected as the best alternatives for the proposed smart clothing system design as a sensor, actuator and power supply, respectively.

2.3 Adaptation of sensor methodology to textile structure

2.3.1. Introduction

According to results mentioned in Section 2.2, firstly, types of ultrasonic sensors were investigated due to the aim of the study. Then, ultrasonic sensor was chosen according to criteria identified earlier. In order to integrate ultrasonic sensor to textile structure, types of conductive yarns were also investigated and realized. Therefore, in this section, the integration of sensor methodology to textile structure was briefly explained with respect to smart clothing system.

2.3.2. Materials

2.3.2.1 Characteristics of ultrasonic sensor

Towards our aim, in order to select ultrasonic sensor, following criteria should be considered:

- Criterion 1: Dimension of sensor should be as small as possible.
- Criterion 2: Ranging distance of sensor should be between the ranges of 0.2m-6m for identifying objects in front of the user.
- Criterion 3: Interface of sensor should satisfy analog voltage as output for easy programming, and pulse width output for obtaining digital measurement.

- Criterion 4: Voltage requirements of sensor should be around 5V because of microcontroller and actuator's working constraints.
- Criterion 5: Beam pattern of sensor should be as narrow as possible. To detect objects in front of the user along walking direction, beam angle should not be expanded so much to the environment in order not to misguide the user.

Considering Appendix-A1, Table 2.8 shows the comparison of ultrasonic sensor types. In the table, the sign (+) shows that related sensor meets criterion requirement, whereas sign (-) shows that it does not meet the criterion requirement. As a result, since Maxbotix Inc. Max Sonar-EZ type matches with our requirements, it was chosen in the scope of this study.

Table 2.8: Comparison of ultrasonic sensor types

Ultrasonic Sensors Type	Dimensions	Ranging Distance	Interface	Power Requirements	Beam Pattern
Maxbotix MaxSonar-EZ	+	+	+	+	+
Devantec SRF04	-	-	-	-	-
Devantec SRF05	-	-	-	+	-
Devantec SRF08	-	+	-	-	-
Devantec SRF10	-	+	-	-	-
Devantec SRF235	-	-	-	-	+
Devantec SRF02	+	+	-	+	-

LV-MaxSonar ®-EZ3™ (MaxBotix) has small dimensions and low power requirements, 2.5V to 5.5V supply with low (2mA) typical current draw [204]. Fig. 2.5 shows the ultrasonic sensor with its dimensions. These dimensions were taken into account during the insertion of conductive yarns to textile structure. The detection capability of this sensor ranges between 6 to 254 inches [see Appendix-A2].

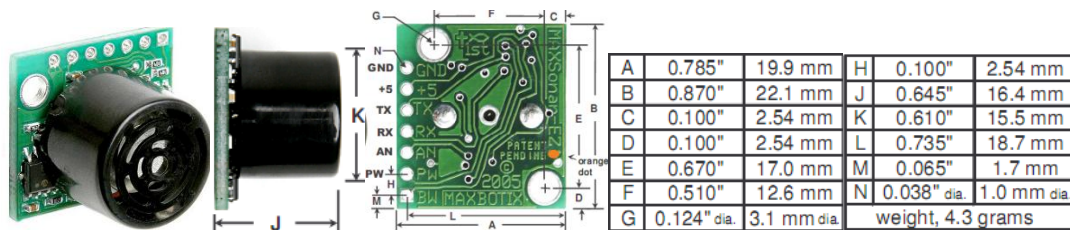


Fig. 2.5: Overview of ultrasonic sensor and its dimensions [204]

2.3.2.2 Characteristics of conductive yarns

Different conductive yarns were studied to integrate ultrasonic sensor to textile structure in order to compare system performance. Therefore, five different conductive yarns with different linear resistances were used to form electrical circuits in woven fabric samples.

The details of the conductive yarns used in our research are summarized in Table 2.9. Additionally, polyester yarn was used to form electrical insulation in the structure.

Table 2.9: Characteristics of yarns for integration of ultrasonic sensor

Sample no	Role of yarn in fabric	Material type	Yarn count	Linear resistance
	Non-conductive Yarn	Polyester Microfiber	330dtex	-
1	Conductive Yarn	100% Stainless Steel	260 2-ply tex	<15ohm/m
2	Conductive Yarn	Silver Plated Nylon 66-4 ply	312/34f 4-ply dtex	<50ohm/m
3	Conductive Yarn	Silver Plated Nylon 66-2 ply	140/17f 2-ply dtex	<230ohm/m
4	Conductive Yarn	Silver Plated Nylon 66	312/34f dtex	<240ohm/m
5	Conductive Yarn	Insulated Copper Yarn	144tex	<10ohm/m

Electrical resistivity (ρ) is a measure of how strongly a material shows resistance to the flow of electric current. The SI unit of electrical resistivity is the ohm metre [Ωm]. Electrical conductivity is the reciprocal quantity of electrical resistivity. Its SI unit is siemens per metre (Sm^{-1}).

In our study, to measure the conductivity of yarns, *TTi 1906* computing multimeter was used. Both the electrical resistivity and linear resistance of yarns were calculated in ohm meter (Ωm) and ohm per meter (Ω/m), respectively. For instance; Table 2.10 shows the conductivity calculations for yarn sample 2 (silver plated nylon 66-4 ply).

By using length and measured resistance values, Fig. 2.6 was obtained. According to Equation seen on the graph (see Fig. 2.6), resistance of the multimeter circuit was identified as 0.74Ω .

Table 2.10: Conductivity calculations for yarn sample 2

Measurement no	Length(cm)	Measured Resistance- R(Ω)	Resistance of Circuit- Rc (Ω)	R-Rc (Ω)	Resistivity Ωcm
1	1	1,3	0,74	0,56	0,000703
2	2	1,8	0,74	1,06	0,000666
3	3	2,2	0,74	1,46	0,000611
4	4	2,7	0,74	1,96	0,000615
5	5	3,1	0,74	2,36	0,000593
6	6	3,6	0,74	2,86	0,000599
7	7	4,2	0,74	3,46	0,000621
8	8	4,7	0,74	3,96	0,000622
9	9	5,1	0,74	4,36	0,000608
10	10	5,6	0,74	4,86	0,00061
11	11	6,2	0,74	5,46	0,000623
12	12	6,7	0,74	5,96	0,000624
13	13	7,2	0,74	6,46	0,000624
14	14	7,6	0,74	6,86	0,000615
15	15	8,1	0,74	7,36	0,000616
average					0,000623

Then, resistivity values were calculated by using following equation:

$$\rho = \frac{R - Rc}{l} A \tag{2.11}$$

where,

l is the length of the piece of material (measured in meters, m)

A is the cross-sectional area of the yarn (measured in square meters, m²).

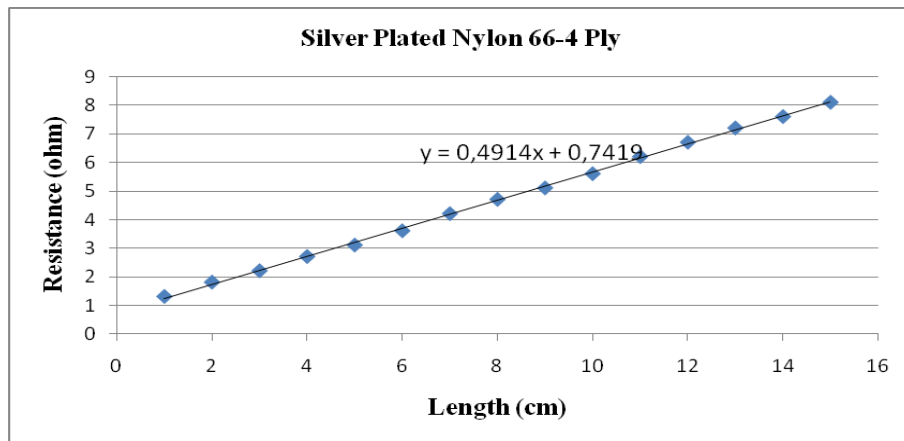


Fig. 2.6: Linear resistance graph of sample 2 (Silver Plated Nylon 66-4 ply)

2.3.3. Design of woven fabric structure

To prevent formation of short circuits, conductive yarns were hidden into structure. A fabric structure was considered as a double-woven fabric, and conductive yarns were placed in the middle layer of the structure. A double woven cloth containing weft stuffer yarns was woven with polyester yarns on an ARM loom (see Fig. 2.7b). The set of warp yarns of upper layer was linked to the set of weft yarns from bottom layer and thus, two layers were held together. A four-harness satin weave was chosen for both layers. Fig. 2.7a shows the diagram representing the drawdown, threading and lift-plan of the double-woven cloth. The design process was created by using Pointcarre Textile Software ® [205].

3D-graphical representation of the woven fabric structure (TexGen software ® [206]) is shown in Fig. 2.8.

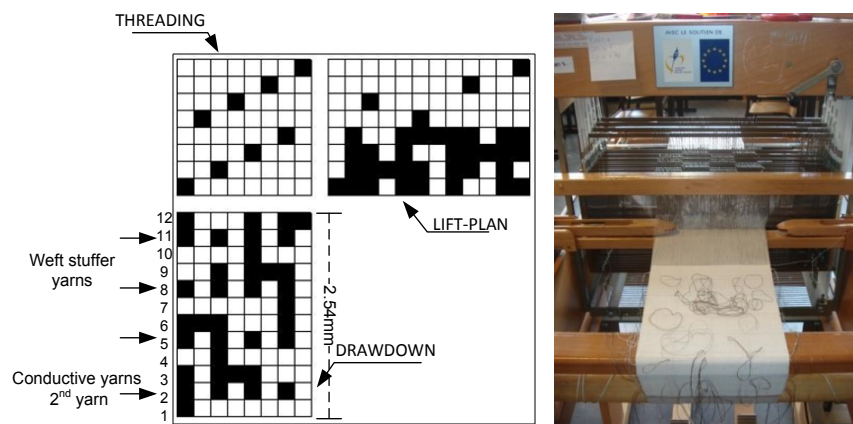


Fig. 2.7: a) The draft for double-woven cloth with weft stuffers and conductive yarn position b) fabric on the loom

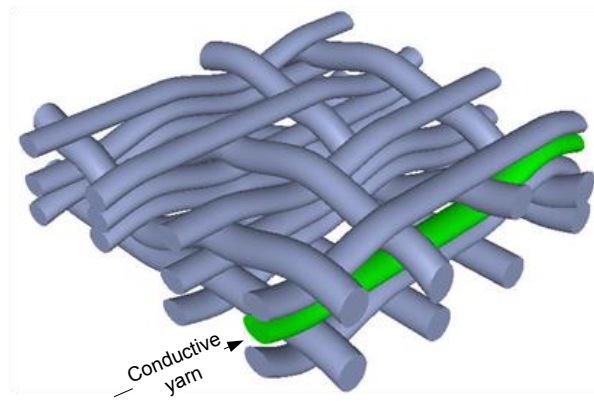


Fig. 2.8: 3D representation of the double-woven cloth (TexGen software®)

2.3.4. Integration of ultrasonic sensor

In our research, to measure the signal quality and beam pattern of sensor, single ultrasonic sensor integrated to textile structure was used. However, our other experiments showed that obstacle detection required multi-connection of sensors. Since the number of insertion of conductive yarns changes according to connection procedure, integration of single sensor and multi connected sensors was presented separately.

2.3.4.1 Integration of single ultrasonic sensor

For single sensor measurements, only analog voltage output was used. Therefore, to integrate single sensor to textile structure, three electrical connection points that are Ground, Voltage (Vcc) and Analog Voltage at specified distances (see Fig. 2.5), were taken into account.

During the weaving process, some of polyester weft stuffers were replaced with conductive yarns at the distances required by sonar sensor's technical data book [204]. The conductive yarns were positioned in the middle of the fabric and they had a straight trajectory without crimp. Thus, in each sample the same conductive yarn was used three times in weft direction at desired distances to satisfy three electrical connection points. Finally, for signal quality experiments, five different samples including five different conductive yarns with the same fabric design were produced (see Fig. 2.9).



Fig. 2.9: Samples

Final sample corresponding sensor's connection points is shown in Fig. 2.10. As seen in the figure, the conductive yarns are in grey color in the middle part of fabric and non-conductive polyester microfibers are in white color. Conductive yarns were placed in order to match Ground, Voltage (Vcc) and Analog Voltage Output pins. Furthermore, to construct electrical circuit and to connect sensor with fabric, loops were formed among conductive yarns, and snap fasteners were sewn onto these loops.

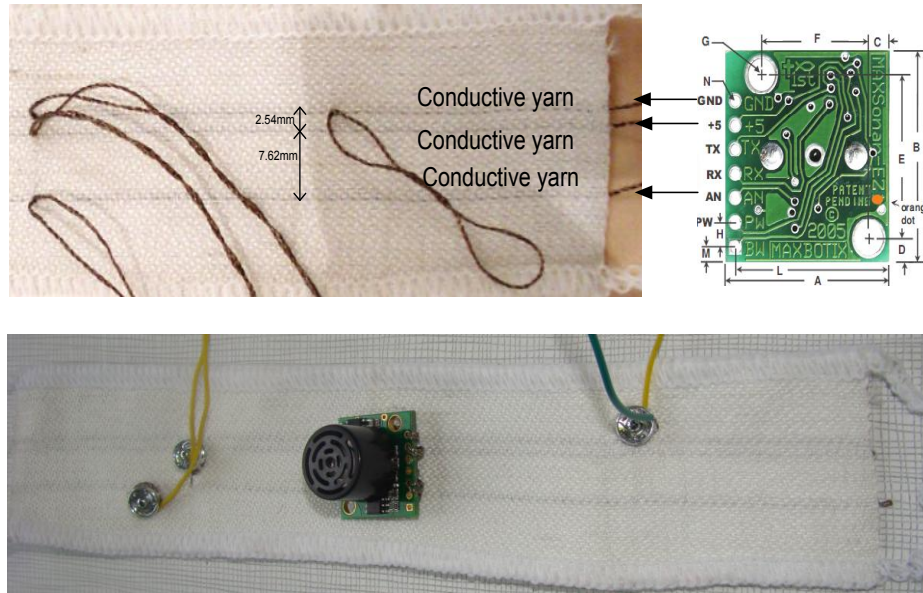


Fig. 2.10: a) Sample overview: conductive yarns corresponding to sensor ground, Vcc and analog voltage output points

2.3.4.2 Integration of multi-connected ultrasonic sensors

According to our objective, to detect obstacles it is necessary to work with several sensors. Therefore, we performed our obstacle detection experiments by using multi-connected sensors integrated to textile structure. Before giving the integration procedure of multi-connected sensors, it is necessary to define multi connection procedure of sensors at first.

In order to work with multi-sensors, sensors should be chained together as shown in Fig. 2.11. Therefore, to keep running and constantly loop sensors, mainly three things were done:

Firstly, a resistor $1K\Omega$ was added between the last sensor's TX back to the RX of the first sensor. Secondly, BW pin was pulled high. Thirdly, to "kick start" sensors; the RX pin on the first sensor was pulled high for at least $20\mu S$. This lets the microcontroller return its pin to a high impedance state so that the next time around the TX output from the last sensor made its way to the RX of the first sensor. Thus, all of the sensors in the chain run in sequence. This "ring of sensors" cycle around and around provided constantly maintaining the validity of their analog values.

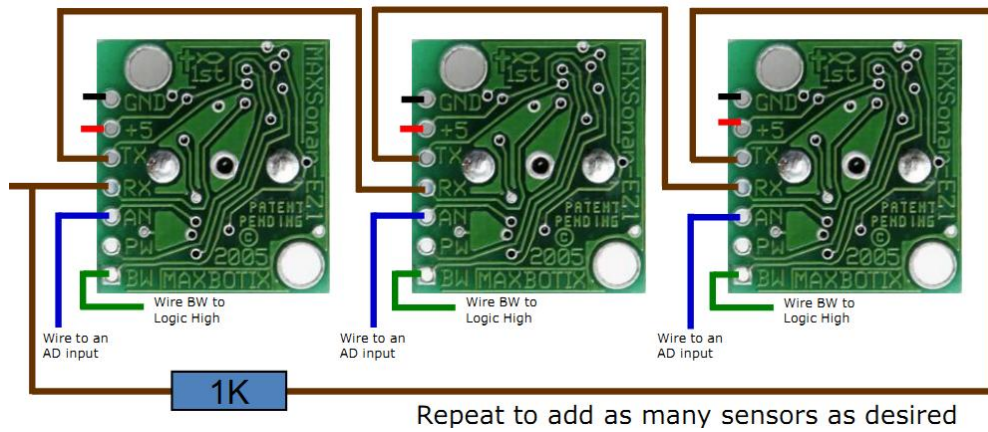


Fig. 2.11: Chaining of ultrasonic sensors [204]

Within this concept the most recent range reading was always ready to be read on the analog voltage pin, so once the chain in continuous mode, the values at any time are read. Fig. 2.12 shows the MATLAB file for sensors constantly looping. As summarized above, BW pin of sensors was pulled to high, which corresponds to Analog output of DAQ (Data Acquisition) Card with constant value of 5 voltage. RX pin also was pulled high with step function, which corresponds to Analog output1 of DAQ Card, for $20\mu\text{S}$ with initial value of 5 volts.

After brief explanation of multi-sensor connection procedure, integration procedure of multi-connected sensors is defined as follow:

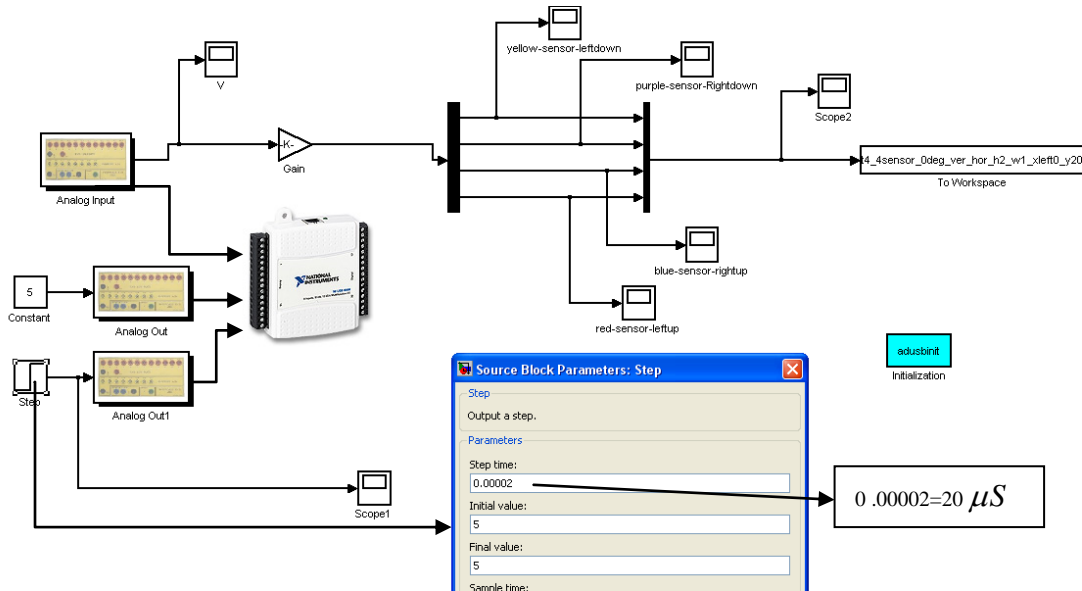


Fig. 2.12: MATLAB file for sensors constantly looping

As presented above, to integrate multi-connected sensors to textile structure, it was necessary to use Voltage, Ground, AN, TX, RX and BW pins of the sensor. Therefore, six electrical connection points (Voltage, Ground, AN, TX, RX and BW pins) at specified distances (see Fig. 2.5), were taken into account.

Similar to single sensor integration, during the weaving process, some of polyester weft stuffers were replaced with conductive yarns at the distances required by sonar sensor's technical data book [204].

Thus, in each sample the conductive yarn was used six times in weft direction at desired distances to satisfy six electrical connection points.

To construct electrical circuit and to connect sensor with fabric, loops were formed among conductive yarns, and snap fasteners were sewn onto these loops. Final sample corresponding sensor's connection points is shown in Fig. 2.13. As seen in the figure, the conductive yarns are in grey color in the middle part of fabric and non-conductive polyester microfibers are in white color.

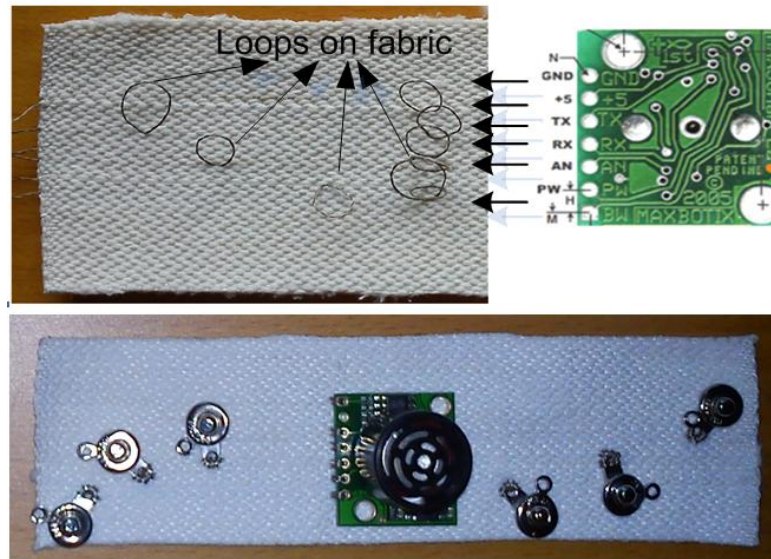


Fig. 2.13: Sample overview: conductive yarns corresponding to sensor ground, Vcc, TX, RX, analog voltage, and BW output points

2.3.5. Conclusion

In this section, ultrasonic sensor integration methodology to textile structure was studied. It was observed that single sensor and multi sensors integration procedure varied with sensors' connection technique.

2.4 Adaptation of actuator methodology to textile structures

2.4.1. Introduction

Towards the objective of the study, vibrotactile feedback was chosen in order to guide visually impaired people. Therefore, according to results in Section 2.2, vibration motors to be used as actuators were investigated. Considering clothing system requirements and ultrasonic sensor power requirements, type of vibration motor was selected.

In order to investigate vibrotactile perception, two different fabric structures with two different conductive yarns were produced. In this part, the integration of vibration motor to textile structure was briefly explained with respect to smart clothing system.

2.4.2. Materials

2.4.2.1 Characteristics of vibration motor

In this research, Arduino LilyPad Vibe Board® vibration motor was used as an actuator to ensure vibrotactile sensation due to its small dimensions, low power requirement and easy implementation. Fig. 2.14 shows the vibration motor with its properties.



20 mm outer diameter
Thin, 0.8 mm PCB
0.002 kg
Max Applied Voltage: 5.5 V

Fig. 2.14: Arduino LilyPad Vibe Board® [207]

2.4.2.2 Characteristics of conductive yarns

Two different conductive yarns were used to form electric circuits in the structure in order to integrate the vibration motors to textile structures.

Since silver plated nylon yarns show the best compromise between the signal quality and textile properties e.g. handle, stable and elastic, easy to weave, easy to integrate sensor etc.; they were chosen to form electric circuits. Table 2.11 shows the characteristics of yarns used for integration of vibration motor. Two conductive yarns with different linear resistances were taken into account to evaluate their performances on the resulting vibrotactile perception level.

Table 2.11: Characteristics of yarns for integration of vibration motor

Role of yarn in fabric	Material type	Yarn count	Linear resistance
Non-conductive Yarn	100% Acrylic	24x2 tex	-
Conductive Yarn	Silver Plated Nylon 66-4 ply	312/34f 4-ply dtex	<50 ohm/m
Conductive Yarn	Silver Plated Nylon 66	312/34f dtex	<240 ohm/m

2.4.3. Formation of e-textile structures

To prevent short circuits, the woven fabric sample was designed as a double-woven structure as mentioned in Section 2.3 (see Fig. 2.8), and a knitted fabric sample was designed using lay-in technique with the stitch density of 1×1 rib . The model of the knitted structure is seen in Fig. 2.15. Thus, conductive yarns were hidden in the middle layer of both woven and knitted fabrics.

Double-woven fabric and 1x1 rib fabric samples were produced by using handloom weaving machine and handloom flat knitting machine, respectively.

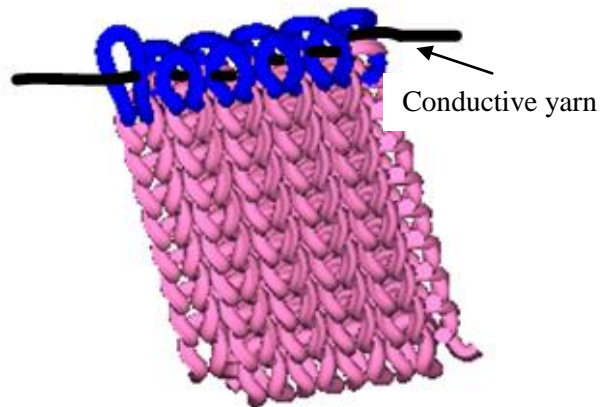


Fig. 2.15: 3D representation of the 1x1 rib fabric

2.4.4. Integration of vibration motor

During the production of samples, loops were formed among conductive yarns and then, snap fasteners were sewn onto these loops.

Thus, the connection of vibration motor to textile structure was provided by these loops. Eventually, signals were transmitted to vibration motor passing through conductive yarns via snap fasteners. Fig. 2.16 shows the samples that were produced and Table 2.12 shows the physical characteristics of samples. In order to optimize the fabric pressure effect on the skin, the weights of samples were adjusted approximately to the same value.

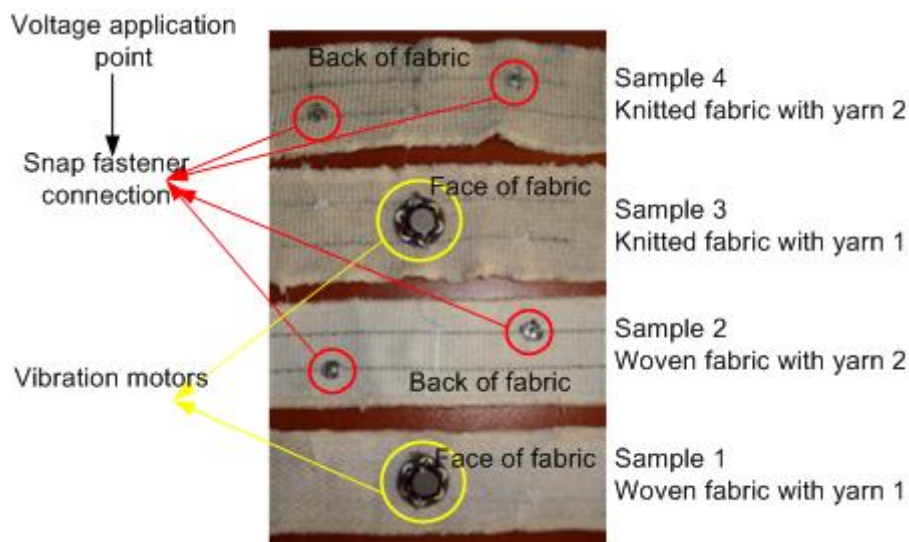


Fig. 2.16: Samples

Table 2.12: Physical characteristic of samples

	Sample 1	Sample 2	Sample 3	Sample 4
Weight	5.184 g	4.819 g	5.194 g	4.836 g
Length	19 cm	19 cm	14 cm	14 cm
Width	4 cm	4 cm	4 cm	4 cm
 d (distance between snap fastener-vibration motor)	4 cm	4 cm	4 cm	4 cm

2.4.5. Conclusion

Since vibration motion was chosen as a guidance alert in smart clothing concept, vibration motors were investigated and selected for the proposed system. To evaluate vibration effect in terms of vibrotactile perception, two different fabric structures with two different conductive yarns were produced. Then the vibration motors were integrated to fabric structures. In this part, a brief explanation about integration of vibration motors to textile structure was given.

Chapter 3

System analysis & results for e-textile architecture

3.1 Analysis on signal quality of ultrasonic sensor

3.1.1 Introduction

The main function of ultrasonic sensor is to detect obstacles and to measure the distance to obstacle through reflected sound waves. In sonar systems, electrical impulse is converted into sound waves, and the echoes of reflected sound waves are picked up by the sonar equipment. Thus, in ultrasonic sensor system, the distance to an object is identified by the measurement of the time from transmission of a pulse to reception, and performance of the system is analyzed according to detection capabilities and signal accuracy.

In this part, in order to find the influence of conductive yarn type for our smart clothing system, conductive yarns on the performance of ultrasonic sensor integrated to textile structure were investigated and discussed. The performance of ultrasonic sensors was tested in terms of signal quality by using five different conductive yarns used as transmission lines in three different configurations regarding disturbances.

3.1.2 Experimental

In this part, the produced samples described in Section 2.3. (see Fig. 2.9) were used.

3.1.2.1 Measurement set up

As seen in Fig. 3.1, in order to evaluate performance of integrated sensor, Textronix®TDS 210 scope was used. Textile circuit was connected to oscilloscope from V_{AN} snap fastener. V_{CC} snap fastener

(Feeding voltage) and GND snap fastener was connected to power supply. Since the working range of sensor is between 2.5 V-5.5 V, 5 V (Voltage) was fed to Vcc snap fastener.

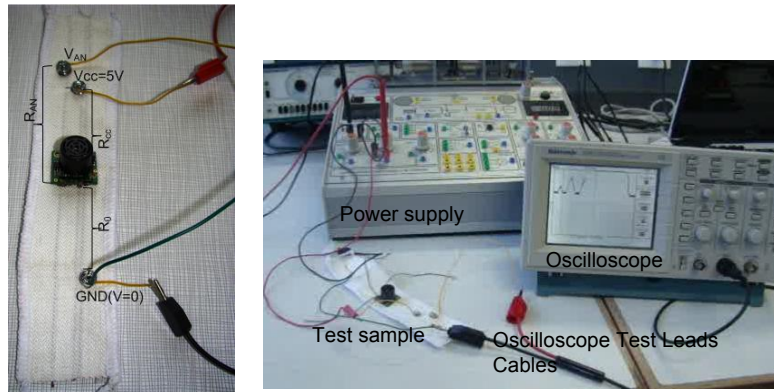


Fig. 3.1: Electrical circuit of integrated ultrasonic sensor and experimental set up

3.1.2.2 Measurement procedure

In order to observe disturbances effect, measurements were conducted in three different cases using an obstacle above the height of 20 cm as seen in Fig. 3.2. In the first case, ultrasonic sensor fabric sample was only tested using an obstacle. In the second and third cases, mobile phones were used in order to disturb measurements, and simulate real conditions of the sonars utilization. They were placed vertically and horizontally according to test sample at the same distance of 10 cm. During the 2nd and 3rd case, to observe if there is any differences between calling and non-calling situations, phones were subjected to ring. As a result, in order to present the performance of ultrasonic sensor and to show the effect of yarn type on the signal quality of the sensor, samples woven with five different conductive yarns were tested in three different cases, and situations as summarized in Table 3.1.

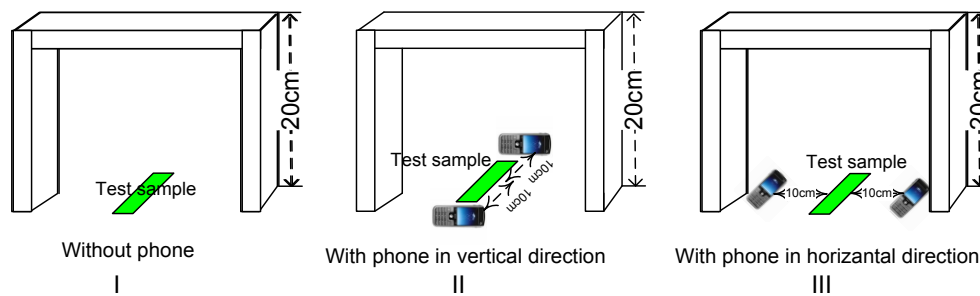


Fig. 3.2: Measurement configurations

Table 3.1: Cases for measurement procedure

Cases	Situation
I. Without Phone	-
II. With Phone in vertical direction	Calling No calling (standby)
III. With Phone in horizontal direction	Calling No calling (standby)

3.1.2.3 Noise level identification

The noise level (unwanted signal) and noise amplitude was determined by the signal processing in MATLAB. The signal to noise ratio (SNR) was estimated by calculating the ratio of signal power to noise power as described below:

$$SNR = \frac{P_{signal}}{P_{noise}} \quad (3.1)$$

Since signal and noise were measured in the same impedance, the SNR was obtained by calculating the square of the amplitude ratio, where A is root mean square (RMS) amplitude.

$$SNR = \left(\frac{A_{signal}}{A_{noise}} \right)^2 \quad (3.2)$$

Generally, SNRs expressed in logarithmic decibel scale. Therefore, in order to quantify signal quality of each sample, SNR_{dB} value of each sample was calculated by using following equations [208].

$$SNR_{dB} = 10 \log_{10} \left(\frac{P_{signal}}{P_{noise}} \right) = P_{signal,dB} - P_{noise,dB}, \quad (3.3)$$

$$SNR_{dB} = 10 \log_{10} \left(\frac{A_{signal}}{A_{noise}} \right)^2 = 20 \log_{10} \left(\frac{A_{signal}}{A_{noise}} \right) \quad (3.4)$$

3.1.3 Results

A random fluctuation in an electrical signal is called an electronic noise. The level of noise, which is the level of unwanted alteration of the signal waveform, gives an idea about the signal quality [209]. In our case study due to the material characteristics, conductive yarns woven so close to each other create an undesired effect on themselves when they are transmitting signals. Thus, they are acting as a noise sources between each other creating crosstalk [110]. For instance in Fig. 3.3, the noisy signal recorded by sample 3 woven with silver-plated nylon 66-2 ply yarn can be easily noticed.

Fig. 3.4 and Fig. 3.5 show the comparison of signals and SNRs during the sensor measurement without using mobile phones, respectively. From a first visual examination, it is possible to notice that there is significant difference between the morphology of signals. Samples woven with 100% stainless steel, silver plated nylon 66-4 ply yarn, and insulated copper yarn, which have linear resistance of <15 ohm/m, <50 ohm/m, <10 ohm/m respectively, showed better signal quality than samples woven with

silver plated nylon 66-2 ply yarn and silver plated nylon 66 yarn with a linear resistance of <230 ohm/m and <240 ohm/m, respectively (see Fig. 3.4).

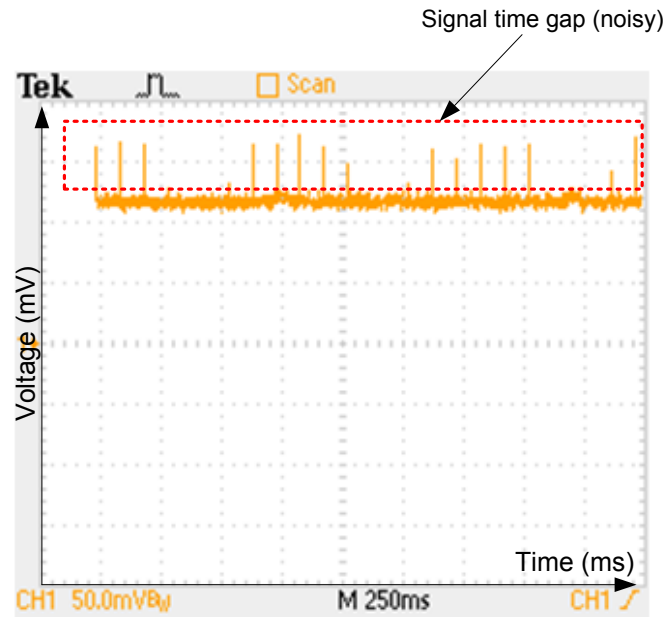


Fig. 3.3: Signal recorded by sample 3 woven with silver-plated nylon 66-2 ply yarn during the sensor measurement with case I (without phone)

Furthermore; as seen in Fig. 3.5, SNR values of samples woven with 100% stainless steel (29.11), silver plated nylon 66-4 ply yarn (29.37) and insulated copper yarn (29.38) were higher than samples woven with silver plated nylon 66-2 ply yarn (27.77) and silver plated nylon 66 yarn (27.92). SNR values of samples also explained that the signal qualities of sample 1, sample 2 and sample 5 were better than sample 3 and sample 4. These differences in signal quality permitted us to state that as the linear resistance of yarn increases noise level increases also.

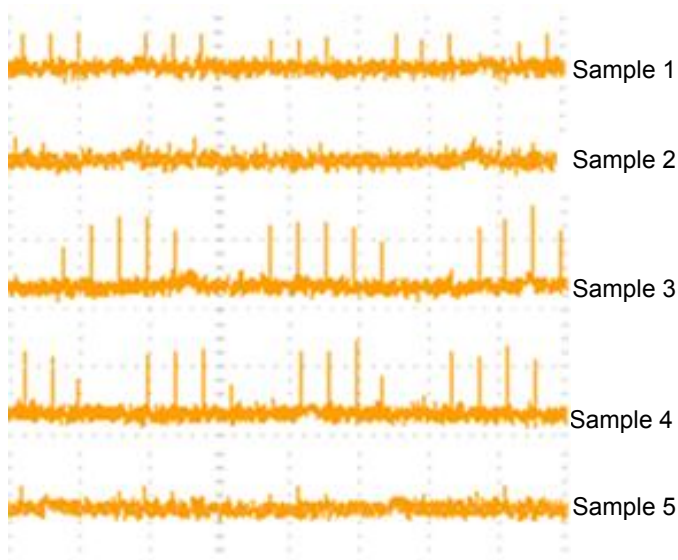


Fig. 3.4: Comparison of signals during the sensor measurement with case I (without phone)

Furthermore, it was clearly identifiable that there was no significant difference between the morphology of the signals obtained by samples woven with 100% stainless steel and silver plated nylon 66-4 ply yarn. In addition, it was noticed that sample woven with insulated copper yarn showed better signal quality than others.

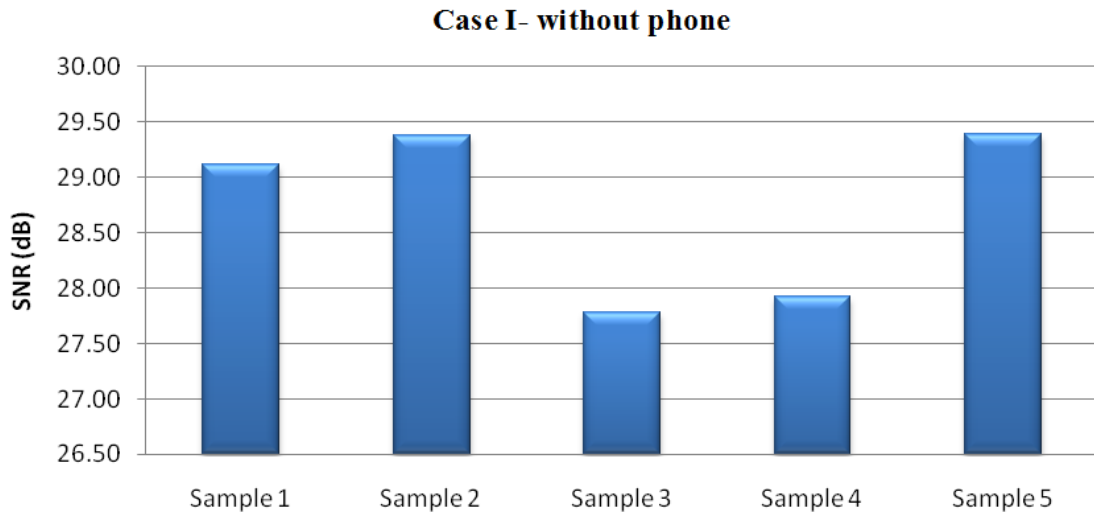


Fig. 3.5: Comparison of SNRs during the sensor measurement with case I (without phone)

In order to check if the calling situation influences performance of sensor due to the direction, phones were subjected to ring, and replaced in different positions according to sensor range. Figs. 3.6-3.8 show comparison of signals and SNRs during calling situation in vertical and horizontal position. As it can be seen from the figures, when phones were replaced in vertical position (see case II-Fig. 3.2), calling situation presented a significant effect on the signal performance whereas it has no significant effect when the phones were replaced in horizontal position. Different peaks can be clearly observed from the Fig. 3.6 during the calling situation in vertical position.

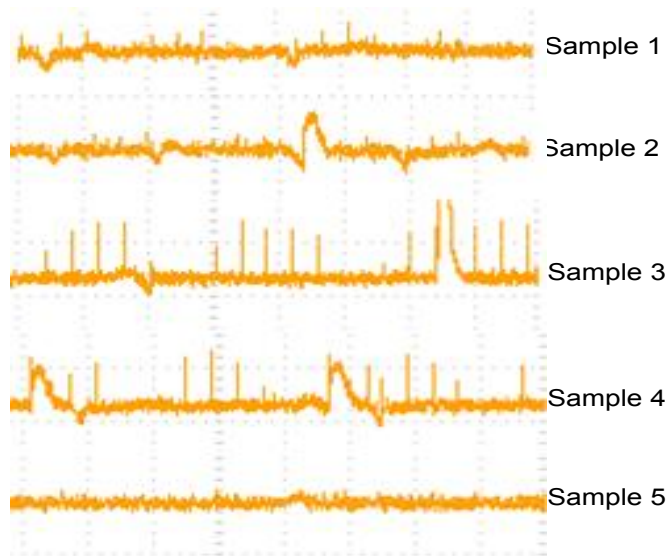


Fig. 3.6: Comparison of signals during the sensor measurement with case II (with phone vertical direction during calling)

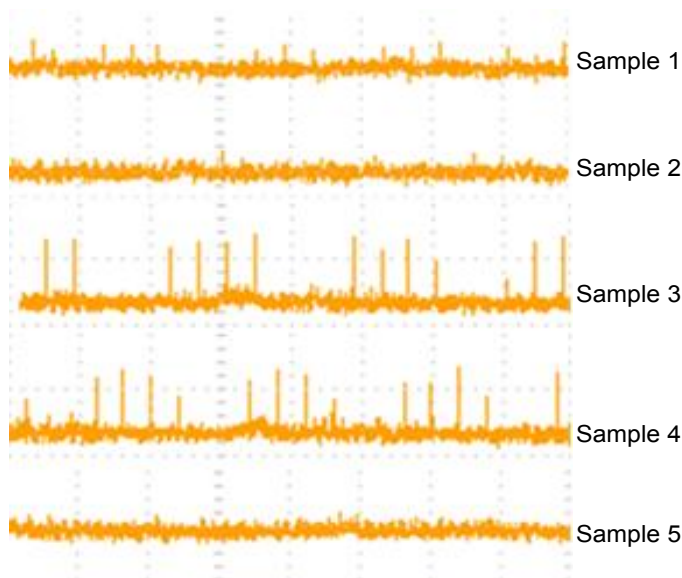


Fig. 3.7: Comparison of signals during the sensor measurement with case III (with phone horizontal direction during calling)

Moreover, with reference to Fig. 3.8, SNR value of each sample decreased during calling situation in vertical position. This phenomenon can be linked to the working range of sensor. Therefore, it should be outlined that if the sensor's beam is parallel to the position of calling situation, it may cause a decrease in signal quality. Despite this phenomenon, sample woven with insulated copper yarn also showed good signal quality once again.

Additionally, in order to distinguish if there is any difference between horizontal and vertical position during standby situation, samples were tested. Fig. 3.9 and Fig. 3.10 show the comparison of signals in horizontal and vertical direction, when the phones were subjected to standby situation, respectively. With reference to Fig. 3.9-3.10, from a first visual examination, it can be noticed that, standby situation of phones has no considerable effect on the signal quality of sensor due to the direction.

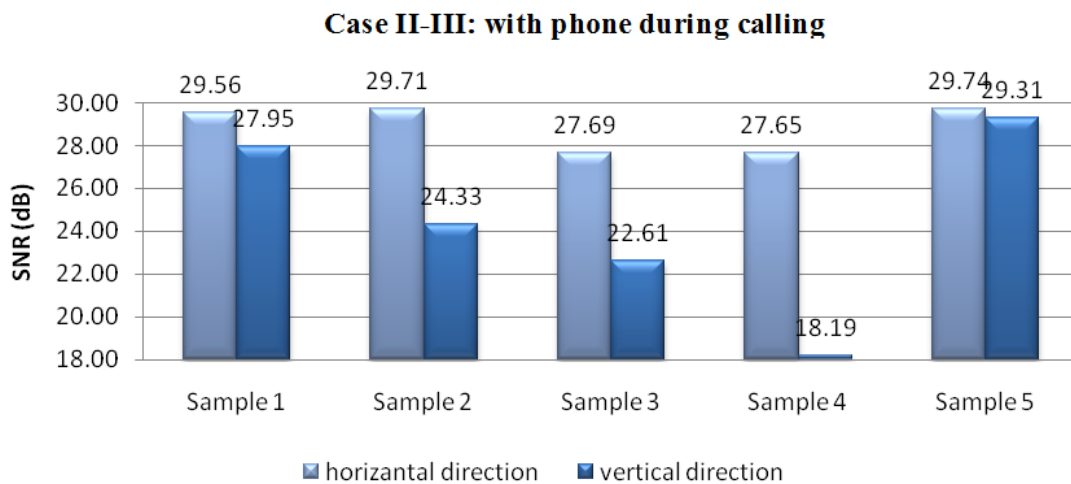


Fig. 3.8: Comparison of SNRs during the sensor measurement with case II and III (with phone horizontal and vertical direction during calling)

Even if the morphology of signals seems similar between vertical and horizontal direction, a slight decrease was seen in the SNR value of each sample when the phones were replaced in vertical direction rather than horizontal direction (see Fig. 3.11).

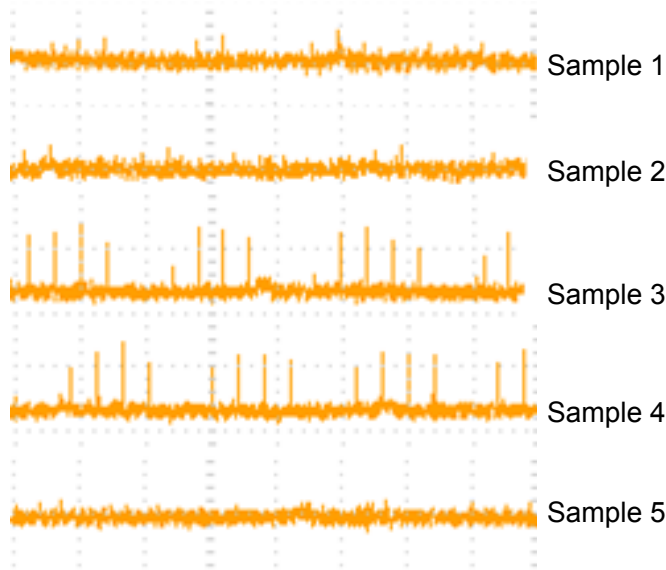


Fig. 3.9: Comparison of signals during the sensor measurement with case II (with phone in horizontal position during standby)

Hence, this proves that if the working range of sensor is parallel to the position of standby situation, it may also cause a slight decrease in signal quality.

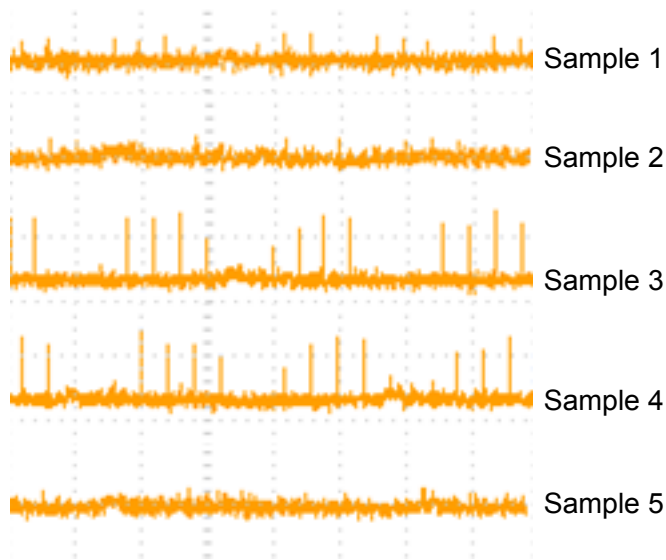


Fig. 3.10: Comparison of signals during the sensor measurement with case II (with phone in vertical position during standby)

Fig. 3.12 shows the change in SNRs according to situations. In this figure, codes were arranged according to details of cases. “wp” indicates with phone, “H” indicates horizontal position, “V” indicates vertical position and “woutp” indicates without phone . As seen in the figure, a change occurs apparently in vertical position during calling.

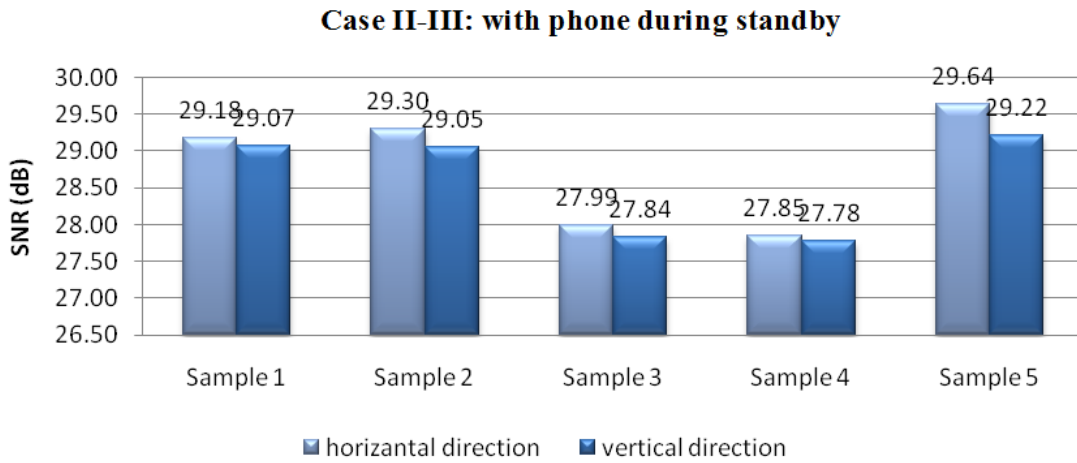


Fig. 3.11: Comparison of SNRs during the sensor measurement with case II and III (with phone in horizontal and vertical position during standby)

It is found that the change in SNR value of sample 4 (silver plated nylon 66 yarn with a linear resistance of <240 ohm/m) was extremely high; on the other hand change in SNR value of sample 5 (insulated copper yarn with a linear resistance of <10 ohm/m) was low in vertical position during calling. The changes in rank from higher to lower are sample 4, sample 3, sample 2, sample 1, and sample 5, respectively. These results can be attributed to the conductivity of yarns and working range of sensors as mentioned above.

From Fig. 3.12, it is possible to notice that when the linear resistance increases, change in SNRs increases also. Therefore, it can be concluded that the change in SNRs is proportional with linear resistance of yarns. This means when the conductivity of yarn increases, the noise level decreases, resulting in better signal quality.

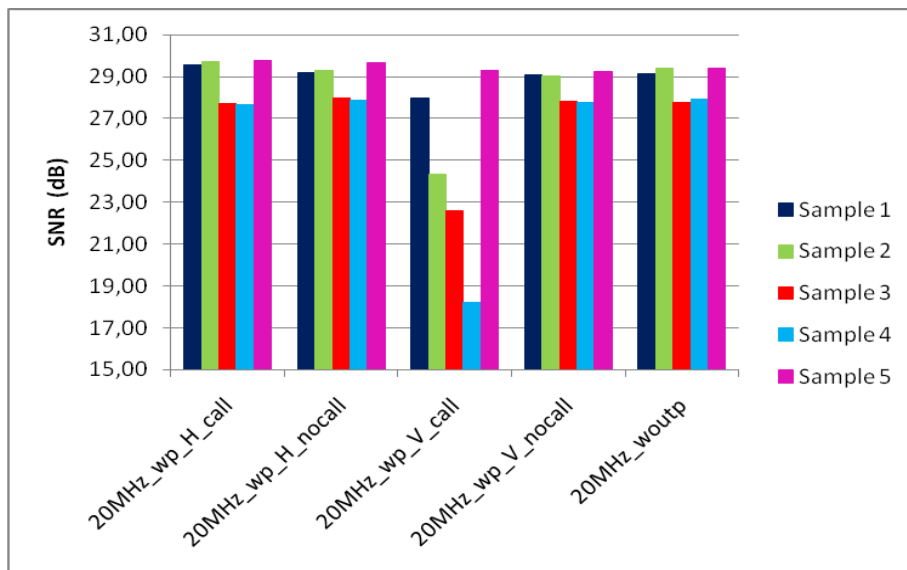


Fig. 3.12: Change in SNRs according to situations

3.1.4 Conclusion

In this part, the performance of ultrasonic sensor integrated to textile structure was analyzed and discussed by using five different conductive yarns in different cases. In order to measure signal quality of ultrasonic sensor, measurements were performed in three different configurations of disturbances: without using phones, with phones in vertical and horizontal directions, during the calling and standby situations.

The results reported that linear resistance of conductive yarns affects the signal quality of sensors. It was found that when the linear resistance increases, noise level increases and signal quality decreases. According to our results, insulated copper yarn showed the best signal quality. Nevertheless, our experiences showed that silver plated nylon 66-4ply yarn achieve the best compromise between signal quality and preserving textile properties e.g. handle, stable and elastic, easy to weave, easy to integrate sensor etc. Another result issued was that the direction of calling and standby situation has an important effect on the signal quality of sensor and it gives us an idea about their working range. Therefore, it should be noted that the working range (beam) of sensor is noise sensitive.

3.2 Analysis of the Beam Pattern of Ultrasonic Sensor

3.2.1 Introduction

In order to detect obstacles in front of the user, first the detection capability of our sensor should be known. Therefore, in this part the detection angle and capability of ultrasonic sensor were analyzed. By this way, the beam pattern of the ultrasonic sensor was presented related to identified object and compared with the actual one given in sensor's datasheet in order to test the efficiency of the proposed method of detection.

To do this, according to results of Section 3.1, single ultrasonic sensor integrated to textile structure with silver plated nylon 66-4 ply yarn having linear resistance of <50 ohm/m was tested for detection of obstacles. An electronic circuit was designed with PIC 16F877 microcontroller unit used to convert and record measured signal to meaningful data.

3.2.2 Experimental

3.2.2.1 Distance and object direction measurement by ultrasonic sensor

An ultrasonic sensor wave is a sound speed of about $c=344$ m/s in 20 C° at sea level. Distance measurement in ultrasonic sensor is based on the "time of flight" principle (TOF) [210]. That means,

the distance to an object is identified by the measurement of the time from transmission of a pulse to reception. In other words, the distance (L) to an object is calculated by Equation (4.5) (t : arrival time after reflection) [211].

$$L=c*t/2 \text{ (m)} \tag{3.5}$$

However, there is a difficulty in measuring the azimuth of an object by using a single ultrasonic sensor. Fig. 3.13 shows a drawing of the geometrical relationship in measuring azimuth of objects where they are vertically arranged at the same distances to a sensor. Let us define O_1, O_2, O_3 and O_4 as objects and $L_1, L_2, L_3,$ and L_4 as the distances measured respectively from the objects O_1, O_2, O_3 and O_4 . The azimuth of objects can be expressed by using triangle rule as following:

For object 2:
$$\theta_{12} = \cos^{-1}\left(\frac{L_1}{L_2}\right) \tag{3.6}$$

For object 3:
$$\theta_{13} = \cos^{-1}\left(\frac{L_1}{L_3}\right) \tag{3.7}$$

Since object 4 is outside of the sensor's detection range, the azimuth value of this object cannot be determined by sensor.

Due to known facts explained above, in our experiments, only the measured distances to an object was taken into account by considering triangular rule. The object either is detected by the sensor or not was noted, and if it is detected then the measured distance was taken.

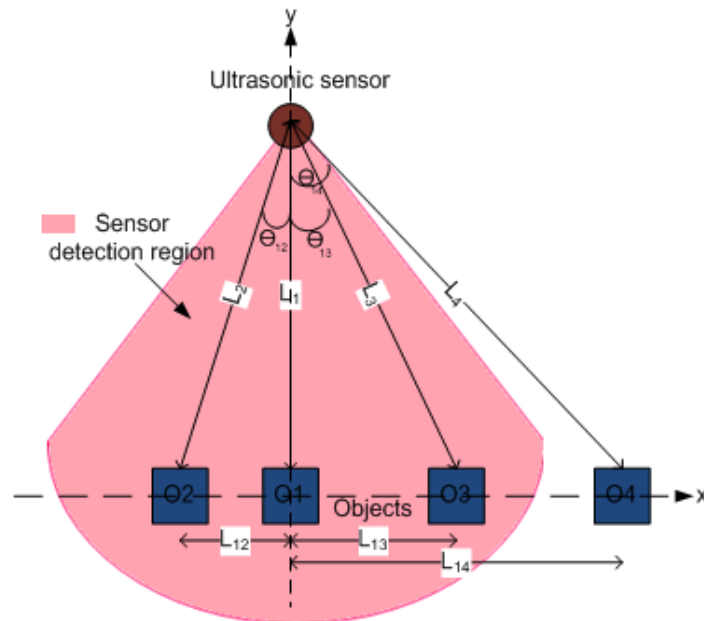


Fig. 3.13: Geometrical relationship in measuring azimuth of objects

3.2.2.2 Measurement set up

Measurements were performed using TekoPIC Programming Experimental Set Kit as shown in Fig. 3.14. Our system consisted of power supply, ultrasonic sensor integrated to textile structure, microcontroller and a LCD panel.

To control the system 16F877 peripheral interface microcontroller was used. Its code was written in the PIC C language by using MPLAB®IDE software and then, to compile HI-TECH C® Compiler was used. Since our ultrasonic sensor analog voltage output works with a scaling factor of $V_{cc}/512$ per inch that means a supply of 5V yields ~ 9.8 mV/inch ($5V/512 \approx 9.8$ mV) whereas 3V ($3V/512 \approx 5.8$ mV) yields 5.8 mV/inch, programming was done according to this information [204]. LCD screen was used to display the distance values to an object.

The block diagram of system is shown in Figure 3.14b. Once the sensor was triggered, ultrasound waves transmitted and if any object was presented within working range, ultrasound waves reflected back. In that system, a counter using 40 KHz clock frequency measured the time taken by sensor from transmission of a pulse to reception.

By using this control system, the detection capability of our sensor was measured within the working range of 50 cm to 2.5 meter.

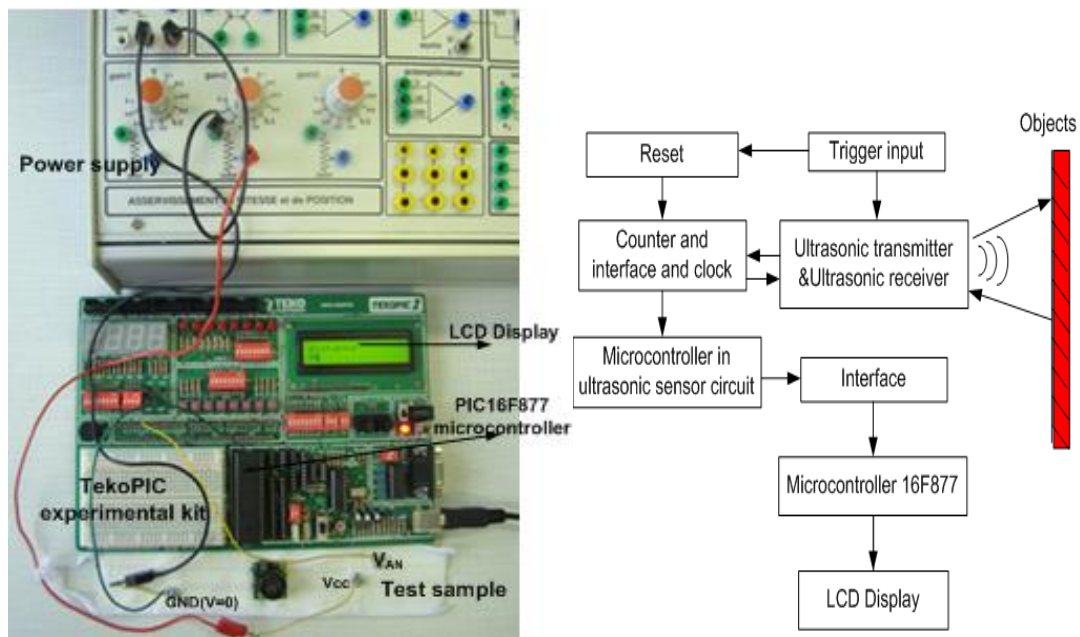


Fig. 3.14: (a) Experiment set-up (b) Block diagram of system

3.2.2.3 Measurement procedure

To determine the beam pattern of ultrasonic sensor, experiments were conducted as shown in Fig. 3.15 by using proposed measurement set-up above. First, consider the ultrasonic sensor is positioned at (0,0) and to detect the border of working range, object is positioned to a distance starting from (0, 50)

to (x, 250) in cm. Measurements were repeated in every 5 cm starting from 50 cm to 250 cm of y-axis. Then, the actual position of object at the border of working range was compared with the one measured by the sensor.

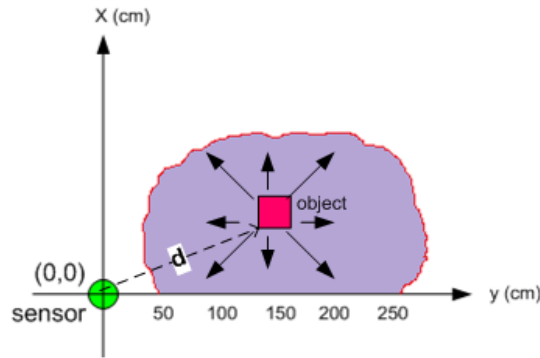


Fig. 3.15: Experimental procedure to determine border of sensor working range

3.2.3 Results

Table 3.2 shows the comparison of actual distance and measured distance to an object. According to this table results, beam pattern of ultrasonic sensor integrated to textile structure was determined as seen in Fig. 3.16. Furthermore, determined beam pattern of sensor was compared with the sensor's beam pattern in its datasheet (Fig. 3.16b). It is clear from the figure that the beam pattern that we determined in our study is similar to the sensor's beam pattern given in its datasheet [204].

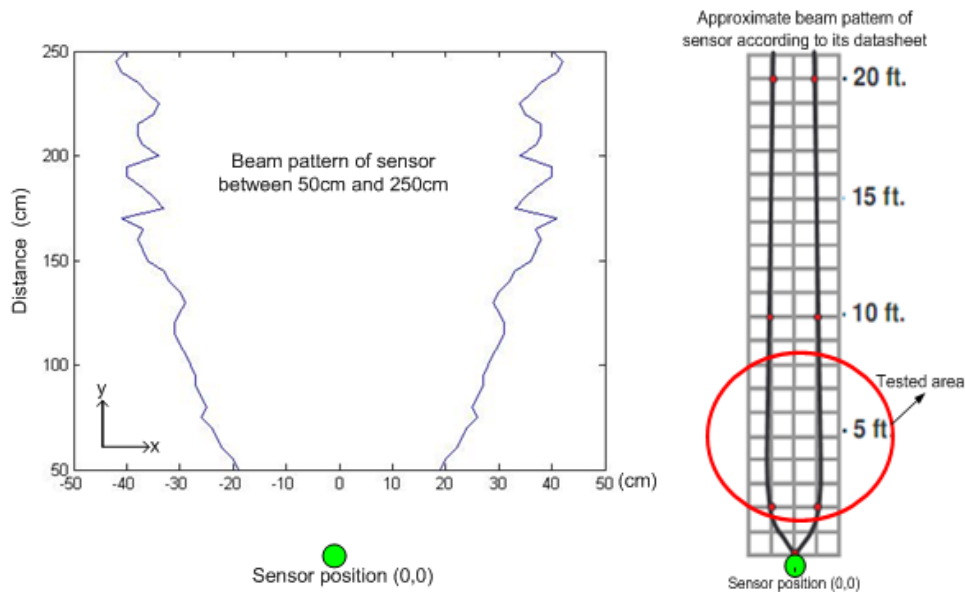


Fig. 3.16: a) Determined beam pattern of ultrasonic sensor integrated to the woven fabric b) Beam pattern of sensor according to its datasheet [204]

Furthermore, achieved results showed that the error between actual distance and measured distance increases as the distance to an object increases. If the object is in the range of 50 and 100cm, the error

will be 0-5 % and if the object is in the range of 200 to 250cm, then the error will increase with 13-15 % (see Fig. 3.17).

Table 3.2: Results of experiments at the border of working range of sensor in one direction

Measurement no	Position of object (x,y)	Actual distance (d) (cm)	Measured distance (d) (cm)	Error	Error %
1	(19,50)	53,5	54	0,5	0,96
2	(20,55)	58,5	58	0,5	0,89
3	(22,60)	63,9	62	1,9	2,98
4	(23,65)	68,9	66	2,9	4,28
5	(24,70)	74,0	72	2,0	2,70
6	(26,75)	79,4	76	3,4	4,26
7	(25,80)	83,8	82	1,8	2,17
8	(26,85)	88,9	85	3,9	4,37
9	(27,90)	94,0	90	4,0	4,22
10	(27,95)	98,8	94	4,8	4,82
11	(28,100)	103,8	97	6,8	6,59
12	(29,105)	108,9	102	6,9	6,36
13	(30,110)	114,0	106	8,0	7,03
14	(31,115)	119,1	110	9,1	7,64
15	(31,120)	123,9	115	8,9	7,21
16	(30,125)	128,5	117	11,5	8,98
17	(29,130)	133,2	120	13,2	9,91
18	(30,135)	138,3	125	13,3	9,61
19	(32,140)	143,6	128	15,6	10,87
20	(33,145)	148,7	133	15,7	10,56
21	(36,150)	154,3	137	17,3	11,19
22	(37,155)	159,4	141	18,4	11,52
23	(38,160)	164,5	146	18,5	11,22
24	(37,165)	169,1	149	20,1	11,89
25	(41,170)	174,9	154	20,9	11,94
26	(33,175)	178,1	158	20,1	11,28
27	(35,180)	183,4	160	23,4	12,75
28	(37,185)	188,7	164	24,7	13,07
29	(40,190)	194,2	168	26,2	13,48
30	(40,195)	199,1	172	27,1	13,59
31	(34,200)	202,9	175	27,9	13,74
32	(37,205)	208,3	180	28,3	13,59
33	(38,210)	213,4	185	28,4	13,31
34	(38,215)	218,3	188	30,3	13,89
35	(35,220)	222,8	190	32,8	14,71
36	(34,225)	227,6	195	32,6	14,31
37	(36,230)	232,8	200	32,8	14,09
38	(38,235)	238,1	205	33,1	13,88
39	(41,240)	243,5	210	33,5	13,75
40	(42,245)	248,6	214	34,6	13,91
41	(40,250)	253,2	217	36,2	14,29

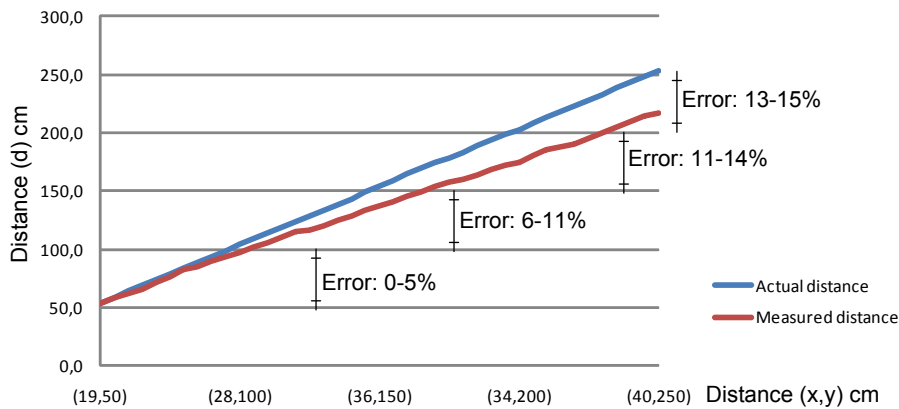


Fig. 3.17: Error differentiation between actual and measured distance

3.2.4 Conclusion

In this part, detection capability of sensor was analyzed. To observe the detection capability of sensor in an environment, objects were placed in front of the sensor in various positions. Measurements were performed by using single ultrasonic sensor that was integrated to fabric. Fabric was connected to a control system that includes power supply, microcontroller and LCD panel. By using this system, the beam pattern of sensor was determined.

The achieved results showed that the determined beam pattern matches with the actual one given in its datasheet. Therefore, it can be concluded that the integration of sensor was successful. Nevertheless, according to our results it should be noted that as the distance to an object increases measurement error increases. Thus to get right results through completely smart clothing system, some coefficients could be added into final programming language considering the errors due to the distance ranges.

3.3 Analysis of Obstacle Detection with Multi-Connected Ultrasonic Sensors

3.3.1 Introduction

In order to find required number of sensors for obstacle avoidance algorithm of smart clothing system, various scenarios were developed by using various numbers of sensors. At first in developed scenarios, sensors were connected by using electrical wires, and then the suitable scenarios were chosen to be tested within textile structure. Moreover, considering the detection capability of single sensor which was found before as approximately changes between -30 cm to 30 cm of x-axis, four sensors were decided finally to be used in two different manner: Two groups of sensors were considered to be placed at left and right position in order to distinguish left and right obstacles. On the other hand, the other two were considered to be placed up and down position in order to differentiate height of obstacles. Considering this arrangement four sensor connected with each other depending on the construction as explained in Section 2.3.4.2 were used to perform experiments within textile structure in order to analyze obstacle's position. Thus, detection capability of four scenarios within textile structure were analyzed and discussed in detail.

3.3.2 Experimental

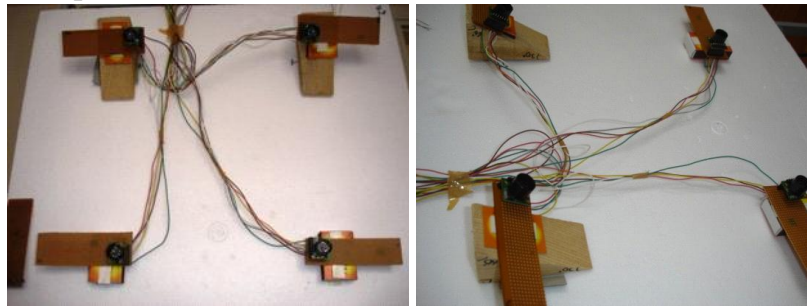
3.3.2.1 Developed scenarios by using wires

After connecting sensors as explained in Section 2.3.4.2, the analog values taken via sensors were checked and found to be successful. Then, scenarios about sensor replacement were designed by

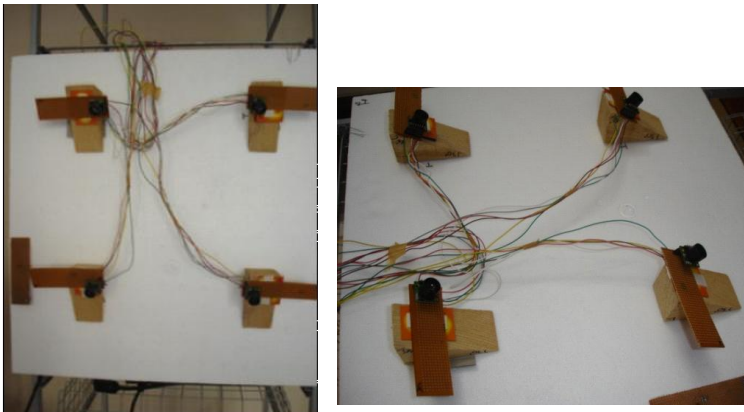
changing the degree of sensor's position to 0° , 30° , 45° as well as arranging the distribution of sensors in a square form or line form. Furthermore, during scenarios the number of sensors was also changed. Two, three and four sensors combinations were tried. Fig. 3.18 shows some developed scenarios related to sensors' positions.



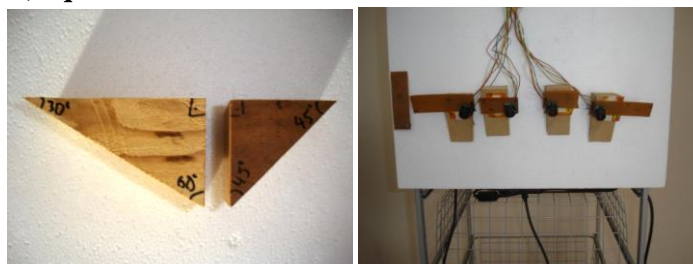
a) square form all sensors at 0°



b) square form: 2 sensor up at 30° and 2 sensor down at 0°



c) square form: 4 sensors at 30°



d) line form: 4 sensor at 30°

Fig. 3.18: Various scenarios related to sensor positions

Due to developed scenarios, it was observed that analysis of detection of obstacles is easier with four-sensor combination in a square form than the other scenarios.

Therefore, experiments continued with textile structure by using four sensor combinations.

3.3.2.2 Developed scenarios in textile structure using conductive yarns

In this case, only combinations of 0° , 30° , and 45° in a square form were found to be precious to continue experiments within textile structure. At this step, instead of wires conductive yarns were used for integrating sensors. The samples mentioned at Section 2.3.4.2 were used. Fig. 3.19 shows four different scenarios, which were developed by using four sensors integrated to textile structure with conductive yarns (white fabrics) and mounting them onto textile surface (green fabric).

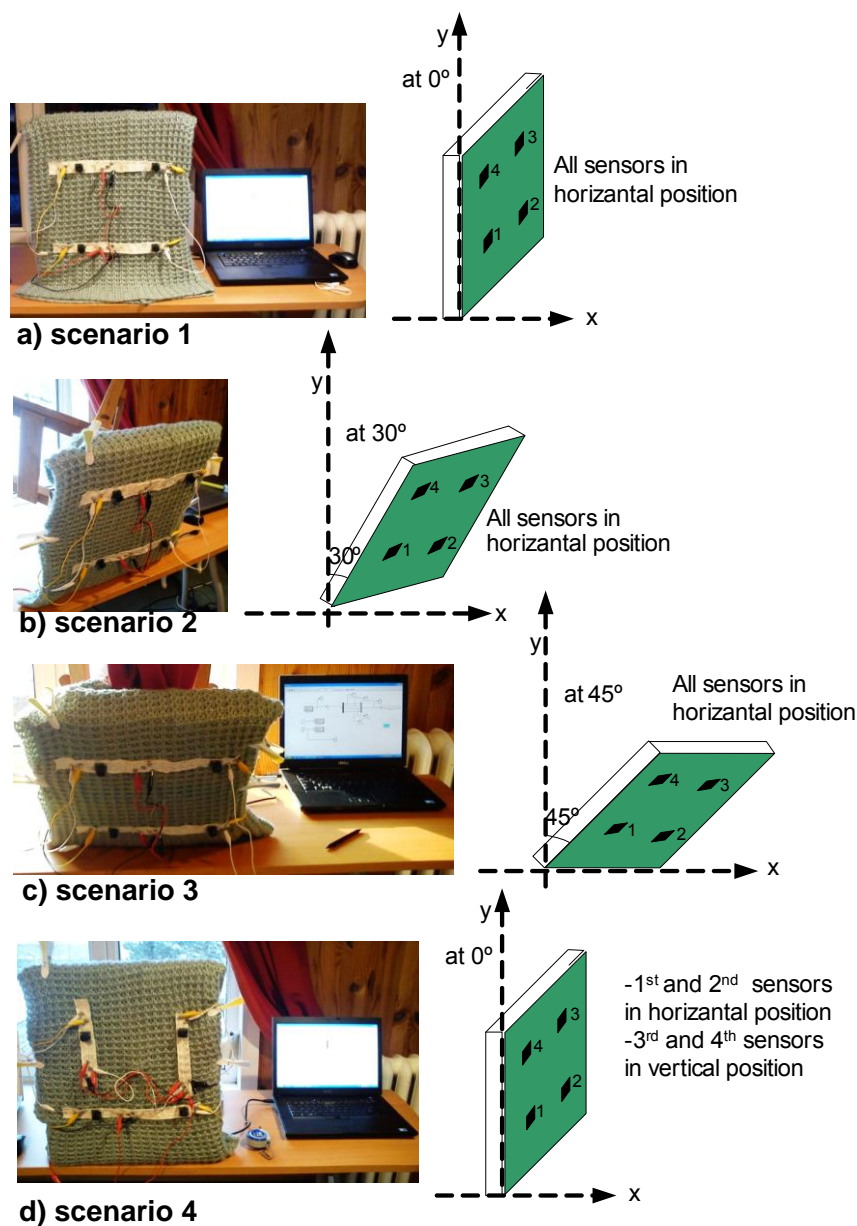


Fig. 3.19: Scenarios developed by mounting sensors onto textile surface

3.3.2.3 Measurement set up

By considering human body physiology, the distance between each sensor was arranged as 20 cm in both horizontal and vertical position as shown in Fig. 3.20. The heights of down sensors and up sensors were adjusted to 90cm and 110cm, respectively. The height and width of obstacle that was used in the experiments were 100cm and 30cm, respectively.

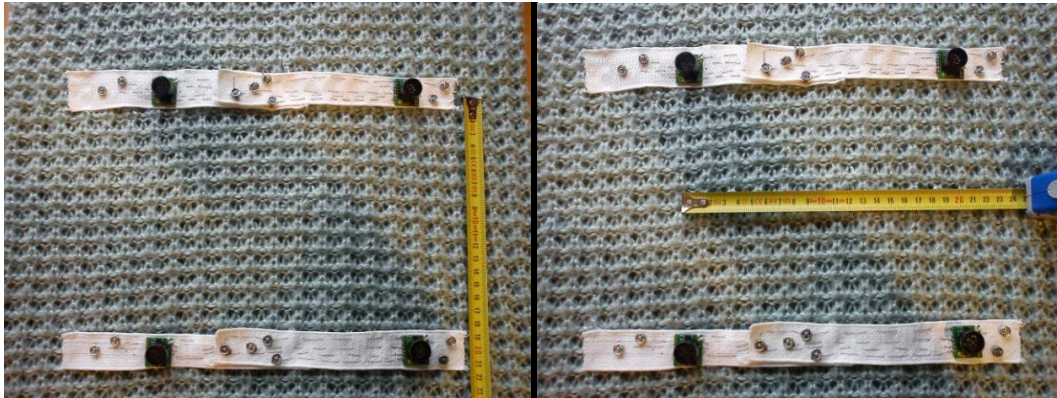


Fig. 3.20: Distances between sensors

To analyze the detection capability of ultrasonic sensors, experiments were conducted as seen in Fig. 3.21. Measurements were recorded in MATLAB by using National Instruments® DAQ (Data Acquisition) Card.

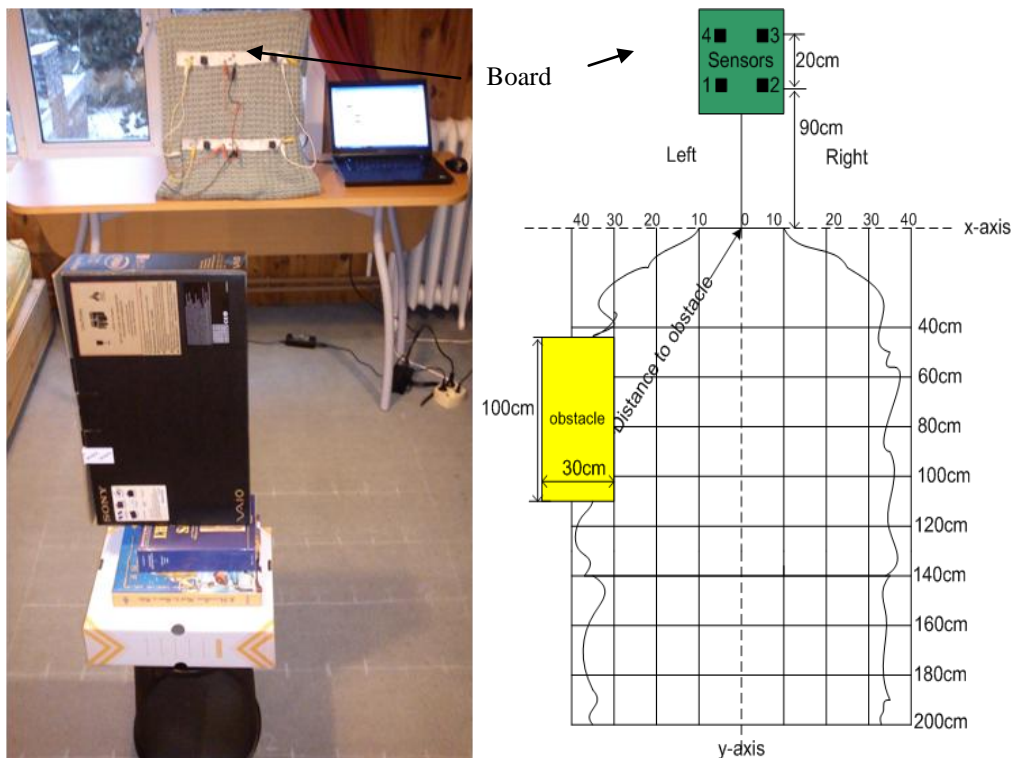


Fig. 3.21: Overview of experiment set-up for obstacle detection

First, the board (green fabric) on which ultrasonic sensors were attached, was positioned at (0, 0) to detect the obstacle in the working range. Then obstacle was positioned to a distance starting from (0,

0) to $(\pm 40, 200)$ in cm by taking into account its detection range (see Fig. 3.16). Then, measurements were repeated every 20cm starting from 40cm to 200cm of y-axis. Then, the actual position of obstacle was compared with the one measured by the sensors. During the experiments, sensor 1 and 4 locates at left side; sensor 2 and 3 locates at right side. Furthermore, both sensor 1 and 2 were placed at down position, on the other hand both sensor 3 and 4 were placed at the up position. For each position of obstacle 100 data was taken and then recorded and analyzed for each sensor, separately.

3.3.3 Results

3.3.3.1 Comparison of scenarios according to position of obstacle

To compare the results of scenarios according to position of obstacle, firstly three examples are given to explain the situations. For instance, consider the obstacle is located at $(0, 60)$, $(0+, 60)$, and $(-0, 60)$. “ $(0, 60)$ ” denotes the center of obstacle at 0 of x-axis, and 60cm of y-axis. “ $(0+, 60)$ ” denotes the border of obstacle locates at 0 from the right side of x-axis, and at 60cm of y-axis. On the contrary, “ $(-0, 60)$ ” denotes the border of object locates at 0 from the left side of x-axis, and at 60cm of y-axis.

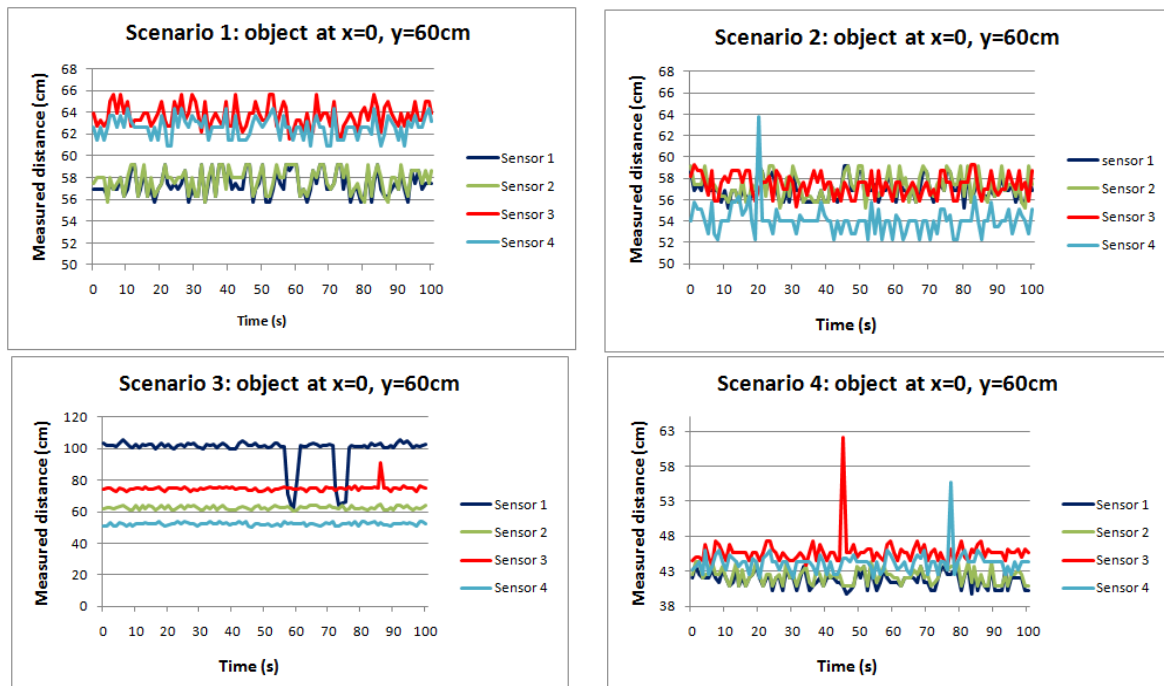


Fig. 3.22: Comparison of scenarios when object locates at $x=0, y=60\text{cm}$

Fig. 3.22 explains that the real position of obstacle is $x=0$ and $y=60$ cm. The expected result or the measured distance by sensors should be around 60 cm. Since the obstacle located at just in front of the all sensors, it was expected that all sensors normally should detect obstacle. When we analyzed the results obstacle was detected correctly at around 60 cm with all sensors of both scenario 1 and 2. However, with scenario 4 obstacle was also detected unfortunately the measured distance value by

sensors was wrong around 45 cm. Moreover, the worst results were recorded by Scenario 3. Scenario 3 appeared hardly incapable of detecting obstacle position.

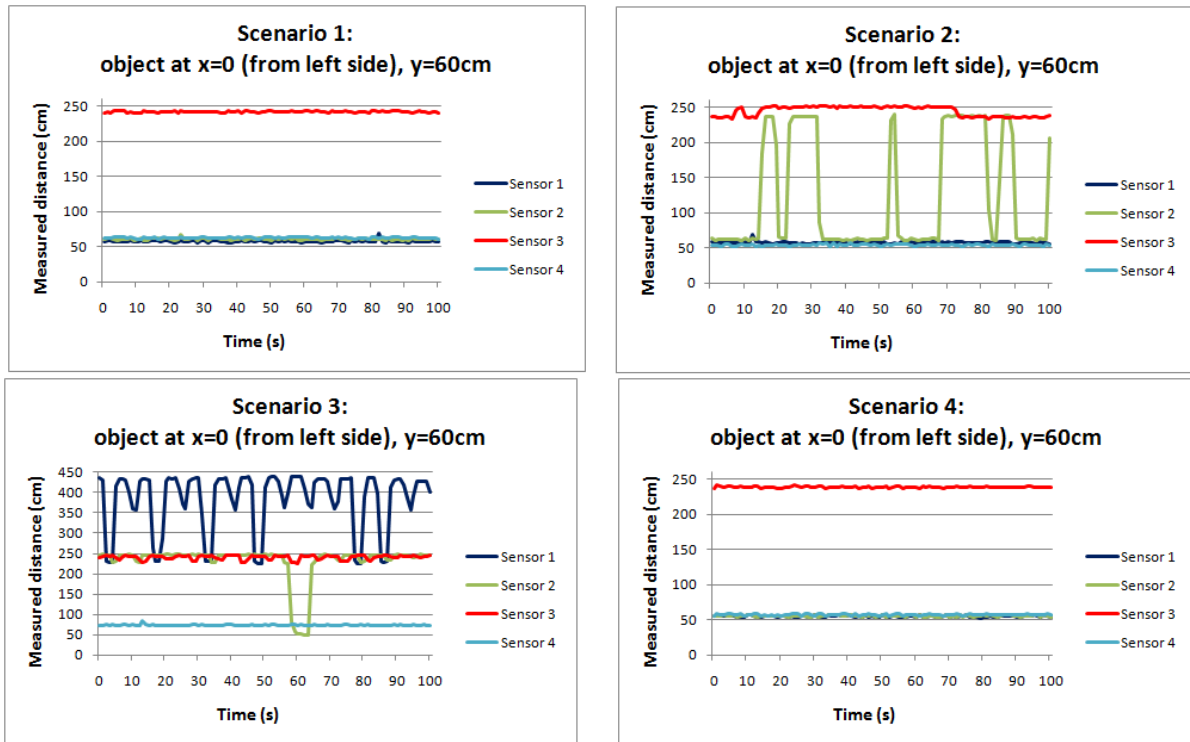


Fig. 3.23: Comparison of scenarios when object locates at $x=0$ (from left side), $y=60\text{cm}$

In the case that obstacle was located at $x=0$ (from left side), $y=60\text{cm}$; the expected result should be that sensors which are positioned at left side should read the object's position definitely. On the other hand, considering hypotenuse rule and distance from sensors to obstacle, sensors at right side may detect the obstacle's position. According to Fig. 3.23, both Scenario 1 and Scenario 4 detected the obstacle well. As it was expected, apart from sensor 3 (up right sensor); sensor 1 (down left sensor), sensor 2 (down right sensor), and sensor 4 (up left sensor) detected the obstacle position correctly. Nevertheless, with Scenario 2 only sensors, which were positioned at left side detected the obstacle. Similar to above, the worst results were recorded by Scenario 3 once again.

When the obstacle position was slid to $x=0$ (from right side), $y=60\text{cm}$; that time the expected result should be reverse to information described above. As seen in Fig. 3.24 in all scenarios sensors at the right (sensor 2 and sensor 3) detected obstacle position correctly, besides with both scenario 1 and 4, obstacle position was detected by also sensor 1 (left down) correctly. However, it was clear to state with scenario 4 that the reading of sensor 4 is not stable.

As a summary, as described above by only analyzing each position of obstacle in a working range separately is not sufficient and easy way to assess which scenario is the best. Therefore, in order to compare the scenarios, all data taken by each sensor in each scenario was analyzed individually according to detection success of obstacle.

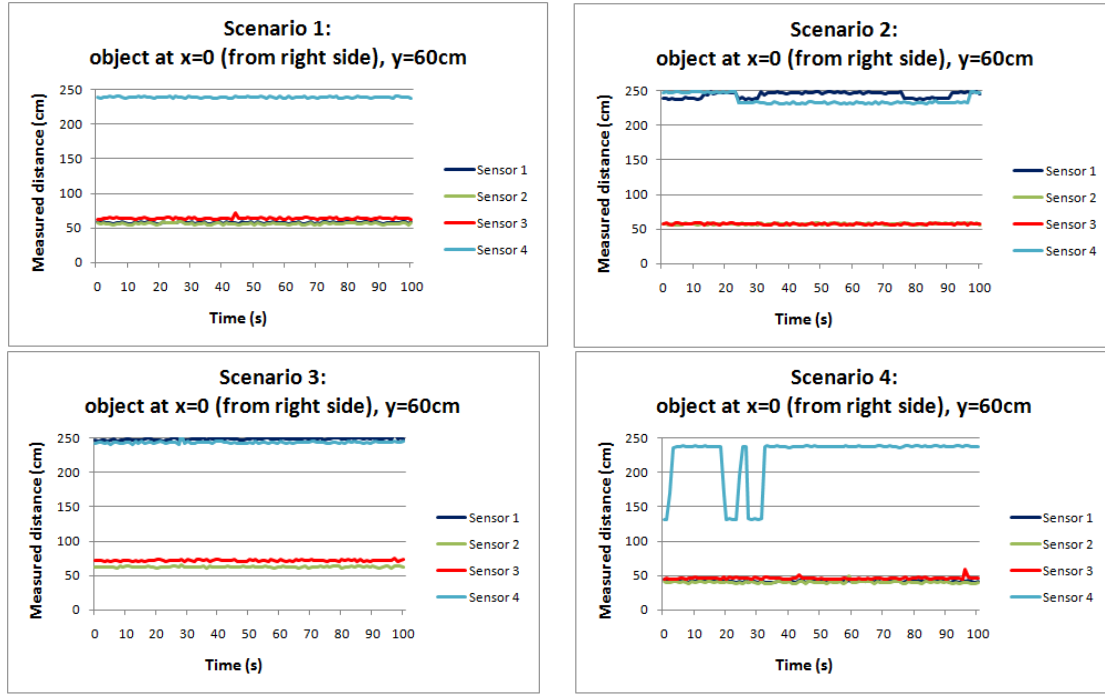


Fig. 3.24: Comparison of scenarios when object locates at $x=0$ (from right side), $y=60\text{cm}$

3.3.3.2 Comparison of scenarios according to detection success

For each position of obstacle, 100 data was taken to measure the distance value to an obstacle. The arithmetical averages and standard deviations of measured distance values were calculated. Table 3.3-3.4 show the summary of average and standard deviation values of scenarios with obstacle at various positions in the range of $\pm 40, 200\text{ cm}$. According to our experimental set, if the object was detected by sensor then the table was colored (see Table 3.3). Dark blue, green, red and blue colors show the regions detected by sensor 1, sensor 2, sensor 3, and sensor 4 respectively.

During the detection phase, the measured distances and real distances were compared relatively by considering triangular rule. Since the hypotenuse is larger than the sides of triangular, the distance to an obstacle increases when the position of obstacle is slid along x-axis compared to the centre (at $x=0$). For instance, if the obstacle's real position is $x=\pm 40\text{cm}$, $y=40\text{cm}$; then by the triangular rule:

$$z = \sqrt{x^2 + y^2}; \text{ the distance to obstacle is } z=56,56\text{cm. Therefore, by also giving some toleration value}$$

($\pm 25\text{ cm}$) all the measured distances were checked within an interval of $y-25\text{cm} \leq z \leq y+25\text{cm}$, where z and y denote the measured distance and real distance values, respectively. Thus, as an assumption $y-25\text{cm} \leq z \leq y+25\text{cm}$ was accepted for evaluation of detection phase. Then, each scenario was assessed according to total number of detection success. According to Table 3.3, it is clear to say that the total detection rate of scenario 1, scenario 2, scenario 3, and scenario 4 are 161, 105, 64, 149 respectively. The total success of scenarios is ranked in descending order as scenario 1 > scenario 4 > scenario 2 > scenario 3. As seen in Fig. 3.25, as the angle of sensor increases from 0° up to 45° detection success decreases.

Table 3.3: Average values of measured distance data taken by different sensors in each scenario

a) scenario 1

		Object at x-axis (cm)																																											
		Object at left												Object at middle				Object at right																											
		-40				-30				-20				-10				0--				0				0++				10				20				30				40			
		S1	S2	S3	S4	S1	S2	S3	S4	S1	S2	S3	S4	S1	S2	S3	S4	S1	S2	S3	S4	S1	S2	S3	S4	S1	S2	S3	S4	S1	S2	S3	S4	S1	S2	S3	S4	S1	S2	S3	S4	S1	S2	S3	S4
object at y axis (cm)	40	239	238	242	239	239	238	243	240	44	238	242	239	42	238	242	239	42	47	242	49	42	43	51	50	47	45	52	240	239	45	240	240	239	45	240	240	239	238	240	240	239	238	240	240
	60	239	238	242	239	224	238	242	239	59	238	242	239	57	64	242	239	57	60	242	62	57	58	64	63	58	56	64	239	64	58	66	240	239	58	241	239	239	62	240	240	239	238	240	240
	80	239	238	242	239	79	238	243	240	76	238	243	240	74	78	242	239	76	78	242	81	78	79	85	83	79	77	85	240	81	77	83	239	239	79	240	239	239	81	240	240	239	238	240	240
	100	239	238	242	240	95	238	242	240	93	238	242	239	91	96	242	239	91	94	243	96	95	96	102	99	95	94	100	240	95	94	99	239	239	94	242	239	239	98	240	240	239	238	240	240
	120	239	238	243	240	112	238	243	239	110	238	243	239	110	114	243	113	110	110	242	113	108	108	114	113	112	110	116	239	239	110	240	239	239	110	241	240	239	114	240	240	239	238	241	240
	140	129	238	243	240	127	238	242	239	125	129	243	240	125	129	243	130	127	127	242	130	127	127	133	132	131	129	242	240	239	127	241	240	239	130	242	240	239	238	241	239	239	238	241	239
	160	239	238	243	240	146	238	242	239	144	148	242	239	144	146	243	148	144	144	242	147	148	148	154	151	148	148	243	240	150	146	242	240	239	148	241	239	239	148	241	239	239	150	243	240
	180	239	238	243	240	163	238	242	240	161	165	243	240	161	163	243	240	159	161	242	164	163	163	169	240	163	161	167	240	219	163	243	240	239	165	242	239	239	165	242	239	239	167	242	240
	200	239	238	243	240	180	238	243	240	178	182	242	240	176	180	243	240	176	178	242	179	178	180	242	183	178	177	242	240	182	179	243	240	239	180	243	240	239	182	243	240	239	238	242	239

b) scenario 2

		Object at x-axis (cm)																																											
		Object at left												Object at middle				Object at right																											
		-40				-30				-20				-10				0--				0				0++				10				20				30				40			
		S1	S2	S3	S4	S1	S2	S3	S4	S1	S2	S3	S4	S1	S2	S3	S4	S1	S2	S3	S4	S1	S2	S3	S4	S1	S2	S3	S4	S1	S2	S3	S4	S1	S2	S3	S4	S1	S2	S3	S4	S1	S2	S3	S4
object at y axis (cm)	40	239	238	236	233	239	238	236	233	239	238	236	233	40	238	236	44	40	237	240	46	40	40	43	39	248	41	43	237	247	43	234	233	240	64	236	233	248	236	242	233	247	236	245	236
	60	239	238	240	234	231	238	236	233	61	238	237	233	59	238	236	56	57	123	245	54	57	57	57	54	245	58	58	237	247	57	58	233	248	73	238	241	244	237	246	233	247	238	242	246
	80	241	238	236	234	240	238	236	233	78	238	236	233	76	238	237	229	74	162	184	71	74	74	75	71	248	74	74	248	247	76	230	235	244	238	234	240	248	238	251	234	247	238	234	238
	100	239	238	236	234	237	238	239	234	95	238	247	235	91	238	238	233	92	189	239	90	93	93	91	90	239	95	93	239	247	91	105	235	239	238	244	236	244	237	239	233	245	238	235	233
	120	239	238	240	233	239	238	237	234	157	238	237	233	108	204	236	107	106	129	239	105	110	110	108	107	248	110	108	235	247	114	110	233	248	158	242	233	247	160	236	233	239	161	234	239
	140	242	238	236	234	239	238	236	234	127	218	236	233	125	201	238	233	125	172	236	132	127	125	123	123	237	125	122	233	241	169	244	237	243	171	234	233	241	171	234	235	239	173	236	235
	160	239	238	236	233	198	238	236	233	223	197	236	233	140	233	236	234	142	186	236	232	142	141	139	138	248	145	234	233	247	186	235	233	239	184	236	233	239	186	236	233	239	188	236	233
	180	241	238	236	234	206	227	236	234	236	238	236	233	157	200	236	233	157	160	239	163	159	158	186	185	202	156	235	233	240	200	242	234	239	201	236	233	239	201	236	234	239	203	236	233
	200	239	238	236	233	228	237	238	233	220	230	236	233	175	224	236	233	174	212	236	233	178	177	183	233	239	175	235	233	239	177	234	234	239	213	236	234	239	215	236	233	239	217	236	233

Table 3.3: Average values of measured distance data taken by different sensors in each scenario (continue)

c) scenario 3

		Object at x-axis (cm)																																											
		Object at left												Object at middle								Object at right																							
		-40				-30				-20				-10				0--				0				0++				10				20				30				40			
		S1	S2	S3	S4	S1	S2	S3	S4	S1	S2	S3	S4	S1	S2	S3	S4	S1	S2	S3	S4	S1	S2	S3	S4	S1	S2	S3	S4	S1	S2	S3	S4	S1	S2	S3	S4	S1	S2	S3	S4	S1	S2	S3	S4
object at y axis (cm)	40	247	247	244	244	247	247	244	244	247	246	245	247	55	247	244	158	60	244	243	77	55	49	66	75	145	49	66	244	249	55	146	244	247	56	246	244	241	241	246	243	241	240	246	244
	60	248	247	244	244	245	246	244	243	242	243	240	239	137	246	244	181	382	232	241	74	99	63	75	52	249	63	72	244	248	312	75	244	247	312	246	244	248	246	246	244	249	247	247	244
	80	247	247	244	244	247	247	244	244	248	247	245	243	82	246	244	83	82	246	244	82	114	79	87	112	248	81	87	244	248	128	85	244	247	246	244	244	234	202	244	244	247	247	244	245
	100	248	247	244	244	247	247	244	244	247	246	244	244	125	247	244	329	95	139	245	96	345	96	131	121	229	96	100	244	248	98	102	244	247	247	244	244	221	215	245	244	247	209	244	244
	120	247	247	244	244	154	247	244	244	248	247	244	243	254	246	245	141	355	168	244	111	137	142	254	296	236	121	142	244	233	119	142	244	217	161	244	244	222	157	246	244	219	220	244	244
	140	239	240	244	244	222	232	244	244	239	171	244	244	339	171	245	392	153	169	244	128	327	168	394	384	247	161	133	244	247	159	439	244	247	169	244	244	248	247	244	244	248	247	244	244
	160	239	238	246	244	240	238	244	244	241	241	244	244	253	243	244	305	163	165	244	140	306	146	265	513	229	163	170	244	217	165	487	244	222	228	245	244	245	212	244	244	218	218	244	244
	180	244	245	245	244	246	246	244	244	236	227	244	244	241	242	245	256	159	226	245	414	249	182	183	183	247	181	514	244	247	226	246	244	247	229	247	247	248	247	245	244	247	247	244	244
200	247	247	244	244	248	247	244	244	247	247	245	244	248	247	244	193	248	247	244	245	209	224	246	241	238	228	310	244	209	244	246	244	197	242	244	244	223	222	244	244	218	217	244	244	

d) scenario 4

		Object at x-axis (cm)																																												
		Object at left												Object at middle								Object at right																								
		-40				-30				-20				-10				0--				0				0++				10				20				30				40				
		S1	S2	S3	S4	S1	S2	S3	S4	S1	S2	S3	S4	S1	S2	S3	S4	S1	S2	S3	S4	S1	S2	S3	S4	S1	S2	S3	S4	S1	S2	S3	S4	S1	S2	S3	S4	S1	S2	S3	S4	S1	S2	S3	S4	
object at y axis (cm)	40	239	237	239	239	239	238	239	239	239	238	239	239	37	237	239	40	37	41	239	40	40	40	46	42	42	40	46	118	238	40	46	238	239	236	239	238	239	238	239	238	239	239	236	239	238
	60	239	238	239	238	236	238	239	238	55	237	239	238	54	59	239	57	54	55	239	57	42	42	46	44	42	40	46	225	220	40	239	239	239	233	239	239	222	235	239	239	234	229	239	239	
	80	239	238	239	239	239	237	239	238	73	80	239	238	71	76	239	238	71	72	239	74	74	67	79	70	76	74	77	158	78	72	86	159	171	74	177	174	163	76	167	163	238	231	239	238	
	100	239	238	239	239	92	237	239	238	90	95	239	239	88	93	239	238	88	89	239	91	91	91	94	93	93	91	94	238	95	91	96	238	190	93	239	239	239	93	239	239	238	229	239	238	
	120	239	238	239	238	238	238	239	239	105	110	239	238	103	106	239	238	103	105	239	108	103	103	109	108	106	106	109	239	108	106	109	238	129	108	239	239	235	110	239	238	239	160	239	238	
	140	238	238	239	238	239	238	239	238	239	238	239	238	120	238	239	205	120	122	239	124	124	124	128	127	124	122	126	229	130	122	128	238	160	125	239	238	239	123	239	232	239	132	239	238	
	160	239	238	239	238	238	237	239	239	219	237	239	238	137	141	239	141	135	139	239	139	134	133	147	145	141	139	239	239	150	139	144	239	230	139	239	238	238	144	239	238	235	203	239	238	
	180	239	238	239	238	228	238	239	239	158	238	239	238	156	158	239	200	156	161	239	158	158	158	161	161	221	156	239	239	238	156	239	238	239	158	239	238	239	171	239	239	238	162	239	238	
200	238	236	239	238	175	236	239	238	175	234	239	238	173	238	239	238	173	237	240	211	175	175	178	177	181	173	178	238	237	173	239	239	239	175	239	239	230	236	239	239	238	236	239	238		

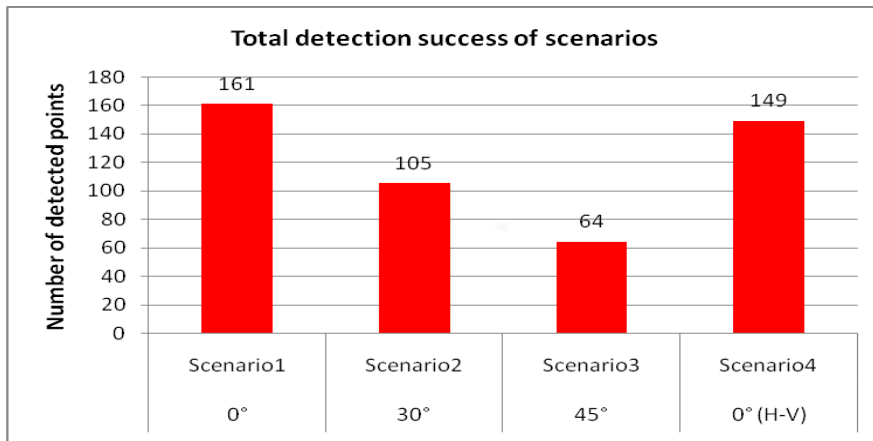


Fig. 3.25: Total detection success of scenarios

Fig. 3.26 shows the detection success rate of different sensors in each scenario. In the figure, R and L denote the right and left, whereas U and D denote the up and down positions of sensors, respectively. In all the scenarios, detection success of down sensors is larger than the up sensors. This can be apparently attributed to the height of obstacle. Since the obstacle height is smaller than the position of up sensors' height and when the distance to an obstacle increases, detection range of up sensors decreases. This shows that sensor is sensitive to height of obstacle. Especially, it should be noted that if the obstacle height is larger than the sensors' position height then the detection of obstacle becomes easier when compared with detection of smaller obstacles.

Moreover, according to Table 3.4, the less variation occurs with scenario 1. In scenario 1, all of the results are more stable as compared to other scenarios.

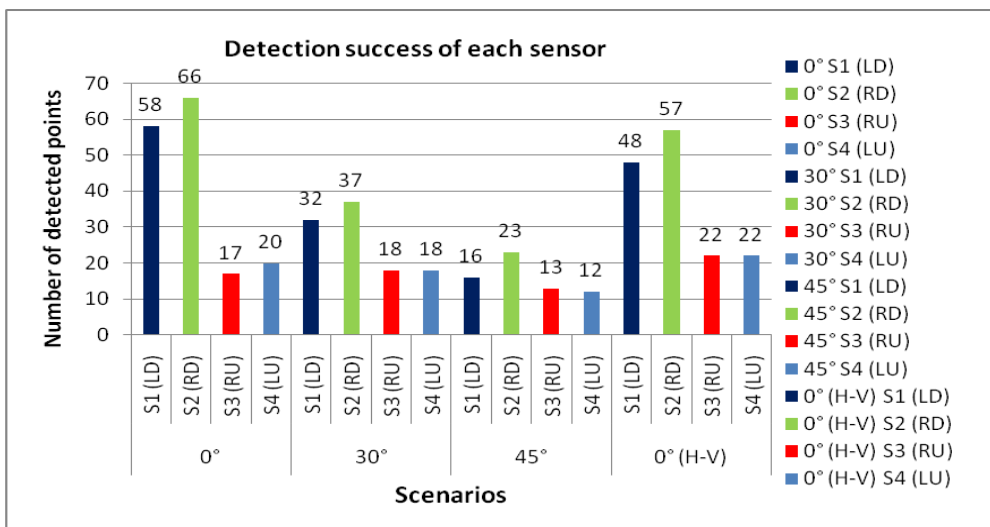


Fig. 3.26: Detection success of each sensor in each scenario

Table 3.4: Standard deviations of measured distance data taken by different sensors in each scenario

a) scenario 1

		Object at x-axis (cm)																																											
		Object at left																Object at middle				Object at right																							
		-40				-30				-20				-10				0--				0				0++				10				20				30				40			
		S1	S2	S3	S4	S1	S2	S3	S4	S1	S2	S3	S4	S1	S2	S3	S4	S1	S2	S3	S4	S1	S2	S3	S4	S1	S2	S3	S4	S1	S2	S3	S4	S1	S2	S3	S4	S1	S2	S3	S4	S1	S2	S3	S4
object at y axis (cm)	40	1	1,3	1,1	1,2	1,1	1	1,1	1,2	1,2	1,1	1	1,2	1,4	1	1	1,3	1	1,1	1	1,1	1,2	1,2	0,9	0,9	1,1	1,2	1,4	1,1	1,2	1,2	1,9	1,1	1,1	1	1,1	1,2	1,5	1,4	1,8	1,2	1,1	1,6	1,7	1,2
	60	1,1	1	1,5	1,1	1	1	1,1	1,7	1	1	1,5	1	1,1	1	1	1,2	1,5	1,3	1,1	1	1,1	1,1	1,1	1	1,1	1,2	1,2	1,1	1,1	1,1	1	1,1	1,1	1	1,5	1,6	1,4	1,1	2	1,1	1,5	1	1	1,2
	80	0,9	0,9	1,1	1,3	1	1	1	1,6	1	1,1	1	1,1	1	1,2	1,3	1,2	1	1,1	1	1,1	1	0,9	1,3	1,3	1	1	1,1	1,1	1,2	1	1,1	1,1	1,4	1,1	1,2	1	1,1	1	1,1	1,1	1	0,9	1,1	1,2
	100	1,3	1,2	1,1	1,2	1,2	1	1,1	1,1	1	1	1,1	1,2	1,6	1,1	1	1,6	1,2	1,2	2,2	1,1	1,2	1,4	1	1,1	1,1	1	1,2	1,2	1,3	1,5	1,1	1,2	1,5	1,2	1,2	1,1	1,1	1,2	1,9	1,2	1,6	1,5	1,1	1,2
	120	1,2	1,1	1,1	1,2	1,1	1,5	1	1,2	1,1	1,1	1,1	1,2	1,4	1,5	1,2	1,8	1,1	1,1	1,1	1,2	1	1	1,1	1,6	1,1	1	1,1	1,3	1,1	1	1,1	1,3	1,1	1,1	1,3	1,2	1,2	1,2	1,1	1,1	1,1	1,1	1,4	1,2
	140	1,1	1,1	1,1	1,2	1,4	1,1	1,1	1,2	1	1,4	1,5	1,2	1,1	1,1	1,9	1,4	1,6	1,5	1,2	1,7	1,2	1	1,1	1,2	1,1	1,6	1,6	1,3	1,2	1,3	2,1	1,3	1	1,5	1,2	1,3	1,2	1,1	1,9	1,2	1,7	1,2	1,6	1,2
	160	1,1	1,6	1,9	1,3	1,4	1,1	1,7	1,2	1,1	1,2	2	1,4	1,1	1,2	1,6	1,6	1	1,2	1,2	1,1	1,5	1,6	1,2	1,2	1,1	1,2	1	1,2	1,6	1,1	1,3	1,2	1,2	1,2	1,9	1,2	1,1	1,1	2,4	1,2	1,1	1,4	1	1,3
	180	1,2	1,1	1,1	1,2	1,1	1,2	1,1	1,1	1,2	1,3	2	1,1	1,1	1	1	1,3	1,3	1,6	1,2	1,2	1,1	1	1,1	1,2	1,2	1,2	1,1	1,7	35	1,2	1,2	1,2	1,1	1,1	1	1,1	1,2	1,1	1	1,2	1,1	1,3	1,2	1,3
200	1,2	1,1	1,1	1,4	1,1	1,1	1,2	1,5	1,3	1,6	1,2	1,2	1,2	1,8	1,2	1,2	1,8	1,1	1,2	1,3	1,3	1,7	1,2	1,2	1,6	1,1	1,1	1,9	1,2	1,3	1,2	1,3	1,4	1,3	1,2	1,2	1,1	1,3	1,2	1,8	1,6	1,1	1,1	1,3	

b) scenario 2

		Object at x-axis (cm)																																															
		Object at left																Object at middle				Object at right																											
		-40				-30				-20				-10				0--				0				0++				10				20				30				40							
		S1	S2	S3	S4	S1	S2	S3	S4	S1	S2	S3	S4	S1	S2	S3	S4	S1	S2	S3	S4	S1	S2	S3	S4	S1	S2	S3	S4	S1	S2	S3	S4	S1	S2	S3	S4	S1	S2	S3	S4	S1	S2	S3	S4	S1	S2	S3	S4
object at y axis (cm)	40	1,7	1	1,2	1,5	1	1,2	1,2	1,2	1,9	1,2	1,1	1,1	1	1	1,1	1,2	1,1	4,6	6,3	1,5	1,1	1,2	1,2	1,8	1	1	1,2	6,4	1,3	1,2	1	1	2,7	0,9	5,7	1,1	1,1	1	7,3	1,3	2,5	1,2	6,5	6,1				
	60	1,1	1,4	6,9	2	1,4	1,5	2	1,7	1	1	4,4	1	1,5	1,2	1,1	1,1	1,5	82	7,3	1,1	1	1,2	1	1,4	4,2	1	1	6,9	1,4	1,1	1,4	1	1,1	3,5	7,1	7,5	4,3	1,5	7,6	1,6	1,2	1	7,4	5,2				
	80	3,3	1	1,1	1,6	3,3	2	1,2	1,2	1	1,2	1,1	1,4	1	1,2	3,5	1,3	1	76	66	1,3	1,3	1	2,7	1,6	1,9	1,1	1	1,1	1,4	1,2	4,8	3,9	4,1	1,5	1	6,8	1,1	1	1,1	2,5	1	1,1	1	6,7				
	100	1,6	1,7	1,1	1,3	4,9	1,6	6,2	1,7	1,1	1	6,4	1	1,2	1,4	4,9	1,6	1,8	68	6	1	1,3	1,2	1,1	1	1,1	1,1	1	7,6	1,1	1,2	1,3	4,9	1,1	1	8,1	5,6	4,8	1,4	7,1	0,9	4,4	1,5	4,1	1				
	120	1,4	1,1	7,1	1,2	3,4	1,2	3,8	1,6	1,1	1,1	3,6	1,2	1,1	41	1,4	1,3	1,1	23	7,9	2,6	1,3	1,1	1,1	1,3	1,2	1,2	1	4,7	1,3	1,6	2	1,1	1,5	1,2	8,9	1,4	1,1	1,2	2	2	1,1	1,2	1,7	6,5				
	140	4,5	1,5	1,3	1,3	1,1	1	1,3	2	1,1	31	1,1	1	1	33	5,4	1,2	1,1	1,7	2,6	4,1	1,2	1,7	2,3	1,5	1,3	1,3	1,2	1,5	4,3	1,1	8,1	4,6	4,6	1,3	1,3	1,2	3,9	1,3	1,1	1,5	1,7	1,2	1,6	1,6				
	160	1,2	1,1	1,3	1,4	22	1,3	2,4	1,8	31	20	1,3	1,2	1,3	15	1,2	1,7	1,2	1,1	1,2	2,9	1,3	1,2	1,1	1,1	1,1	2,1	2,2	1,2	2,9	1,2	2	1,1	1,9	1,4	1,1	1,1	1,2	1,2	2,2	1,5	1,1	1,5	1,3	1,5				
	180	3,6	1,5	1,2	1,6	13	16	1,1	1,3	21	1,1	1,3	1,3	1,1	1,2	1,2	1,1	1,6	2,2	5,8	1	1,2	1,1	1,8	1,2	5,2	1	1,5	1,2	2,8	1	7,9	1,5	1,6	1,5	1,1	1,1	1,5	1,6	1,8	1,3	1,1	1,1	1,1	1,1				
200	1,3	1,2	1,2	1,3	11	3,8	5,5	1,3	10	10	1,2	1,1	1,2	11	2	1,2	1,3	7,5	1,9	1,3	1,2	1,1	1,2	1,2	1,2	1,3	1,6	1,1	1,2	1,3	1,4	1,5	1,6	1,2	2,9	1,4	1,3	1,1	1,3	1,8	1,2	1,3	1,1	1,1					

Table 3.4: Standard deviations of measured distance data taken by different sensors in each scenario (continued)

c) scenario 3

		Object at x-axis (cm)																																															
		Object at left												Object at middle				Object at right																															
		-40				-30				-20				-10				0--				0				0++				10				20				30				40							
		S1	S2	S3	S4	S1	S2	S3	S4	S1	S2	S3	S4	S1	S2	S3	S4	S1	S2	S3	S4	S1	S2	S3	S4	S1	S2	S3	S4	S1	S2	S3	S4	S1	S2	S3	S4	S1	S2	S3	S4	S1	S2	S3	S4	S1	S2	S3	S4
object at y axis (cm)	40	1,1	1,0	1,2	1,4	1,0	1,0	1,0	1,1	1,0	1,0	1,3	1,2	1,0	1,3	1,6	1,9	15	2,8	1,4	20	1,5	1,1	1,1	1,1	1,0	1,0	2,3	1,0	1,5	2,7	7,4	1,4	1,2	1,1	1,1	1,4	5,4	5,0	1,4	1,5	6,6	6,0	1,2	1,1				
	60	1,6	1,0	0,9	1,1	3,2	2,0	1,4	1,8	7,9	5,9	5,5	6,5	1,3	1,6	1,7	1,1	76	45	5,4	1,4	9,3	1,0	1,9	1,0	1,8	0,9	1,1	1,6	1,5	1,1	2,0	1,1	1,0	1,1	1,1	1,9	1,2	1,0	1,2	1,1	1,4	1,4	1,1	1,1				
	80	1,1	1,0	1,0	1,1	1,1	1,5	1,9	1,7	1,1	1,0	2,4	1,6	0,9	0,9	1,0	1,1	2,3	1,1	1,1	1,1	1,5	2,0	1,9	78	0,9	0,9	1,0	1,2	1,4	1,7	1,1	1,1	1,5	1,0	1,1	1,1	28	55	0,9	1,1	1,1	1,4	1,2	1,4				
	100	1,1	1,0	1,2	1,3	1,1	1,6	1,1	1,2	1,1	1,0	1,2	1,1	1,1	1,2	1,0	79	1,1	1,6	1,7	1,1	73	1,0	2,1	14	13	1,0	1,1	2,0	1,2	1,4	1,0	1,2	1,1	1,1	1,1	1,1	22	25	2,2	1,7	1,2	49	1,0	1,2				
	120	1,1	1,1	1,2	1,2	1,1	1,6	1,1	1,1	1,8	1,0	1,1	1,4	25	1,9	1,1	1,6	80	33	1,1	1,1	2,4	19	84	95	9,4	11	1,3	1,7	11	6,7	1,2	1,2	29	23	1,1	1,2	41	1,1	1,2	1,5	22	22	2,1	1,6				
	140	7,1	6,3	1,1	1,2	24	12	2,0	1,1	7,4	1,2	1,0	1,8	85	1,1	1,3	43	1,1	1,1	1,2	1,1	90	6,2	40	44	1,0	17	25	1,2	1,4	9,2	47	1,7	1,2	1,5	1,6	1,0	1,1	1,1	1,3	1,2	1,2	1,1	1,2	1,7				
	160	8,3	7,3	1,6	1,1	6,4	11	1,1	1,2	6,2	5,3	1,0	1,7	107	5,7	1,3	118	1,4	15	1,1	1,2	69	6,7	42	52	15	1,2	22	1,1	26	1,6	54	1,2	38	30	2,4	1,4	14	39	1,1	1,7	29	33	1,1	1,2				
	180	3,1	2,4	1,1	1,8	2,4	2,1	1,1	1,1	10	18	1,2	1,2	5,6	5,1	1,9	45	20	40	2,0	129	1,4	1,6	1,1	1,0	1,2	1,1	57	1,1	1,5	25	1,1	1,0	1,2	25	2,4	9,7	1,1	1,5	2,0	1,2	1,0	1,6	1,1	1,2				
200	1,2	1,7	1,2	1,6	1,6	1,4	1,1	1,2	1,1	1,1	1,7	1,7	1,2	1,6	1,1	1,4	1,2	1,1	1,1	1,5	20	27	1,3	13	10	22	95	1,6	33	13	1,2	1,6	43	27	1,2	1,2	20	20	1,1	1,2	25	25	1,0	1,2					

d) scenario 4

		Object at x-axis (cm)																																															
		Object at left												Object at middle				Object at right																															
		-40				-30				-20				-10				0--				0				0++				10				20				30				40							
		S1	S2	S3	S4	S1	S2	S3	S4	S1	S2	S3	S4	S1	S2	S3	S4	S1	S2	S3	S4	S1	S2	S3	S4	S1	S2	S3	S4	S1	S2	S3	S4	S1	S2	S3	S4	S1	S2	S3	S4	S1	S2	S3	S4	S1	S2	S3	S4
object at y axis (cm)	40	1,7	1,3	1,1	1,0	1,0	1,5	1,0	1,8	1,7	1,1	1,0	1,0	1,1	1,3	1,0	0,9	1,4	1,3	1,1	1,1	1,1	1,1	1,5	1,0	1,4	1,1	1,0	22	1,8	1,0	1,0	1,6	1,0	2,2	1,3	1,4	1,0	1,0	1,0	1,0	1,4	1,2	2,0	1,0				
	60	1,2	1,2	1,1	0,9	5,3	1,0	1,0	1,2	1,6	1,1	1,1	1,1	1,9	1,7	1,3	1,1	1,2	1,0	1,1	1,1	1,1	1,1	1,9	1,5	1,2	1,4	1,7	34	35	1,1	0,9	1,4	1,5	5,2	1,7	1,6	34	3,6	1,0	1,1	7,6	9,0	1,0	1,7				
	80	1,5	1,5	1,2	1,7	1,6	1,3	1,9	1,0	1,1	1,1	1,0	1,4	1,0	1,1	1,2	1,0	0,9	1,4	1,0	1,0	1,3	6,8	1,4	6,6	1,4	1,4	1,7	36	1,0	1,0	31	38	53	1,0	57	56	68	1,0	67	68	1,4	18	1,1	1,4				
	100	1,2	2,1	0,9	1,6	1,1	1,0	1,3	1,1	1,5	1,7	1,9	1,0	1,1	1,6	1,1	0,9	1,1	1,1	1,1	1,2	1,1	1,1	2,1	1,2	1,6	1,0	1,1	1,1	1,2	1,1	1,0	1,0	53	1,2	1,8	1,0	1,1	1,6	1,1	1,5	1,8	31	1,9	1,1				
	120	1,2	1,2	1,1	1,2	1,1	1,0	1,1	1,4	1,2	1,1	0,9	1,0	1,1	1,7	1,2	1,1	1,1	1,4	2,0	1,2	1,7	1,2	1,1	1,0	1,2	1,0	1,9	1,1	1,1	1,1	2,1	1,1	45	1,2	1,3	1,1	22	1,1	1,8	1,7	1,2	47	1,2	1,2				
	140	1,4	1,5	2,5	1,1	1,7	1,1	1,0	1,0	1,5	1,2	1,1	1,0	1,4	1,1	1,1	53	1,0	1,0	1,1	1,4	1,5	1,2	1,2	1,5	1,0	1,2	1,8	44	18	1,2	1,1	1,0	51	1,2	1,2	1,1	1,1	8,5	1,2	11	1,2	15	2,0	1,1				
	160	1,1	1,7	2,1	1,1	1,1	1,0	2,0	1,1	40	1,2	1,2	1,1	1,6	1,1	1,2	1,5	4,3	1,1	2,6	1,3	8,7	9,0	1,9	1,8	1,2	1,2	1,1	1,7	25	1,2	1,0	1,7	26	1,2	1,2	1,4	1,7	1,8	2,2	1,5	19	45	1,8	1,1				
	180	1,1	1,4	1,1	1,3	28	1,3	1,1	1,2	1,7	1,2	1,4	1,1	1,0	1,9	1,1	41	1,2	21	1,9	1,1	1,1	1,5	1,2	1,9	33	1,6	1,4	1,9	1,6	1,1	1,1	2,0	1,1	1,9	1,0	1,0	1,9	28	1,5	1,5	1,6	2,2	1,2	1,1				
200	1,5	6,6	1,0	1,0	1,2	6,7	1,9	1,1	1,8	15	1,2	1,4	1,6	1,9	1,2	1,2	1,4	1,0	2,1	33	1,2	1,7	1,3	1,3	16	2,3	1,1	1,5	1,5	1,3	1,1	1,1	1,6	1,4	1,2	2,0	11	1,2	1,1	1,1	4,6	1,3	1,7	1,7					

3.3.3.3 Comparison of scenarios according to detection error

After the comparison of detection success, scenarios were also compared according to detection error. In order to do this, detection error of each sensor in each scenario was calculated as follows:

Firstly, the average values of gathered data were calculated. Since 100 data was taken for each position of obstacle, the average value of 100 data was calculated for each sensor in each scenario by using Equation 3.8. By using these data, Table 3.3 was obtained.

$$\bar{X} = \frac{1}{n} \sum_{i=1}^n X_i \quad (3.8)$$

Secondly, the expected value of each position of obstacle (μ) or in other words the each actual position of obstacle was used to calculate the mean square error (MSE) by using Equation 3.9.

It should be noted that the actual distance of each position of obstacle was computed according to each sensor's position separately by using triangular rule ($z = \sqrt{x^2 + y^2}$). Error was calculated if the obstacle is detected by sensor, therefore the colored values in Table 3.3 were used for error calculation.

$$MSE(\bar{X}) = E ((\bar{X} - \mu)^2) \quad (3.9)$$

Finally, the total mean square error of each sensor in each scenario was summed up and divided by each sensor's detection rate (γ) separately in order to calculate average detection error (ADE) of each sensor:

$$ADE = \frac{\sum E ((\bar{X} - \mu)^2)}{\gamma} \quad (3.10)$$

In Appendix B, Tables B1-4 summarizes the calculations of average detection error for each scenario. For instance with reference to Table B1, case no 66 shows that obstacle located at $x=10$ (right) and $y=80$. The actual distances according to sensors were calculated as following:

-Since sensor 2 and sensor 3 locates at (10, 0), then the actual distance to obstacle from these sensors should be $z = \sqrt{(10-10)^2 + (80-0)^2} = 80$ cm.

-Since sensor 1 and sensor 4 locates at (-10,0), then the actual distance to obstacle from these sensors should be $z = \sqrt{(10-(-10))^2 + (80-0)^2} = 82.5$ cm.

According to table, the measured average distances are 80.7cm, 76.8cm, 82.7cm and 239.3cm for sensor 1, sensor 2, sensor 3, and sensor 4 respectively. This shows that obstacle was detected by only sensor 1, sensor2 and sensor 3. Thus, the table was colored. Then by the colored (detected) values, mean squared errors for sensor 1, sensor 2 and sensor 3 were calculated as $(80.7 - 82.5)^2 = 3.1$ cm, $(76.8 - 80)^2 = 10.4$ cm and $(82.7 - 80)^2 = 7.1$ cm, respectively.

Finally, considering all cases, average detection errors were calculated by Equation 3.10. The detection rate of a sensor explains the number of detected points by the sensor and it can be computed by counting the number of detected points.

Table 3.5 summarizes the average detection error for each sensor in each scenario. Fig. 3.27 shows the total average detection error of each scenario. It can be easily seen from the figure that the minimum error occurs with scenario 1 while the maximum error occurs with scenario 4.

Table 3.5: Average detection error for each sensor in each scenario in cm

	Sensor 1	Sensor 2	Sensor 3	Sensor 4	Total Average Detection Error
Scenario 1	161.4	153.3	48.0	102.3	464.9
Scenario 2	191.6	230.5	110.6	122.0	654.7
Scenario 3	194.2	114.4	139.4	151.1	599.1
Scenario 4	244.0	243.8	148.4	188.2	824.3

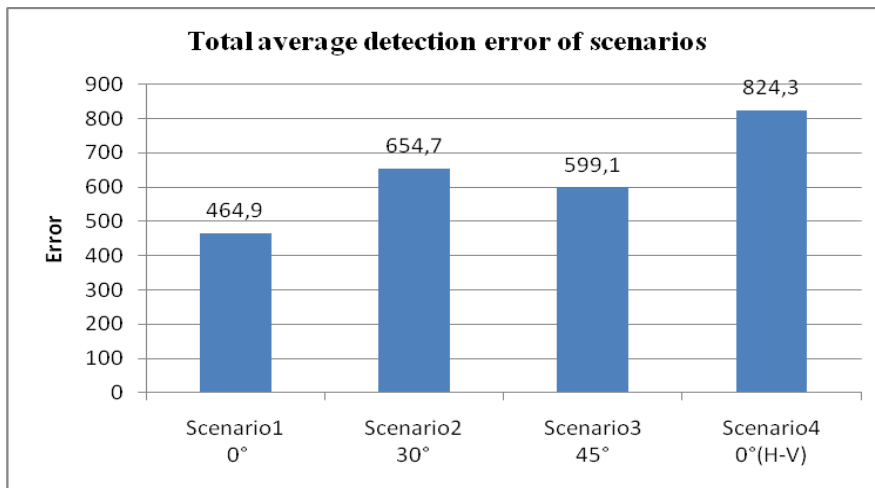


Fig. 3.27: Total average detection error of each scenario

3.3.3.4 Comparison of scenarios according to detection range

Moreover, scenarios were compared according to detection range capabilities. For instance, Fig. 3.28 shows the detection range of sensors when obstacle located at $y=80$ cm along whole x -axis. With scenario 1; sensor 1 (left down sensor), sensor 2 (right down sensor), sensor 3 (right up sensor), and

sensor 4 (left up sensor) detect the obstacle in the range of [-35 15]cm, [-15 35]cm, [0 12]cm, [-8 0]cm on the x-axis respectively. Indeed, this proves that obstacles located at right side can be easily detected by right positioned sensors than the left positioned ones, or vice versa as expected logically.

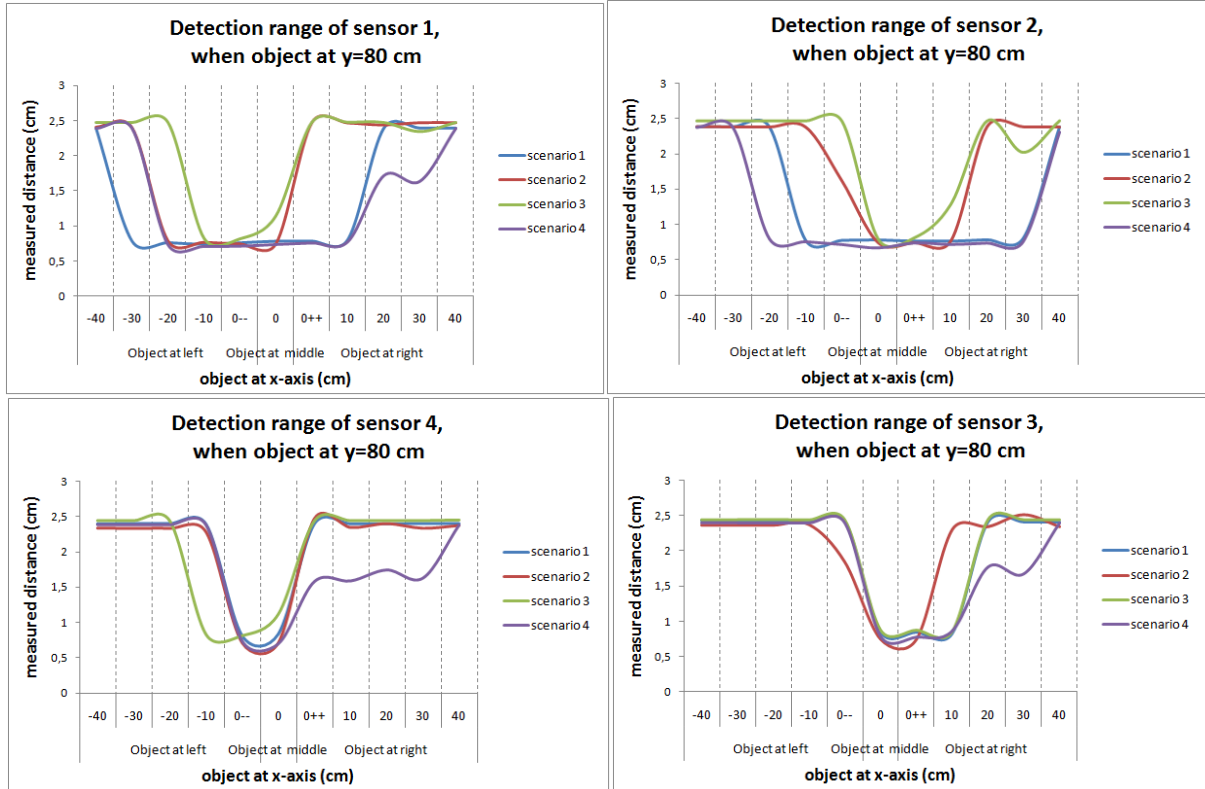


Fig. 3.28: Comparison of detection range of sensors when object at $y=80\text{cm}$

However, detection range capabilities showed differences according to scenarios. In order to compare detection range of scenarios easily, Fig. 3.29 and 3.30 are presented. As seen from the Fig. 3.29, with scenario 2 and scenario 3 the detection range capabilities of sensor 1 decreases as well as its detection beam angle becomes narrower. On the other hand, scenario 1 and scenario 2 present larger detection angle to sensor 1 that means sensor 1 is capable of detect obstacles within wider range.

Moreover, it can be noticed that sensor 1 can detect the area mainly at the left rather than at the right. However, with reference to Fig. 3.30 sensor 2 can detect the area mainly at the right rather than at the left. This can be attributed to sensor's position. As described above and expected logically, if the position of sensor is at the right then the right sided obstacles are mainly detected clearly, in contrast if the position of sensor is at the left then the left sided obstacles are mainly detected. Additionally, when scenarios are compared, with Scenario 1 and Scenario 4 detection capability of sensor 2 increases like sensor 1, whereas it decreases with Scenario 2 and Scenario 3.

As a result, according to detection range capabilities Scenario 1 and Scenario 4 present better results than the other two scenarios.

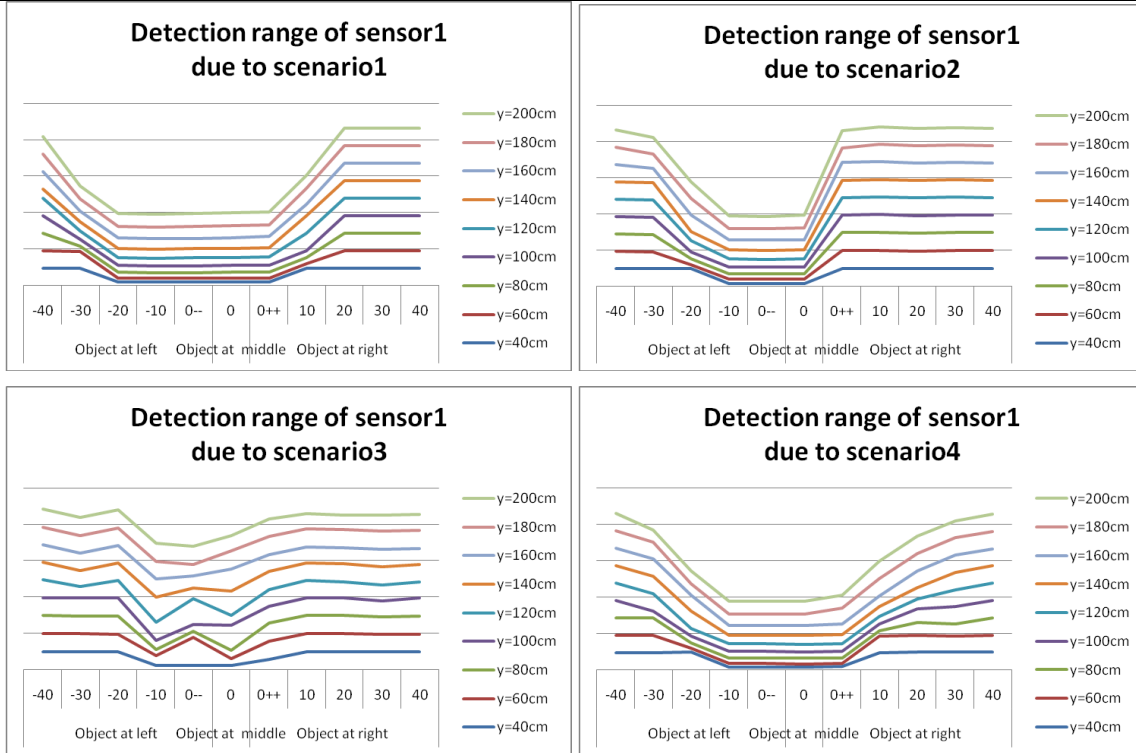


Fig. 3.29: Detection range of sensor 1 according to scenarios

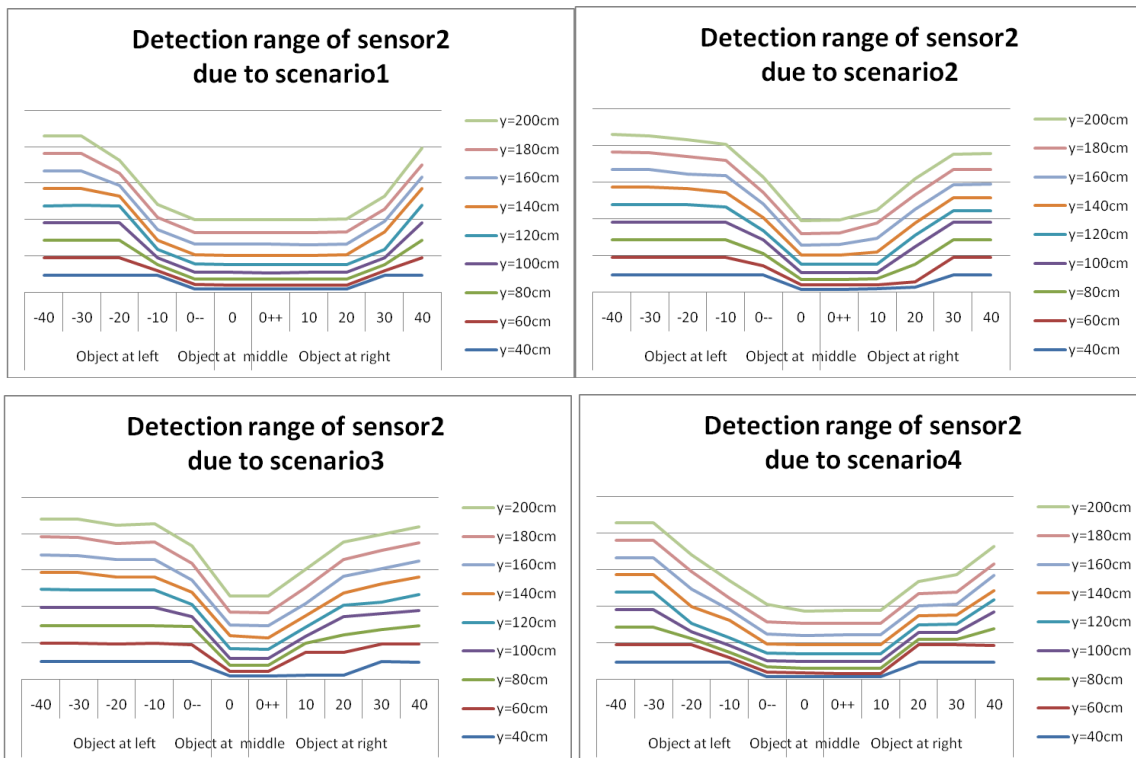


Fig. 3.30: Detection range of sensor 2 according to scenarios

3.3.4 Conclusion

In this part, in order to find required number of sensors as well as develop suitable obstacle avoidance algorithm for smart clothing system, different scenarios were developed by connecting sensors together. According to developed scenarios by using electrical wires, only four scenarios were selected to continue experiments within textile structures. Then, sensors integrated to textile structures by using conductive yarns and snap fasteners were mounted on textile surface. In 1st, 2nd, and 3rd scenario, four sensors positioned horizontally onto textile surface with an angle of 0°, 30°, and 45°, respectively. Additionally, in 4th scenario, two sensors at down were positioned horizontally, on the contrary two sensors at up were positioned vertically with an angle of 0°. Then, all data taken by each sensor in each scenario were analyzed and compared.

Results showed that when the scenarios were evaluated according to total detection success, rank in descending order was scenario 1 > scenario 4 > scenario 2 > scenario 3. Furthermore, it was found that as the angle of sensor increases from 0° up to 45°, detection success decreases. Moreover, in all scenarios detection success of down sensors was larger than the up sensors. This can be associated with the height of obstacle. Therefore, height of obstacle has a considerable effect on the detection success. It should be noted that if the object height is smaller than the sensors' position height relatively, then the detection of objects will be difficult.

According to standard deviation results, the less variation occurred with scenario 1. In scenario 1, all of the results seemed to be more stable as compared to other scenarios.

When the results were compared according to detection error, minimum error occurred with scenario 1 while the maximum error occurred with scenario 4.

Moreover, due to detection range capabilities scenario 1 and scenario 4 presented better results than the other two scenarios.

Another result issued from this section was that position of detection range of sensors was shaped by position of sensors. That means, if the position of sensor is at the right then the number of detected objects will be greater at the right side than the left side, or vice versa.

To sum up, scenario 1 in which all sensors were placed horizontally at 0° presented us the best compromising results not only in terms of detection success, detection error and detection range capabilities but also integration and mounting of sensors onto textile structure. Therefore, for our smart clothing system scenario 1 was chosen to arrange position and number of sensors onto garment.

3.4 Analysis of Vibrotactile Perception via Vibration Motors by using Fuzzy Logic

3.4.1 Introduction

According to results of the Section 2.2, in order to guide visually impaired people, vibration motion was determined as guidance alert. Therefore, as mentioned in Section 2.4, vibration motor was selected towards our aim and it was successfully integrated to textile structure. However, the critical question was that to where vibration motor should be placed in proposed smart clothing system? In which areas of human body are more sensitive to vibrotactile perception e.g wrists, abdomen, arm? Which fabric structure can transfer vibration motion better? Therefore, in order to answer these questions, first we made a literature review about vibrotactile perception and then, we conducted a comprehensive study in order to analyze the vibrotactile perception via our e-textile structures by using fuzzy logic.

3.4.1.1 Vibrotactile sensation

Tactile sensations activate numerous mechanoreceptors in the outer layers of the skin. Tactile information is then, transmitted directly to the brain from these mechanoreceptors to provide information about tactile sensations. Vibrotactile sensation is a kind of tactile sensation based on vibration motions [212].

In a number of developed tactile displays, vibrotactile feedback stimulation is used to provide information about the direction or orientation of person or vehicle [80, 213-219], for deaf people to support speech vocalization [220], for blind people to detect 3D patterns of an obstacle distribution [221-222], and to read printed material [223] etc.

3.4.1.2 Factors effecting vibrotactile perception

In vibrotactile sensations, the perception level depends on many factors connected with the characteristic of vibration stimuli such as contact and friction values between the human skin and a sensed object, vibration frequency, magnitude, duration of vibration, type of applied vibration motions and the area of the contactor stimulating the skin [212, 224-226]

The literature review mainly summarizes the effect of vibration frequency ranging from 0.4 Hz to 1 KHz on vibrotactile perception level. The effect was studied by a different contactor measuring device [227-231]. Some researchers reported that when the vibration frequency increases, perception level increases also [232-234], whereas others found that the perception level is independent of vibration

frequency [235-237]. Indeed, since frequency working range is different in various studies, perception level results according to used frequencies, showed differences. Furthermore, some researchers concluded that factors such as the size of the contactor/handle [230, 238-240], its shape [230], and its surroundings [240] have significant effect on the vibrotactile sensation at different frequencies. Furthermore, in most of the studies three regions of the body, which are fingertip, forearm, and abdomen, are often used as a stimulated contact area.

Indeed, the perception level of vibrotactile stimulation varies in different regions of the body. This may be explained by the innervation density of mechanoreceptors in the skin [241-242].

For instance, the perception level in areas with high innervation densities, e.g. fingertips, is stronger than in areas with low innervation densities, e.g. the arm [243]. In some of the studies, parts of the body (i) upper body: abdomen, chest, shoulders, or head; (ii) lower body: feet and legs, or buttocks, back were subjected to vibration [244-246]. It was reported that low frequencies (from 0.5 to 1.25 Hz) caused discomfort in the upper body, whereas high frequencies (from 6.3 to 16.0 Hz) caused discomfort in the lower body [245].

Vibrations are not in the form of unitary stimuli. They are composed of a certain waveform, which can be regular or irregular [246]. Waveforms can also affect the level of vibrotactile perception. It has been shown that in a modulated sinusoid waveform study, in which the amplitude of a base signal (e.g. 250 Hz) is modulated by a second sinusoid (e.g. 50 to 20 Hz), the level of perception has changed [247].

As seen from the factors mentioned above, during the design of a vibrotactile display there are many parameters, which should be considered carefully. Therefore, considering our smart clothing system we conducted a comprehensive study in order to analyze vibrotactile perception level. Herewith, we intended to discover the influence of conductive yarns, signal waveforms and frequencies, and different body local areas on the resulting vibrotactile perception level.

By this way, which kind of fabric structure should be used, in which area of smart clothing system vibration motors should be fixed, which kind of signal waveform at which frequency level should be applied to vibration motor were decided by using fuzzy logic.

3.4.2 Experimental

In order to perform experiments, samples that were mentioned in Section 2.4 (see Fig. 2.16) were used.

3.4.2.1 Measurement set up

Experiments were conducted by applying three types of signal waveforms as seen in Fig. 3.31 (square wave, sin wave, and saw tooth wave) in three different frequencies (0.5 Hz, 5 Hz and 50 Hz) to different parts of the user's body (see Fig. 3.32), by using samples mentioned above.

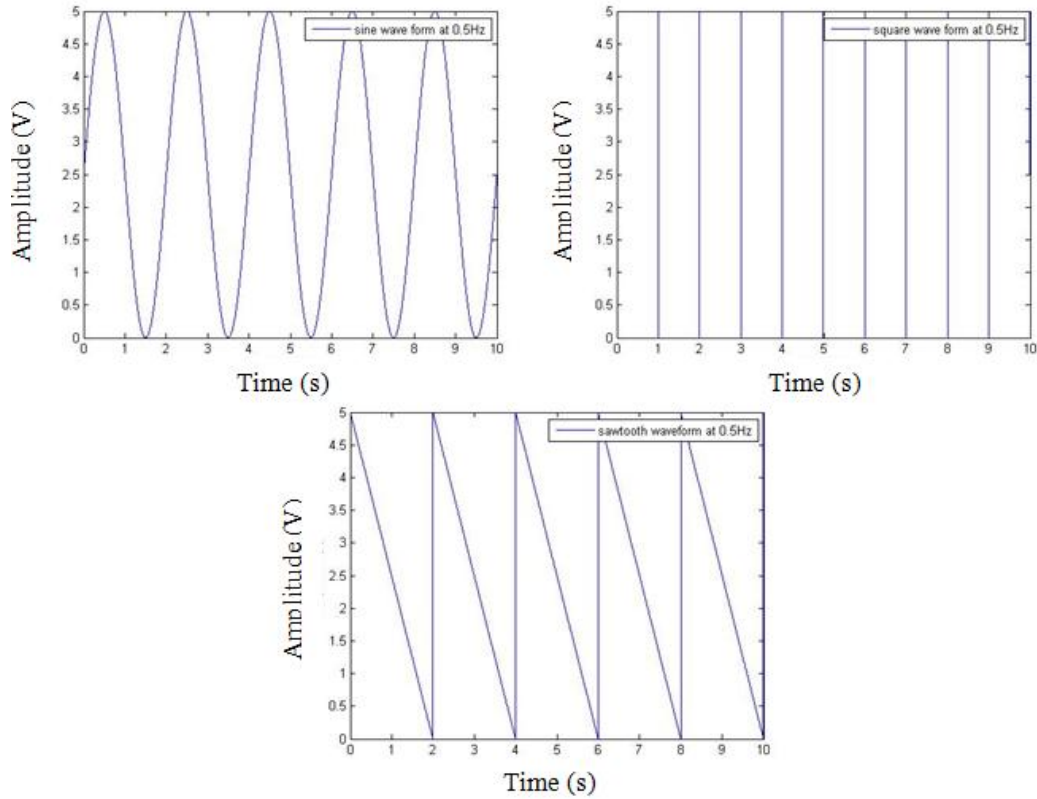


Fig. 3.31: Generated signals: sinwave, square wave, sawtooth wave with 5V amplitude at 0.5Hz

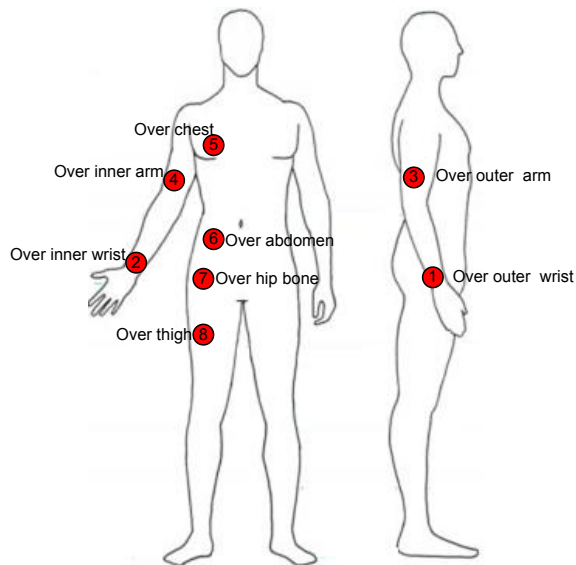


Fig. 3.32: Stimulated contact areas of human body during the measurements

Signals were generated in MATLAB, and transmitted via National Instruments® DAQ (Data Acquisition) Card. Frequency level was measured with oscilloscope. Duration for each experiment was adjusted to 30 seconds [231].

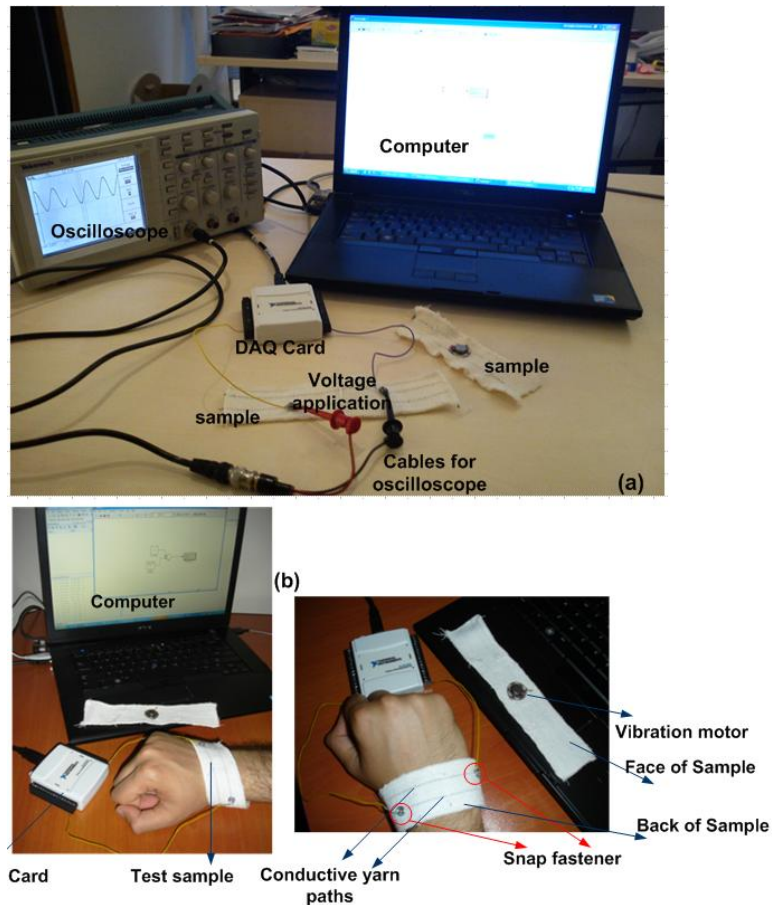


Fig. 3.33: Measurement-set up (a) measurement over outer wrist (b)

In order to analyze and compare the perceived vibrotactile sensations, samples woven and knitted with two different conductive yarns were tested with three different waveforms at three different frequencies, on eight different body parts of the eight people.

Fig. 3.33 shows measurement set-up and measurement over outer wrist. In order to avoid pressure effect, fabrics were placed on human body under relaxed conditions i.e. without any stress. Therefore, for some parts of the body, test was done when evaluator was lying on the bed to prevent fall down of fabric by gravitational force.

3.4.2.2 Evaluation method

Fig. 3.34 explains the framework of the evaluation method according to fuzzy relations. As seen in Fig. 3.34; to construct team, due to the known decreasing sensitivity of elderly humans, eight people (four men and four women) aged between 24 and 30 were selected for experiments [255]. Since all of

the evaluators self-reported having a normal sense of touch, the weighting factor of each evaluator was considered equally:

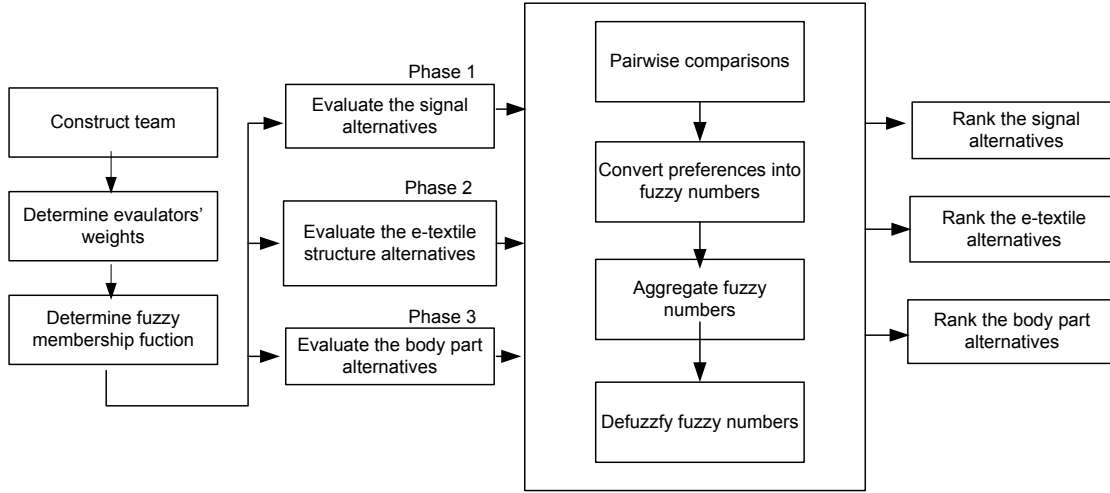


Fig. 3.34: Framework of the fuzzy evaluation method

Then, fuzzy membership function for vibrotactile perception was determined. The fuzzy data can be in linguistic terms, fuzzy sets or fuzzy numbers. Fuzzy scale is a set of fuzzy numbers P_1, \dots, P_n defined in the interval $\langle A, B \rangle$ and they are numbered according to their order to make a fuzzy decomposition:

$$\forall x \in \langle A, B \rangle : \sum_{i=1}^n P_i(x) = 1 \quad (3.11)$$

If the data are in linguistic terms instead of fuzzy numbers, then fuzzy scale is formed by fuzzy linguistic variables [249]. We used fuzzy linguistic terms according to study of Kulak and Kahraman [192]. Hence, the values of vibrotactile perception were expressed in fuzzy linguistic scale ranging from very low (VL) to very high (VH) as seen in Fig. 3.35. During the evaluation phase; at first, a training session was prepared to help the evaluators to become familiar with the linguistic terms of perception levels along body parts and situations. The training procedure can easily make the evaluator to understand and unify the meaning of the evaluation terms such as “very high” and “medium”.

Then, since the fuzzy data are in linguistic terms, evaluations were transformed into standard fuzzy numbers. They all were assigned to crisp scores, and evaluations for pairwise comparisons were aggregated by using following equation:

$$\tilde{S}_i = \tilde{S}_{i1} \otimes w_{e1} \oplus \tilde{S}_{i2} \otimes w_{e2} \oplus \dots \oplus \tilde{S}_{im} \otimes w_{em} \quad (3.12)$$

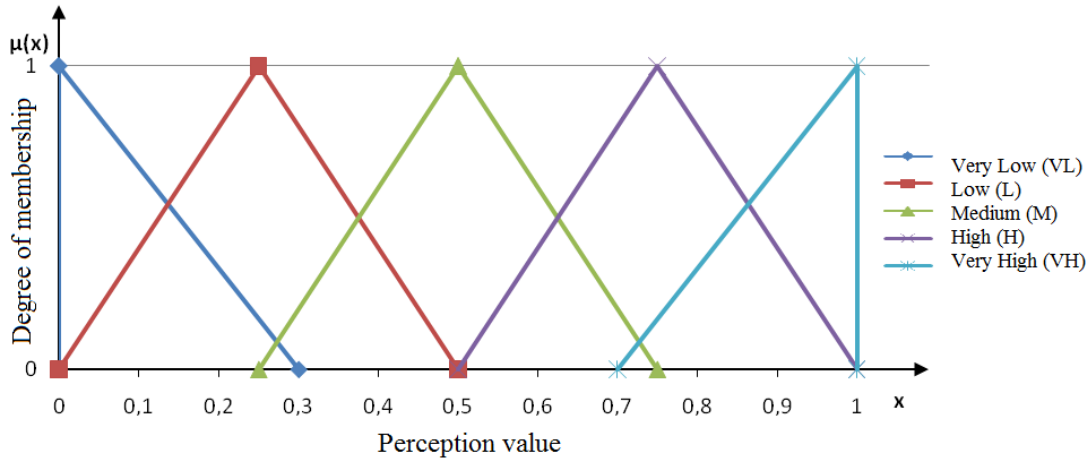


Fig. 3.35: Triangular fuzzy numbers for linguistic terms

where \tilde{S}_i is the fuzzy aggregated score of the i^{th} criterion and where w_{ei} is the weight of i^{th} evaluator and $w_{ei} \in [0,1]$. \otimes and \oplus denote the fuzzy multiplication and fuzzy addition operators, respectively.

Then, defuzzification operation was used to defuzzify the fuzzy numbers [195]. Finally, the best alternative with having highest perception level was selected.

Results were also compared statistically. ANOVA was performed to compare the significance value between different alternatives (signal type and frequency, e-textile structures, and body parts) and perception level. In order to do test, SPSS program was used and statistical significance was set at $p < 0.05$. Fig. 3.36 shows the hierarchy of the evaluation phase. At first, signal alternatives were evaluated, compared, and ranked for perception level. Secondly, by applying and combining the best signal alternative with e-textile structure alternatives, e-textile structure alternatives were evaluated, compared, and ranked. Thirdly, the best e-textile structure alternative with the best signal alternative was applied on the different parts of the human body (see Fig. 3.32). Finally, the best combination and situation were selected to show the highest vibrotactile perception information.

3.4.3 Results

3.4.3.1 Results according to signal alternatives

Vibrotactile perception values of eight evaluators according to signal alternatives were summarized in Table 3.6 in fuzzy linguistic terms. In the table, the evaluators were denoted as E1, E2., E8. The perception values in fuzzy terms were transformed into fuzzy numbers by using linguistic scale as shown in Fig. 3.35. Then, they were aggregated, and defuzzified as mentioned above. Hence, the result of total evaluation of vibrotactile perception according to signal alternatives is shown in Fig. 3.37.

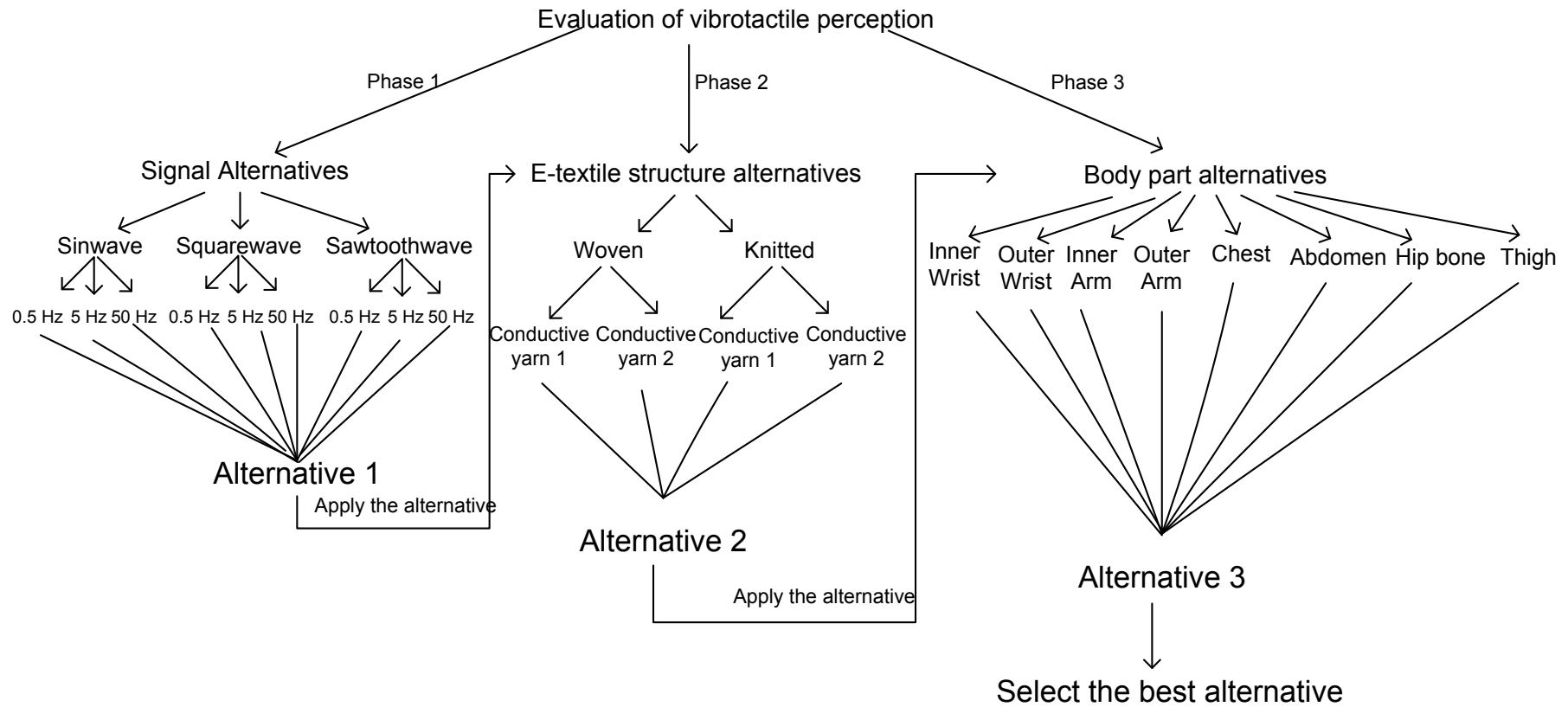


Fig. 3.36: Hierarchy of the evaluation

Table 3.6: Vibrotactile perception values of each evaluator according to signal alternatives

	Sine wave			Square wave			Sawtooth wave		
	0.5	5	50	0.5	5	50	0.5	5	50
E1	VH	H	M	M	M	L	M	M	M
E2	H	M	M	H	M	M	H	H	M
E3	H	H	M	M	L	L	H	M	L
E4	VH	H	M	M	M	L	M	L	L
E5	VH	M	L	M	L	VL	M	M	L
E6	H	M	M	M	M	L	M	M	M
E7	H	M	M	M	M	L	H	M	L
E8	H	M	L	M	L	VL	H	M	M

As it can be noticed from the Fig. 3.37, when the frequency of signal increases, the perception level decreases. Moreover, in the same frequencies the perception level of square wave form is lower than the perception level of both saw tooth and sine wave forms.

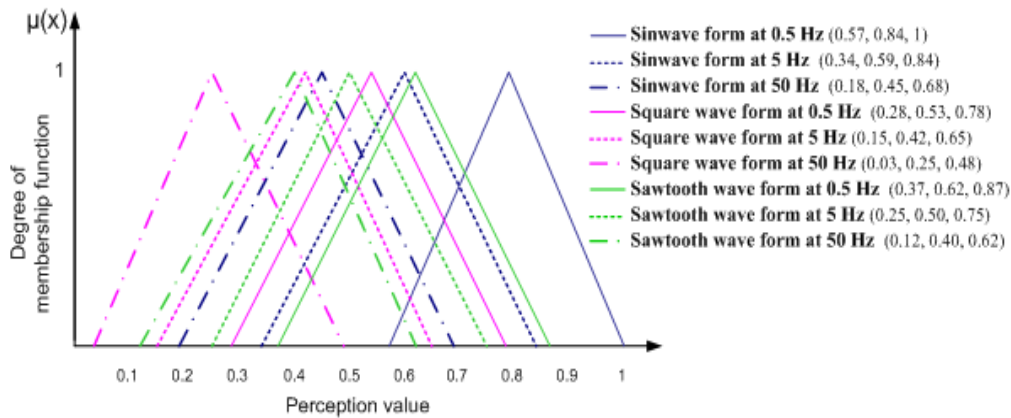


Fig. 3.37: Result of total evaluation of vibrotactile perception according to signal alternatives

Furthermore, as it can be seen from the figure, sine wave form at 0.5 Hz showed highest vibrotactile perception level. The order of vibrotactile perception level of waveforms at the same frequencies was: sine wave > saw tooth > square. Moreover, based on ANOVA results (see Table 3.7-3.8); the level of vibrotactile perception varied significantly with both signal type and frequency ($p < 0.001$; ANOVA).

Table 3.7: Perception Level & Signal Type ANOVA Results

	Sum of Squares	df	Mean Square	F	Significance
Between Groups	11,028	2	5,514	10,023	0,000
Within Groups	37,958	69	0,550		
Total	48,986	71			

Table 3.8: Perception Level & Frequency ANOVA Results

	Sum of Squares	df	Mean Square	F	Significance
Between Groups	20,028	2	10,014	23,860	0,000
Within Groups	28,958	69	0,420		
Total	48,986	71			

These results can be explained by the structure of wave forms. In sine wave form, an increase and decrease are seen uniformly. But in both saw tooth wave and square wave forms, a sudden increase is seen, and this directly reflects to vibration motion. By this way, it can be said that tactile sensation is smooth in sin wave form whereas it is rough in both saw tooth and square wave form [252]. This may affect the evaluators' perception negatively. Furthermore, as the frequency increases, continuity in vibration motion increases. However, in low frequencies the vibration motion is more discrete. From the results, it can be concluded that people prefer to feel discrete vibrations instead continuous vibrations as an alert. Therefore, in order to continue our experiments with different e-textile structure alternatives, sine wave form at 0.5 Hz signal alternative was chosen, and applied with e-textile structure alternatives for the comparison.

3.4.3.2 Results according to e-textile structure alternatives

Table 3.9 shows the vibrotactile perception values of eight evaluators according to e-textile structure alternatives in fuzzy linguistic terms and Fig. 3.38 shows the result of total evaluation of vibrotactile perception according to e-textile structure alternatives in fuzzy membership functions.

Table 3.9: Vibrotactile perception values of each evaluator according to e-textile structure alternatives

	Woven Fabric		Knitted fabric	
	Conductive yarn 1	Conductive yarn 2	Conductive yarn 1	Conductive yarn 2
	Sample 1	Sample 2	Sample 3	Sample 4
E1	H	H	M	M
E2	VH	VH	H	H
E3	VH	H	VH	VH
E4	H	M	H	M
E5	M	M	M	M
E6	H	H	H	H
E7	VH	H	H	H
E8	H	H	H	H

According to evaluation results as shown in Table 3.9 and in Fig. 3.38, vibrotactile perception of sample 1 was higher than other samples. This explained that the perception level in woven fabrics integrated with highly conductive yarn was higher than other samples. Furthermore, it was found that the perception level in woven samples was a bit higher than in knitted samples. This may be attributed to fabric structure. According to our study, woven samples were more compact than knitted ones, and consequently this let the fabric transfer vibrotactile motion better.

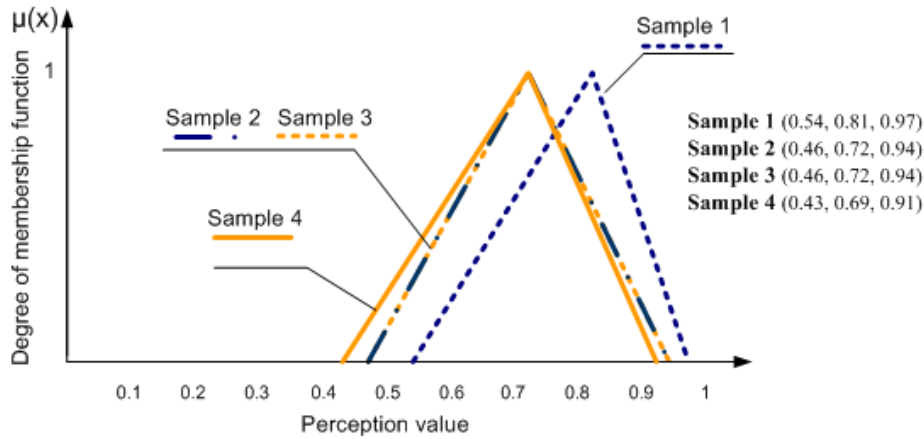


Fig. 3.38: Result of total evaluation of vibrotactile perception according to e-textile structure alternatives

Nevertheless, when samples are compared with respect to conductive yarn type, it cannot be said that there is significant difference between them ($p=0.205$; ANOVA Table 3.10). This result can be attributed to less distance between snap fastener and vibration motor. If the distance between snap fastener and vibration motor increases, resistance of the circuit will also increase. This may affect the duration of beginning of vibration motion and in this way; the perception level can show difference.

Table 3.10: Perception Level & Conductive yarn ANOVA Results

	Sum of Squares	df	Mean Square	F	Significance
Between Groups	0,781	1	0,781	1,682	0,205
Within Groups	13,938	30	0,465		
Total	14,719	31			

3.4.3.3 Results according to body part alternatives

To compare the perceived vibrotactile sensation on different parts of the human body, the woven e-textile fabric including silver plated nylon 66-4ply yarn with a linear resistance of <50 ohm/m was used during the experiments by applying sine wave form signal at 0.5 Hz on the evaluators' different body parts.

Vibrotactile perception values of eight evaluators according to body part alternatives in fuzzy linguistic terms, and total evaluation of vibrotactile perception were shown in Table 3.11 and Fig. 3.39-3.40, respectively.

Table 3.11: Vibrotactile perception values of each evaluator according to body part alternatives

	Over Outer	Over Inner	Over Outer	Over Inner	Over Chest	Over Abdomen	Over Hip bone	Over Thigh
E1	H	M	L	M	M	L	VH	VL
E2	VH	H	M	H	H	M	H	L
E3	H	M	M	H	H	M	VH	L
E4	VH	M	M	H	M	L	H	VL
E5	H	M	M	H	M	L	H	L
E6	VH	H	M	H	M	M	VH	VL
E7	H	M	M	M	M	L	H	L
E8	VH	H	M	H	M	L	VH	L

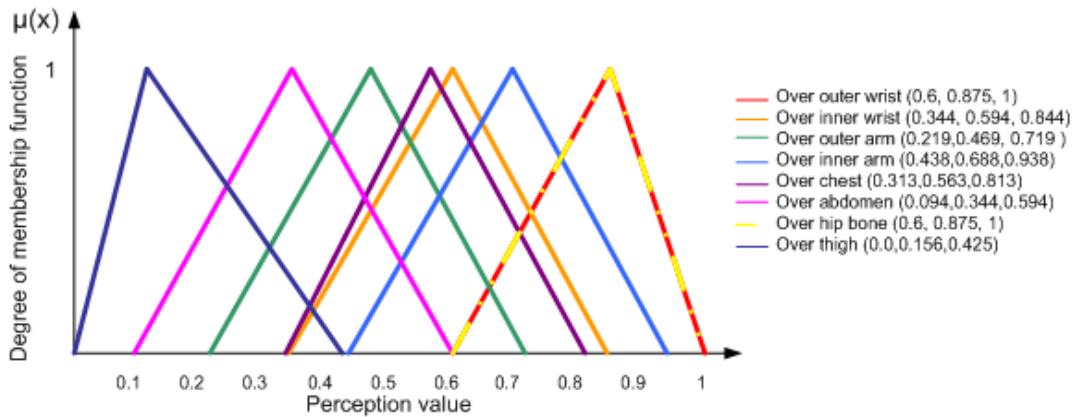


Fig. 3.39: Result of total evaluation of vibrotactile perception according to body parts alternatives

As seen in Fig. 3.39 and Fig. 3.40, the highest vibrotactile sensation was perceived over the outer wrist and hip bone area of the evaluators' body, whereas the lowest was perceived over thigh. The perceived vibrotactile sensation in rank from higher to lower on the body parts were over outer wrist/over hip bone, over inner arm, over inner wrist, over chest, over outer arm, over abdomen, and over thigh, respectively. Furthermore, it was also found that the perception level over the outer wrist was higher than the perception level over the inner wrist. On the contrary, the perception level over the outer arm was lower than the perception level over the inner arm. Therefore, it can be concluded that vibrotactile perception level significantly changed according to body parts ($p < 0.001$; ANOVA, see Table 3.12). This could be attributed entirely to the distribution of sensory nerves on the human body as mentioned in the literature.

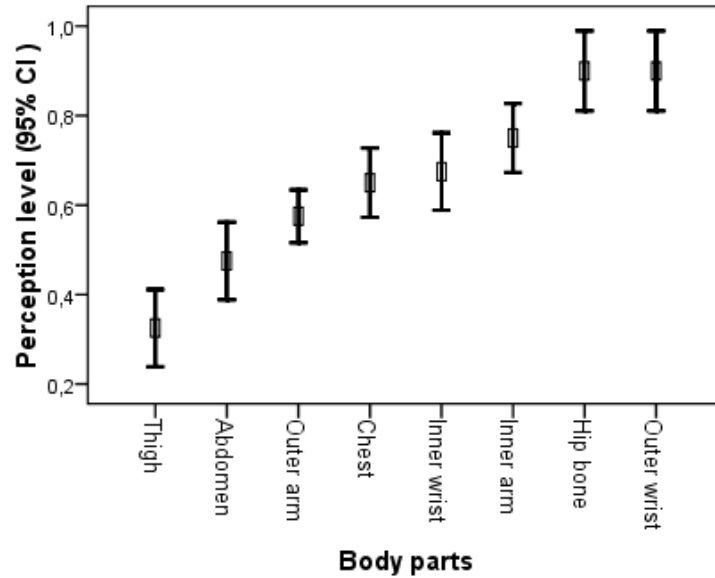


Fig. 3.40: Result of total evaluation of vibrotactile perception according to body parts alternatives (95% Confidence Interval)

For instance, in a study on tactile displays, it was also reported that vibratory threshold was higher in hips than in abdomen and thigh respectively at 100 Hz [226]. Moreover, in another study in which five people were exposed to a vertical sinusoidal wave force vibrating at various frequencies; it was reported that at 5 Hz the vibration was more sensible on the chest than abdomen and thigh [244].

Table 3.12: Perception Level & Body parts ANOVA Results

	Sum of Squares	df	Mean Square	F	Significance.
Between Groups	55,438	7	7,920	32,852	0,000
Within Groups	13,500	56	0,241		
Total	68,938	63			

3.4.4 Conclusion

In this section, vibrotactile perception level was investigated in terms of fuzzy relations. The influence of woven and knitted e-textile structures with two different conductive yarns, different signal wave forms (sine wave, square wave, and saw tooth wave) at three different frequencies (0.5 Hz, 5 Hz, and 50 Hz) and different body parts (wrist, arm, chest, abdomen, hip bone, thigh) on the resulting vibrotactile perception were evaluated by eight people (evaluators).

Results showed that e-textile structure type influenced the vibrotactile perception level. Nevertheless, conductive yarn type had no significant effect on the perception level of vibrotactile when the distance (resistance) between snap fastener and vibration motor (in the e-textile circuit) is small. According to

our study, the highest perception level in the e-textile structures was obtained by woven e-fabric integrated with highly conductive yarn. This may be related with more compactness of woven fabrics.

Moreover, signal waveform and the frequency had a significant effect on the vibrotactile perception level. It was found that as the frequency of signal increases the perception level decreases. Correspondingly, it can be concluded that people prefer to feel discrete vibrations instead continuous vibrations as an alert. According to our results, sine wave form at 0.5 Hz showed highest vibrotactile perception level within the signal type alternatives.

Another result issued from this study was that perception level of vibrotactile sensation showed differences due to contact areas of human body. The highest level of vibrotactile sensation was perceived over the outer wrist and hip bone area of the evaluators' body, whereas the lowest was perceived over thigh.

To conclude; the best combination for highest vibrotactile perception was to use woven e-fabric including highly conductive yarn over the outer wrist and/or over the hip bone by applying sine wave form at 0.5 Hz. Therefore, this combination was considered during the design of smart clothing prototype.

Chapter 4

Design and development of smart clothing prototype with an algorithm for obstacles avoidance

4.1. An algorithm for obstacle avoidance

4.1.1 Introduction

The ability to navigate visually impaired person through an environment cluttered with obstacles is a crucial issue. Navigation towards a target is a complex task and an important research field especially in robotic applications. The real-time obstacle avoidance algorithm is one of the key issues for mobile robots as well. A great number of different obstacle avoidance algorithms for mobile robots have been developed for indoor and outdoor environments. However, there is no obstacle avoidance algorithm developed for visually impaired people through an integrated system that consists of sonar sensors mounted on a garment. Since the obstacle avoidance strategy of visually impaired people is based on similar principles with obstacle avoidance strategy of mobile robots, the algorithms developed for mobile robots thus are given.

The general theory for mobile robotic navigation is based on such principles: First the robot can perceive the surroundings by sensors mounted on it like cameras, sonars, laser range finders, GPS etc. Then it is able to plan its operations based on the artificial intelligence model developed for navigation and obstacle avoidance task.

In the literature, a large number of algorithmic approaches were used in order to plan mobile robot motion such as grid method [251], vector field histogram method [252], potential field method [253],

path planning [254], geometry based approach, pattern generation method [255], switching control approach [256-258], self localization [259], soft computing based approaches like fuzzy logic, neural network, genetic algorithm and their different combinations [260].

Fuzzy logic is easily used when a mathematical model of the process is difficult to be proved or implemented in a real-time operation [261]. In recent years, fuzzy logic, neural network and genetic algorithm based approaches have been successfully applied to control mobile robots.

Ragaruman et al proposed a fuzzy logic based model for navigation of mobile robots in indoor environment [262]. Guo et al. developed an algorithm by using fuzzy logic to control the lower limbs rehabilitation robot with the known environment information [263]. Jincong et al. introduced the design of an intelligent four-wheel obstacle avoidance robot based on fuzzy control [260]. Pradhan et al. discussed different fuzzy logic controllers with different membership functions in order to navigate mobile robots [264]. Park and Zhang used a dual fuzzy logic approach for navigation of mobile robot. The first controller was designed to control target steering while the second one to follow the edge of obstacles [265]. Similarly, Chen and Juang designed two model based on fuzzy logic controllers in order to control wheeled mobile robot The first model was set up to avoid short distance obstacles while the second one was for target seeking [261]. Farooq et al designed a fuzzy logic based hurdle avoidance controller for mobile robot navigation in noisy and uncertain environments [266]. Maaref and Barret presented a study about the problem of navigating mobile robot either in an unknown environment or in a partially known one. A navigation method based on fuzzy inference proposed for avoiding convex and concave obstacles [267]. In most of the fuzzy logic controllers, the performance of the controller depends on the selection of membership functions and fuzzy if-then rules. Since the if-then rules designed by human experts, it is hard to choose and implement correct rules in the controller [268-273]. Therefore, there are some attempts were made in order to extract rules automatically. Hui and Pratihar used genetic algorithm to extract rules for fuzzy controller, thus they developed an algorithm based on combination of genetic and fuzzy approaches to avoid obstacles [274]. Moreover, Liu et al. adjusted the rules of fuzzy obstacle avoidance controller of autonomous mobile robot by using genetic algorithm [275, 276]. For the mentioned problem, some researchers have focused on using neural network approach to control the mobile robot. For instance, Szemes et al. applied the observation of human walking behavior to train fuzzy neural networks (FNN). The trained FNNs were applied to approximate the obstacle avoidance behavior of human walking as well as to control the mobile robot in a human-robot shared environment [277], similarly Mahyuddin et al. designed a neuro-fuzzy algorithm which is able to control the operations such as sense, map, plan and act. In their system, they used neuro-fuzzy approach in order to modify and extract new rules from a properly training [278, 279]. He et al. used fuzzy neural network method based on the Takagi-Sugeno information fusion arithmetic to avoid obstacles. First, the information get by sensors was classified and fused. Then the fused results were considered as the inputs of fuzzy neural network [280]. In

another study, the neural network approach was combined with GPS. In that system, a radial basis function network (RBFN) based on neural network was used to map the GPS data into the robot coordinates and then, trained data was combined with sonar based navigation system of the mobile robot [281]. Hui and Pratihari developed various algorithms based on genetic-fuzzy, genetic neural and potential field method (PFM) approaches and compared them as well. They found that soft computing based approaches (genetic fuzzy and genetic neural) were more adaptive and robust compared to the PFM [282].

Therefore, considering literature review and mainly focusing on recent studies, we decided to use combination of neural network and fuzzy logic approaches in our study. Hence, in order to navigate visually impaired person through an environment cluttered with obstacles, neuro-fuzzy logic based obstacle avoidance control algorithm was developed for our smart clothing system. Before, giving details of developed neuro-fuzzy control algorithm, the kinematic analysis of walking person, obstacle avoidance strategy, principals of neural network and fuzzy logic are presented in this part.

4.1.2 Kinematics analysis of walking person

Assume that person position is $P_b = (x_b, y_b, \theta_b)^T$, where (x_b, y_b) represents the coordinate of the person body and θ_b represents his heading angle from the horizontal axis as seen in Fig. 4.1. In the figure, w_b and v_b are the angular and linear velocities of walking person's body, respectively. The angular velocity of person depends on both angular velocities of the left (wl_l) and right (wl_r) legs where it can be demonstrated as $w_b = (wl_l, wl_r)^T$

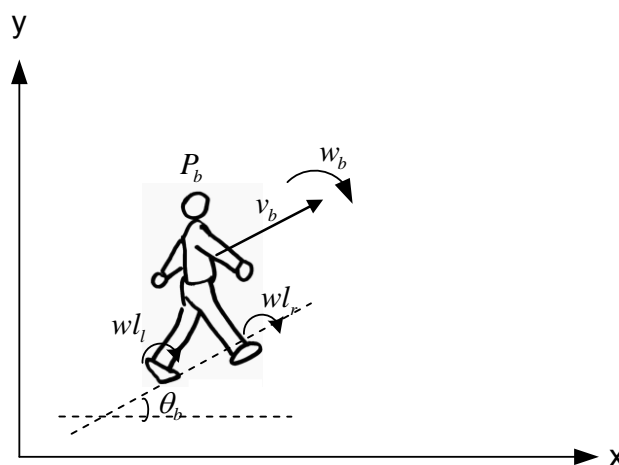


Fig. 4.1: Model of walking person in coordinate system

According to heading angular velocity w_b , the corresponding motion state of walking person can be summarized as in Table 4.1

Table 4.1: Motion state of walking person

w_b	$w_b=0$	$w_b>0$	$w_b<0$
Motion state	Go straight	Turn right	Turn left

If $w_l = -w_r$, then the angular velocity is $w_b = 0$ which implies that there is no turning action: go straight. Thus, the desired state of motion can be obtained by changing w_l and w_r .

Motion state of the walking person can be shown as $M_b = (v_b, w_b)^T$ by using his linear v_b and angular w_b velocities. Thus, the first kinematic equation can be written as follows:

$$\dot{P}_b = \begin{bmatrix} \dot{x}_b \\ \dot{y}_b \\ \dot{\theta}_b \end{bmatrix} = \begin{bmatrix} \cos \theta_b & 0 \\ \sin \theta_b & 0 \\ 0 & 1 \end{bmatrix} \begin{bmatrix} v_b \\ w_b \end{bmatrix} \quad (4.1)$$

and the coordinate of moving person is

$$\begin{bmatrix} x_{b(i+1)} \\ y_{b(i+1)} \\ \theta_{b(i+1)} \end{bmatrix} = \begin{bmatrix} x_{b(i)} \\ y_{b(i)} \\ \theta_{b(i)} \end{bmatrix} + \begin{bmatrix} \cos \theta_b & 0 \\ \sin \theta_b & 0 \\ 0 & 1 \end{bmatrix} \begin{bmatrix} v_b \\ w_b \end{bmatrix} \times \Delta t \quad (4.2)$$

where Δt is the sampled time, i is the current time index, and $i+1$ is the next time index.

Hence, according to above equations, the position of walking person can be estimated by controlling his/her angular w_b and linear v_b velocities.

4.1.3 Obstacle avoidance strategy

In the presence of obstacles, to guide person becomes more and more difficult. To guide user, firstly three important things should be determined:

- Target
- Obstacles
- Person's position

Then, guidance strategy can be implemented as seen in Fig. 4.2. The notation of observer used in this diagram is equivalent to the notation of control system.

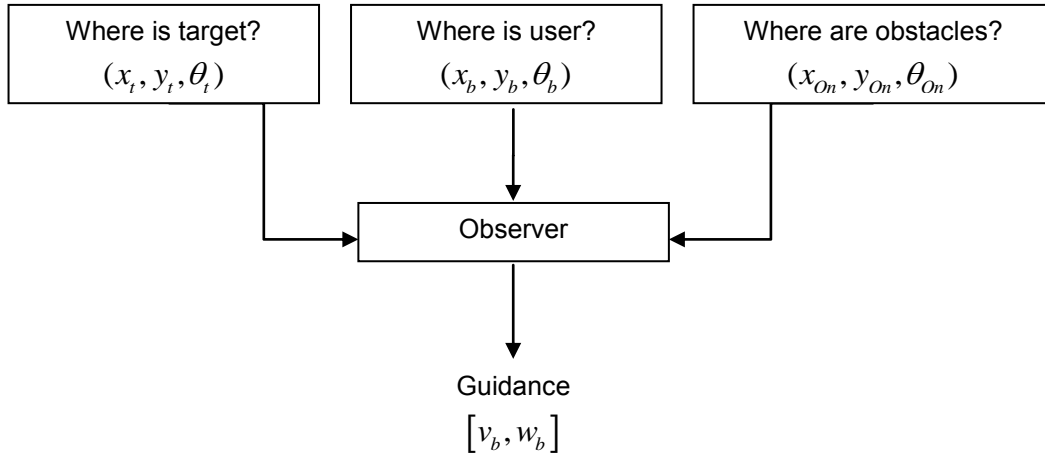


Fig. 4.2: Block diagram of guidance strategy

Suppose that the workspace W is cluttered up with N stationary obstacles O_n , $n \in \{1, \dots, N\}$ and a target point as seen in Fig.5.3

In the case of n obstacles and one target point, the distance to the target point is computed as

$$d_{t(i+1)} = \sqrt{(x_t - x_{b(i+1)})^2 + (y_t - y_{b(i+1)})^2} \quad (4.3)$$

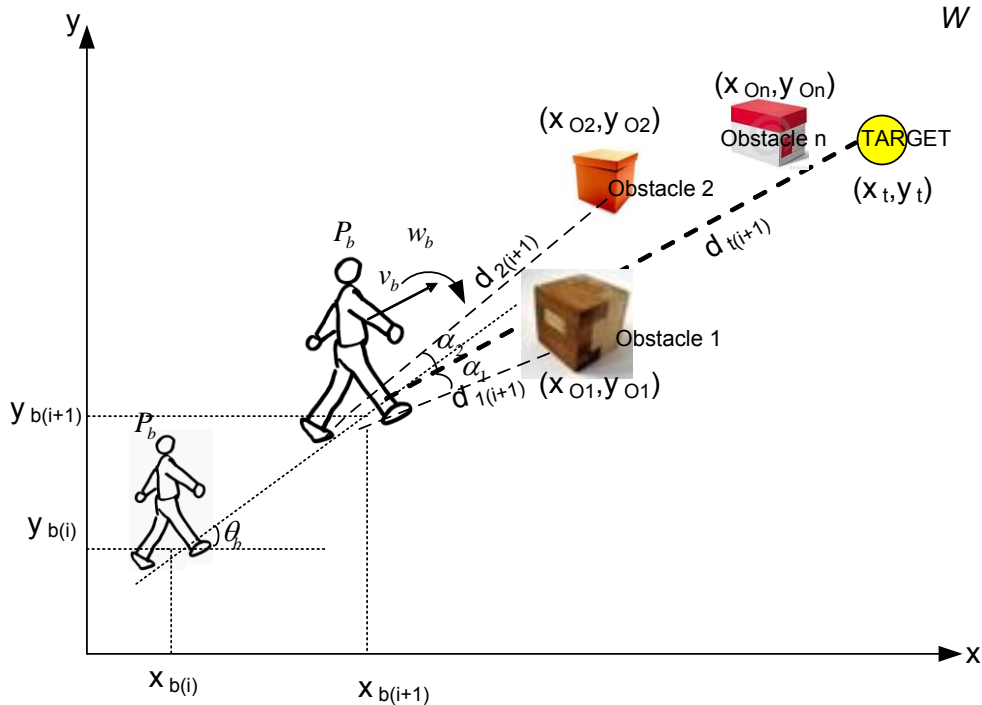


Fig. 4.3: Navigation of walking person under multi-obstacles environment

and desired direction angle (ϕ) is modified according to person as follows:

$$\phi_{i+1} = \tan^{-1} \left(\frac{y_t - y_{b(i+1)}}{x_t - x_{b(i+1)}} \right) \quad (4.4)$$

By considering Equation 4.2 and 4.4, it can be concluded that there is a relation between recommended direction angle (ϕ) and velocity of person.

Therefore, while guiding person, variables distance to target (d_t) and direction angle (ϕ) have to be controlled at each decision point regarding obstacles. For example; if there are two obstacles in front of the walking person with a distance of $d_{1(i+1)}$ and $d_{2(i+1)}$ as shown in Fig. 4.3, then the distances to obstacles can be calculated as

$$d_{1(i+1)} = \sqrt{(x_{01} - x_{b(i+1)})^2 + (y_{01} - y_{b(i+1)})^2} \quad (4.5)$$

$$d_{2(i+1)} = \sqrt{(x_{02} - x_{b(i+1)})^2 + (y_{02} - y_{b(i+1)})^2} \quad (4.6)$$

and the angle (α_1) between obstacle 1 and target point, and similarly the angle (α_2) between obstacle 2 and target point can be computed as

$$\alpha_{1(i+1)} = \left\| \tan^{-1} \left(\frac{y_t - y_{b(i+1)}}{x_t - x_{b(i+1)}} \right) - \tan^{-1} \left(\frac{y_{01} - y_{b(i+1)}}{x_{01} - x_{b(i+1)}} \right) \right\| \quad (4.7)$$

$$\alpha_{2(i+1)} = \left\| \tan^{-1} \left(\frac{y_t - y_{b(i+1)}}{x_t - x_{b(i+1)}} \right) - \tan^{-1} \left(\frac{y_{02} - y_{b(i+1)}}{x_{02} - x_{b(i+1)}} \right) \right\| \quad (4.8)$$

Assume that α_k represents the system's detection range in terms of angle and let $\alpha_{k_{\max}}$ denotes the maximum detection angle or in other words the border of detection range, then to avoid obstacles following rules should be taken into account [276]:

- (i) If $(\alpha_{1(i+1)} > \alpha_{k_{\max}}) \wedge (\alpha_{2(i+1)} > \alpha_{k_{\max}})$, which represents that there is no obstacle in the detection range, then there will be no avoidance strategy. This means go straight (zero) or $w_b = 0$ (Table 4.1).
- (ii) If $((\alpha_{1(i+1)} \leq \alpha_{k_{\max}}) \wedge (\alpha_{2(i+1)} > \alpha_{k_{\max}})) \vee ((\alpha_{1(i+1)} > \alpha_{k_{\max}}) \wedge (\alpha_{2(i+1)} \leq \alpha_{k_{\max}}))$, which represents only either one is in the detection range, then there is only one obstacle to be avoided. Therefore, the question is simplified as how to avoid just one obstacle; turn right or left, or in other words $w_b > 0$ or $w_b < 0$ (Table 4.1).

(iii) If $((\alpha_{1(i+1)} \leq \alpha_{k_{max}}) \wedge (\alpha_{2(i+1)} \leq \alpha_{k_{max}}))$, which represents both are in the detection range then, there are two obstacles to be avoided. Thus, select the obstacle that should be avoided by considering the minimum distance rule $(\min(d_{1(i+1)}, d_{2(i+1)}))$ as follows [276]:

- 1) If $d_{1(i+1)} < d_{2(i+1)}$, then firstly avoid first obstacle (O1), secondly avoid second obstacle (O2).
- 2) If $d_{1(i+1)} > d_{2(i+1)}$, then first avoid second obstacle (O2), secondly avoid first obstacle (O1).
- 3) If $d_{1(i+1)} = d_{2(i+1)}$, then compare $\alpha_{1(i+1)}$ and $\alpha_{2(i+1)}$
 - a) If $\alpha_{1(i+1)} < \alpha_{2(i+1)}$, then select obstacle 1 (O1) as target obstacle to be avoided.
 - b) If $\alpha_{1(i+1)} > \alpha_{2(i+1)}$, then select obstacle (O2) as target obstacle to be avoided.
 - c) If $\alpha_{1(i+1)} = \alpha_{2(i+1)}$, then select one of them randomly: Obstacle 1 or Obstacle 2 as target obstacle to be avoided.

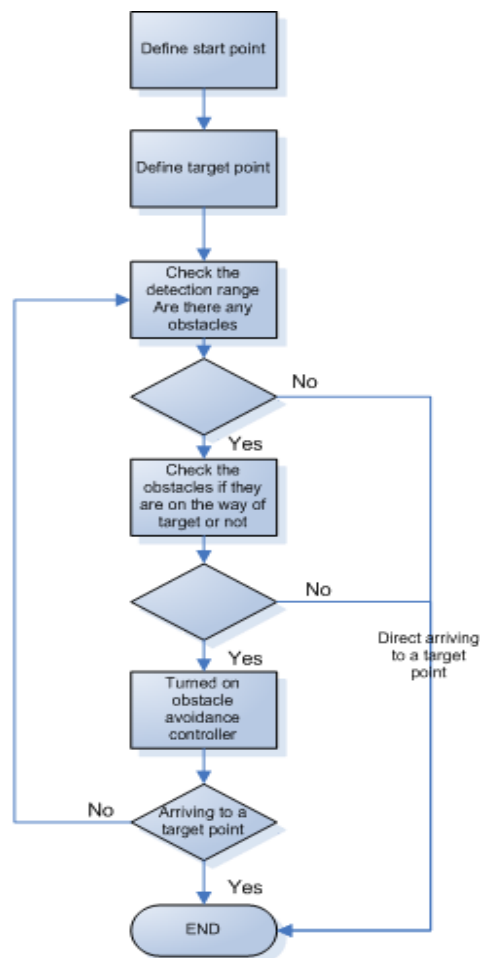


Fig. 4.4: Basic flow diagram of obstacle avoidance strategy

According to above obstacle avoidance strategy, a control system was considered and developed in order to guide visually impaired person. Fig. 4.4 shows the basic flow diagram of avoidance strategy.

During the design of control system, fuzzy and neural network approaches were used. Before explaining our neuro-fuzzy controller in detail, the basic principles of neural network and fuzzy logic are given.

4.1.4 Principals of neural network architecture

A neuron with a single scalar input and bias are given in Fig. 4.5. The scalar input p is transmitted through a connection with its strength by the scalar weight w to form the product wp , again a scalar. Additionally, a scalar bias b is simply added to product wp as shown by the summing junction. Finally, the transfer function net input n , again a scalar, becomes the sum of the weighted input wp and the bias b . Here f is a transfer function that takes the argument n and produces the output a .

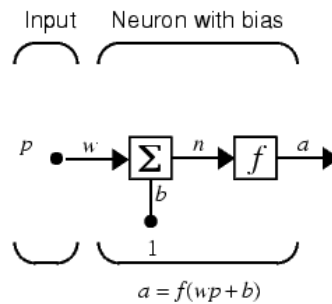


Fig. 4.5: Simple neuron model

Two or more of the neurons can be combined in a layer to form a network. A network can include one or more such layers. In Figure 4.6, a one-layer network with R input elements and S neurons are shown.

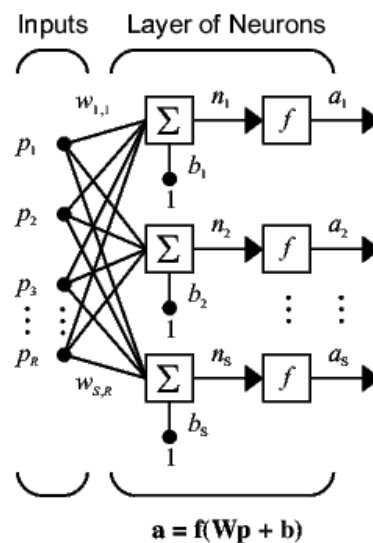


Fig. 4.6: One-layer neural network

R denotes the number of input elements in input vector and S denotes the number of neurons in layer. In this network, each element of the input vector p is connected to each neuron input through the weight matrix W . Finally, the neuron layer outputs form a column vector a . The expression for output a can be summarized as on below figure:

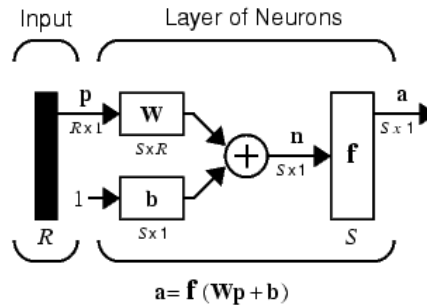


Fig. 4.7: Abbreviated notation of one layer neural network

In this figure, p is an R length input vector, W is an $S \times R$ matrix, and a and b are S length vectors. As defined previously, the neuron layer includes the weight matrix, the multiplication operations, the bias vector b , the summer, and the transfer function boxes [283].

4.1.5 Basis of fuzzy logic

Fuzzy logic starts with the concept of a fuzzy set. A fuzzy set is a set that contains elements with only a partial degree of membership. Let X denote the universe and its elements denote x , then a fuzzy set A in X is defined as a set of ordered pairs.

$$A = \{x, \mu_A(x) \mid x \in X\}$$

$\mu_A(x)$ is called the membership function (or MF) of x in A . A membership function (MF) is a curve that represents how each point in the input space is mapped to a membership value (or degree of membership) between 0 and 1. Fig. 4.8 shows some examples of membership functions [284].

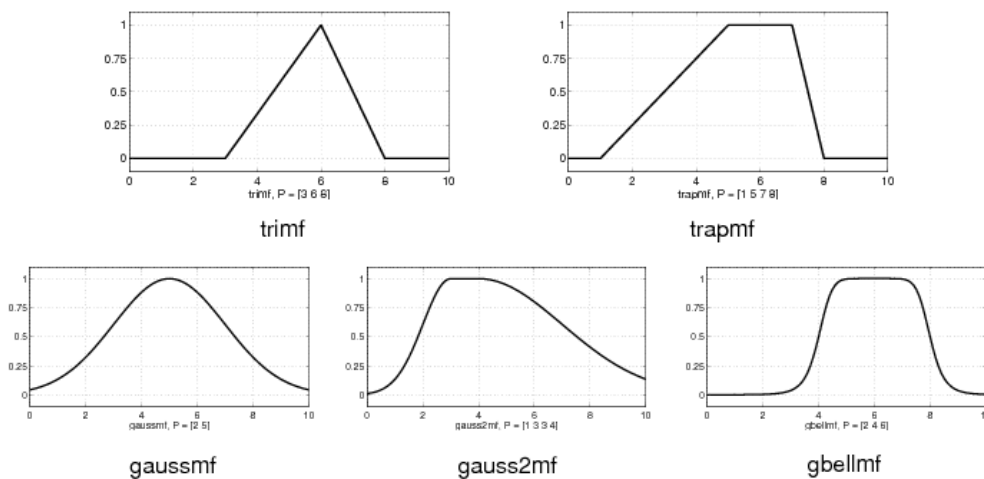


Fig. 4.8: Examples of membership functions

A	B	$\min(A,B)$
0	0	0
0	1	0
1	0	0
1	1	1

AND

A	B	$\max(A,B)$
0	0	0
0	1	1
1	0	1
1	1	1

OR

A	$1 - A$
0	1
1	0

NOT

Fig. 4.9: Boolean logic ANDs and ORs and NOTs [284]

In fuzzy logic, the operations are based on standard Boolean logic as seen in Fig. 4.9. Moreover, because there is a function behind the truth table rather than just the truth table itself, values other than 1 and 0 take place. Fig. 4.10 shows how fuzzy inference connects with logical operations.

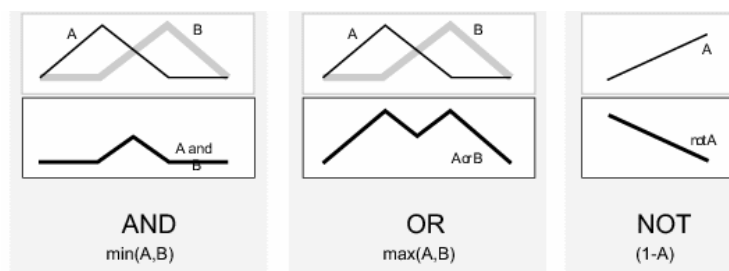


Fig. 4.10: Fuzzy inference with logical operations [284]

By considering logical operations, if-then rules are formed. These if-then rule statements are used to formulate the conditional statements that comprise fuzzy logic.

Fuzzy inference process comprises five parts: fuzzification of the input variables, application of the fuzzy operator (AND or OR) in the antecedent, implication from the antecedent to the consequent, aggregation of the consequents across the rules, and defuzzification [284].

Step 1-Fuzzify inputs: Take the inputs and determine the degree of membership between 0 and 1 (Fig. 4.11)

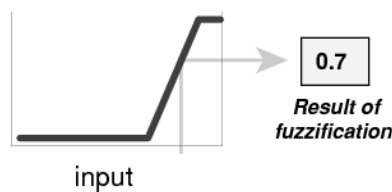


Fig. 4.11: Fuzzify inputs [284]

Step 2- Apply fuzzy operator: The input to the fuzzy operator is two or more membership values from fuzzified input variables. If there are multiple parts to the antecedent, apply fuzzy logic operators in order to obtain a single number between 0 and 1. This is the degree of support for the rule. This number is then applied to the output function. Fig. 4.12 shows the example of OR operator application.

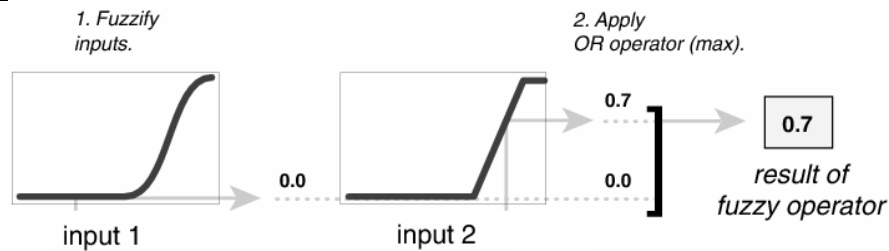


Fig. 4.12: Example of Step:2-Apply fuzzy operator [284]

Step 3-Apply implication method: Use the degree of support for the entire rule to shape the output fuzzy set. The consequent of a fuzzy rule assigns an entire fuzzy set to the output. Fig. 4.13 shows the example of application of implication operator (MIN).

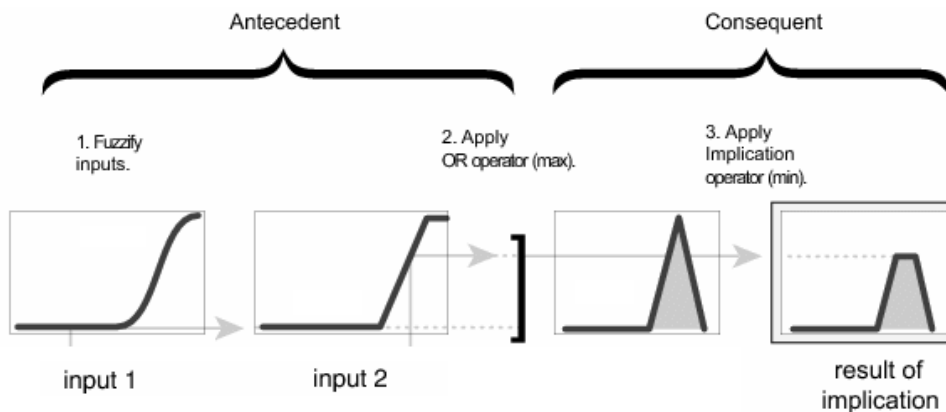


Fig. 4.13: Example of Step:3-Apply implication method [284]

Step 4-Aggregate all outputs: In order to make a decision about system, the rules must be combined in some manner. Aggregation is the process that transfers the output fuzzy sets for each rule into a single fuzzy set. Aggregation occurs before the defuzzification. The inputs of the aggregation process are the output functions returned by the implication process for each rule. For aggregation process, three methods are commonly used: Maximum, probabilistic OR, sum (simply the sum of each rule's output set). Fig. 4.14 shows how the outputs of each three rule are combined or aggregated into a single fuzzy set

Step 5- Defuzzification: Result of aggregation includes a range of output values that must be defuzzified in order to resolve a single output value from the set. There are different methods for defuzzification, however the most popular defuzzification method is the centroid calculation, which calculates the center of area under the curve. An example of centroid defuzzification methods is shown in Fig. 4.15

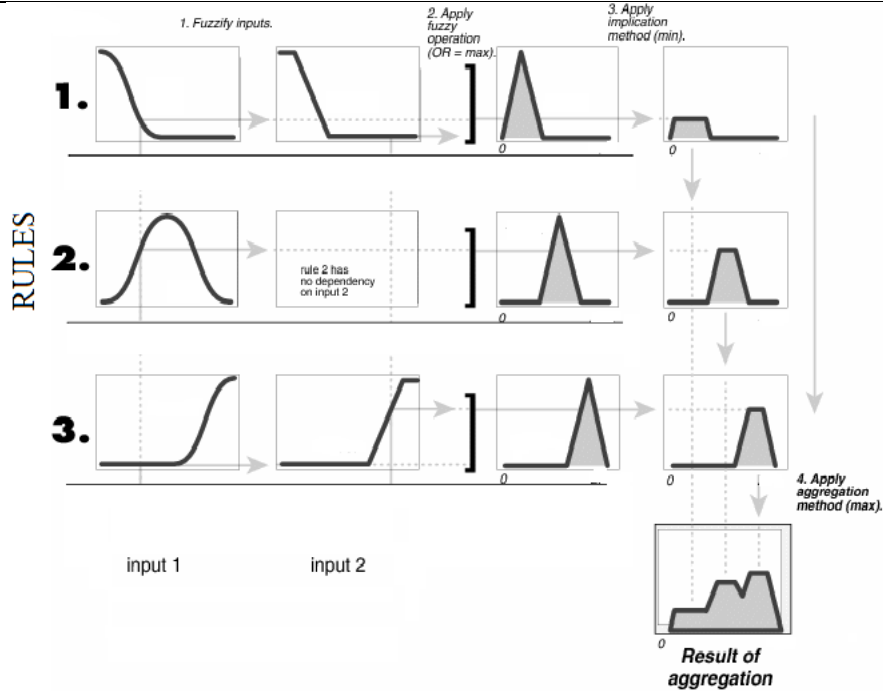


Fig. 4.14: Example of aggregation method (max) [284]

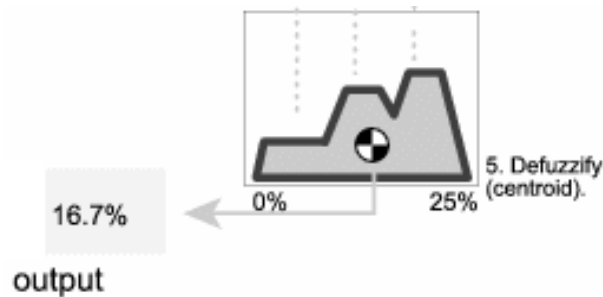


Fig. 4.15: Example of defuzzification method (centroid) [284]

Finally, steps mentioned above from beginning to end describes the whole process of Fuzzy Inference System. By using fuzzy inference systems, fuzzy logic controllers can be designed as shown in Fig. 4.16.

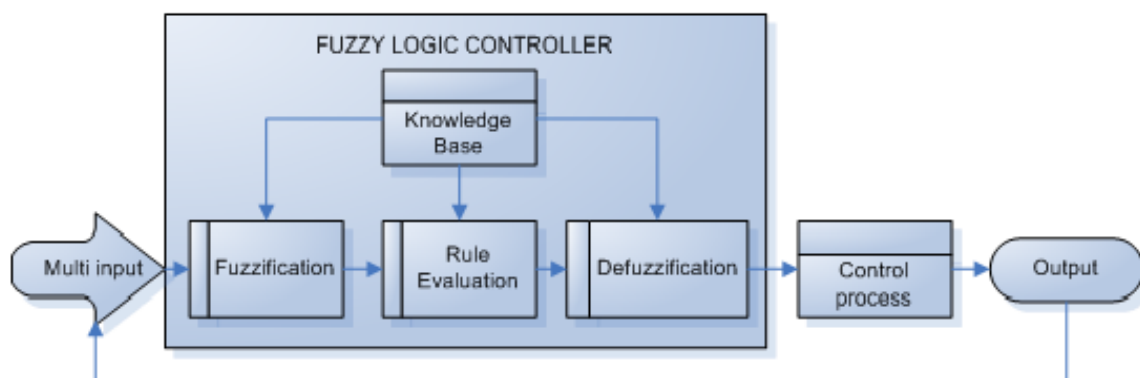


Fig. 4.16: Composition diagram of fuzzy controller

4.1.6 Neuro-fuzzy control algorithm for obstacle avoidance

In our smart clothing system, four sensors integrated to front side of garment perceive surroundings. While the wearer navigates in an unknown environment, ultrasonic sensors detect the presence of obstacles as well as measure the distance to obstacles. During the design process, four sensors were divided into two groups (see Fig. 4.17). In order to differentiate height of obstacles, two ultrasonic sensors were considered to be placed up position on the garment while the other two placed down position. Besides, in order to differentiate position of obstacles whether they are on the left side or right side due to wearer's position, two sensors were considered to be placed at left part of the garment while the other two at right part. Thus, by considering two groups of four-sensor situation; probable cases for detection of obstacles were determined and obstacles' potential positions with regard to person position were examined. Fig. 4.18 shows some cases for obstacle's position.

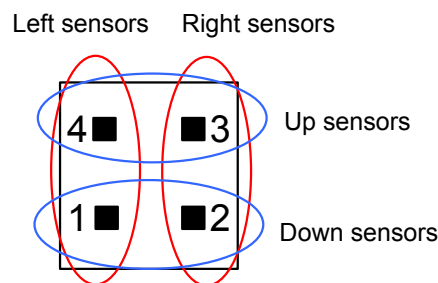


Fig. 4.17: Sensor's position on the garment

Before developing control system, at first some assumptions were made according to our study. The target location and user's location was considered to be known variables by the user heuristically. Thus, in our system only the data got by sensors were used as inputs of controller (see Fig. 4.2). The framework of the proposed control system is shown in Fig. 4.19

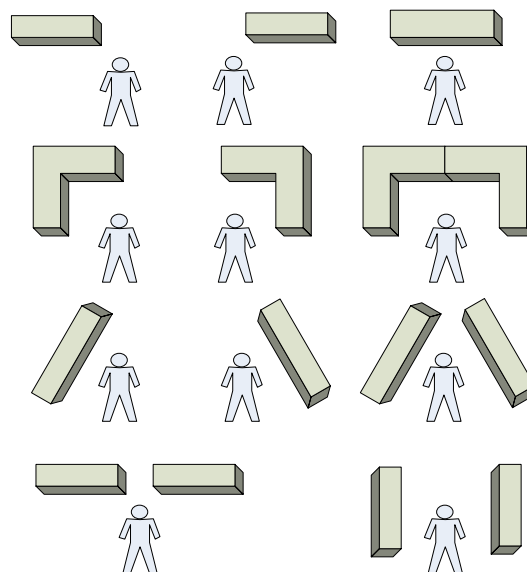


Fig. 4.18: Different cases between obstacles and user

In the control system, data filtration and pre-processing is conducted based on data from all sensors in order to understand if there are any obstacles or not. When the user's path is blocked by an obstacle, the avoiding action is necessary not to crash obstacle by this way neuro-fuzzy obstacle avoidance controller takes place and gives output to make turns to avoid collision. When all distance values got from sensors are larger than a predefined value range, this situation is regarded as there is no obstacle to be avoided. As a result, user is guided to go straight (zero/no turn) as an output response.

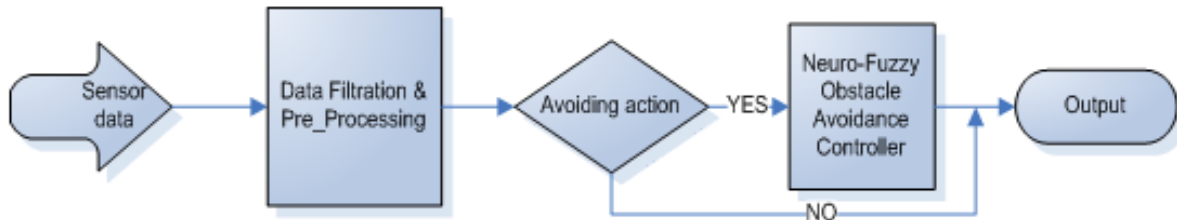


Fig. 4.19: Framework of control system for proposed smart clothing

After the data filtration and pre-processing by using neural network and fuzzy logic principles, a neuro-fuzzy obstacle avoidance controller for smart clothing system was designed. The structure of the proposed neuro-fuzzy controller is shown in Fig. 4.20. The inputs of controller are the outputs of sensors: the averaged distances to obstacles Xd_{1i} , Xd_{2i} , Xd_{3i} , Xd_{4i} obtained from the sensor 1, sensor 2, sensor 3, and sensor 4 respectively. The output signal from the neuro-fuzzy controller is the turning angle and direction. The algorithm starts with the data filtration process.

4.1.6.1 Data filtration and pre-processing

In this process, data generating by sensors are either eliminated or transmitted to controller. It was known that our sensor detection range is up to 6.45 meter [204].

In order to give controller decision, by considering our requirements a predefined value was determined at first. A value of 2.5 meter (predefined value) was considered for elimination of data that means if the sensor detects the distance to an object larger than 2.5 meter or in other words if the object locates 2.5 meter or further away from user's location then, the data is eliminated and considered as there is no object on the way of user. Thus, in the first algorithm all averaged input data larger than 2.5 meter is being filtered and directly sent to go straight position (zero) which is interpreted as no turning action.

Secondly, for the averaged data smaller than 2.5 meter was interpreted as there is an object/s on the way of user, and according to decision of position of object, it is sent to avoidance strategy to be processed. Fig. 4.20. explains the data elimination process.

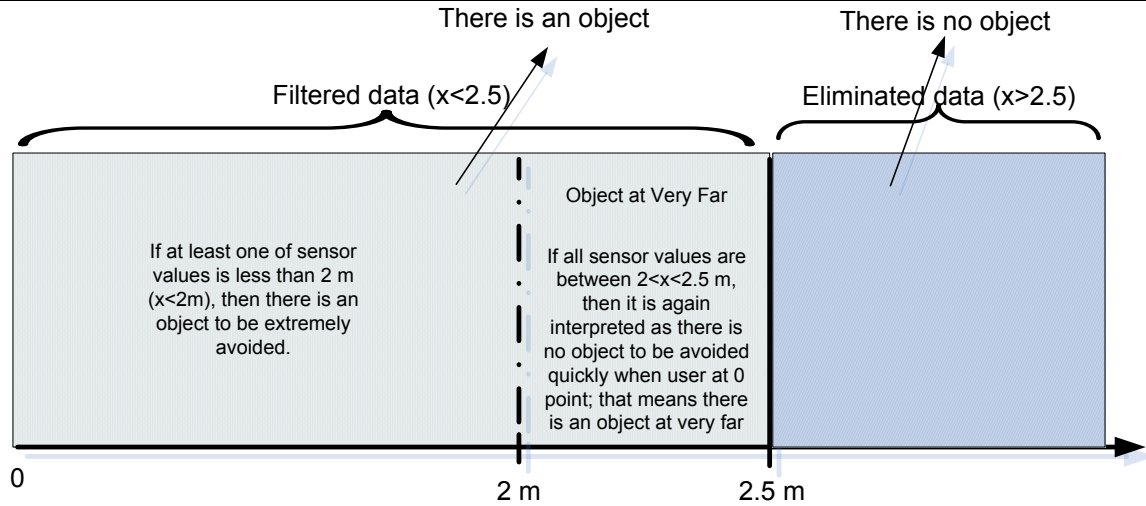


Fig. 4.20: Data elimination process

In fact, when the all sensor values are between 2 and 2.5 meter, they are interpreted as there is an object at very far and it is not necessary to avoid this obstacle at this time interval quickly. Thus, this situation is again assigned to go straight position (zero) as if there is no obstacle that should be avoided. However, sometimes one, two or three of sensors may measure between 2 and 2.5 m because of detection of obstacle at far away or noisy data, while the other/s detects an obstacle within 2 meter. In this case, if at least one of the sensor values is less than 2 meter, it is interpreted as there is an obstacle that should be extremely avoided.

In order to decide object's position, experiments were conducted with various object's position in x and y-axis in a real-time environment as explained in Section 3.3. For each sensor 9900 data was obtained. In this concept, possible scenarios for detection of objects by using four sensors were formed as follows:

<Algorithm 1- Data filtration and pre-processing>

```

if  $Xd_{1i} > 2 \ \& \ Xd_{2i} > 2 \ \& \ Xd_{3i} > 2 \ \& \ Xd_{4i} > 2$ 
    there is no obstacle;

elseif  $Xd_{1i} < 2 \ \& \ Xd_{4i} < 2 \ \& \ (Xd_{2i} > 2 \ | \ Xd_{3i} > 2)$ 
    obstacle at the left;

elseif  $(Xd_{1i} > 2 \ | \ Xd_{4i} > 2) \ \& \ Xd_{2i} < 2 \ \& \ Xd_{3i} < 2$ 
    obstacle at the right;

elseif  $(Xd_{1i} < 2 \ | \ Xd_{4i} < 2) \ \& \ Xd_{2i} > 2 \ \& \ Xd_{3i} > 2$ 
    obstacle at the left;

elseif  $Xd_{1i} > 2 \ \& \ Xd_{4i} > 2 \ \& \ (Xd_{2i} < 2 \ | \ Xd_{3i} < 2)$ 
    obstacle at the right;
    
```

```
elseif  $Xd_{1i} < 2 \ \& \ Xd_{2i} < 2 \ \& \ Xd_{3i} > 2 \ \& \ Xd_{4i} > 2$ 
    if  $Xd_{1i} > Xd_{2i}$ 
        obstacle at the right;
    else
        obstacle at the left;
    end

elseif  $Xd_{1i} > 2 \ \& \ Xd_{2i} > 2 \ \& \ Xd_{3i} < 2 \ \& \ Xd_{4i} < 2$ 
    if  $Xd_{4i} > Xd_{3i}$ 
        obstacle at the right;
    else
        obstacle at the left;
    end

elseif  $Xd_{1i} < 2 \ \& \ Xd_{2i} > 2 \ \& \ Xd_{3i} > 2 \ \& \ Xd_{4i} < 2$ 
    obstacle at the left;

elseif  $Xd_{1i} > 2 \ \& \ Xd_{2i} < 2 \ \& \ Xd_{3i} < 2 \ \& \ Xd_{4i} > 2$ 
    obstacle at the right;

elseif  $Xd_{1i} < 2 \ \& \ Xd_{2i} < 2 \ \& \ Xd_{3i} < 2 \ \& \ Xd_{4i} < 2$ 
    obstacle at the front;
else
    there is no obstacle;
end
```

After determining object's position with Algorithm 1, (Algorithm 1 was tested with real time measurements and regarding Table 3.3 results the success of the algorithm was found 97.98 % by using MATLAB), data is sent to one of the avoidance strategy: left, front, and right obstacle avoidance.

This time, neuro-fuzzy algorithm starts processing data. Neuro-fuzzy algorithm is composed of

A- Input layer

B- Hidden layer (rule layer and consequence layer)

C- Output layer

In the input layer and hidden layer of algorithm, fuzzy inference system (FIS) takes place. To set up the fuzzy inference system, MATLAB® Fuzzy Logic Toolbox was used. As shown in Fig. 4.21, three types of fuzzy inference system was developed namely; (i) left obstacle avoidance, (ii) front and (iii) right obstacle avoidance fuzzy inference system. Fig. 4.22 shows the developed fuzzy inference system for left obstacle avoidance. Similarly, front and right obstacle avoidance fuzzy inference system were also developed.

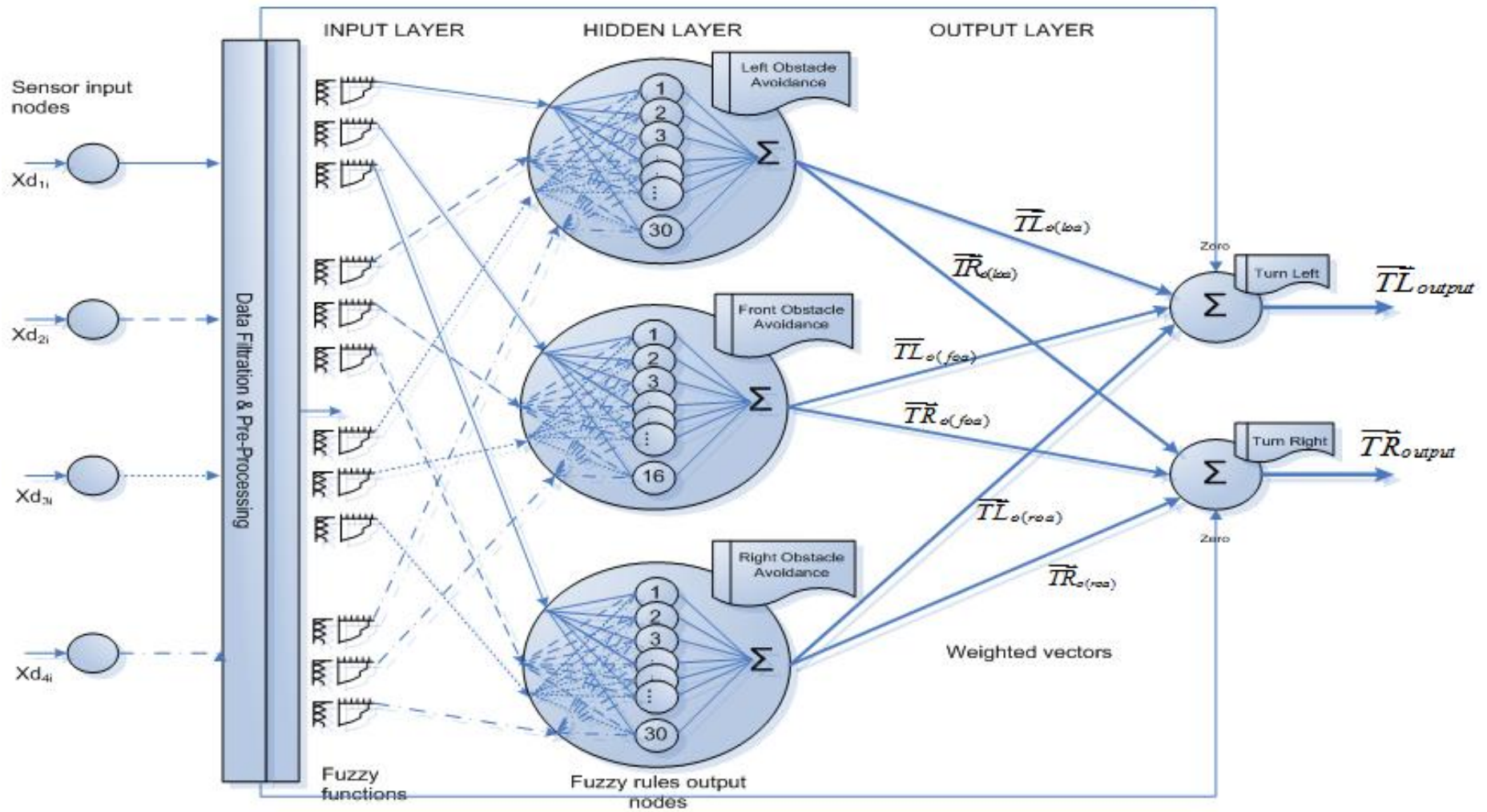


Fig. 4.21: Proposed neuro-fuzzy control system for the smart clothing

4.1.6.2 Input layer / Fuzzification

The fuzzification procedure maps the crisp input values to the linguistic fuzzy terms with membership values between 0 and 1.

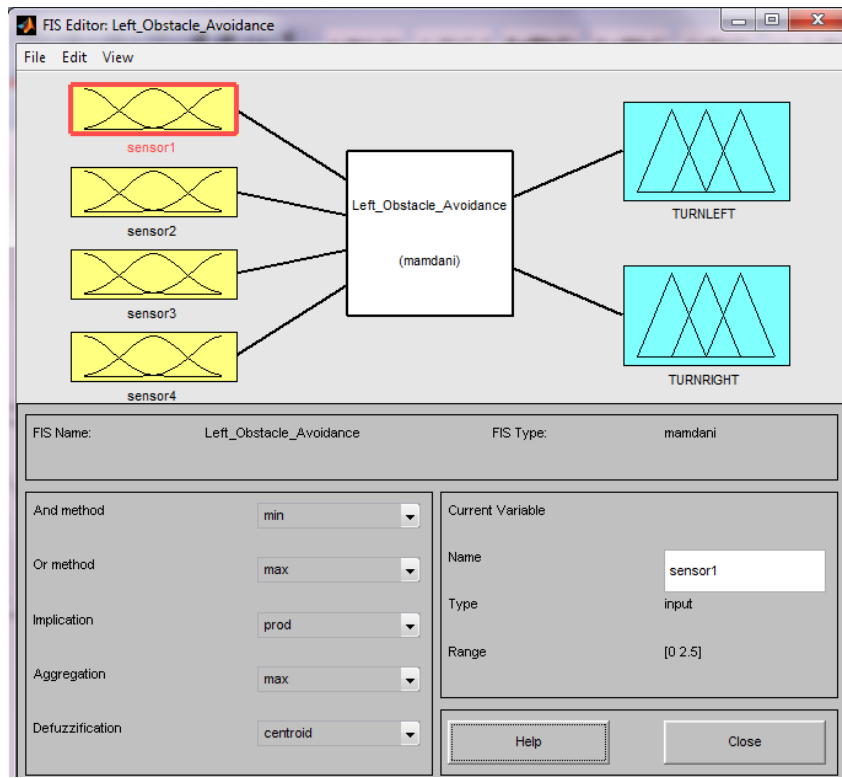


Fig. 4.22: Fuzzy Inference System (FIS) for left obstacle avoidance

In this layer, the inputs are the filtered data and each of these inputs is classified to fuzzy set membership functions. The inputs of fuzzy inference system are “averaged measured distances to an obstacle” information from sensor 1, sensor 2, sensor 3 and sensor 4, which are described by three linguistic variables: Near, Far and Very Far. The domain of functions is being from 0 (minimum) to 2.5 meter (maximum) for each sensor.

The two linguistic variables near and far were described by triangular membership functions, whereas very far described by trapezoidal membership function as shown in Fig. 4.23.

Indeed, the input values between $2 < X_{di} \leq 2.5$ was regarded as there is no detected obstacles neither at far nor near, thus they were interpreted as Very Far (see developed fuzzy rules).

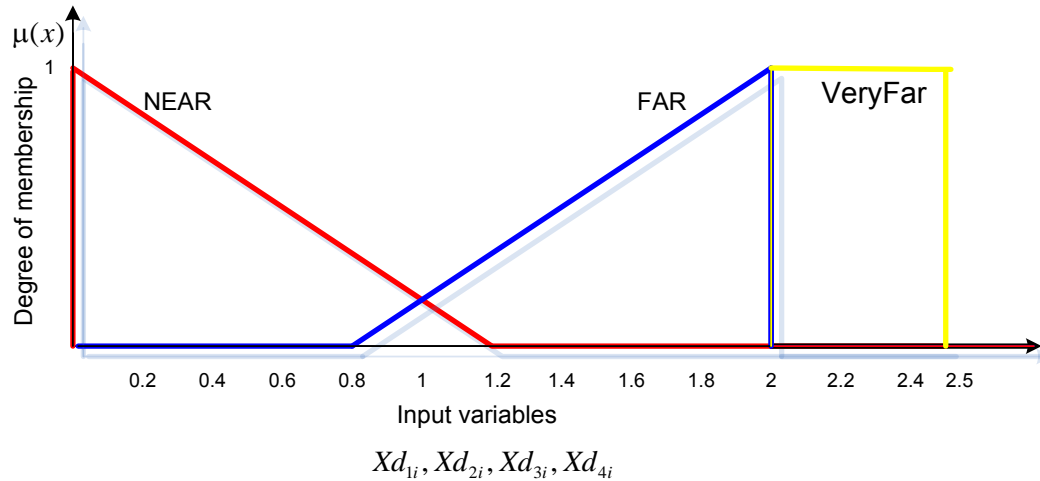


Fig. 4.23: The membership functions for input variables

For instance, the measured distances by sensors to an obstacle located at (-10, 60) cm are shown in Fig. 4.24. As seen in the figure, sensor 1 and sensor 2 detect the obstacle around 60 cm while sensor 3 and sensor 4 does not detect the obstacle. When the averaged values of these data are taken, firstly they are filtered and then each of these inputs is classified to fuzzy set membership functions as follows:

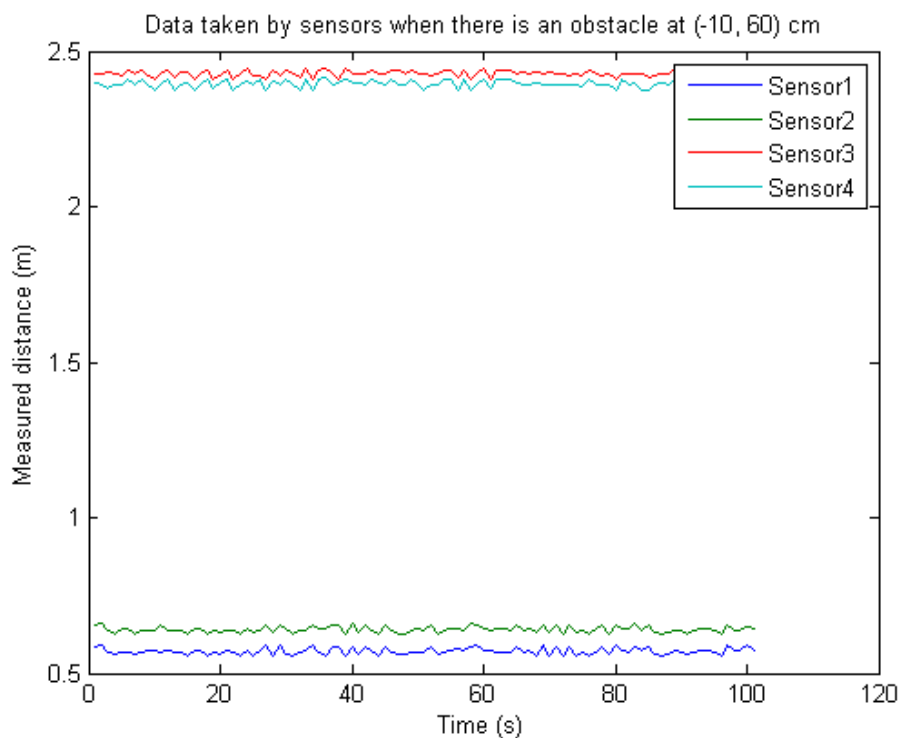


Fig. 4.24: Measurement results when the obstacle at (-10, 60) cm

(i) Since the “averaged measured distances to an obstacle” information from sensor 1 and sensor 2 is about 60cm, they are classified as “Near” and (ii) Since the “averaged measured distances to an obstacle” information from sensor 3 and sensor 4 is about 2.4 m, they are classified as “Very Far”.

The outputs of fuzzy inference system were also described by fuzzy linguistic variables, which are turn left small (S), medium (M), large (L), and very large (VL), and similarly turn right small (S), medium (M), large (L), and very large (VL) as shown in Fig. 4.25 and Fig. 4.26, respectively. The domain of functions is [-90 90]. All the linguistic variables were denoted by triangular membership functions (MF).

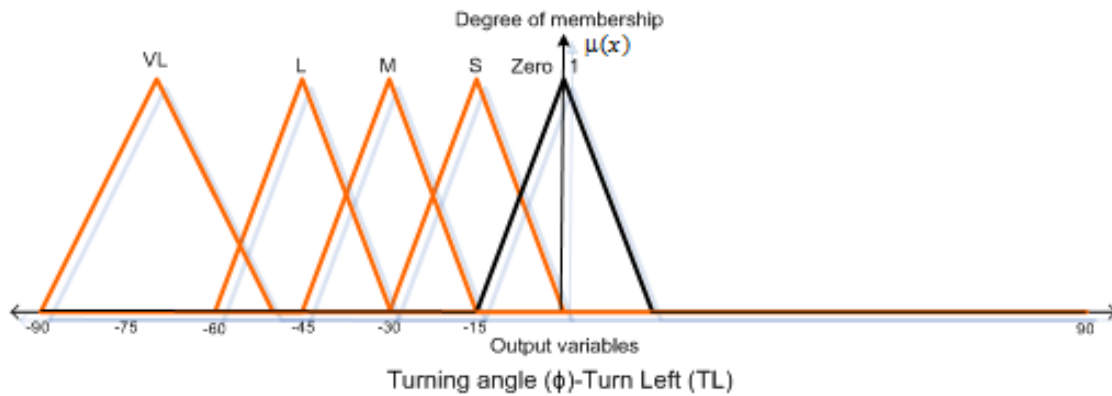


Fig. 4.25: The membership functions for output variables “turn left”

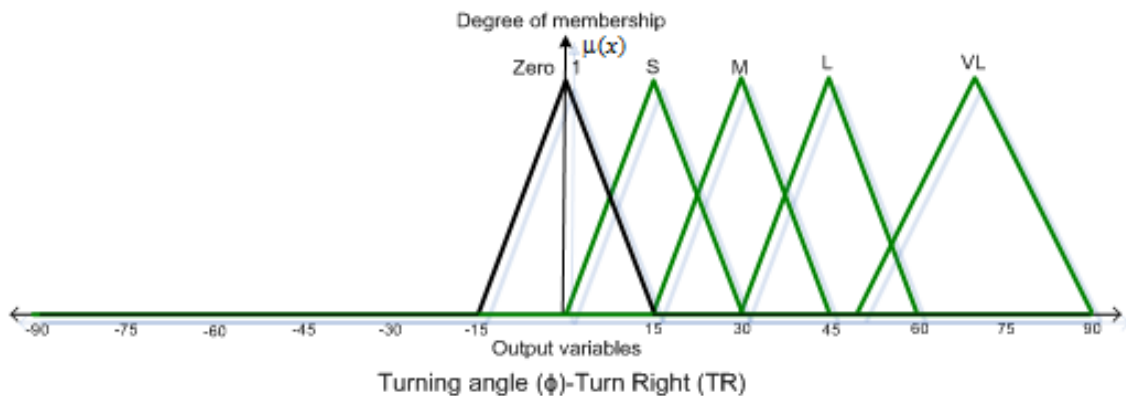


Fig. 4.26: The membership functions for output variables “turn right”

Triangular MF was mainly selected because of limited computational resources of microcontroller. In general, it is specified by three parameters {a, b, c} [266]:

$$triangle(x; a, b, c) = \begin{cases} 0, & x < a \\ \frac{x-a}{b-a}, & a \leq x \leq b \\ \frac{c-x}{c-b}, & b \leq x \leq c \\ 0, & c \leq x \end{cases} \quad (4.9)$$

By using min and max, an alternate expression can be written as:

$$triangle(x; a, b, c) = \max\left(\min\left(\frac{x-a}{b-a}, \frac{c-x}{c-b}\right), 0\right) \quad (4.10)$$

The parameters {a, b, c} determine the x coordinates of three corners of the underlying membership function.

4.1.6.3 Hidden layer-1 / Fuzzy rule layer

In this layer in order to control user’s motion in an environment as well as establish the relation between sensor values and turning angle, 77 rules were designed considering algorithm 1 and by taking Table 3.3-scenario 1 results into account. Hence, the rules are defined by human knowledge by using observed data (Table 3.3-scenario 1) taken by real time measurements and training of data was done off-line. Regarding Table 3.3 results according to object’s position determined by training of data, the turning angle of user was decided. Table 4.2 shows the recommended turning angle for user to avoid obstacle concerning its position. In the table “R” and “L” indicate the turn right and turn left, respectively. Additionally, as mentioned above, {Z, S, M, L, VL} values denote the turning angle in terms of linguistic variables.

Table 4.2: The relation between turning angle and detected object position

		Object at x-axis (cm)											
		-∞	-40	-30	-20	-10	0	10	20	30	40	-∞	
Object at y-axis (cm)	Turning angle (φ)												
	0-100	Z	RS	RS	RM	RL	RVL/LVL	LL	LM	LS	LS	Z	
	100-200	Z	RS	RS	RS	RM	RL/LL	LM	LS	LS	LS	Z	
	∞	Z	Z	Z	Z	Z	Z	Z	Z	Z	Z	Z	

Fuzzy rule layer (b)

During the fuzzy rules design; one rule was designed for the situation when there is not any obstacle on the way of user that means go straight or zero (no turning action). Besides, when there is an obstacle/s on the left, right or front of the user, 30, 30 and 16 rules were designed for left, right and front obstacle avoidance, respectively as shown in Appendix-C.

The reason for designing separate fuzzy inference systems (left, right, front) is that there are some rules which are common for left and right positioned obstacles. For instance; consider rules for left obstacle avoidance-algorithm 1 (Rule 6) and rules for right obstacle avoidance-algorithm 1 (Rule 6) (see Appendix-C):

-Algorithm 1 (Rule 6): $Xd_{1i} < 2$ & $Xd_{2i} < 2$ & $Xd_{3i} > 2$ & $Xd_{4i} > 2$

According to fuzzy inference system, the values Xd_{1i} and Xd_{2i} can correspond both Near or Far. Consider, both Xd_{1i} and Xd_{2i} correspond to Near. In this case by one fuzzy inference system, the position of obstacle can not be determined correctly whether the obstacle is on the left or right. However, it is known that if $Xd_{1i} > Xd_{2i}$ then, obstacle at the right; if $Xd_{1i} < Xd_{2i}$ then, obstacle at the left. Therefore, since there is no rule definition in FIS that identifies $Xd_{1i} > Xd_{2i}$ or $Xd_{1i} < Xd_{2i}$ condition, three fuzzy inference systems (left, right, front) have been separately considered to overcome this problem and not to guide user wrongly. Particularly, rules 21-22 and 24-25 in the left obstacle avoidance neuron and in the right obstacle avoidance neuron (see APPENDIX-C) explain this situation clearly.

4.1.6.4 Hidden layer-2/ Consequence layer: Fuzzy Implication - Defuzzification

c) Fuzzy Implication

The choice of fuzzy implication rule is very important when designing a fuzzy control system. Fuzzy implication evaluates the consequent part of each rule.

After the inputs have been fuzzified and degree of each rule is calculated using AND operator (see rules), the output membership function is then truncated by fuzzy implication. In this research, among the various implication methods, Larsen product implication method was used. The Larsen product implication is given by

$$\mu_{A \rightarrow B}(x, y) \equiv \mu_A(x) \cdot \mu_B(y) \quad (4.11)$$

where $A \rightarrow B$ denotes an implication in the universe U and V. It uses the arithmetic product between the two membership functions in the universe of discourses U and V [285].

All the rules were evaluated in this manner and output membership functions were aggregated using MAX operator to result in fuzzy output.

d) Defuzzification

The fuzzy implication and as well as aggregation yield the fuzzy output, which is the union of all individual rules that are validated for the control action in a cumulative manner using MAX (OR) operator. Conversion of this fuzzy output to crisp output is defined as defuzzification.

In our research the centroid method, which returns the center of area under the curve, was used for the proposed controller.

Let $\mu_{out}(TL_r)$ and $\mu_{out}(TR_r)$ show the center of membership functions of the output variables for left (*l*), front (*f*), and right (*r*) obstacle avoidance neurons after the evaluation of rules, where $r=1,2,3\dots n$ are the rule numbers for each avoidance neuron and TL_o and TR_o are the crisp values which describe the outputs for Turn Left and Turn Right commands. The value of the output control for each avoidance by centroid method is described as:

For left obstacle avoidance (*loa*) neuron, final output:

$$TR_{o(loa)} = \frac{\sum_{lr=1}^{30} TR_{lr} \mu_{out}(TR_{lr})}{\sum_{lr=1}^{30} \mu_{out}(TR_{lr})}, \quad TL_{o(loa)} = 0 \quad (4.12)$$

For right obstacle avoidance (*roa*) neuron, final output:

$$TL_{o(roa)} = \frac{\sum_{rr=1}^{30} TL_{rr} \mu_{out}(TL_{rr})}{\sum_{rr=1}^{30} \mu_{out}(TL_{rr})}, \quad TR_{o(roa)} = 0 \quad (4.13)$$

For front obstacle avoidance (*foa*) neuron, final output:

$$TL_{o(foa)} = \frac{\sum_{fr=1}^{16} TL_{fr} \mu_{out}(TL_{fr})}{\sum_{fr=1}^{16} \mu_{out}(TL_{fr})}, \quad TR_{o(foa)} = \frac{\sum_{fr=1}^{16} TR_{fr} \mu_{out}(TR_{fr})}{\sum_{fr=1}^{16} \mu_{out}(TR_{fr})} \quad (4.14)$$

When there is no object: $TL_{o(none)}=0$ and $TR_{o(none)}=0$

Example for working principle of FIS in Hidden layer of Neural Network

An example of proposed fuzzy inference system for front obstacle avoidance neuron is shown in Fig. 4.27, where sensor 1, sensor 2 and sensor 4 measure “near” while sensor 3 measures “far”. Let us explain how the FIS works.

As seen from the figure that sensor 1, sensor 2, sensor 3 and sensor 4 detect the obstacle at 0.496m, 0.539m, 1.70m and 0.453m, respectively. These inputs correspond to “near” and “far” linguistic variables in fuzzy inference as shown by yellow triangular.

Step 1- Fuzzification

First fuzzification procedure starts and by this way the degree of memberships $\mu(Xd_{1i}), \mu(Xd_{2i}), \mu(Xd_{3i}), \mu(Xd_{4i})$ are determined. Fig. 4.28-4.31 shows the fuzzification process for the 3rd rule in whole control system or in other words 3rd rule for front obstacle avoidance neuron.



Fig. 4.27: Implication and defuzzification process of front obstacle avoidance neuron fuzzy inference

Step 2- Apply fuzzy operator MIN

For 3rd rule: $\min (\mu(Xd_{1i}), \mu(Xd_{2i}), \mu(Xd_{3i}), \mu(Xd_{4i})) = 0.55$

For the rules between 1 and 16 rules except 3rd rule:

$\min (\mu(Xd_{1i}), \mu(Xd_{2i}), \mu(Xd_{3i}), \mu(Xd_{4i}))=0$ as also it can be noticed from the Fig. 4.27.

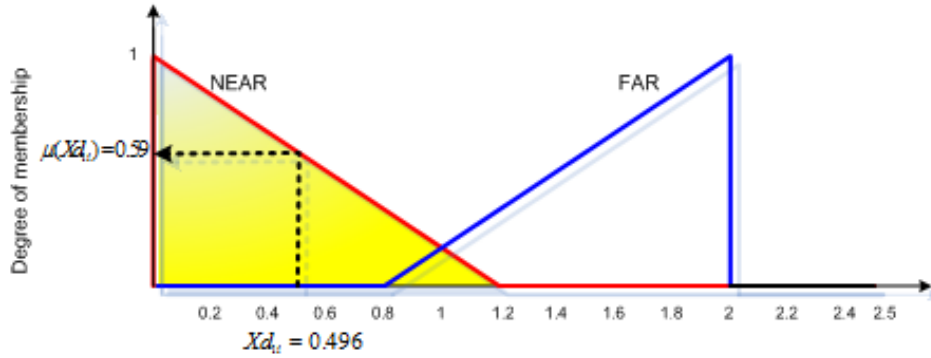


Fig. 4.28: Fuzzification for input 1 (data read by sensor 1) for the 3rd rule in front obstacle avoidance

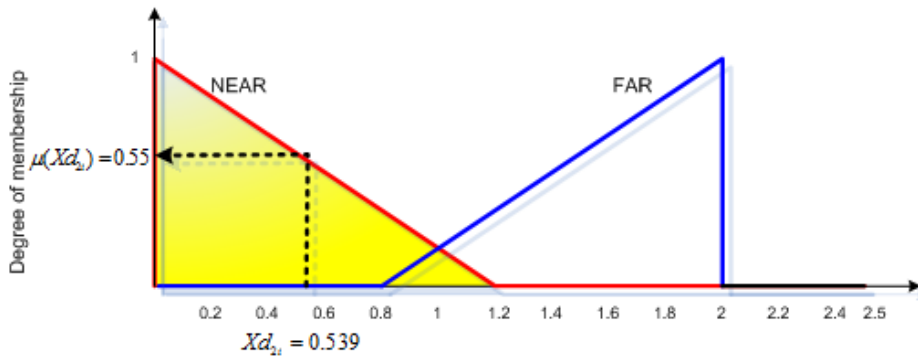


Fig. 4.29: Fuzzification for input 2 (data read by sensor 2) for the 3rd rule in front obstacle avoidance

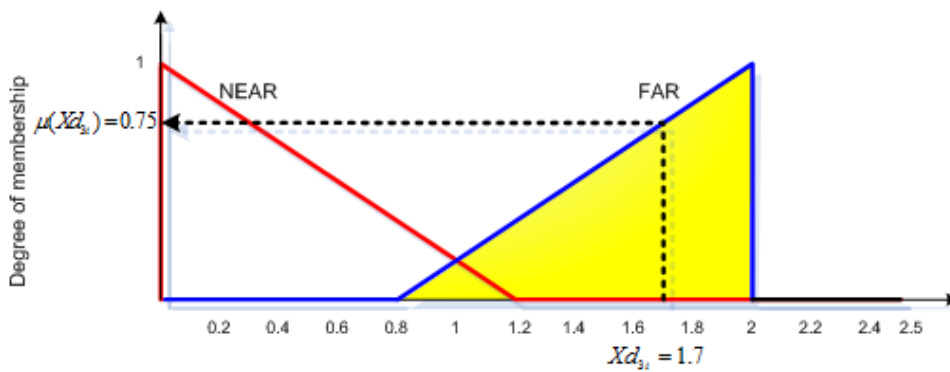


Fig. 4.30: Fuzzification for input 3 (data read by sensor 3) for the 3rd rule in front obstacle avoidance

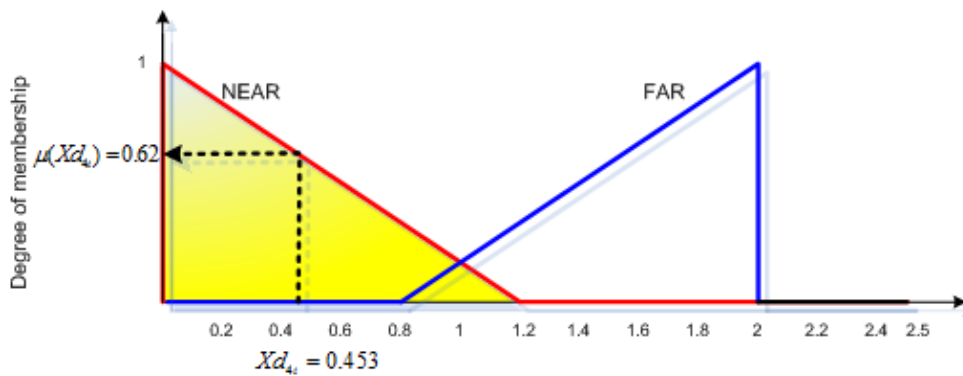


Fig. 4.31: Fuzzification for input 4 (data read by sensor 4) for the 3rd rule in front obstacle avoidance

Step 3- Fuzzy Implication

– Rule 3 implies that:

If $Xd_{1i} = \text{Near} \ \& \ Xd_{2i} = \text{Near} \ \& \ Xd_{3i} = \text{Far} \ \& \ Xd_{4i} = \text{Near} \Rightarrow \text{Turn Right VL}$

and fuzzy implication for this rule can be computed as

$$\mu_{[0-2.5] \rightarrow [0-90]}(Xd_{2i}, TR_{f3}) \equiv \mu_{[0-2.5]}(Xd_{2i}) \cdot \mu_{[0-90]}(TR_{f3}) \quad (4.15)$$

According to rule 3, $TR_{f3} = \text{VL}$ (Very Large) as shown in Fig. 4.32.

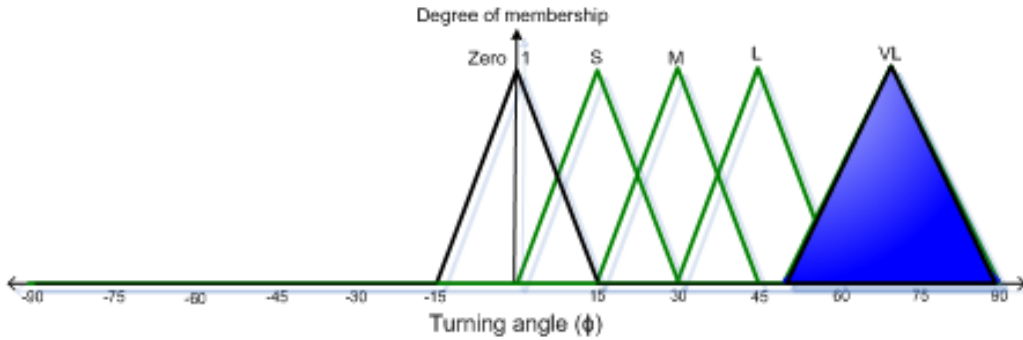


Fig. 4.32: Output membership function for 3rd rule in front obstacle avoidance

Since VL represents triangular function (50, 70, 90) then,

$$\mu_{[0-2.5] \rightarrow [0-90]}(Xd_{2i}, TR_{f3}) \equiv 0.55 \cdot \mu_{[0-90]}((50, 70, 90)) \quad (4.16)$$

$\mu_{[0-2.5] \rightarrow [0-90]}(Xd_{2i}, TR_{f3}) \equiv 0.55 \otimes (0, 1, 0)$ which shows the triangular function (50,70,90) with a degree of 0.55 as shown in Fig. 4.33

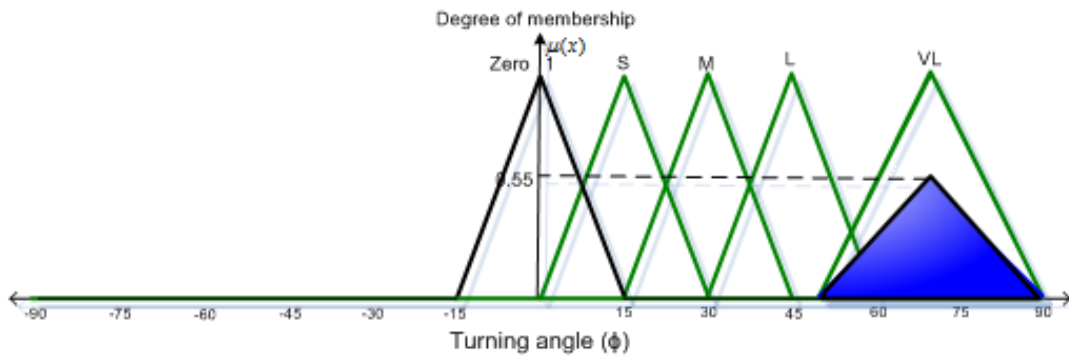


Fig. 4.33: Implication process for 3rd rule in front obstacle avoidance

For the rules between 1 and 16 rules except 3rd rule, since the

$\min(\mu(Xd_{1i}), \mu(Xd_{2i}), \mu(Xd_{3i}), \mu(Xd_{4i}))$ is zero then the fuzzy implication computed as below is also zero:

$$\mu_{[0-2.5] \rightarrow [0-90]}(\min(Xd_i), TR_{fr}) \equiv \mu_{[0-2.5]}(Xd_i) \cdot \mu_{[0-90]}(TR_{fr}) \wedge \mu_{[0-2.5] \rightarrow [0-90]}(\min(Xd_i), TL_{fr}) \equiv \mu_{[0-2.5]}(Xd_i) \cdot \mu_{[0-90]}(TL_{fr}) \quad (4.17)$$

$$= 0$$

Step 4- Defuzzification

After all 16 rules are evaluated in this manner and output membership functions are aggregated in a cumulative manner using MAX (or) operator to result in fuzzy output, defuzzification takes place. The output function for the front obstacle avoidance neuron is shown in Fig. 4.34.

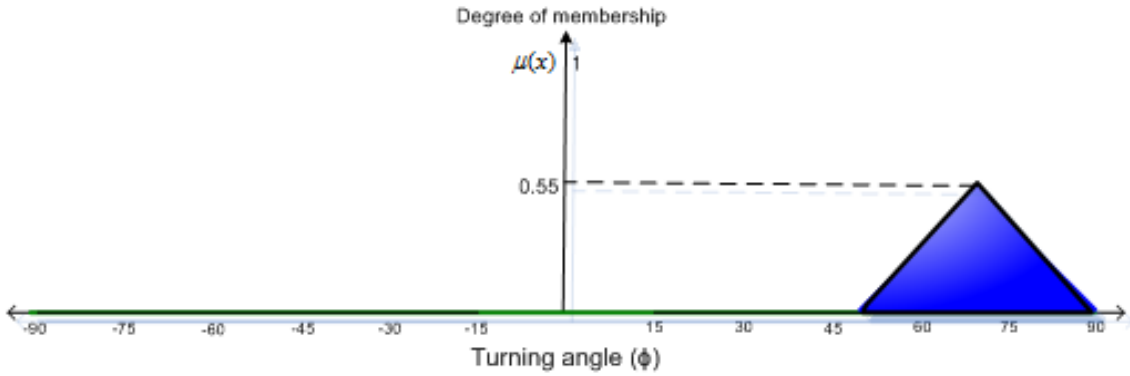


Fig. 4.34: Final output function for the front obstacle avoidance neuron for a given example

Since the output is computed for front obstacle avoidance (foa) neuron as Equation 4.14 and since $TL_{o(foa)}$ is calculated as zero then, $TR_{o(foa)}$ can be written as

$$TR_{o(foa)} = \frac{\sum_{fr=1}^{16} TR_{fr} \mu_{out}(TR_{fr}) - TR_{f3} \mu_{out}(TR_{f3}) + TR_{f3} \mu_{out}(TR_{f3})}{\sum_{fr=1}^{16} \mu_{out}(TR_{fi}) - \mu_{out}(TR_{f3}) + \mu_{out}(TR_{f3})} \quad (4.18)$$

which implies

$TR_{o(foa)} = \frac{0 + TR_{f3} \mu_{out}(TR_{f3})}{0 + \mu_{out}(TR_{f3})}$. As described above and seen in Fig. 4.34, TR_{f3} represents the triangular function (50, 70, 90) and $\mu_{out}(TR_{f3})$ shows the (0, 0.55, 0) for each point of triangular. By using the center point of triangular, the formula can be computed as

$$TR_{o(foa)} = \frac{70 \cdot 0.55}{0.55} = 70 \quad (4.19)$$

As a result; the recommended turning angles for user in order to avoid front obstacle are $TL_{o(foa)} = 0$ and $TR_{o(foa)} = 70$ as seen in Fig. 4.27, which means only Turn Right with an angle of 70° .

Indeed, this shows the object is just in front of the user at left. Therefore, user should be guided to avoid obstacle as soon as possible by recommending turning right with a large angle. As explained above, the given example was only for the front obstacle and processed by only front obstacle avoidance neuron.

Moreover, by using fuzzy logic toolbox in MATLAB, the control surface can be demonstrated. For instance, by processing the designed rules in right obstacle neuron, the relation between sensor values and turning angle in terms of linguistic values was established. A control surface was plotted to visualize the variation in turning angle with given sensor values when the sensor 3 reads 1.2 m (Far) and sensor 4 reads 2.4 m (VeryFar) in right obstacle avoidance neuron (see Fig. 4.35). In this figure for turn left, blue colors represent the critical regions corresponding turning angle very large while yellow colors represent the turning angle very small regions.

Besides as expected from the rules, it seems that there is no turning action for right, which corresponds 0° for the figure at right. Thus, control surface can explain us the relation between sensor readings and recommended turning angles.

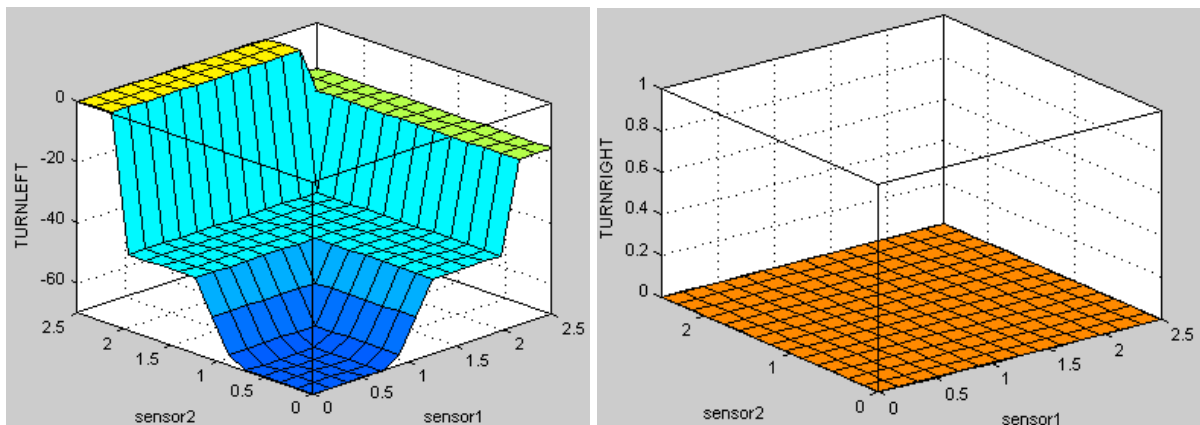


Fig. 4.35: Example of control surface for right obstacle avoidance neuron

4.1.6.5 Output Layer/Fuzzy-Neural Approximation and Final Outputs

Fig. 4.36 shows the basic diagram of fuzzy neural approximation of proposed controller. Here the weight functions are approximated by fuzzy sets.

In this output layer, the outputs of consequence layer will be the inputs of output layer and the final output will be desired turning angle in order to avoid obstacle. Thus, the weight functions of output layer will be the output functions $(O_{N_{TL}}, O_{N_{TR}})$ as shown in Fig. 4.36, where N denotes the number of neurons that are left obstacle avoidance neuron (1), front obstacle avoidance (2), and right obstacle avoidance (3), and TL denotes the turning position to left whereas TR denotes the turning position to right.

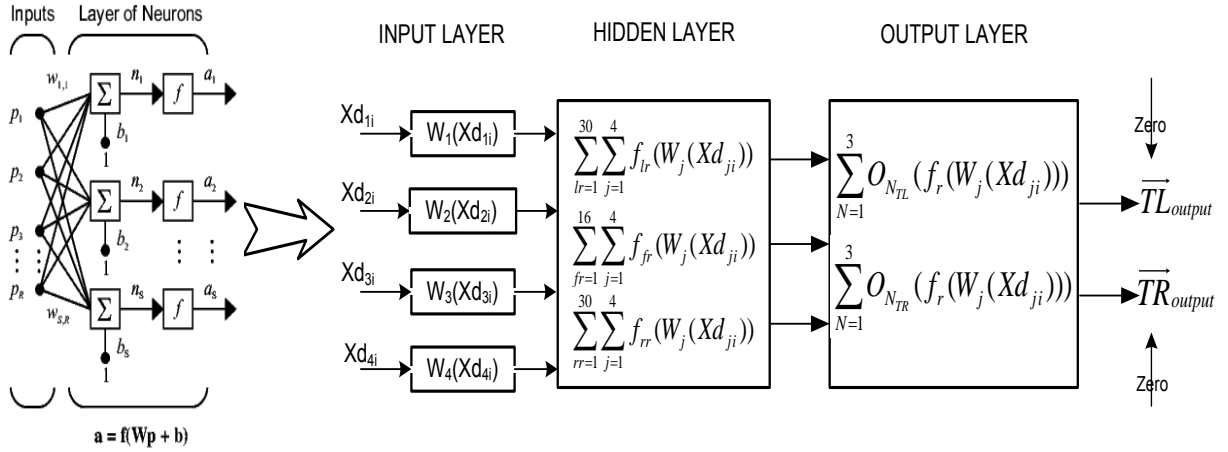


Fig. 4.36: Basic diagram of fuzzy neural approximation of proposed controller

As explained in Section 4.1.6.4, the output functions for left, front, and right obstacle avoidance neurons become:

$$O_{1TL} = TL_{o(loa)} = 0; \quad O_{1TR} = TR_{o(loa)} = \frac{\sum_{lr=1}^{30} TR_{lr} \mu_{out}(TR_{lr})}{\sum_{lr=1}^{30} \mu_{out}(TR_{lr})} \quad (4.20)$$

$$O_{2TL} = TL_{o(foa)} = \frac{\sum_{fr=1}^{16} TL_{fr} \mu_{out}(TL_{fr})}{\sum_{fr=1}^{16} \mu_{out}(TL_{fr})}; \quad O_{2TR} = TR_{o(foa)} = \frac{\sum_{fr=1}^{16} TR_{fr} \mu_{out}(TR_{fr})}{\sum_{fr=1}^{16} \mu_{out}(TR_{fr})} \quad (4.21)$$

$$O_{3TL} = TL_{o(roa)} = \frac{\sum_{rr=1}^{30} TL_{rr} \mu_{out}(TL_{rr})}{\sum_{rr=1}^{30} \mu_{out}(TL_{rr})}; \quad O_{3TR} = TR_{o(roa)} = 0 \quad (4.22)$$

Unless data is not processed in the avoidance neurons, which means it is eliminated by the data filtration and pre-processing, zero function ($Z(0)=0$) that demonstrates there is no obstacle on the way of user will come additionally, thus the final outputs are calculated as follows:

$$\overline{TL}_{output} = \sum_{N=1}^3 O_{N_{TL}} \vee Z(0) \quad (4.23)$$

$$\overline{TR}_{output} = \sum_{N=1}^3 O_{N_{TR}} \vee Z(0) \quad (4.24)$$

By combining Equations 4.20-4.24 the final outputs of the proposed neuro-fuzzy controller can be written finally as

$$\overline{TL}_{output} = \left(\frac{\sum_{fr=1}^{16} TL_{fr} \mu_{out}(TL_{fr})}{\sum_{fr=1}^{16} \mu_{out}(TL_{fr})} + \frac{\sum_{rr=1}^{30} TL_{rr} \mu_{out}(TL_{rr})}{\sum_{rr=1}^{30} \mu_{out}(TL_{rr})} \right) \vee Z(0) \quad (4.25)$$

$$\overline{TR}_{output} = \left(\frac{\sum_{lr=1}^{30} TR_{lr} \mu_{out}(TR_{lr})}{\sum_{lr=1}^{30} \mu_{out}(TR_{lr})} + \frac{\sum_{fr=1}^{16} TR_{fr} \mu_{out}(TR_{fr})}{\sum_{fr=1}^{16} \mu_{out}(TR_{fr})} \right) \vee Z(0) \quad (4.26)$$

Consequently, an algorithm for smart clothing system was described by fuzzy neural approaches. The system inputs were evaluated in terms of fuzzy relations, and then the outputs which are recommended turning angles in order to avoid obstacle were deduced by using neural network architecture.

As a result, the outputs of described neuro-fuzzy controller will be processed by microcontroller and thus, they will be transmitted to vibration motors as signals defined by intervals of “S”, “M”, “L”, “VL” for turning action in order to guide user. Before microcontroller programming, the success of the multi-layer fuzzy controller was given with comparison of one layer fuzzy inference system.

4.1.7 Implementation and comparison of multi-layer fuzzy controller with one layer fuzzy controller

The success of the proposed system was tested in real environment for its detection and avoidance capability. Data taken by real time experiment results were used to compare multi-layer fuzzy inference systems (left, right, front) with one layer fuzzy inference system.

One layer fuzzy system was designed using the same 77 rules presented in Appendix-C. The rules in left, right and front obstacle avoidance neurons (30, 30 and 16 rules) were gathered into one fuzzy inference to define one layer fuzzy inference system.

In order to validate the efficiency of the proposed system, it has been implemented on the real data acquired in the experimentation phase (using Table 3.3). Our system is then compared with a basic one layer FIS described above.

The outputs of these two systems are presented in Figures 4.37-4.39. These results demonstrate that in most of cases, the outputs of the two systems are the same or very close (less than 15°) of the target angles.

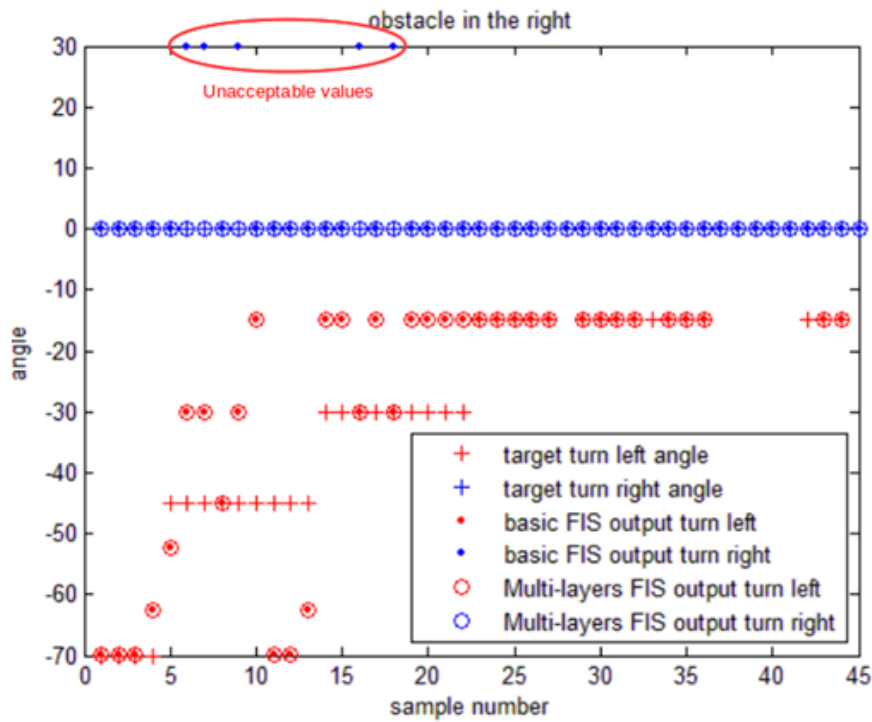


Fig. 4.37: Outputs of the multi-layer FIS and one-layer FIS and target angles when the obstacle is at the right

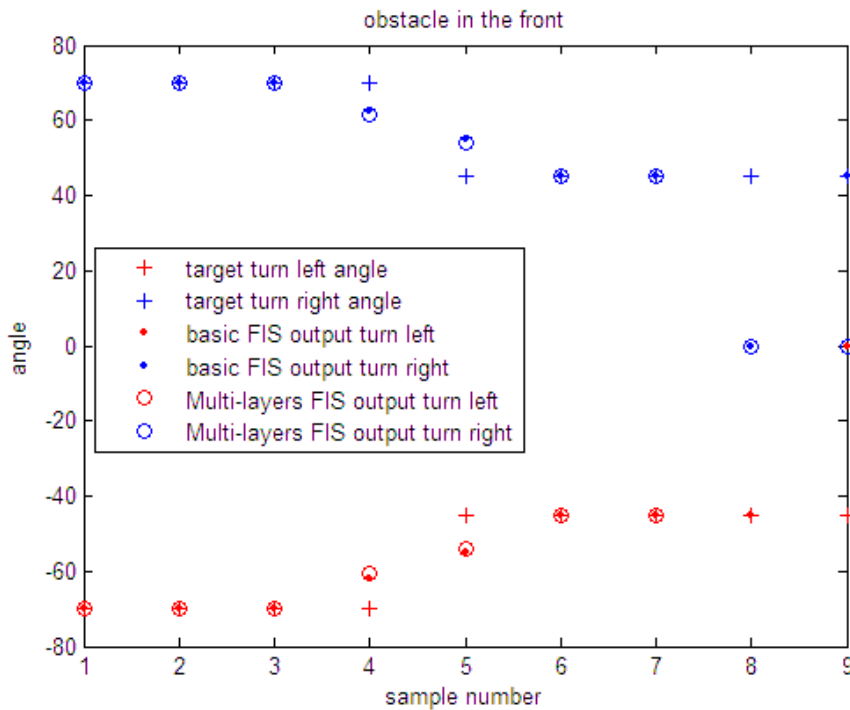


Fig. 4.38: Outputs of the multi-layer FIS and one layer FIS and target angles when the obstacle is in the front

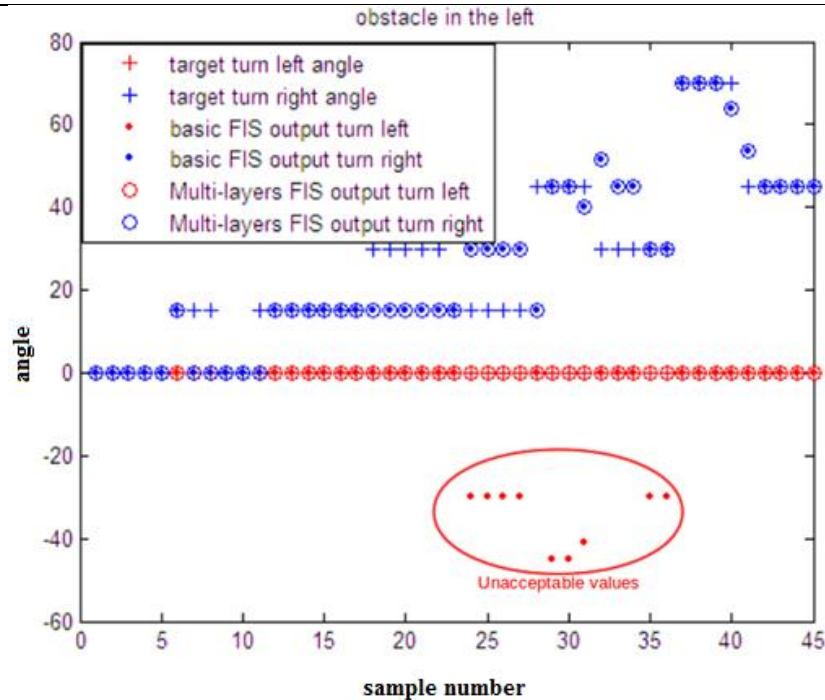


Fig. 4.39: Outputs of the multi-layer FIS and basic FIS and target angles when the obstacle is at the left

However, in specific cases that we explained earlier (see Section 4.1.6.3), the multi-layers FIS outperforms the basic FIS. Indeed, the basic FIS is not able to find the right direction especially for right and left avoidances.

In particular; when the obstacle is at the right, user should be guided by turning left in order to avoid it. Therefore; the expected output value of the fuzzy controller should be “Turn left with an angle and Turn right=0”. According to Fig.4.37, in some cases, basic one layer FIS presented unacceptable output values such as Turn Right with an angle of 30° instead of 0°. On the contrary, when the obstacle is at the left, user should be guided by turning right in order to avoid obstacle. Then, the expected output value of the fuzzy controller should be “Turn right with an angle and Turn Left=0”. Again, in some cases as seen in Fig.4.39, single FIS presented some unacceptable output values by giving wrong decision as “Turn Left with an angle” instead “Turn Left=0”. Therefore, in some cases single FIS did not present right decision output in terms of direction.

These errors are not acceptable in this kind of application since this leads to wrong orientation of the user and a probable collision with the obstacle. On the other side, for all the cases, multi-layer FIS presented right decision output in terms of direction. It has only errors in definition of angles like single FIS also has. For instance, in some cases instead of 45°, it presented 30°, or instead of 30°, it presented 15°. Indeed, the error in terms of angles can be acceptable because of the noisy data taken by sensors. It does not let the user a direct collision with an obstacle.

As a result, it is apparent that the multi-layer FIS gives better results than the one layer FIS and it is capable of guiding user in right decision output in terms of direction.

4.1.8 Microcontroller programming

In our study, Lilypad Arduino® microcontroller board was used. The board was based on ATmega328 (20MHz, 6-channel 10-bit ADC, 14-channel programmable I/O Lines) which the instruction set and technical specifications of the chip was given in ATMEL® Technical Data Manual [286]. In order to program microcontroller, Arduino developed a C based software. Thus, in this study Arduino’s own software® was preferred against assembly language due to easy programming.

The design of program is aimed at analysing signals acquired by the ultrasonic sensors and transforming them into different vibration intervals in the case of obstacles as mentioned earlier section for guiding person with recommended turning action. Fig. 4.40 shows the flow diagram of the microcontroller’s main program used in our study.

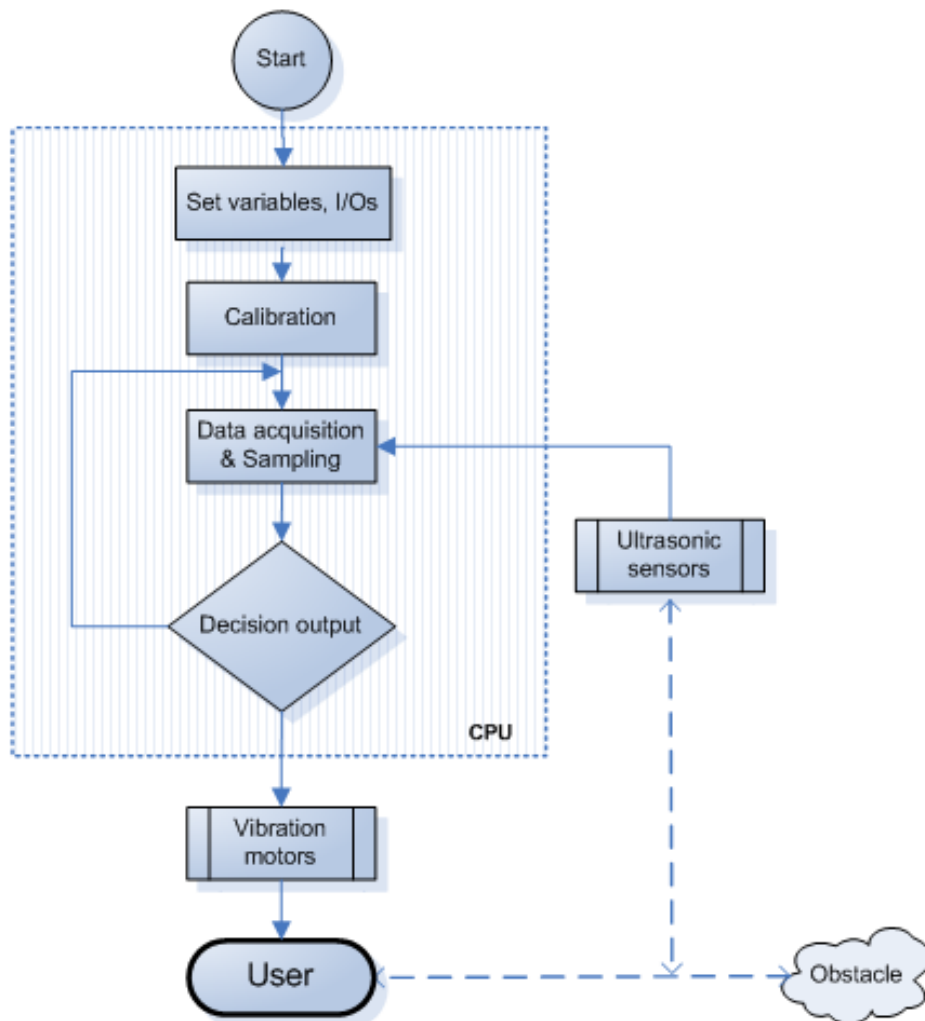


Fig. 4.40: Flow diagram of microcontroller’s main program

The main program works as follows: Firstly, program goes through an initialization phase where all variables are set, all I/O (Input/Output) ports are initialized and the external devices are enabled.

Next the processor waits for calibration during 5 seconds. In the calibration phase, all sensor outputs assign to the same range. Thus, they are capable of measuring the same interval.

Then, data acquisition and sampling loop starts. Signals acquired by ultrasonic sensors are processed within a sampling period. In that period, data processing is done in order to understand if there is an obstacle on the way of user or not.

According to data assessment, decision output is given as mentioned in earlier section such that if the obstacle is detected at the right, then actuation signals are transformed to left vibration motors in order to guide person by turning left or vice versa. If data assessment results in there is no obstacle on the way of the user, then there is no decision output as turn left or right, that means no actuation signals are transformed to vibration motors (zero=go straight) and by this way the next data acquisition and sampling loop takes place within a next time interval.

During the sampling process, smoothing algorithm was used in order to prevent noise or unexpected rapid changes. In this way, data sets are smoothed or in other words moving average values of data sets are calculated as shown in Fig. 4.41.

In microcontroller programming, the critical point is the period for sampling of data acquisition and output order. For our study, in order to determine sampling period as well as output order to guide user at a right time interval before crashing obstacle, first walking speed of visually impaired people was searched. Some studies reported that walking speed of normal pedestrian is between 1.22 m/sec (younger pedestrians) and 0.91 m/sec (older pedestrians) [287-288].

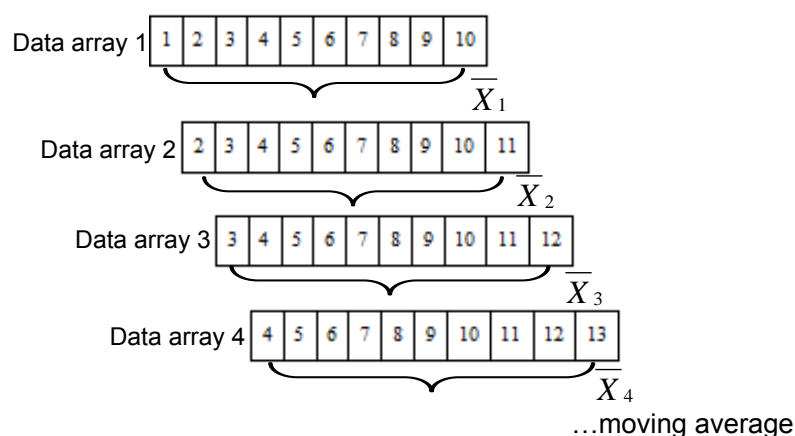


Fig. 4.41: Smoothing algorithm working principle

Considering this known fact and our observations, walking speed of visually impaired person was assumed as 0.6 m/sec. Furthermore, during walking the distance to be checked for obstacles was defined as 2.5 meters in earlier section.

Hence, maximum timing diagram for microcontroller programming including sampling loop and decision output period in a safety margins is shown in Fig. 4.42. At the 1st second, data acquisition as well as sampling is performed. Minimum sampling time of data was calculated and determined as approximately 10 ms (1 sampling loop \approx 10 ms). According to one data assessed after the sampling; one element of the decision matrix is updated. Hence, for the new condition, the decision output can be given after the ten sampling process at least approximately in 100 ms. As soon as decision output is given, actuation signals are transferred to vibration motors and thus, user can sense vibration motions in one second time. Sensation of vibration motions can start before the 2nd time interval ($t_{start-vib} \leq 1s$, $t_{duration-vib} \leq 1s$) due to decision output (The intervals given in the Fig. 4.42 shows the maximum timing including safety margins in order to be able to guide user before crashing an obstacle). After the sensations, one more second is given to user to compensate forward motion during turning action. In this manner, user's avoidance from an obstacle within a 2-2.5 m range is guaranteed.

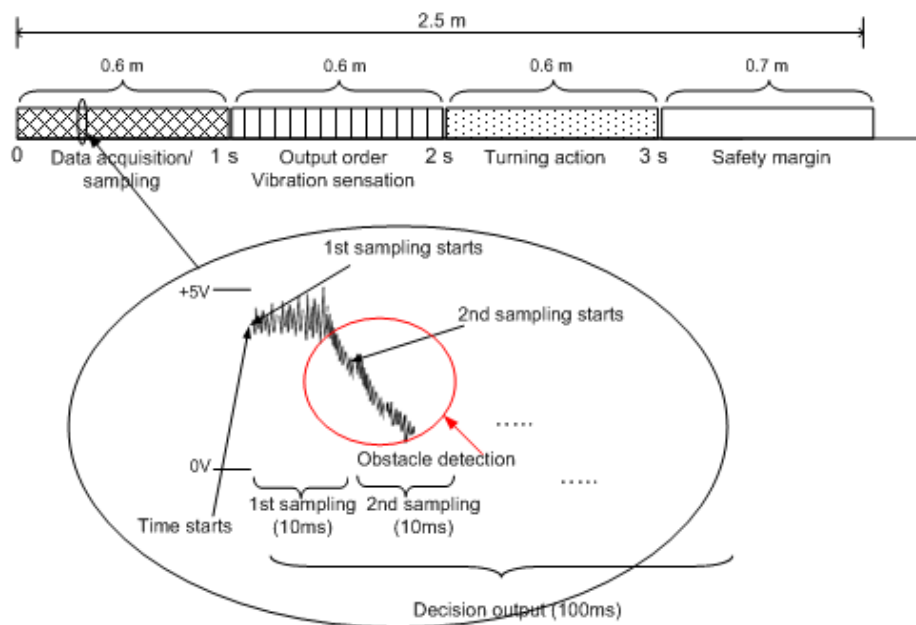


Fig. 4.42: Timing diagram for microcontroller

Thus, considering timing diagram and above mentioned information microcontroller programming has been done.

4.2. Design and Development Concept of Smart Clothing Prototype for Visually Impaired People

A smart clothing system is essentially a hierarchical process. At each level of hierarchy there are different factors which should be taken into account in order to transform garment into an interactive, intelligent infrastructure to facilitate information processing. During the design of interactive garment

two main critical issues which are requirements for electronic software and hardware components, and wearability performance should be elaborated together and compromised. Therefore a smart clothing system is a combination of different research fields especially electronics, information technology, control engineering, and textiles design.

Present research is aimed at designing and developing a smart clothing system to be able to guide visually impaired people during navigation by detecting as well as avoiding obstacles. In chapter 2, sensors and actuators have been realized for designing e-textile architecture of the aimed smart clothing system. In chapter 3, the system of e-textile architecture has been analyzed in detail. Towards our aim, how many sensors, actuators should be placed on the garment, which areas of the garment are suitable for higher vibrotactile perception as well as position of actuators, which type of conductive yarns should be used for acquiring better signal quality from the sensors have been found. In chapter 4, the algorithm for obstacle detection and avoidance was developed and by this way, microcontroller programming of the smart clothing prototype has been done. Within this section, all results and findings have been combined into a unique smart clothing system. Thus, the prototype development combined four key research fields; electronics, control engineering, information processing-technology and textiles.

During the development of prototype, firstly, the electronic circuit of the system according to electronic software and hardware requirements has been designed and then by considering wearability requirements and comfort of the user, the layout of the system has been devised.

4.2.1. Circuit design

The circuit was designed mainly considering multi-connection of ultrasonic sensors as discussed in Chapter 2. The schematic diagram of smart clothing system circuit is shown in Fig. 4.43.

The function of this circuitry is to digitize as well as transform analog signals acquired by sensors into vibration signal. It modulates analog signals into different levels of vibrations by identifying correlation between position of obstacle and required turning action (direction and angle) for user.

There are four key connections and elements for this circuitry; (i) one microcontroller, (ii) four ultrasonic sensors, (iii) eight vibration motors, and (iv) two power supply. Owing to findings earlier, four sensors were used to detect obstacles, eight vibration motors (each of four on the left and right) were used in order to guide user by recommending him/her turning direction and angle. As mentioned in the developed algorithm section commands for required turning action, which were processed through microcontroller by linguistic variables namely; turning left or right with an angle of small (S), medium (M), large (L), and very large (VL), were provided by eight vibration motors. In that purpose, microcontroller was used in order to process as well as transform data into commands.

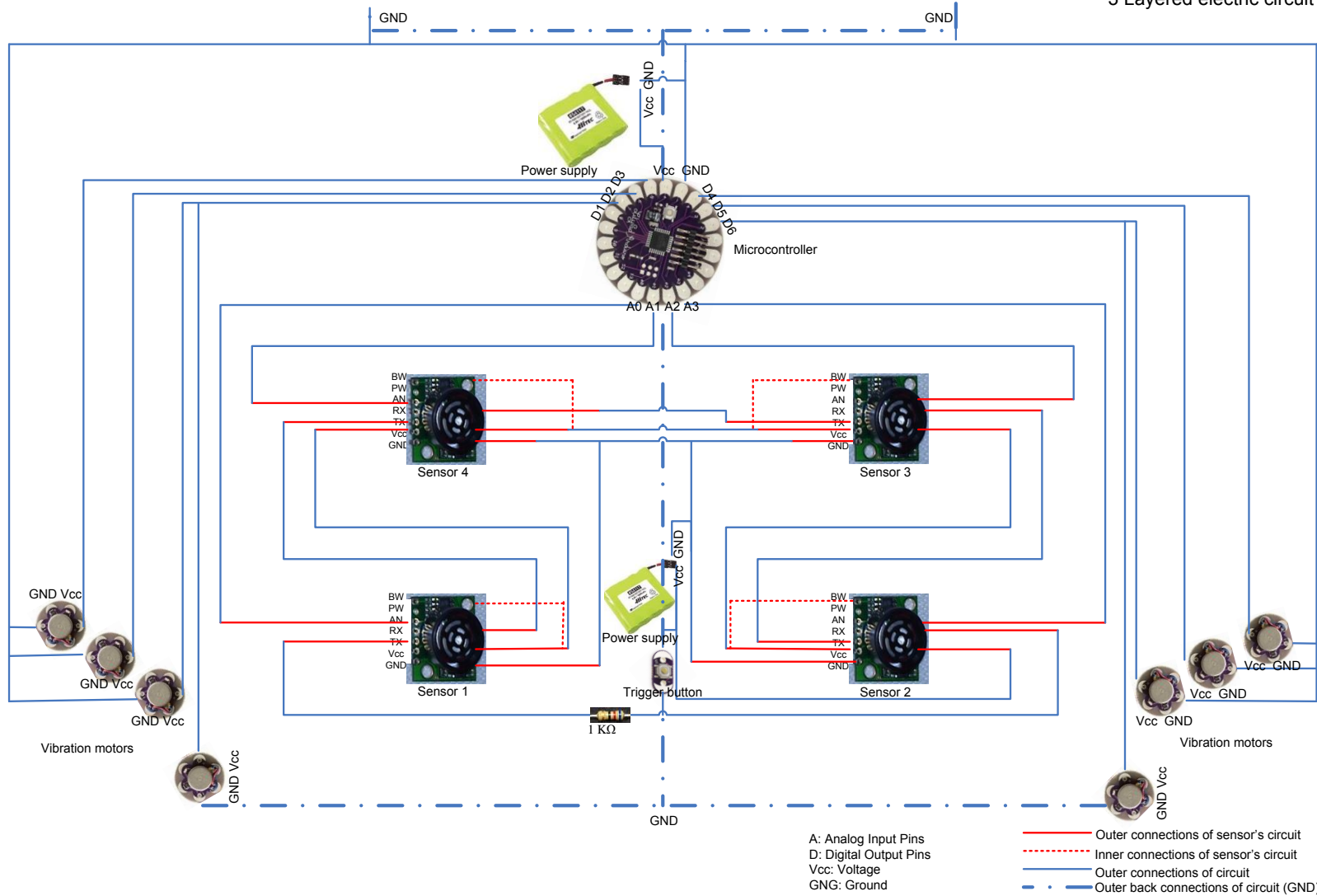


Fig. 4.43: Schematic diagram of smart clothing system circuit

4.2.1.1 Schematic circuit diagram of microcontroller

The LilyPad Arduino® microcontroller board was used. The LilyPad Arduino has a circle shape, approximately 50mm in diameter. The thickness of the board itself is 0.8mm and with the attached electronics it is approximately 3mm. As mentioned in section 4.1.8, the LilyPad Arduino can be powered via USB connection or with an external power supply. In our circuit design, it was powered with a 4.8V NiMH flat battery. The board is based on ATmega328 [289]. The schematic diagram of the board is shown in Fig. 4.44.

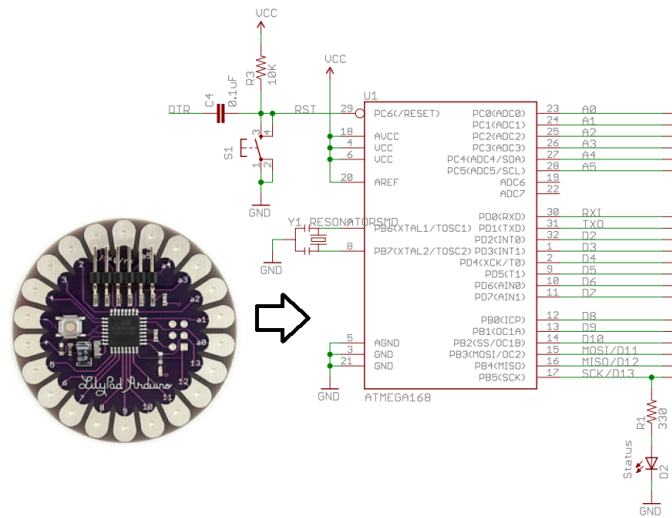


Fig. 4.44: Schematic diagram of LilyPad Mainboard Microcontroller [289]

With reference to Fig. 4.43 and 4.44, the pins for analog inputs; A0(23), A1(24), A2(25) and A3(26) were connected with the analog output pins of ultrasonic sensors. Vcc and GND pins were connected with the power supply, the pins for the digital outputs D2(32), D3(1), D4(2), D5(9), D6(10) and D7(11) were connected with the vibration motors' input pins.

4.2.1.2 Schematic circuit diagram of ultrasonic sensors

Fig. 4.45 shows the schematic circuit diagram of ultrasonic sensor. Sensor functions using active components consisting of an LM234, a diode array, PIC 16F676 microcontroller, together with a variety of passive components [204].

Here, the out pins GND, 5V, TX, RX, AN, and PW of each sensor were connected with the whole circuit according to multiconnection principles of sensor as discussed in Section 2.3.4. GND and Vcc (operates on 2.5V - 5.5V) pins were connected with 4.8V NiMH flat battery.

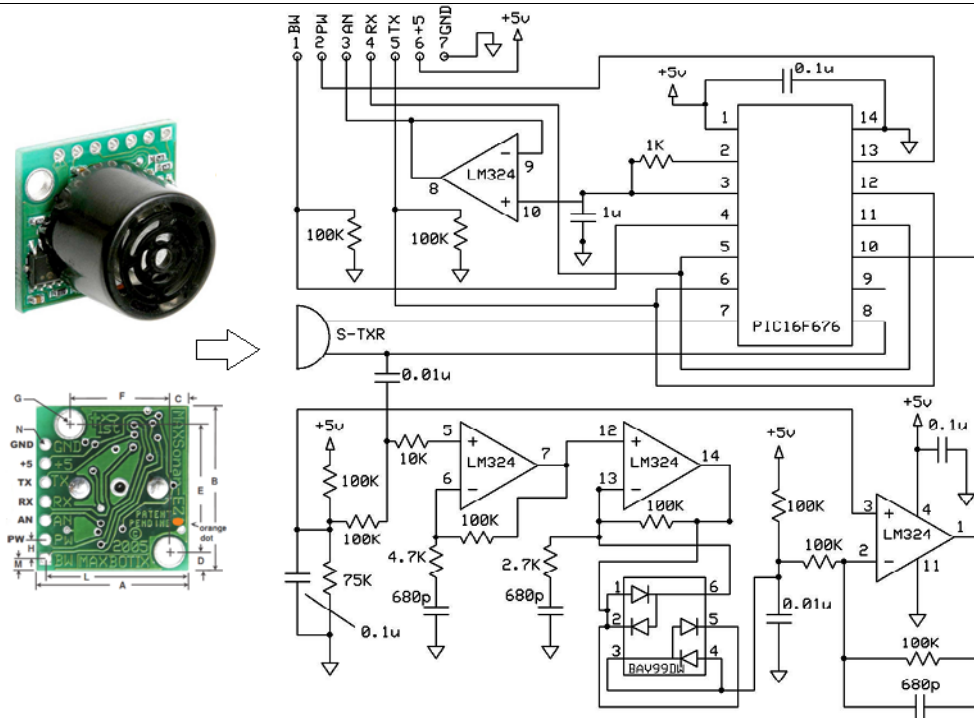


Fig. 4.45: Schematic circuit diagram of LV-MaxSonar®-EZ3 sensor [204]

The TX pin of the first sensor was connected with the RX pins of the second sensor (follow red colors in Fig. 4.43), and this was repeated up to 4th sensor. By this way the RX pin of each sensor was internally pulled high. This synchronization yields the communication of sensors within each other. The AN (analog output) pin of the each sensor was connected with the microcontrollers analog inputs (AI). AN pin of the sensor outputs analog voltage with a scaling factor of $V_{cc}/512$ per inch. This voltage calculation was used in microcontroller programming for interpreting distance to an obstacle. Moreover, BW pin of each sensor was held high by connecting it to Vcc pin of the sensor (follow red discrete line in Fig. 4.43). It was done in order to get low noise chaining. As mentioned in Section 2.3.4, a resistor $1\text{ K}\Omega$ was added to circuit between the last sensor’s TX back to the RX of the first sensor in order to keep running and constantly loop sensors. Furthermore, to “kick start” or in other words to trigger sensors, Arduino Lily Pad Button Board® was added to circuit. In Fig. 4.46, Arduino Lily Pad Button Board® is shown. It has small dimensions (8x16mm) with a thickness of 0.8mm. It was connected to circuit from GND and Vcc pins [290].



Fig. 4.46: Arduino LilyPad Button Board® [290]

4.2.1.3 Schematic circuit diagram of vibration motors

Fig. 4.47 shows the schematic circuit diagram of Arduino LilyPad Vibe Board®. Here, the GND pin of the each vibration motor was connected with the GND of the circuit. Vcc pin of the each vibration motor was connected with the microcontroller digital outputs.

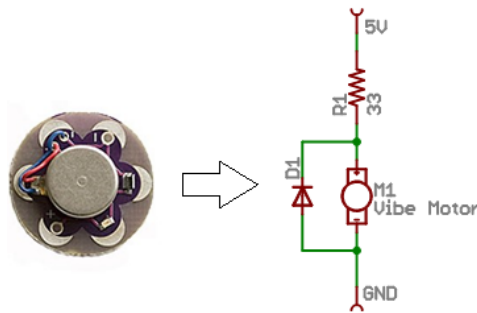


Fig. 4.47: Schematic circuit diagram of Arduino LilyPad Vibe Board® [291]

4.2.2. Design Layout

Considering Fig. 4.43, the circuit layout of the prototype was designed as seen in Fig. 4.48. In Fig. 4.44 (a) and (b), the circuit was designed over the front and back of garment, and over the arms, respectively.

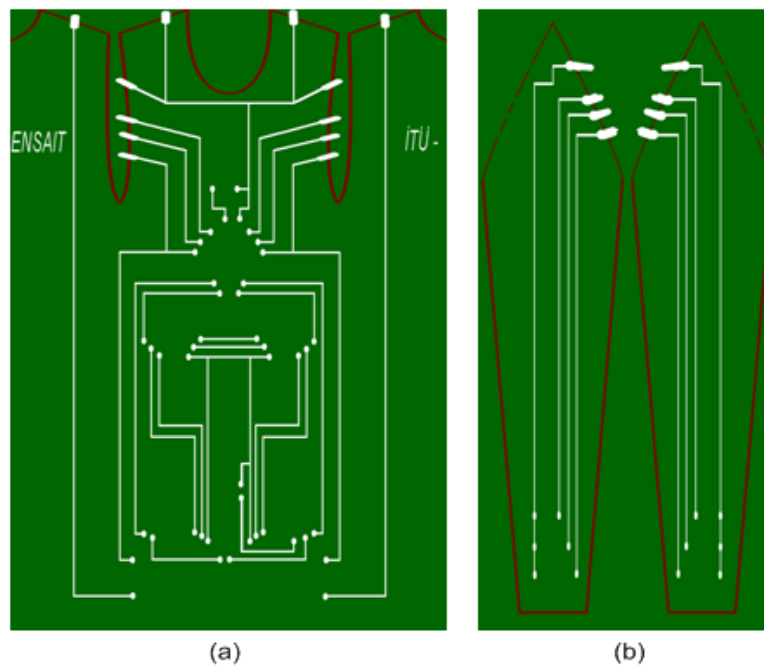


Fig. 4.48: Circuit layout design on the garment

4.2.2.1 Sensor placement

In Chapter 3, it was found that the best scenario was to use four sensors with an angle of 0° . Moreover, since the distance between four sensors were previously adjusted to 20 cm considering human body physiology, the position of sensors on the garment were decided as placing them under the breast zone of the garment taking account of both women's and men's body.

Indeed, the position of sensor plays a great role on the detection of obstacles. They should be placed in a region where the garment does not move so much during the walking. Within this concept, there can be two alternative zones: Shoulders zone or zone under the breast. If the sensors are placed over the shoulders zone, then obstacles with higher height such as wardrobe, wall will be detected. On the other hand, if the sensors are placed over the zone under breast, then the obstacles not only with higher height but also lower than that of height such as tables can also be detected. Towards our aim and considering environmental conditions, since there are more obstacles with lower height, then the zone under the breast on the garment was chosen for position of sensors in order to avoid more obstacle collision.

4.2.2.2 Actuator-vibration motor placement

According to Section 3.4 results, it was found that the highest level of vibrotactile sensation was perceived over the outer wrist and hip bone area of the evaluators' body. Therefore, to guide user, vibration motors were decided to be placed over the outer wrist and hip bone area of the garment. Three of the vibration motors were decided to be placed on the wrist of left arm, whereas the other three on the wrist of right arm. The left and right hip bone area was chosen for summer clothing usage. The garment was designed for both summer and winter periods. Therefore, when the arms of the proposed garment are taken out, the system is designed to be able to generate control by the vibration motors placed on the left and right hip bone area of the garment. To sum up, eight vibration motors were decided to be placed as follows: Each three of the six vibration motors are on the left and right arm over the outer wrist of garment and the other two are on the left and right hip bone area of the garment. Three vibration motors are used on one arm to give to user information about the location of obstacles as well as about required turning angle.

For instance, in the case of right turn with a small angle, only the 1st vibration motor on the right arm will act. Similarly, if the required turning action is right turn with a large angle, then three vibration motors on the right arm will act.

4.2.2.3 Microcontroller and power supply placement

After the decision of actuator's and sensor's placement, the positions of microcontroller and power supplies were planned out. Considering circuit and resistance constraints, microcontroller and power supplies should be placed as close as possible to each other. Moreover, critical point in microcontroller placement is that it is the network of inputs and outputs. Therefore, it should be placed in a region that is able to gather all analog outputs from sensors and send inputs to actuators without any overlapping. Therefore, the best possible position for microcontroller is in the center of garment regarding to whole circuit.

Due to microcontroller position and circuit constraints, positions of power supplies were determined close to microcontroller. Hence, they were decided to be placed around the vertical centerline of the garment.

4.2.3. Smart clothing prototype

4.2.3.1 Base structure of interactive garment

In order to obtain the circuit layout design shown in Fig. 4.48 on the garment, production of seamless products was considered. By this way, MBS Merz ® single-jersey circular knitting machine as seen in Fig. 4.49, with a cylinder diameter of 13 inches and E28 gauge was used to produce base structure of interactive garment.



Fig. 4.49: MBS Merz ® single-jersey circular knitting machine

Considering wearability and durability performance requirements mentioned in Section 2.1 such as comfortable, breathable, moisture absorption, lightweight, strength etc., Polyamide 66 yarns with a linear density of 78/68x2 dtex were used. Additionally, in order to get tightly fit in the garment, elastomeric yarns composed of PA (22 Denier) including Lycra® (16 Denier) were also used during the production of base structure of interactive garment.

According to results of Section 3.1, since the silver plated nylon 66-4ply yarns with a linear density and resistance of 312/34x4 dtex and $50\Omega/m$, respectively, presented the best compromise between signal quality and textile properties, they were used to satisfy electrical conduction in the garment. The arm and body parts of the garment were produced seamless. Then, they were sewn together in order to produce a base structure of the interactive garment (see Fig. 4.50). As shown in that figure, conductive yarns are in grey color, whereas polyamide yarns are in white. This structure is also washable. The other electronic parts are removable and their washing is not recommended.



Fig. 4.50: Base structure of developed interactive garment

4.2.3.2 Removable structures of interactive garment

Since the higher vibrotactile perception was obtained by woven fabric samples according to Section 3.4 results, woven structure was chosen for vibration motors' integration. Indeed, the compactness of woven structure provides better impact resistance than knitting structure and by this way, it will prevent the swinging of sensors and actuators during walking. Therefore, instead of knitting structure,

woven structure was considered to produce removable parts. Ultrasonic sensors and vibration motors integrated to textile structure were designed as described in Section 2.3-2.4.



Fig. 4.51: The production of removable parts for sensor and vibration motor integration

The production of removable parts for sensors and vibration motors was done by a hand loom weaving machine as shown in Fig. 4.51. Double-woven structure was defined. Again, the same conductive yarns and polyamide 66 yarns with a linear density of 78/68x4 dtex were used. Conductive yarns were inserted as well as hidden in the middle part of the double woven structure. Fig. 4.52 - Fig. 4.54 show the removable parts for vibration motor and sensor integration.

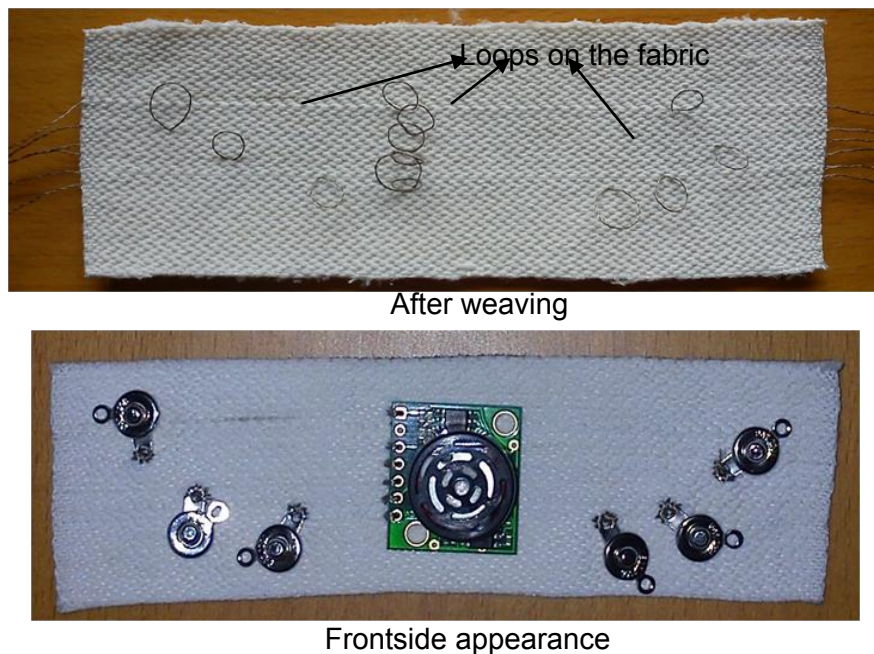


Fig. 4.52: Ultrasonic sensor integrated to woven fabric to attach under the breast zone of garment

To build electrical circuit and to connect sensor and vibration motor with fabric, loops were formed among conductive yarns, and snap fasteners were sewn onto these loops. As seen in the figures, the conductive yarns are in grey color in the middle part of fabric and polyamide yarns are in white color.

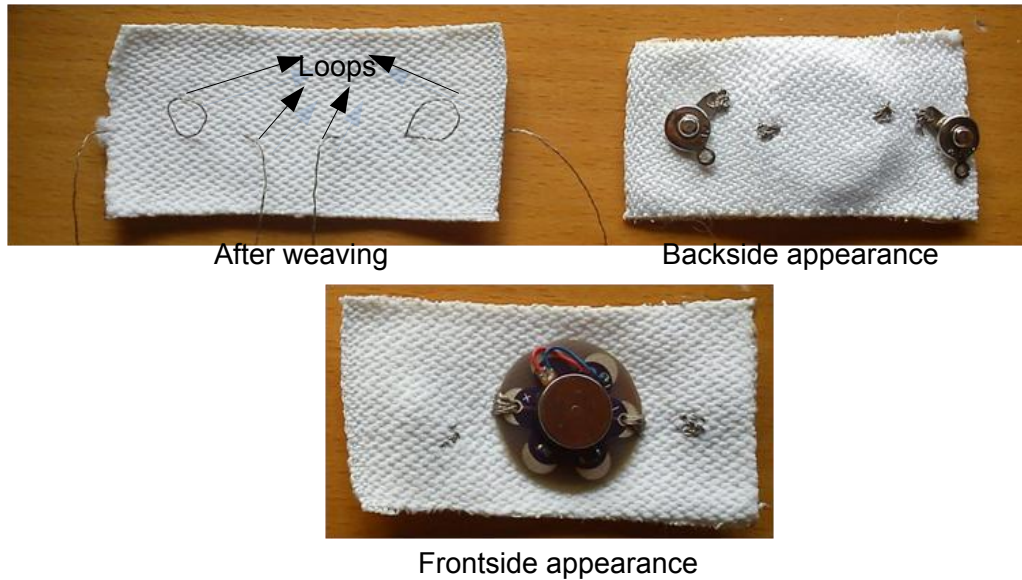


Fig. 4.53: Vibration motors integrated to woven fabric to attach over hip bone area of the garment

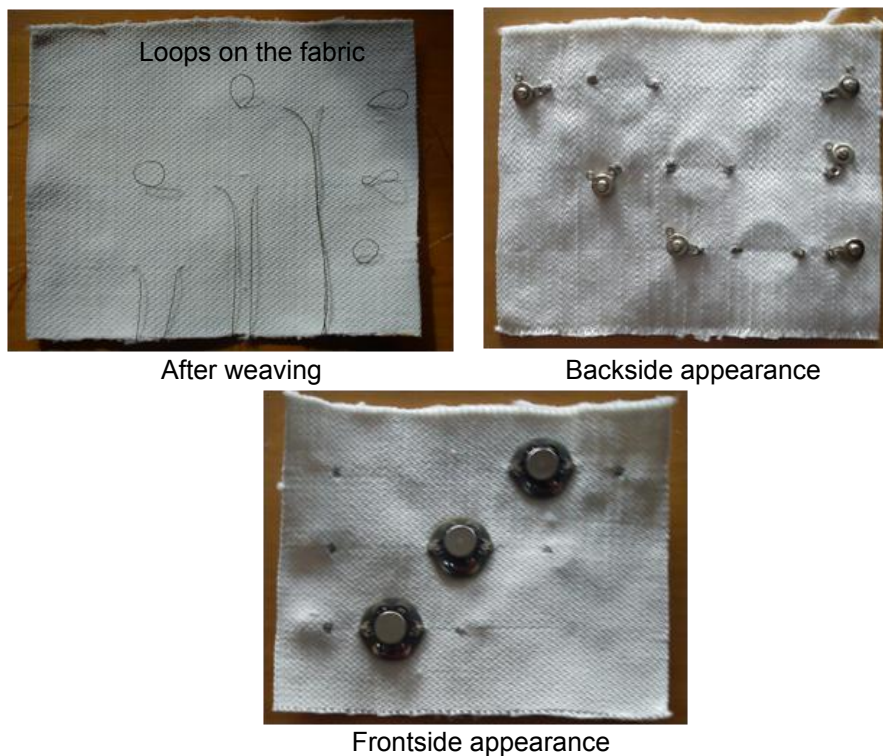


Fig. 4.54: Vibration motors integrated to woven fabric to attach over wrist area of the garment

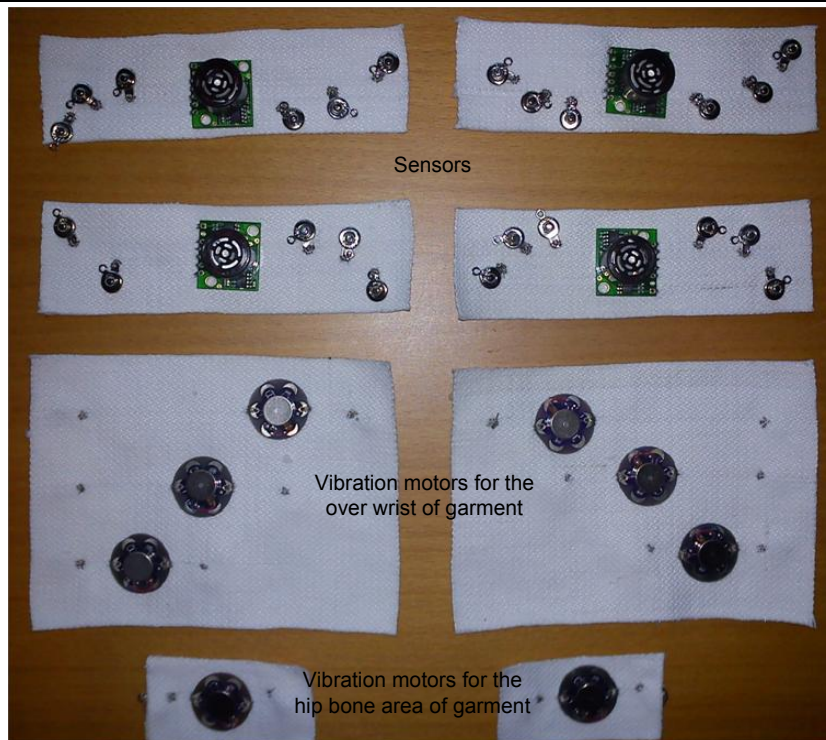


Fig. 4.55: Removable fabrics for sensor and actuator connections to main circuit

The total removable parts for sensor and actuator connections are shown in Fig 4.55. There are totally four sensors and eight vibration motors integrated to woven fabrics. The connection of these removable parts to main circuit in base structure of the interactive garment was provided by snap fasteners.

The removable fabric for microcontroller connection was produced by sewing. Similarly, snap fasteners provided connections among main circuit and microcontroller. The fabric used for producing base structure of interactive garment was also used to produce both microcontroller connection and pockets for batteries (see Fig. 4.56). The conductive yarns were again inserted as well as hidden in the middle part of knitted fabric.

Microcontroller integrated to knitted fabric



Pockets for batteries



Fig. 4.56: Removable fabrics for microcontroller and pockets for batteries

4.2.3.3 Interactive garment prototype

Finally, an interactive garment with its removable parts is shown in Fig. 4.57. Sensors were positioned in front of the garment under the breast zone. Vibration motors were positioned over the wrist and hip bone area of the garment. Microcontroller and batteries were positioned along the vertical centerline of the garment.



Fig. 4.57: Interactive garment with its removable parts

Parts for ultrasonic sensors, vibration motors and batteries were designed to be attached from the inner side of the garment and thus, they are not visible when they are attached. However, only microcontroller is visible on the garment when attached. By this way, user can open and close the system easily via button on the microcontroller.

Fig. 4.58 shows the final smart clothing prototype worn by mannequin. The weight of the final prototype without batteries is about 250 g, whereas the weight including two batteries is 458 g. Smart garment enabling detection and avoidance of obstacles is easy to handle, light enough to wear and carry, and washable when removable parts are detached from the main structure.



Fig. 4.58: Final smart clothing prototype for visually impaired people

4.3. Final Experiments and Performances of Smart Clothing System

Our smart clothing was tested for the following purposes:

- ✓ Detection capability and robustness
- ✓ Power consumption
- ✓ Heating behaviour
- ✓ Washability performances

4.3.1. Detection capability and robustness of the developed system

Detection capability of the developed system was defined as the degree of detection range in terms of distance along y and x-axis that is able to detect obstacles during operations. Robustness was defined as the ability of developed system to detect obstacles' position accurately in order to navigate avoiding collisions.

For experimental purposes, intelligent garment placed on the mannequin was tested for its detection range as shown in Fig. 4.59. During measurements, obstacles were placed in front of the mannequin in different positions in order to find maximum detection range. For instance, (see Fig. 4.59), white drawings on the ground were obtained during operation in different time intervals.



Fig. 4.59: Measurements for detection capability of the developed system

According to measurement results, during the first two hour the detection capability of the system was up to 2.5 m in y-axis as seen in Fig. 4.60. However, as the operation time increased, the detection range decreased. After 4 hour and 6 hour working time, the detection range decreased to 2.2 m and 1.8 m, respectively. This result can be attributed to a decrease in battery voltage. As the time passes, batteries run out. Thus, the feeding voltage going to sensors decreases. Since the analog voltage output of our ultrasonic sensor works with a scaling factor of V_{cc} (Feeding voltage)/512 per inch as mentioned in Section 3.2, the measured distance values acquired by sensors decrease due to a decrease in V_{cc} and the detection range as time passes also decreases.

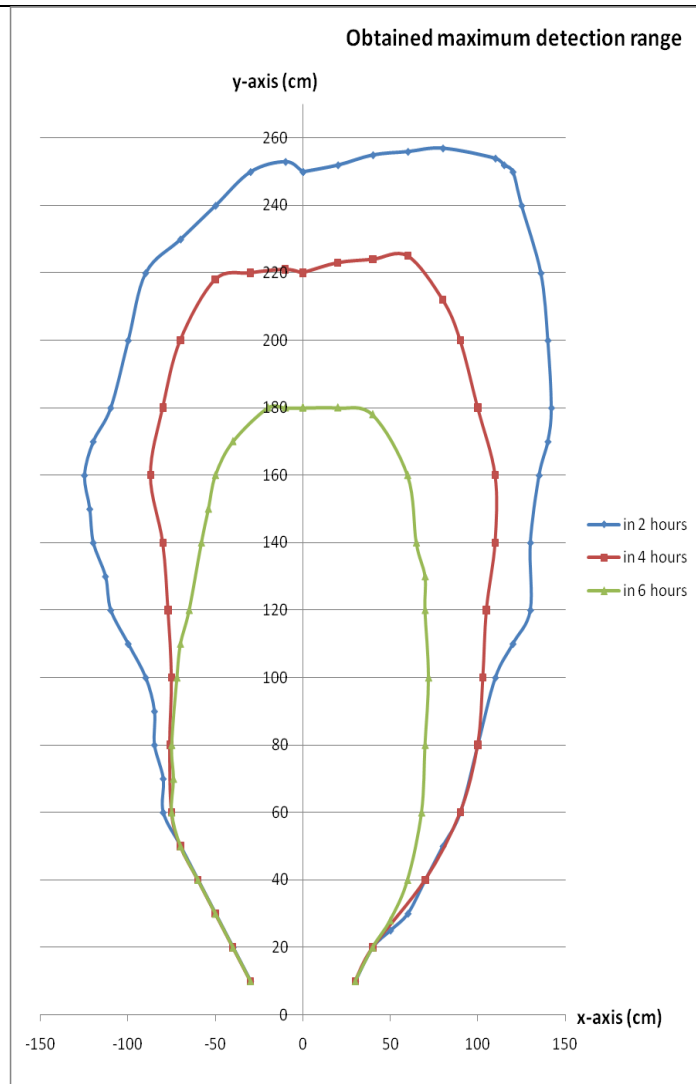


Fig. 4.60: Detection capability of the developed smart clothing

Moreover, as shown in Fig. 4.60, it was observed that detection ranges of left and right sensors are a little bit different. The areas detected by left and right sensors are not symmetrical. This may be related to different sensitivities of sensors.

For experimental environment, different indoor configurations with various layouts were chosen in order to identify obstacle's position. For instance, one layout of the environment including obstacles is shown in Fig. 4.61.

Before conducting experiments since lengths and widths of obstacles are critical issues for obstacle detection due to sensors' locations on the garment, following assumptions were made: (i) the widths of obstacles used in experiments were larger than 30cm, (ii) the heights of obstacles used in experiments were higher than 90cm.



Fig. 4.61: Layout of environment including obstacles

Experimental results showed that developed system is able to identify obstacle's position without any failure within the detection range (see Fig. 4.60). It means system is able to detect obstacles accurately, when they are at the right, system gives an output to turn left or vice versa. When obstacles are in front, system gives an output to turn right and left at the same time.

Therefore, an user can choose his/her way randomly by turning right or left in order to avoid an obstacle. In case of smaller obstacles having a width of ~15cm, it was observed that our system is still able of detecting an obstacle when it is located left or right. It is however unable to detect it when it is in front. It detects the obstacle as it was right or left randomly. This result may be explained by the distance between two sensors equal to 20cm defining the threshold value regarding the detection of the smallest possible obstacle. Therefore, obstacles smaller than 20cm in width are not correctly detected.

In conclusion, it may be noted that the increase in obstacle width increases accuracy of its detection. Similarly, the height of obstacles is critical for their detection. They should be higher than sensors' height.

Overall, the developed smart clothing detection system is robust and reliable if obstacles are large and tall.

4.3.2. Power consumption

Smart clothing system power supply system consists of two 4.8V NiMH flat batteries with a capacity of 2200mAh. As mentioned previously, in the circuit one of them supplies four ultrasonic sensors, while the other supplies the rest of the circuit, especially microcontroller and vibration motors.

Therefore, in order to find the life time of the smart clothing system (without any spare battery), experiments were made as follows:

First, the currents drawn by the vibration motors, ultrasonic sensors and microcontroller were investigated. It was observed that voltage coming to one vibration motor during the operation was measured as approximately 3.3 V. Therefore, the current passing through this vibration motor can be computed as:

$$I_{vib} = \frac{V_{vib}}{R_{vib}} \quad (4.27)$$

where $V_{vib}, I_{vib}, R_{vib}$ represents voltage, current, and resistance value of one vibration motor. According to datasheet of Arduino LilyPad Vibe Board® [291], since (see Fig. 4.47), $R_{vib} = 33\Omega$ then $I_{vib} = 100mA$. Therefore, the current passing through one vibration motor is 100mA. According to our control algorithm, all vibration motors can be activate (e.g. when the obstacle in front of the visually impaired person, six vibration motors should be turned on at the same time in order to warn). In this manner, the total current is equal to $6 \times 100mA = 600mA$ in the case of winter period utilization.

For summer period, only a hip bones area vibration motors (2 vibration motors) will be turned on and the maximal current will be equal to $2 \times 100mA = 200mA$.

Concerning sensors and microcontroller according to technical datasheet of our microcontroller [286], as shown in Fig. 4.62, the current is about 5mA for 4.8V, at 25°C during the operation (active mode). However, microcontroller is functioning all the time and the vibration motors are activated only during short periods of time (1s) when necessary.

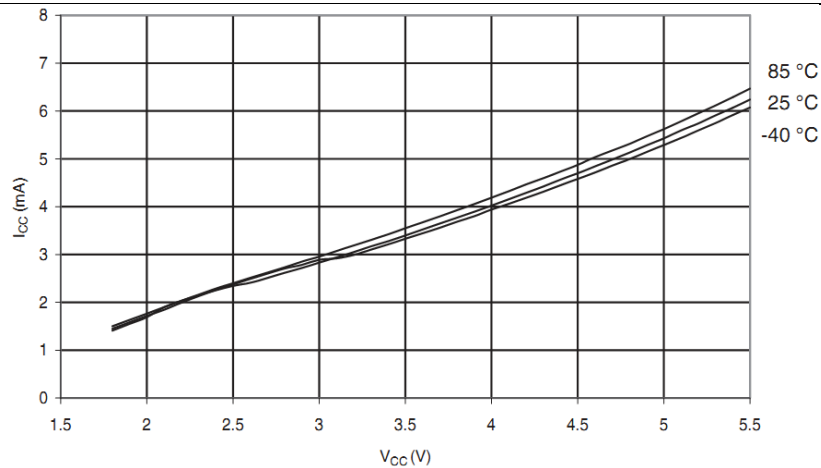


Fig. 4.62: ATmega328: Active Supply Current vs. V_{cc} [286]

Similarly, according to datasheet of ultrasonic sensors, it was found that the current for one operating sensor at 5V is 3mA. As there are four sensors the total required current is $4 \times 3\text{mA} = 12\text{mA}$. Sensors are also supplied continually, it means that in the operating mode the power necessary to supply our detection system is less than 12mA, therefore the life time is equal approximately to 8 days with one 2200mAh battery. Concerning vibration motors, six of them may vibrate during approximately 4 hours without interruptions.

Like microcontroller's current draw, sensors' current draw is highly smaller than the vibration motors' current draw. It has been considered the power loss in conductive yarns was negligible. Therefore, those currents would also be eliminated against vibration motors' current in the circuit.

In real experimental conditions with a lot of obstacles, measurements approve the our estimations and the battery supplying vibration motors runs out faster than the other one.

4.3.3. Heating behavior

Thermal analysis was carried out in order to find out whether the garment heats up above the level when the comfort of user can be affected or it may provoke injuries.

A thermal camera (Testo 880 ®, Testo Inc.) was used to take infrared images of the structure. Testo 880 ® Thermal Camera has a thermal resolution of $<0,1 \text{ }^\circ\text{C}$ at $30 \text{ }^\circ\text{C}$ and was set to record temperatures every 5 seconds.

A multichannel DC power source (Keithley 2400 SourceMeter®, Keithley Instruments Inc.) was used as power supply. Experiments were done in standard laboratory conditions (20°C , %65RH). The base structure of the interactive garment was placed on a plastic stand about 50cm away from thermal camera. Then, conductive parts of the garment were clamped with the probe of the DC power supply.

At first, measurement started with supplying 5V to the garment considering system's real working conditions. Afterwards, measurements were conducted by increasing voltage value from 1V to 16V in order to test the system's heating behaviour. During the measurements, Testo IRSoft software® was used to acquire images of temperature distribution on the fabric sample.

For instance, Fig. 4.63 shows the thermal image of a structure at 5V with its temperature distribution along conductive yarn. Moreover, Fig. 4.64 shows the thermal images of the structure over the sample area along conductive yarns when the voltage value is adjusted to 1V, 4V, 10V and 16V respectively.

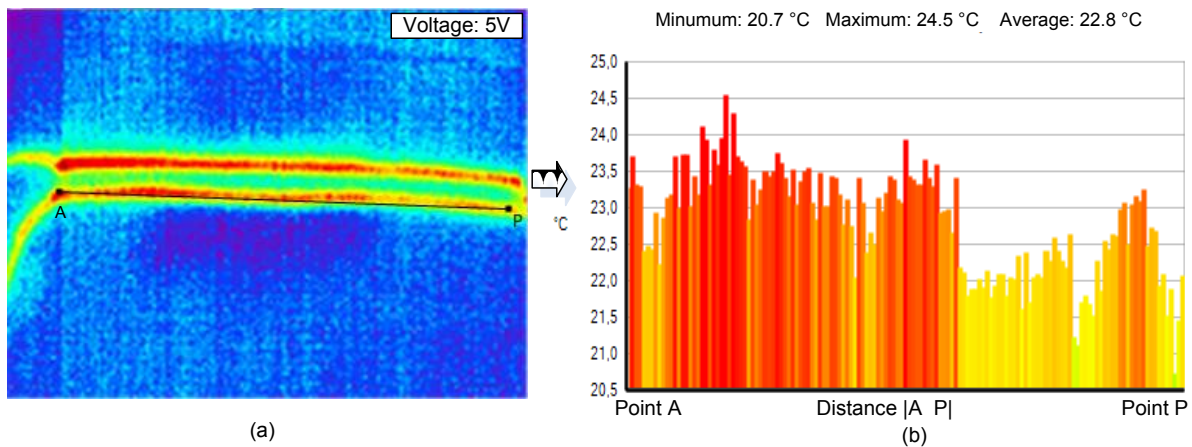


Fig. 4.63: Thermal image of the structure at 5V (a) and its temperature distribution along conductive yarn with a distance of $|AP|$ (b)

According to Fig. 4.63, it was observed that the average temperature along the conductive yarn is about 22.8 °C. Concerning our intelligent garment, since the system's working range is around 5V, it can be concluded that during the operation mode the temperature on the intelligent garment will be around 22 °C along the conductive yarns (transmission lines). Indeed, this result was found as satisfying regarding thermal comfort of a human body.

According to ASHRAE STANDARD 55-2010 [292], to maintain comfort of human body, the amount of insulation required to keep a resting person warm in a windless room at 70 °F (21.1 °C) is equal to one clo.

Moreover, as shown in Fig. 4.64 it was observed that the temperature of the conductive yarns increases rapidly with the voltage increase (see Fig. 4.65). With five voltages 1 V, 4 V, 8 V, 12 V and 16 V, the obtained average temperature values are 18.3 °C, 20.8 °C, 30.5 °C, 46 °C, and 64.4 °C, respectively.

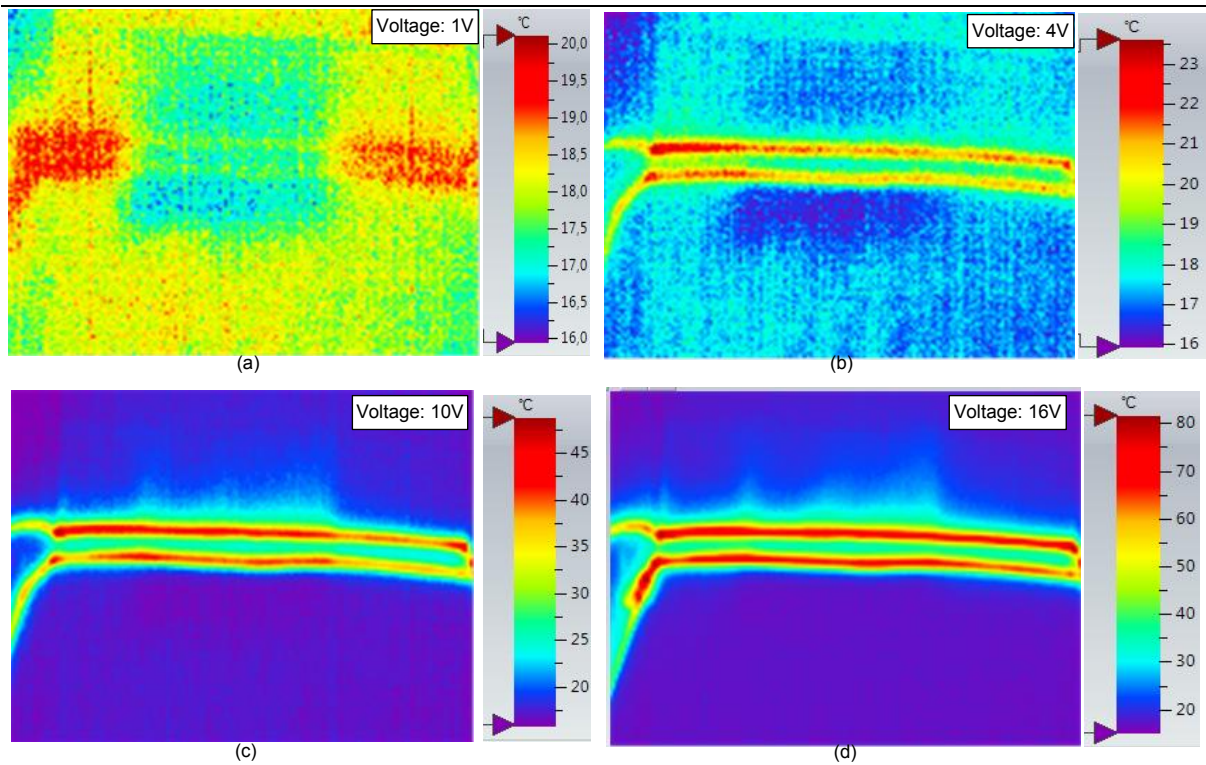


Fig. 4.64: Thermal images of the structure over a sample area at 1V, 4V, 10V,16V

Based on these results, the recommended voltage range to be applied on intelligent garments should not exceed 6-7 V in case of utilization of silver plated conductive yarns (<50ohm/m) in order to guarantee comfort and safety.

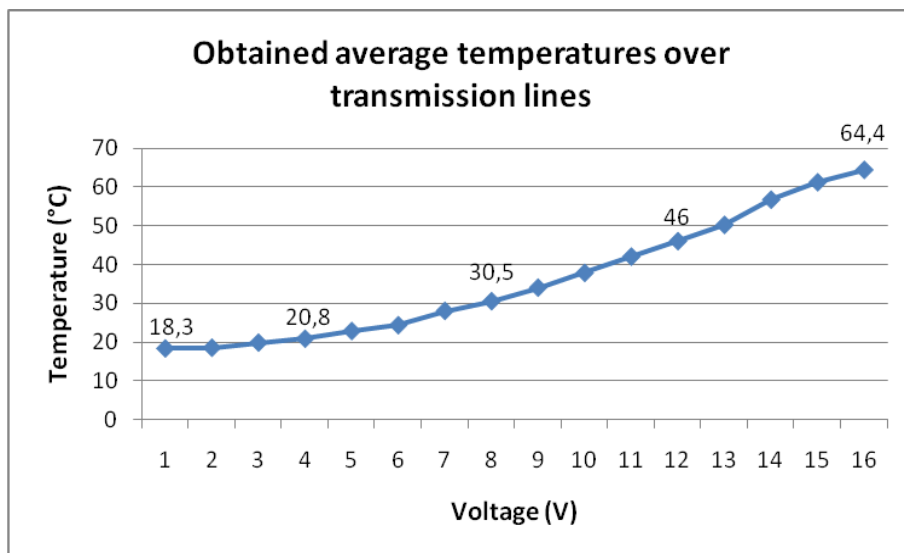


Fig. 4.65: Average temperatures over the transmission lines on the garment vs. voltage

4.3.4. Washability

In order to test the changes in electrical conductivity of the system after home laundering, a sample of base structure (without microcontroller, sensors and vibration motors) was washed 10 cycles under AATCC Test Method 135-2004 [293]. Test conditions were chosen according to Table I-III in the standard (see Appendix-D) as follows:

- Table I---(1) Normal/cotton sturdy machine cycle, (III) 40 °C, (A) tumble drying
- Table II---Normal
- Table III---Cotton sturdy

Hence, specimen was washed with a detergent of 66 g/l, dummy load of 1.8 kg, water level of 18±1 gal (washing time:12 min and final spin time: 6 min). After each washing cycle, the conductivity of the transmission line was tested. No significant difference could be noticed after 10 washing cycles along transmission line as shown in Table 4.3

Table 4.3: Resistance variation along transmission line after washing

	Wash cycle										
	0	1	2	3	4	5	6	7	8	9	10
Resistance (Ω)	11.43	11.71	11.82	12.22	12.245	12.263	12.272	12.293	12.32	12.342	12.37

4.4. Summary

In this chapter, an algorithm based on neuro-fuzzy controller has been developed for smart clothing system in order to guide visually impaired people successfully. In this algorithm, system inputs acquired by sensors have been evaluated in terms of fuzzy relations, and then the outputs corresponding to recommended turning angles, indicated by vibration motors, have been deduced by using neural network architecture. Afterwards, a microcontroller programming has been realized according to a control algorithm.

In the second part of the chapter, design and development concepts of the smart clothing prototype have been introduced. Finally, prototype has been tested for detection capability, power consumption, heating behaviour and washability.

Results showed that developed system is able to identify obstacle's position without any failure within its detection range. It is capable of detection of obstacles accurately such that when obstacles are at the right, system gives an output turn left or vice versa. When obstacles are in front, system gives an output like turn right and turn left at the same time. Therefore, it can be concluded that developed system is successful, reliable and robust.

Regarding power consumption, it was found that due to power consumption calculations previously mentioned, the first battery, which supplies vibration motors and microcontroller, runs out more quickly than the second one. Additionally, it was observed that system can work for at least one day (8hours) without any additional battery, however depending on environment this result may change.

Concerning heating behaviour of the system, during the operation mode (Voltage $\approx 5V$), it was found that temperature along transmission lines on the garment is around 22 °C. In addition, when the voltage value is increased from 1 V up to 16 V, it was observed that the temperature increases over the transmission line (conductive yarns) rapidly from 18 °C to 64 °C.

Moreover, washing experiments showed that there is no significant change on the conductivity of transmission lines after 10 washing cycles.

GENERAL CONCLUSION AND FUTURE RESEARCHES WORKS

Summary of Major Results and Conclusions

Based on extensive literature review on theories subjecting both visually impaired issues and intelligent textiles, a smart clothing system able to detect obstacles in order to guide visually impaired people has been successfully developed and studied experimentally and theoretically in this thesis. Major findings obtained from the experiments and the conclusions are summarized as follows:

(1) An overview of the electronic travel aids developed for visually impaired people's navigation concerns has been presented. A state of the art of intelligent textiles from fibres to interactive garment has been given as well. A survey of the literature has shown that there are various types of navigation travel aids developed for visually impaired people that can be mainly classified as (i) GPS Based Systems, (ii) RFID Tag Based Systems, (iii) Camera-Based Systems, and (iv) Sonar Based Systems. In those systems, most of the work does not consider user comfort. However, it is important for a usable electronic travel aid to let the visually impaired be hand free and comfortable during navigation. Therefore, the most suitable approach to let the user be hand free is embedding whole system into clothes. In the literature, some of the researchers suggested this idea. However, none of the studies developed such kind of system; a garment fully integrated with electronics that enables detection of obstacles as well as guidance for visually impaired people.

(2) In order to determine the most suitable electronic components of an intelligent garment structure enabling detection of obstacles as well as guidance for visually impaired people, an algorithm based on fuzzy AHP and fuzzy information axiom has been presented. In the scope of the study, various electronic components sensors, actuators and power supplies were considered and their alternatives in industry and literature were determined. The linguistic judgments of experts for the alternatives under the defined criteria with respect to defined functional requirements led to a conclusion that ultrasonic sensor, vibration motor, and chemical cell batteries are the most solution alternatives for the proposed smart clothing system.

Moreover, the accuracy criterion was found to be the most important among all criteria, while the cost was the least.

(3) In order to decide which conductive yarn is suitable for the planned smart clothing system, the performance of ultrasonic sensor integrated to textile structure regarding its monitoring performance, signal quality and accuracy was analyzed by using various conductive yarn types. Considering real utilization conditions of the garment, mobile phones were only taken into account as disturbance source. Results reported that linear resistance of conductive yarns affects the signal quality of sensors. It was found that when the linear resistance increases, noise level increases and signal quality decreases. Owing to less linear resistance, insulated copper yarn showed the best signal quality. Nevertheless, our experiences showed that silver plated nylon 66-4ply yarn achieved the best compromise between signal quality and preserved textile properties e.g. handle, stable and elastic, easy to weave, easy to integrate sensor etc. Another result issued was that the direction of calling and standby situation of the mobile phones has an important effect on the signal quality of sensor and it gives us an idea about sensors' working range.

(4) Detection capability of single sensor integrated to textile structure was analyzed and compared with its datasheet in terms of detection range. The results showed that the determined beam pattern matches with the actual one given in its datasheet. However, according to our results it should be noted that as the distance to an obstacle increases measurement error also increases. Thus to get right results, it is recommended to add some corrective coefficients into microcontroller programming due to errors related to distances.

(5) In order to find the optimal number of sensors as well as develop suitable obstacle avoidance algorithm for smart clothing system, different scenarios were developed by connecting sensors together. Finally, during the experiments with textile structure, four sensors were decided to be positioned horizontally onto textile surface with an angle of 0° , 30° , and 45° in 1st, 2nd, and 3rd scenarios, respectively. Additionally, in the 4th scenario, two sensors at down were positioned horizontally, on the contrary two sensors at up were positioned vertically with an angle of 0° . Results showed that the total detection success rate of scenario 1 in which four sensors were placed at 0° is higher than the others are. It was found that as the angle of sensor increases from 0° up 45° , detection success rate decreases. Moreover, in all scenarios the rate of detection success of down sensors was higher than those of up sensors. This was related with height of obstacle. It was concluded that height of obstacle has a considerable effect on the detection success. Therefore, it is obvious that if the

obstacle's height is smaller than the sensors' position height relatively, the detection of obstacles will be difficult. Another result issued was that position of detection range of sensors was shaped by position of sensors. This means, if the position of sensor is at the right then the number of detected obstacles will be greater at the right side than the left side and vice versa. To sum up, the scenario 1 in which all sensors were placed horizontally at 0° presented the best compromising results not only in terms of detection success rate, detection error and detection range capabilities, but also in terms of integration and mounting onto textile structure. Hence, four sensors at 0° arrangement were chosen for the proposed smart clothing system.

(6) Vibrotactile perception level was investigated in terms of fuzzy relations in order to find out the influence of conductive yarns, signal waveforms and frequencies, and different body local areas on the resulting vibrotactile perception level. By this way, decisions were taken on a kind of fabric structure that should be used, an area of smart clothing system where vibration motors should be fixed and kind of signal waveform and frequency that should be applied to vibration motors. Results showed that e-textile structure type influenced the vibrotactile perception level. Nevertheless, conductive yarn type had no significant effect on the perception level of vibrotactile when the distance (resistance) between snap fastener and vibration motor (in the e-textile circuit) is small. The highest perception level in e-textile structures was obtained by woven e-fabric integrated with highly conductive yarn. Moreover, signal waveform and the frequency had resulted in a significant effect on the vibrotactile perception. It was noticed that when the frequency of signal increases perception level decreases. Therefore, it was deduced that people prefer to feel discrete vibrations instead continuous vibrations as an alert. According to experimental results, sine wave form at 0.5 Hz showed highest vibrotactile perception level within the signal type alternatives. Another important result issued from this study was that perception level of vibrotactile sensation changes according to contact areas of human body. The highest level of vibrotactile sensation was perceived over the outer wrist and hip bone area of the evaluators' body, whereas the lowest was perceived over thigh. To conclude in order to get highest vibrotactile perception, the use of woven e-fabric including highly conductive yarn over the outer wrist and/or over the hipbone by applying sine wave form at 0.5 Hz was recommended. Therefore, regarding this result, the placement of actuators over the intelligent garment was identified as wrist and hip bone area and the fabric structure for actuators (attachable part) were decided as woven e-fabric including highly conductive yarns.

(7) Smart clothing prototype enabling detection of obstacles named as “Wearable Obstacle Detection System” has been successfully developed. Considering smart clothing system an algorithm based on neuro-fuzzy controller for obstacle avoidance has also been developed in order to navigate visually impaired people through this smart clothing system. The design and development concept of smart clothing prototype has involved four key areas of research, namely (i) electronics, (ii) information technology, (iii) control engineering, and (iv) textiles. The prototype has been tested for detection capability, power consumption, heating behaviour and washability. Results showed that developed system is able to identify obstacle’s position without any failure within its detection range. System is capable of detecting left, right, and front obstacles’ position accurately and giving right output while detecting obstacles such that when obstacles are at the right, system gives an output turn left; when obstacles are at the left, system gives an output turn right. When obstacles are in front, system gives an output like turn right and turn left at the same time, hence user can understand there is an obstacle just in front of user and randomly he/she can choose his/her way by turning right or left at that moment. Therefore, it may be concluded that developed system is successful, reliable and robust. Regarding power consumption of the system, it was found that system can work for at least 1 day without any additional battery, however depending on environment this result can change. Therefore, it is recommended to users to have spare battery for much longer usage and to overcome upsets. Concerning heating behaviour of the system, during the operation mode (Voltage \approx 5V), it was found that temperature along transmission lines on the garment is around 22 °C, which approximately corresponds with ASHRAE STANDARD 55-2010’s thermal comfort degree (21.1 °C). However, owing to findings earlier, it is highly notable that before designing a smart clothing system, since the applied voltage value effects heating behaviour of smart clothing system, comfort level of user should be taken into consideration. Therefore, according to our results recommended voltage range that would be applied to intelligent garments (including silver plated nylon $<50\text{ohm/m}$) should not exceed 6-7V due to comfort and safety margins.

Herewith, four key areas of research, namely (i) electronics, (ii) information technology, (iii) control engineering and (iv) textiles have been combined in order to develop this smart clothing system. The research work presented here holds promises for further development of efficient and reliable smart clothing system named as “Wearable Obstacle Avoidance System” for guiding visually impaired people among obstacles during walking.

The successful outcome of this research will absolutely provide an impetus for future developments of electronic textiles as well as interactive garments.

Recommendations For Future Work

Within this thesis, we have demonstrated that with the aid of developed smart clothing system named as “Wearable Obstacle Detection System”, obstacles with a height of 90 cm or more can be easily detected and their positions can be accurately determined as well. However, based on the study presented here, the following future research works are suggested:

(1) In order to detect smaller obstacles, system could be combined with whole garment of the user such as trousers. In addition, in order to detect obstacles on the ground such as big holes or in order to detect stairs system could be integrated with shoes as well.

(2) This system currently offers accurate detection statically. To guide user during walking accurately avoiding collisions, implementing newly developed neuro-fuzzy controller algorithm for obstacle avoidance into microcontroller programming should be extremely useful. Upgrading the microcontroller to one that has more memory and upgrading programming language by implementing digital filters in microcontroller in order to attenuate noise in signals that are processed inside microcontroller are recommended.

By this way, the degree of navigation and guidance accuracy during walking should increase.

(3) For outdoor environment, developed system can be fully integrated with GPS, RFID, camera and vocal guidance, not only can it track the user, but also find a route to specific destination, and then guide the user to this destination using synthesized speech by ensuring localization information to user such as the street address of the current location etc.

(4) Regarding power consumption of the developed system, a control to warn the user about battery level or the level of voltage supply can be implemented to the system e.g voltage monitoring circuit. Due to information on voltage level decrease, some coefficients related to detection range capability have to be added to microcontroller programming in order to prevent decrease in detection range as well.

(5) Due to the technology miniaturization and reduction of costs in electronics and textile industry, new sensing elements, new flexible technologies, new actuators, new functional yarns can be implemented to our developed system. For instance, flexible textile based solar cells, which is expected to be thinner, lighter in weight and more powerful in the future, would be embedded to newly developed smart clothing system as power supply for further improvement. As an actuator, artificial muscles would be interesting. Finally, a fully textile flexible sonar systems may be developed in order to replace existing miniaturized rigid sensors.

References

- [1] World Health Organization, *World health report*, <<http://www.who.int/mediacentre/factsheets/fs282/en/index.html>> accessed at 10.02. 2011
- [2] Bousbia-Salah, M., Redjati, A., Fezari, M., Bettayeb, M., 2007. An ultrasonic navigation system for blind people, *Signal Processing and Communications*, ICSPC 2007. IEEE International Conference, 24-27 November, pp. 1003 - 1006
- [3] Fink W, Tarbell M, 2009. CYCLOPS: A mobile robotic platform for testing and validating image processing and autonomous navigation algorithms in support of artificial vision prostheses, *Computer methods and programs in biomedicine*, Vol. 96, no.3, pp. 226-33.
- [4] Tsai, J.W. Morley, G.J. Suaning, N.H. Lovell, 2009. A wearable real-time image processor for a vision prosthesis, *Computer Methods and Programs in Biomedicine*, ISSN 0169-2607
- [5] Lee Wee C., Leung, M.K.H., 2004. SINVI: smart indoor navigation for the visually impaired *Control, Automation, Robotics and Vision Conference*, Vol. 2, 6-9 December, pp.1072 - 1077
- [6] Alhajri, K., Al-Salihi, N., Garaj, V., Balachandran, W., 2008. The performance of WiFi network for application in a navigation system for visually impaired people, 24-26 April 2008, pp. 243 - 249
- [7] Velázquez, R., Pissaloux, E.E., Guinot, J.C., Maingreud, F., 2005. Walking using touch: Design and preliminary prototype of a non-invasive ETA for the visually impaired Source: *Annual International Conference of the IEEE Engineering in Medicine and Biology Proceedings*, Vol.7, pp. 6821-6824
- [8] Sakamoto, N., Koshi, K., Tadokoro, Y., Support system for the visually impaired that uses a digital still camera and portable telephones, *Journal of the Institute of Image Information and Television Engineers*, Vol. 51, no. 11, pp. 1906-1914
- [9] Balakrishnan, G., Sainarayanan, G., Nagarajan, R., Yaacob, 2004. Stereopsis method for visually impaired to identify obstacles based on distance, *Proceedings - Third International Conference on Image and Graphics*, pp. 580-583.
- [10] Nagarajan, R., Yaacob, S., Sainarayanan, G., 2002. Fuzzy clustering in vision recognition applied in NAVI, *Fuzzy Information Processing Society, Proceedings. NAFIPS. Annual Meeting of the North American* 27-29 June, pp:261 - 266
- [11] Sainarayanan, R. Nagarajan, Sazali Y., 2007. Fuzzy image processing scheme for autonomous navigation of human blind, *Applied Soft Computing*, Vol. 7, no.1, January 2007, pp. 257-264, ISSN 1568-4946
- [12] Balakrishnan, G., Sainarayanan, G., Nagarajan, R., Yacob, S., 2005. On stereo processing procedure applied towards blind navigation aid – SVETA *Proceedings - 8th International Symposium on Signal Processing and its Applications*, Vol. 2, pp. 567-570

-
- [13] Balakrishnan, G., Sainarayanan, G., Nagarajan, R., Yaacob, S. 2007. Fuzzy matching scheme for stereo vision based electronic travel aid, *IEEE Region 10 Annual International Conference, Proceedings*
- [14] Gonzalez-Mora, A. Rodriguez Hernandez, L. F. Rodriguez-Ramos, L. Diaz-Saco, and N. Sosa, 2009. Development of a new space perception system for blind people, based on the creation of a virtual acoustic space. *Tech. Rep.* [Online]. <<http://www.iac.es/proyect/eavi>>
- [15] Jirawimut, R., Prakoonwit, S., Cecelja, F., Balachandran, W., 2009. Visual odometer for pedestrian navigation, *Instrumentation and Measurement*, Vol. 52, Issue 4, Aug. 2003 pp. 1166 - 1173
- [16] Nicholas M., Stephen S., Michael B., David L., Penny P., 1999. Robotic sensing for the partially sighted, *Robotics and Autonomous Systems*, Vol.26, Issues 2, pp. 185-201.
- [17] Bujacz, M., Baranski, P., Moranski, M., Strumillo, P., Materka, A., 2008. Remote guidance for the blind -A proposed teleassistance system and navigation trials Human System Interactions Conference, 25-27 May pp.888 - 892
- [18] Bourbakis, N.G., Kavraki, D., 2001. An intelligent assistant for navigation of visually impaired people Bioinformatics and Bioengineering Conferenc., Proceedings of the IEEE 2nd International Symposium on 4-6 Nov, pp.230 - 235
- [19] Bourbakis, N., Keefer, R., Dakopoulos, D., Esposito, A. 2008. Multimodal Interaction Scheme between a Blind User and the Tyflos Assistive Prototype, *Tools with Artificial Intelligence*, Vol. 2, 3-5 Nov. pp. 487 - 494
- [20] Dakopoulos, D., Bourbakis, N. 2008. Preserving visual information in low resolution images during navigation of visually impaired, *1st International Conference on Pervasive Technologies Related to Assistive Environments*
- [21] Bourbakis, N., Kavraki, D. 2005. A 2D vibration array for sensing dynamic changes and 3D space for blinds' navigation, Proceedings - BIBE 2005: 5th IEEE Symposium on Bioinformatics and Bioengineering, pp. 222-226.
- [22] Dakopoulos, D., Boddhu, S.K., Bourbakis, N., 2007. A 2D Vibration Array as an Assistive Device for Visually Impaired Bioinformatics and Bioengineering, 14-17 Oct., pp. 930 – 937
- [23] Denshi Joho, T. Gakkai R. 2006. A route comprehension support system for a robotic travel aid, *Systems and Computers in Japan*, Vol. 37, No. 9, 2006 (Translated from, Vol. J86-D-I, No. 4, April 2003, pp. 269–279)
- [24] Kotani, S., Kiyohiro, N., 1994. Human interface of a robotic travel aid Mori, *Robot and Human Communication*, Proceedings 3rd IEEE International Workshop on 18-20 July, pp.90 – 94
- [25] Url-1 <http://www.sagedata.com/learning_centre/RFID_main.html> accessed on February, 2011

-
- [26] Ebrahim, Y., Abdelsalam, W., Ahmed, M., Siu-Cheung Chau. 2005. Proposing a hybrid tag-camera-based identification and navigation aid for the visually impaired, *Consumer Communications and Networking Conference*, 3-6 Jan.pp.172 – 177
- [27] Gharpure, Chaitanya P., 2004. Orientation-free radio frequency identification-based navigation in a robotic guide for the visually impaired, *M.S. dissertation.United States -- Utah: Utah State University*, Publication Number: AAT 1423820.
- [28] Chang, T., Ho, Chien-Ju, Hsu, D., Chawei, L. Yuan-Hsiang, T. Min-Shieh, Wang, M., Hsu, J., 2005. iCane - A partner for the visually impaired, *Lecture Notes in Computer Science*, V. 3823 LNCS, pp.393-402
- [29] Mooi, Wong S., Tan Chong E. NH. 2010.Efficient RFID Tag Placement Framework for In Building Navigation System for the Blind. In: *Information and Telecommunication Technologies (APSITT)*, pp.1-6.
- [30] Yelamarthi K, Haas D, Nielsen D, Mothersell S. 2010. RFID and GPS Integrated Navigation System for the Visually Impaired, *IEEE Engineering and Technology*, pp.1149-1152.
- [31] Zou Ji, Duanyuan B. Research of Region Navigation Based on Radio Frequency Identification. In: 2010 International Conference on Computer, Mechatronics, Control and Electronic Engineering (CMCE), 2010 pp.300-303.
- [32] Seto TKM. 2009. A navigation system for the visually impaired using colored navigation lines and RFID tags. *IEEE Engineering in Medicine and Biology Society. Conference*.pp.831-4.
- [33] Shiizu, Y., Hirahara, Y., Yanashima, K., Magatani, K.. 2007. The development of a white cane which navigates the visually impaired, *Engineering in Medicine and Biology Society. 29th Annual International Conference of the IEEE* 22-26 Aug. pp.5005 - 5008
- [34] Ienaga, T., Yoneda, Y., Wada, C, Kimuro, Y., Matsumoto, Michito, 2008. Development of a direction indicating system for a tele-support for the visually impaired Information Theory and Its Applications, *ISITA International Symposium*, 7-10 Dec., pp.1 - 6
- [35] Chumkamon, S., Tuvaphanthaphiphat, P., Keeratiwintakorn, P., 2008. A blind navigation system using RFID for indoor environments *Electrical Engineering/Electronics, Computer, Telecommunications and Information Technology, 5th International Conference*. Vol. 2, 14-17 May, pp.765 - 768
- [36] D'Atri, E., Medaglia, C.M., Serbanati, A., Ceipidor, 2007. A system to aid blind people in the mobility: A usability test and its results U.B., Systems, *ICONS '07. Second International Conference*, 22-28 April pp.35 – 35
- [37] Koide, S., Kato, M. 2006. 3-D Human Navigation System with Consideration of Neighboring Space, *Information Systems, Man and Cybernetics, SMC '06. IEEE International Conference* V. 2, 8-11 Oct., pp.1693 – 1698
- [38] Fariaj, J , Lopes S, Fernandes H, Martins P B, 2010. Electronic White Cane For Blind People Navigation Assistance. *World Automation Congress*, pp.1-7

-
- [39] Kulyukin, V., Gharpure, C., Nicholson, J., Pavithran, S., 2004. RFID in robot-assisted indoor navigation for the visually impaired. *Intelligent Robots and Systems*, 2004 IEEE/RSJ International Conference on Vol.2, 28 Sept.-2 Oct. pp.1979-1984
- [40] Murai, Y., Araki, T., Miyakawa, M., 2008. RFID localization for the visually impaired Tatsumi, Automation Congress, WAC 2008. World Sept. 28 2008-Oct. 2 2008 pp.1 - 6
- [41] Oktem, R., Aydin, E., Cagiltay, N.E., 2008. An indoor navigation aid designed for visually impaired people, *Industrial Electronics 34th Annual Conference of IEEE*, 10-13 Nov. pp.2982 - 2987
- [42] Murai, Y., Miyakawa, M., 2007. RFID for aiding the visually impaired recognize surroundings, *Conference Proceedings - IEEE International Conference on Systems, Man and Cybernetics*, pp. 3719-3724
- [43] Kulyukin, V., Gharpure, C., Sute, P., De Graw, N., Nicholson, J., 2004. A robotic wayfinding system for the visually impaired, *Proceedings of the National Conference on Artificial Intelligence*, pp.864-869
- [44] Xiaohan L., Makino, H., Kobayashi, S., Maeda, Y., 2007. Design of an Indoor Self-Positioning System for the Visually Impaired - Simulation with RFID and Bluetooth in a Visible Light. *Communication System Engineering in Medicine and Biology Society 29th Annual International Conference of the IEEE*, 22-26 Aug. 2007 pp.1655 - 1658
- [45] Szeto, Andrew Y. J., Sharma, Satish K. 2007. RFID based indoor navigational aid for persons with severe visual impairments, *29th Annual International Conference of IEEE-EMBS, Engineering in Medicine and Biology Society*, pp. 6360-6363
- [46] Soeda, K., Aoki, S., Yanashima, K., Magatani, K. 2004. Development of the visually impaired person guidance system using GPS. *Engineering in Medicine and Biology Society, 26th Annual International Conference of the IEEE*, Vol.2, 1-5 Sept. pp.4870 – 4873
- [47] Brusnighan, D.A., Strauss, M.G., Floyd, J.M., Wheeler, B.C.1989. Orientation aid implementing the global positioning system, *Bioengineering Conference*, Northeast, pp.33 - 34
- [48] Ponchillia, P. E Rak, E. C., Freeland, A. L. LaGrow, S.J, 2007. Accessible GPS: Reorientation and Target Location Among Users with Visual Impairments, *Journal of Visual Impairment & Blindness*, Vol. 101 Issue 7, pp.389-401, 13p
- [49] Marston, James R., Loomis, Jack M. Klatzky, Roberta L , Golledge, R. 2007. Nonvisual Route Following with Guidance from a Simple Haptic or Auditory Display, *Journal of Visual Impairment & Blindness*, Apr2007, Vol. 101 Issue 4, pp.203-211
- [50] Cecelja, F., Garaj, V., Hunaiti, Z., Balachandran, W., 2006. A Navigation System for Visually Impaired, *Instrumentation and Measurement Technology Conference Proceedings of the IEEE*, 24-27 April pp.1690 – 1693

- [51] Ebrahim, Y., Abdelsalam, W., Ahmed, M., Siu-Cheung C. 2005. Proposing a hybrid tag-camera-based identification and navigation aid for the visually impaired, *Consumer Communications and Networking Conference*, 3-6 Jan., pp.172 – 177
- [52] Yelamarthi K, Haas D, Nielsen D, Mothersell S. 2010. RFID and GPS Integrated Navigation System for the Visually Impaired. *IEEE Engineering and Technology*. pp.1149-1152.
- [53] Hunaiti Z, Garaj V, Balachandran W. 2009. An Assessment of a Mobile Communication Link for a System to Navigate Visually Impaired People, *IEEE Transactions on Instrumentation and Measurement*. 58(9) pp.3263-3268.
- [54] Loomis J.M Golledge, R., Klatzky, R.L. 1998. Navigation System for the Blind: Auditory Display Modes and Guidance, *Presence: Teleoperators & Virtual Environments*, Vol. 7 Issue 2, pp.193-203,
- [55] Hunaiti, Z., Garaj, V., Balachandran, W., Cecelja, F., 2004. An assessment of GSM/GPRS link in a navigation system for visually impaired pedestrians, *Electronics, Communications and Computers, 2004. CONIELECOMP 2004. 14th International Conference*, 16-18 Feb. pp.30 - 34
- [56] Loomis,R , Marston, G., Golledge, K., 2005. Personal Guidance System for People with Visual Impairment: A Comparison of Spatial Displays for Route Guidance, *Journal of Visual Impairment & Blindness*, Vol.99, pp.219-232
- [57] Mayerhofer, B., Pressl, B., Wieser, M., 2008. ODILIA - A mobility concept for the visually impaired, *Lecture Notes in Computer Science (including subseries Lecture Notes in Artificial Intelligence and Lecture Notes in Bioinformatics)*, v 5105 LNCS, pp.1109-1116,
- [58] Ran, L., Helal, S., Moore, S., 2004. Drishti: an integrated indoor/outdoor blind navigation system and service, *Pervasive Computing and Communications, Proceedings of the Second IEEE Annual Conference*, pp.23 – 30
- [59] LaPierre, C. M., 1998. Personal navigation system for the visually impaired, Section 0040, Part 0544 Canada: Carleton University (Canada), Publication Number: AAT MQ36892.
- [60] Korgaonkar, S.U. 2008. Low cost localization and navigation system using Global Positioning for visually impaired users, *MSc. Theses*, Section 0241, Part 0800, United States -- Utah: Utah State University, Publication Number: AAT 1454852.
- [61] Hunaiti, Z., Garaj, V., Balachandran, W., Cecelja, F., 2005. An Assessment of 3G Link in a Navigation System for Visually Impaired Pedestrians *Electronics, Communications and Computers, Proceedings. 15th International Conference*, 28-02 Feb. 2005 pp.7 - 9
- [62] Hunaiti, Z., Garaj, V., Balachandran, W., Cecelja, F., 2005. Mobile Link Assessment for Visually Impaired Navigation System. *Instrumentation and Measurement Technology Conference, Proceedings of the IEEE*, Volume 2, 16-19 May pp.883 - 887
- [63] Url-2 <<http://en.wikipedia.org/wiki/Sonar>> accessed at February, 2011

-
- [64] Dakopoulos D, Bourbakis NG. 2010. Wearable Obstacle Avoidance Electronic Travel Aids for Blind: A Survey, *IEEE Transactions On Systems, Man, And Cybernetics—Part C: Applications And Reviews*. 40(1): pp.25-35.
- [65] Ulrich, I., Borenstein, J., 2001. The GuideCane-applying mobile robot technologies to assist the visually impaired. *IEEE Transactions on Systems, Man, and Cybernetics Part A:Systems and Humans.*, v 31, n 2, pp.131-136
- [66] Aigner, P., McCarragher, B., 1999. Shared control framework applied to a robotic aid for the blind, *IEEE Control Systems Magazine*, V 19, n 2, pp.40-46
- [67] Aziz, I., Abdul, M., Sajee, M., Mazlina, S., 2008. Blind echolocation using ultrasonic sensors, *Information Technology International Symposium* .Vol. 4, 26-28 Aug. pp.1 - 7
- [68] Bousbia-Salah, M., Fezari, M., 2006. An ultrasonic mobility system for blind and visually impaired people, *Automatic Control and Computer Sciences*, Vol. 40, No. 3, pp.55-59
- [69] Balakrishnan, M., 2007. Cane mounted knee-above obstacle detection and warning system for the visually impaired, *Proceedings of the ASME International Design Engineering Technical Conferences and Computers and Information in Engineering Conference*, Vol. 4, pp. 143-151.
- [70] Calder DJ. 2009. Assistive technology interfaces for the blind. *3rd IEEE International Conference on Digital Ecosystems and Technologies*. pp.318-323.
- [71] Shraga S., Iwan U., and Johann B., 2001. Computerized obstacle avoidance systems for the blind and visually impaired, *Intelligent Systems and Technologies in Rehabilitation Engineering*, CRC PRESS LLC
- [72] Shoval, S., Borenstein, J., Koren, Y., 1998. Auditory guidance with the Navbelt-a computerized travel aid for the blind, *Systems, Man, and Cybernetics, Part C: Applications and Reviews*, Vol. 28, Issue 3, pp.459 - 467
- [73] Shoval, S., Borenstein, J., Koren, Y., 1994. Mobile robot obstacle avoidance in a computerized travel aid for the blind, *Robotics and Automation, Proceedings IEEE International Conference*, Vol.3. 8-13 May, pp.2023 - 2028
- [74] Sethu Selvi, S., Kamath, U.R., Sudhin, M.A., 2008. Andha Asthra - A navigation system for the visually impaired, *Multisensor Fusion and Integration for Intelligent Systems, IEEE International Conference*, 20-22, pp.137 – 142
- [75] Bousbia-Salah, M., Redjati, A., Fezari, M., Bettayeb, M., 2007. An Ultrasonic Navigation System for Blind People, *Signal Processing and Communications, IEEE International Conference* , 24-27 Nov. pp.1003 - 1006
- [76] Byeong-Seok S., Cheol-Su L., Oakley and S. Brewster, 2007. Obstacle Detection and Avoidance System for Visually Impaired People, LNCS 4813, pp. 78–85
- [77] Cardin, S., Thalmann, D., F. Vexo, 2007. A wearable system for mobility improvement of visually impaired people, *The Visual Computer*, Vol. 23, No. 2

-
- [78] Zhang, J. C.W.Lip, S.K.Ong AYC.N. 2010. A Multiple sensor-based Shoe Mounted User Interface Designed for Navigation Systems for the Visually Impaired. *Wireless Internet Conference (WICON)*, Vol 1, pp.1-8.
- [79] Wada C. ,2009. Basic Study on Presenting Distance Information to the Blind for Navigation. *Fourth International Conference on Innovative Computing, Information and Control*, pp.405-408.
- [80] Shah, C., Bouzit, M., Youssef, M., Vasquez, L., 2006. Evaluation of RU-Netra - Tactile Feedback Navigation System For The Visually Impaired, *Virtual Rehabilitation International Workshop*, pp.72 – 77
- [81] Url-3 Bay Advanced Technologies Ltd. <<http://www.batforblind.co.nz> > accessed on February, 2011
- [82] Url-4 <<http://bestpluton.free.fr/EnglishMiniRadar.htm>> accessed on February 2011, BestPluton World Cie.
- [83] Ito, M. Okamoto, J. Akita, T. Ono, I. Gyobu, T. Tagaki, T. Hoshi, and Y. Mishima, 2005. CyARM: An alternative aid device for blind persons, CHI05, Portland, OR, Apr. 2–7, pp. 1483–1488.
- [84] Akita J, Komatsu T, Ito K, Ono T, Okamoto M. 2009. CyARM: Haptic Sensing Device for Spatial Localization on Basis of Exploration by Arms. *Advances in Human-Computer Interaction*. pp.1-7.
- [85] Rentschler AJ, Simpson R, Cooper RA, Boninger ML, 2008. Clinical evaluation of Guido robotic walker. *Journal Of Rehabilitation Research And Development*, Vol. 45 (9), pp. 1281-93
- [86] D. Cottet, J. Grzyb, T. Kirstein, and G. Troster, 2003. Electrical characterization of textile transmission lines, *IEEE Transactions on Advanced Packaging*, vol. 26, May. 20 pp. 182-190.
- [87] Wallace, G., Campbell, T. E., 2007. Putting Function into Fashion: Organic Conducting Polymer Fibres and Textiles, *Fibers and Polymers*, Vol. 8, pp. 135-142.
- [88] Y. Ouyang and W.J. Chappell, 2008., High Frequency Properties of Electro-Textiles for Wearable Antenna Applications, *IEEE Transactions on Antennas and Propagation*, Vol. 56, pp. 381-389.
- [89] C.tang Huang, C.-lung Shen, C.-fa Tang, and S.-hung Chang, 2008. A wearable yarn-based piezo-resistive sensor, *Sensors And Actuators*, Vol. 141, pp. 396-403.
- [90] C. Huang, C. Tang, M. Lee, and S. Chang, 2008. Parametric design of yarn-based piezoresistive sensors for smart textiles, *Sensors and Actuators A: Physical*, Vol. 148, pp. 10-15.
- [91] Huang, CT., 2007. A Wearable Textile for Monitoring Respiration, Time, p. 1.
- [92] Kaynak, S. Najar, and R. Foitzik, 2008. Conducting nylon, cotton and wool yarns by continuous vapor polymerization of pyrrole, *Synthetic Metals*, Vol. 158, pp. 1-5.
- [93] Ramachandran, T., Vigneswaran, C., Design and Development of Copper Core Conductive Fabrics for Smart Textiles, *Journal of Industrial Textiles*, Vol. 39, pp. 81-93.

-
- [94] Koncar, V., E.B. Nebor, X. Joppin, 2004. FICC (Floatable Intelligent and Communicative Clothing) Project - Conductive Fibers Development, *Eighth International Symposium on Wearable Computers*, pp. 36-39.
- [95] Kim, B., Koncar, V., Devaux, E., Dufour, C. and Viallier, P., 2004. Electrical and morphological properties of PP and PET conductive polymer fibers, *Synthetic Metals*, Vol. 146, pp. 167-174.
- [96] Devaux, E., Koncar, V., Kim, B., Campagne, C. Roux, C., Rochery, M. and Saihi, D., Processing and characterization of conductive yarns by coating or bulk treatment for smart textile applications, *Transactions of the Institute of Measurement and Control*, Vol. 29, pp. 355-376.
- [97] Xue, K. Park, X. Tao, W. Chen, and X. Cheng, 2007. Electrically conductive yarns based on PVA/carbon nanotubes, *Composite Structures*, Vol. 78, pp. 271-277.
- [98] Bedeloglu, A., Demir, A., Bozkurt, Y., Sariciftci, N.S., 2009. A Photovoltaic Fiber Design for Smart Textiles, *Textile Research Journal*, Vol. 80, pp. 1065-1074.
- [99] Toivola, M. Ferenets, P. Lund, and A. Harlin, 2009. Photovoltaic fiber, *Thin Solid Films*, Vol. 517, pp. 2799-2802.
- [100] Wang, C. Too, and G. Wallace, 2005. A highly flexible polymer fibre battery, *Journal of Power Sources*, Vol. 150, pp. 223-228.
- [101] Maccioni, E. Orgiu, P. Cosseddu, S. Locci, and A. Bonfiglio, 2006. The textile transistor: a perspective for distributed, wearable networks of sensor devices, *3rd IEEE/EMBS International Summer School on Medical Devices and Biosensors*, pp. 5-7.
- [102] Lee, J.B. and Subramanian, V., 2005. Weave patterned organic transistors on fiber for E-textiles, *Electron Devices, IEEE Transactions on*, Vol.52 (2), pp. 269-275
- [103] Maccioni, M., Orgiu, E., Cosseddu, P., Locci S., and Bonfiglio, A. 2006. The textile transistor: a perspective for distributed, wearable networks of sensor devices *Applied Physics Letters*, Vol. 89, 143515
- [104] Locci, S., Maccioni, M, Orgiu, E., Bonfiglio, A., 2007. An Analytical Model for Cylindrical Thin-Film Transistors, *Electron Devices, IEEE Transactions on*, Vol.54 (9), pp. 2362 – 2368
- [105] De Rossi, D. 2007. Electronic textiles: A logical step, *Nature Materials*, Vol.6, Iss.5, pp.328
- [106] Hamed, M., Forchheimer, R. Inganas, O. 2007. Towards woven logic from organic electronic fibres, *Nat. Mater.* Vol. 6, pp. 357
- [107] Tao, X., Koncar, V. and Dufour, C.,2011. Novel Geometry Pattern for the Wire Organic Electrochemical Textile Transistor, *Journal of the Electrochemical Society*, Vol. 158, Issue 5, pp. H572-H577
- [108] Dhawan, A., 2007. Development Of Robust Fiber Optic Sensors Suitable For Incorporation Into Textiles, and A Mechanical Analysis Of Electronic Textile Circuits, *Ph.D. Thesis*, North Carolina State University, Pub.No. 3306578

-
- [109] Dhawan, A. A.M. Seyam, T.K. Ghosh, and J.F. Muth, 2004., Woven Fabric-Based Electrical Circuits Part I: Evaluating Interconnect Methods, *Textile Research Journal*, vol. 74, 2004, pp. 913-919.
- [110] Dhawan, A., Tushar K. Ghosh, Abdelfattah M. Seyam, 2010., Woven Fabric-Based Electrical Circuits Part II: Yarn and Fabric Structures to Reduce Crosstalk Noise in Woven Fabric-Based Circuits, *Textile Research Journal*, Vol. 74, 2004, pp. 955-960.
- [111] Locher, I., Enabling Technologies for Electrical Circuits on a Woven Monofilament Hybrid Fabric, *Textile Research Journal*, 2010, Vol. 78, pp. 583-94
- [112] Visser H.J., Reniers, C.F., 2007. Textile antennas, a practical approach, *IET Seminar Digests*, pp. 538-538.
- [113] Sanz-Izquierdo, B. Batchelor, J.C., 2008. A Dual Band Belt Antenna, *International Workshop on Antenna Technology: Small Antennas and Novel Metamaterials*, pp. 374-377.
- [114] Salonen, P., Rahmat-Samii, Y. 2006. Textile antennas: Effects of antenna bending on input matching and impedance bandwidth, *First European Conference on Antennas and Propagation*, Nov. pp. 1-5.
- [115] Salonen, P. and M. Keskilammi, 2008. SoftWear Antenna, *IEEE Military Communications Conference*, Nov. pp. 1-6.
- [116] Hertleer, C., Laere, A.V., H. Rogier, and L.V. Langenhove, 2010. Influence of Relative Humidity on Textile Antenna Performance, *Textile Research Journal*, Vol. 80, pp. 177-183.
- [117] Hertleer, C. Tronquo, A., H. Rogier, and L.V. Langenhove, 2010. The Use of Textile Materials to Design Wearable Microstrip Patch Antennas, *Textile Research Journal*, Vol. 78, pp. 651-658.
- [118] Hertleer, C., Rogier, H., L. Vallozzi, and F. Declercq, 2007. A textile antenna based on high-performance fabrics, *IET Seminar Digests*, pp. 558-558.
- [119] Gimpel, U. Mohring, H. Muller, A. Neudeck, and W. Scheibner, 2004. Textile-Based Electronic Substrate Technology, *Journal of Industrial Textiles*, Vol. 33, pp. 179-189.
- [120] Winterhalter, J. Teverovsky, P. Wilson, J. Slade, W. Horowitz, E. Tierney, and V. Sharma, Development of electronic textiles to support networks, communications, and medical applications in future U.S. military protective clothing systems., *IEEE transactions on information technology in biomedicine*, Vol. 9, pp. 402-6.
- [121] Nakad, Z. M. Jones, T. Martin, and R. Shenoy, 2007. Using electronic textiles to implement an acoustic beamforming array : A case study *Pervasive and Mobile Computing*, Vol. 3, pp. 581-606.
- [122] Cheng, K.B. 2006. Electromagnetic Shielding Effectiveness of the Twill Copper Woven Fabrics, *Journal of Reinforced Plastics and Composites*, Vol. 25, pp. 699-709.
- [123] Sim Roh, Y.-seung Chi, T.J. Kang, and S.-wook Nam, 2008. Electromagnetic Shielding Effectiveness of Multifunctional Metal Composite Fabrics, *Textile Research Journal*, Vol. 78, pp. 825-835.

-
- [124] Lee, S.-E., K.-Y. Park, K.-S. Oh, and C.-G. Kim, 2009. The use of carbon/dielectric fiber woven fabrics as filters for electromagnetic radiation, *Carbon*, Vol. 47, pp. 1896-1904.
- [125] Rothmaier, B. Selm, S. Spichtig, D. Haensse, and M. Wolf, 2008. Photonic textiles for pulse oximetry, *Optics express*, Vol. 16, pp. 12973-86.
- [126] Ashok Kumar, C. Vigneswaran, and T. Ramachandran, 2010. Development of Signal Transferring Fabrics Using Plastic Optical Fibers for Defense Personnel and Study their Performance, *Journal of Industrial Textiles*, Vol. 39, pp. 305-326.
- [127] Hasegawa, M. Shikida, D. Ogura, and K. Sato, 2007. Novel type of fabric tactile sensor made from artificial hollow fiber, *IEEE 20th International Conference on Micro Electro Mechanical Systems (MEMS)*, pp. 603-606.
- [128] Kayacan, O. and Bulgun, E.Y., 2009. Heating behaviors of metallic textile structures, *International Journal of Clothing Science and Technology*, Vol. 21, pp. 127-136.
- [129] Kayacan, O., Bulgun, E. and Sahin, O. 2009. Implementation of Steel-based Fabric Panels in a Heated Garment Design, *Textile Research Journal*, Vol. 79, No.16, pp. 1427-1437.
- [130] Scilingo, E.P., A. Gemignani, R. Paradiso, N. Taccini, B. Ghelarducci, and D. De Rossi, 2005. Performance evaluation of sensing fabrics for monitoring physiological and biomechanical variables., *IEEE transactions on information technology in biomedicine*, Vol. 9, pp. 345-52.
- [131] Wijesiriwardana, R., K. Mitcham, and T. Dias, 2004. Fibre-Meshed Transducers Based Real Time Wearable Physiological Information Monitoring System, *Eighth International Symposium on Wearable Computers*, pp. 40-47.
- [132] Wijesiriwardana, R., 2006. Inductive fiber-meshed strain and displacement transducers for respiratory measuring systems and motion capturing systems, *IEEE Sensors Journal*, Vol. 6, pp. 571-579.
- [133] Soleimani, M. 2008. Knitted switches for smart clothing using double electrode technology, *Sensor Review*, Vol. 28, pp. 229-232.
- [134] Soleimani M. and E. Ogucu, 2008. Electromechanical properties of wearable strain gauge transducers, *Electronics Letters*, Vol. 44, pp. 2008-2009.
- [135] Zhang, H., X. Tao, T. Yu, and S. Wang, 2006. Conductive knitted fabric as large-strain gauge under high temperature, *Sensors and Actuators A: Physical*, Vol. 126, pp. 129-140.
- [136] Wan, K.M, 2010. A Resistive Network Model for Conductive Knitting Stitches Resistive Network of Knitting Stitches, *Textile Research Journal*, Vol.80, no.10, pp. 1-13.
- [137] Li, W.M. Au, Y. Li, K.M. Wan, W.Y. Chung, and K.S. Wong, 2009. A Novel Design Method for an Intelligent Clothing Based on Garment Design and Knitting Technology, *Textile Research Journal*, Vol. 79, pp. 1670-1679.
- [138] Linz, T., C. Kallmayer, R. Aschenbrenner, and H. Reichl, 2005. Embroidering Electrical Interconnects with Conductive Yarn for the Integration of Flexible Electronic Modules into Fabric, *Ninth IEEE International Symposium on Wearable Computers*, pp. 86-91.

- [139] Linz, T., L. Gourmelon, and G. Langereis, 2007. Contactless EMG sensors embroidered onto textile.” 4th International Workshop on Wearable and Implantable Body Sensor Networks, Vol. 13, pp.29-34
- [140] Meyer, J., P. Lukowicz, and G. Troster, 2006. Textile Pressure Sensor for Muscle Activity and Motion Detection, *10th IEEE International Symposium on Wearable Computers*, pp. 69-72.
- [141] Koncar, V. Cochrane, C. Lewandowski, M. Boussu, F. and Dufour, C. 2009. Electro-conductive sensors and heating elements based on conductive polymer composites, *International Journal of Clothing Science and Technology*, Vol. 21, pp. 82-92.
- [142] Li, Y., X.Y. Cheng, M.Y. Leung, J. Tsang, X.M. Tao, and M.C.W. Yuen, 2005. A flexible strain sensor from polypyrrole-coated fabrics, *Synthetic Metals*, Vol. 155, pp. 89-94.
- [143] Chuang, M., Windmiller, J. R., Santhosh, P., Ramirez, V., Galik, M., Chou, T., Wang, J., 2010. Textile-based Electrochemical Sensing: Effect of Fabric Substrate and Detection of Nitroaromatic Explosives, *Electroanalysis*, 22, No. 21, 2511 – 2518, 2010
- [144] Merritt, C., Karaguzel, B., J. Wilson, P. Franzon, B. Pourdeyhimi, E. Grant, and T. Nagle, 2006. Sensors on Textile Substrates for Home-Based Healthcare Monitoring, *1st Transdisciplinary Conference on Distributed Diagnosis and Home Healthcare*, pp. 5-7.
- [145] Locher, I. and Troster, G., Screen-printed Textile Transmission Lines, *Textile Research Journal*, Vol. 77, pp. 837-842.
- [146] Buechley, L. and Eisenberg, M. 2007. Fabric PCBs, electronic sequins, and socket buttons: techniques for e-textile craft, *Personal and Ubiquitous Computing*, Vol. 13, pp. 133-150.
- [147] Panhuis, J. Wu, S. Ashraf, and G. Wallace, 2007. Conducting textiles from single-walled carbon nanotubes, *Synthetic Metals*, Vol. 157, pp. 358-362.
- [148] Gopalsamy, S. Park, R. Rajamanickam, and S. Jayaraman, 1999. The Wearable Motherboard™ : The First Generation Responsive Textile Structures Medical Applications, *Virtual Reality*, pp. 152-168.
- [149] Cho, H. and Lee, J., 2007. A Development of Design Prototype of Smart Healthcare Clothing for Silver Generation Based on Bio-medical, *Development*, pp. 1070-1077.
- [150] D'Angelo, S. Weber, Y. Honda, T. Thiel, F. Narbonneau, and T.C. Luth, 2008. A system for respiratory motion detection using optical fibers embedded into textiles., *IEEE Engineering in Medicine and Biology Society Conference*, pp. 3694-7.
- [151] Di Rienzo, M., F. Rizzo, G. Parati, M. Ferratini, G. Brambilla, and P. Castiglioni, 2005. A textile-based wearable system for vital sign monitoring: applicability in cardiac patients, *Computers in Cardiology*, pp. 699-701.
- [152] Chien Chiu, T.-wei Shyr, H.-chiu Chu, Y.-ching Chung, and C.-yen Lan, 2007. A Wearable e-Health System with Multi-functional Physiological Measurement, *Physiological Measurement*, Vol. 14, pp. 429-432.

- [153] Paradiso, R., G. Loriga, and N. Taccini, 2005. A wearable health care system based on knitted integrated sensors., *IEEE transactions on information technology in biomedicine*, Vol. 9, pp. 337-44.
- [154] Wiklund, M. Karlsson, N. Ostlund, L. Berglin, K. Lindecrantz, S. Karlsson, and L. Sandsjö, 2007. Adaptive spatio-temporal filtering of disturbed ECGs: a multi-channel approach to heartbeat detection in smart clothing., *Medical & biological engineering & computing*, Vol. 45, pp. 515-23.
- [155] Paradiso, R. and D. De Rossi, 2006. Advances in textile technologies for unobtrusive monitoring of vital parameters and movements.,” Conference proceedings : IEEE Engineering in Medicine and Biology Society Conference, Vol. 1, pp. 392-5.
- [156] Campbell, T.E., B.J. Munro, G.G. Wallace, and J.R. Steele, 2007. Can fabric sensors monitor breast motion?, *Journal of biomechanics*, Vol. 40, pp. 3056-9.
- [157] Edmison, D. Lehn, M. Jones, and T. Martin, 2006. E-Textile Based Automatic Activity Diary for Medical Annotation and Analysis, *International Workshop on Wearable and Implantable Body Sensor Networks*, pp. 131-134.
- [158] Carpi, F. and De Rossi, D., 2005. Electroactive polymer-based devices for e-textiles in biomedicine., *IEEE transactions on information technology in biomedicine*, Vol. 9, pp. 295-318.
- [159] Heiss, L. 2006. Enabled apparel: the role of digitally enhanced apparel in promoting remote empathic connection, *Ai & Society*, Vol. 22, pp. 15-24.
- [160] Linz, C. Kallmayer, R. Aschenbrenner, and H. Reichl, 2006. Fully Integrated EKG Shirt based on Embroidered Electrical Interconnections with Conductive Yarn and Miniaturized Flexible Electronics, *International Workshop on Wearable and Implantable Body Sensor Networks* pp. 23-26.
- [161] Kim, S. Leonhardt, N. Zimmermann, P. Kranen, D. Kensche, E. Müller, and C. Quix, 2008. Influence of contact pressure and moisture on the signal quality of a newly developed textile ECG sensor shirt, *Time*, pp. 256-259.
- [162] Coosemans, B. Hermans, and R. Puers, 2006. Integrating wireless ECG monitoring in textiles, *Sensors and Actuators A: Physical*, Vol. 130-131, pp. 48-53.
- [163] Ottenbacher, S. Romer, C. Kunze, U. Grosmann, and W. Stork, Integration of a Bluetooth Based ECG System into Clothing, *Eighth International Symposium on Wearable Computers*, pp. 186-187.
- [164] Di Rienzo, F. Rizzo, G. Parati, G. Brambilla, M. Ferratini, and P. Castiglioni, 2005, MagIC System: a New Textile-Based Wearable Device for Biological Signal Monitoring. Applicability in Daily Life and Clinical Setting.,” *EEE Engineering in Medicine and Biology Society Conference*, Vol. 7, pp. 7167-9.
- [165] De Jonckheere, M. Jeanne, a Grillet, S. Weber, P. Chaud, R. Logier, and J.L. Weber, 2007. OFSETH: optical fibre embedded into technical textile for healthcare, an efficient way to monitor patient under magnetic resonance imaging., *IEEE Engineering in Medicine and Biology Society Conference*, pp. 3950-3.

- [166] Lee, Y.-D. and Chung, W.-Y. 2009. Wireless sensor network based wearable smart shirt for ubiquitous health and activity monitoring, *Sensors and Actuators B: Chemical*, Vol. 140, pp. 390-395.
- [167] Linti, H. Horter, P. Osterreicher, and H. Planck, 2006. Sensory baby vest for the monitoring of infants, *International Workshop on Wearable and Implantable Body Sensor Networks*, pp. 135-137.
- [168] Bouwstra, S. W. Chen, and L. Feijs, 2009. Smart Jacket Design for Neonatal Monitoring with Wearable Sensors, *Sixth International Workshop on Wearable and Implantable Body Sensor Networks*
- [169] Pandian, K. Mohanavelu, K.P. Safeer, T.M. Kotresh, D.T. Shakunthala, P. Gopal, and V.C. Padaki, 2008. Smart Vest: wearable multi-parameter remote physiological monitoring system., *Medical engineering & physics*, Vol. 30, pp. 466-77.
- [170] Catrysse, M., Puers, R., Hertleer, C. and Langenhove, L.V. 2004. Towards the integration of textile sensors in a wireless monitoring suit, *Sensors and Actuators*, Vol. 114, pp. 302-311.
- [171] Taccini, N., G. Loriga, M. Pacelli, and R. Paradiso, 2008. Wearable monitoring system for chronic cardio-respiratory diseases, *IEEE Engineering in Medicine and Biology Society Conference*, pp.3690-93.
- [172] P. Lemmens, F. Crompvoets, D. Brokken, J. van den Eerenbeemd, and G.-J. de Vries, 2009. A body-conforming tactile jacket to enrich movie viewing *Third Joint EuroHaptics conference and Symposium on Haptic Interfaces for Virtual Environment and Teleoperator Systems*, March, pp. 7-12.
- [173] Magnenat-Thalmann, N. , A. Petermier, X. Righetti, M. Lim, G. Papagiannakis, T. Fragopoulos, K. Lambropoulou, P. Barsocchi, and D. Thalmann, 2008. A virtual 3D mobile guide in the INTERMEDIA project, *The Visual Computer*, Vol. 24, pp. 827-836.
- [174] Tormene, P., T. Giorgino, S. Quaglini, and M. Stefanelli, 2009. Matching incomplete time series with dynamic time warping: an algorithm and an application to post-stroke rehabilitation, *Artificial intelligence in medicine*, Vol. 45, pp. 11-34.
- [175] Tognetti, A. N. Carbonaro, G. Zupone, and D. De Rossi, 2006. Characterization of a novel data glove based on textile integrated sensors, *IEEE Engineering in Medicine and Biology Society Conference*, Vol. 1, Jan., pp. 2510-3.
- [176] Tognetti, A., R. Bartalesi, F. Lorussi, and D. De Rossi, 2007. Body segment position reconstruction and posture classification by smart textiles, *Transactions of the Institute of Measurement and Control*, Vol. 29, pp. 215-253.
- [177] Mattmann, C. O. Amft, H. Harms, G. Troster, and F. Clemens, 2007. Recognizing Upper Body Postures using Textile Strain Sensors, *11th IEEE International Symposium on Wearable Computers*, October, pp. 1-8.
- [178] Lorussi, F., W. Rocchia, E.P. Scilingo, a Tognetti, and D. De Rossi, 2004. Wearable, Redundant Fabric-Based Sensor Arrays for Reconstruction of Body Segment Posture, *IEEE Sensors Journal*, Vol. 4, pp. 807-818.
- [179] Whiton, A. and Nugent, Y. 2007. A Wearable for Physical Abuse Detection, *11th IEEE International Symposium on Wearable Computers*, October, pp. 1-2.

-
- [180] Dunne, L.E. , P. Walsh, B. Smyth, and B. Caulfield, 2007. A System for Wearable Monitoring of Seated Posture in Computer Users, *4th International Workshop on Wearable and Implantable Body Sensor Networks* , Vol. 13, pp.203-207
- [181] Wu, D. Zhou, C.O. Too, and G.G. Wallace, 2005. Conducting polymer coated lycra, *Synthetic Metals*, Vol. 155, pp. 698-701.
- [182] Munro, B. T. Campbell, G. Wallace, and J. Steele, 2008. The intelligent knee sleeve: A wearable biofeedback device, *Sensors and Actuators B: Chemical*, Vol. 131, pp. 541-547
- [183] Li, L., W.M. Au, Y. Li, K.M. Wan, S.H. Wan, and K.S. Wong, 2009. Design of Intelligent Garment with Transcutaneous Electrical Nerve Stimulation Function Based on the Intarsia Knitting Technique, *Textile Research Journal*, Vol. 80, pp. 279-286.
- [184] Stead, P. Goulev, C. Evans, and E. Mamdani, 2004. The Emotional Wardrobe, *Personal and Ubiquitous Computing*, Vol. 8, pp. 282-290.
- [185] Goulev, P., 2004. Computer Aided Emotional Fashion, *Computers & Graphics*, Vol. 28, pp. 657-666.
- [186] Scott J, Bisig D, Bugmann V., 2007. E-Skin: Research Into Wearable Interfaces, Cross-Modal Perception and Communication for the Visually Impaired on the Mediated Stage. *Digital Creativity*. Vol.18(4), pp.221-233
- [187] Nagendra B., Stijn, O., Stäger, M., Tröster, G., 2004. Towards Wearable Autonomous Microsystems. *Lecture Notes in Computer Science, Pervasive Computing*, V. 3001.
- [188] Suh, N.P., 1990. *The Principles Of Design*, Oxford University Press, New York.
- [189] Suh, N.P., 2001. *Axiomatic Design: Advances and Applications*, Oxford University Press. New York.
- [190] Suh, N.P., 2005. *Complexity Theory and Applications*, Oxford University Press. New York.
- [191] Kulak, O., Kahraman, C. 2005. Fuzzy multi-attribute selection among transportation companies using axiomatic design and analytic hierarchy process. *Information Sciences*, Vol.170, pp.191-210.
- [192] Kulak, O., Kahraman, C., 2005. Multi-attribute comparison of advanced manufacturing systems using fuzzy vs. crisp axiomatic design approach. *International Journal of Production Economics*, Vol. 95, 415-424.
- [193] Kulak, O., Durmuşoğlu, M.B., Kahraman, C., 2005. Fuzzy multi-attribute equipment selection based on information axiom. *Journal of Materials Processing Technology*, Vol. 169, pp. 337-345.
- [194] Kulak, O., 2005. A decision support system for fuzzy multi-attribute selection of material handling equipments”, *Expert Systems with Applications*, Vol. 29(2), pp. 310-319.
- [195] Kahraman, C., Cebi, S., 2009. A new multi-attribute decision making method: Hierarchical fuzzy axiomatic design, *Expert Systems with Applications*, Vol. 36(3-1), pp.4848-4861.
- [196] Celik, M., Cebi, S., Kahraman, C., and Er, I. D., 2009. An Integrated Fuzzy QFD Model Proposal on Routing of Shipping Investment Decisions in Crude Oil Tanker Market Expert Systems with Applications, Vol. 36 (3),2, 6227-6235

-
- [197] Celik, M., Cebi, S., Kahraman, C., Er, D., 2009. Application of axiomatic design and TOPSIS methodologies under fuzzy environment for proposing competitive strategies on Turkish container ports in maritime transportation network, *Expert Systems with Applications* Vol. 36(3),1, 4541-4557.
- [198] Celik, M., Kahraman, C., Cebi, S., & Er, I. D., 2009. Fuzzy Axiomatic Design-Based Performance Evaluation Model for Docking Facilities in Shipbuilding Industry: The Case of Turkish Shipyards, *Expert Systems with Applications*, Vol. 36, 1, pp. 599-615.
- [199] Coelho, A.M. and Moura J.F., “Axiomatic design as support for decision-making in a design for manufacturing context: A case study”, *International Journal of Production Economics*, 2007, Vol. 109, pp. 81–89
- [200] Kahraman C, Kaya I, Cebi S, 2009. A Comparative Analysis For Multiattribute Selection Among Renewable Energy Alternatives Using Fuzzy Axiomatic Design And Fuzzy Analytic Hierarchy Process, *Energy*: Vol. 34, 2009, pp. 1603–1616.
- [201] Cebi S., Kahraman C, 2010. Developing a Group Decision Support System Based on Fuzzy Information Axiom, *Knowledge-Based Systems*, Vol.23 (1), pp.3-16
- [202] Zeng, J., An, M., Smith, N.J., 2007. Application of a fuzzy based decision making methodology to construction project risk assessment, *international journal of project management*, Vol. 25, pp. 589-600.
- [203] Saaty, T.L., 1980. *The Analytic Hierarchy Process*, McGraw-Hill, New York,
- [204] Maxbotix Inc., LV-Maxsonar ®-EZ3™ Data Sheet and LV Chaining Application Notes, available at <www.maxbotix.com> accessed February 2011
- [205] Url-5 <<http://www.pointcarre.com/> accessed> February 2011
- [206] TexGen Software® developed at University of Nottingham
- [207] Arduino LilyPad Vibe Board® available on <<http://www.arduino.cc/>> accessed February 2011
- [208] Choma, A.M., Sarunic, M. V. , Yang,C., Izatt,J.I, 2003. Sensitivity advantage of swept source and Fourier domain optical coherence tomography, *Optics Express*, Vol. 11(18)
- [209] Alvarezetal J., Yanez Y., Prego L., Turo A., Chavez J, Garcia M., Salazar J., 2006. Noise level analysis in bufferrod geometries for ultrasonic sensors, *Ultrasonics*, Vol. 44, 1093–1100
- [210] Peter K. and Schweinzer, H. 2006. Localization Of Object Edges In Arbitrary Spatial Positions Based On Ultrasonic Data, *IEEE Sensors Journal*, Vol. 6, no. 1
- [211] Cheol-Hong M., Young-Soo R., and Hwa-Young K. 2007, An Soc Embedded System Implementation Using An Array Sensor, *Proceddings of 4th International Conference On Fuzzy Systems and Knowledge Discovery*
- [212] Chouvardas, V.G., Miliou, A.N, Hatalis, M.K., 2008. Tactiledisplays: Overview and recent advances, *Displays*, Vol. 29, 185–194
- [213] Rupert, A. H. 2000. An instrumentation solution for reducing spatial disorientation mishaps: Amore “natural” approach to maintaining spatial orientation. *IEEE Engineering in Medicine and Biology Magazine*, pp. 71–80

-
- [214] Van Veen, H. A. H. C., van Erp, J. B. F. 2003. Providing directional information with tactile torso displays. *Eurohaptics*, pp.471–474
- [215] Rochlis, J. L., Newman, D. J. 2000. A tactile display for International Space Station (ISS) extravehicular activity (EVA). *Aviation, Space, and Environmental Medicine* Vol. 7, pp. 571–578
- [216] Traylor, R., Tan, H. Z. 2002. Development of a wearable haptic display for situation awareness in altered-gravity environment: Some initial findings. *10th International Symposium on Haptic Interfaces for Virtual Environment and Teleoperation Systems, Los Alamitos, CA: IEEE Computer Society*, pp. 159–164
- [217] Gilson, R. D., Redden, E. S., Elliott, L. R. 2007. Remote tactile displays for future soldiers, *Tech. Rep. ARL-SR-0152*. Aberdeen Proving Ground, MD: Army Research Laboratory
- [218] Jones, L. A., Lockyer, B., Piatieski, E. 2006. Tactile display and vibrotactile recognition on the torso. *Advanced Robotics*, Vol. 20, pp. 1359–1374
- [219] Lindeman, R. W., Sibert, J. L., Lathan, C. E., Vice, J. M. 2004. The design and deployment of a wearable vibrotactile feedback system. *Proceedings of the Eighth International Symposium on Wearable Computers, Los Alamitos, CA: IEEE Computer Society*, pp. 56–59
- [220] Barbacena, I. L., Barros, A T, Freire, R C S, Vieira, E C A, 2007. Evaluation of pitch coding alternatives for vibrotactile stimulation in speech training of the deaf, *Journal of Physics: Conference Series* 90, 012092
- [221] Yoon, M.-jong, Jeong, G.-young, & Yu, K.-ho. 2009. A Study on Recognition of Obstacle Distribution by Tactile Stimulation, 2. *ICROS-SICE International Joint Conference*, August 18-21, Fukuoka International Congress Center, Japan, pp. 503-508
- [222] Yoon, M.-J., & Yu, K.-H, 2008. Psychophysical experiment of vibrotactile pattern perception by human fingertip. *IEEE transactions on neural systems and rehabilitation engineering*, Vol. 16(2), pp. 171-177
- [223] Bliss, J. C., Katcher, M. H., Rogers, C. H., & Shepard, R. P. 1970. Optical-to-tactile image conversion for the blind. *IEEE Transactions on Man-Machine Systems*, MMS-11, pp. 58–65.
- [224] Chang, A. S., Jacob, R., Gunther, E., Ishii, H. 2002. ComTouch: Design of a Vibrotactile Communication Device, *Proceedings of the conference on Designing interactive systems: processes, practices, methods, and techniques*, London, England, ACM Press, 312, 320
- [225] Harazin, B., Lechowska, H. A., Kalamarz, J., Zielinski, G. , 2005. Measurements of Vibrotactile Perception Thresholds at the Fingertips in Poland, *Industrial Health*, Vol.43, pp. 535–541
- [226] Lynette A. Jones, 2008. Tactile Displays: Guidance for Their Design and Application, *Human Factors*, Vol. 50(1), 90-111
- [227] Bolanowski, S. J., Gescheider, G. A., & Verrillo, R. T.1994. Hairy skin: Psychophysical channels and their physiological substrates. *Somato- sensory and Motor Research*, Vol. 11, 279–290

-
- [228] Gescheider, G. A., Bolanowski, S. J., Pope, J. V., & Verrillo, R. T. 2002. A four-channel analysis of the tactile sensitivity of the fingertip: Frequency selectivity, spatial summation, and temporal summation, *Somatosensory and Motor Research*, Vol. 19, pp. 114–124
- [229] Sherrick, C. E. 1953. Variables affecting sensitivity of the human skin to mechanical vibration. *Journal of Experimental Psychology*, Vol. 45, pp. 273–282
- [230] Verrillo, R. 1963. Effect on contactor area on the vibrotactile threshold, *Journal of the Acoustical Society of America*, Vol. 35, pp. 1962–1966
- [231] Wyllie, I. H., & Griffin, M. J. 2009. Discomfort from sinusoidal oscillation in the pitch and fore and-aft axes at frequencies between 0.2 and 1.6Hz. *Journal of Sound and Vibration*, Vol. 324(1-2), 453-467
- [232] Goff, G.D., 1967. Differential discrimination of frequency of cutaneous mechanical vibration, *Journal of Experimental Psychology*, Vol. 74(2), pp. 294-299
- [233] Rothenberg, G.D., Verrillo, R.T., Zahorian, S.A., Brachman, M.L. and Bolanowski, S.J. 1977. Vibrotactile frequency for encoding a speech parameter, *Journal of the Acoustical Society of America* Vol. 62 (4), pp. 1003-1012
- [234] Mowbray, G.H., Gebhard, J.W., 1957. Sensitivity of the skin to changes in rate of intermittent mechanical stimuli, *Science*, Vol. 125, pp. 1297- 1298
- [235] Franzén, O., Nordmark, J. 1975. Vibrotactile frequency discrimination, *Perception and Psychophysics*, Vol. 17 (5), pp. 480-484
- [236] Craig, J.C., 1972. Difference threshold for intensity of tactile stimuli, *Perception and Psychophysics*, Vol. 11(2), pp.150-152
- [237] Craig, J.C., 1974. Vibrotactile difference thresholds for intensity and the effect of a masking stimulus, *Perception and Psychophysics*, Vol.15(1), pp. 123-127
- [238] Shibata, N., Maeda, S. 2008. Effect of tool handle diameter on temporary threshold shift (TTS) of vibrotactile perception. *International Journal of Industrial Ergonomics*, Vol. 38(9-10), pp. 697–702
- [239] Soneda, T., Nakano, K. 2010. Investigation of vibrotactile sensation of human fingerpads by observation of contact zones. *Tribology International*, Vol. 43(1-2), pp.210-217
- [240] Harada N, Griffin MJ, 1991. Factors influencing vibration sense thresholds used to assess occupational exposures to hand transmitted vibration., *Br J Industr Medic*, Vol. 48, pp. 185–92
- [241] Rowe M.J., 2002. Synaptic transmission between single tactile and kinaesthetic sensory nerve fibers and their central target neurones, *Behavioural Brain Research* Vol. 135, pp.197-212
- [242] Schultz, A. E, Marasco, P. D, Kuiken, T. A, 2009. Vibrotactile detection thresholds for chest skin of amputees following targeted reinnervation surgery, *Brain Research*, Vol. 1251, pp. 121- 129
- [243] Békésy, G. von. 1962. Can we feel the nervous discharges of the end organs during vibratory stimulation of the skin? *Journal of the Acoustical Society of America* Vol. 34, pp. 850–856
- [244] Kubo, M. 2001. An investigation into a synthetic vibration model for humans: An investigation into a mechanical vibration human model constructed according to the relations between the physical,

- psychological and physiological reactions of humans exposed to vibration. *International Journal of Industrial Ergonomics*, Vol. 27(4), pp. 219-232
- [245] Ahn, S.-J., Griffin, M. J. 2008. Effects of frequency, magnitude, damping, and direction on the discomfort of vertical whole-body mechanical shocks. *Journal of Sound and Vibration*, Vol. 311(1-2), pp. 485-497
- [246] Pongrac, H. 2006. Vibrotactile Perception: Differential Effects of Frequency, Amplitude, and Acceleration. *2006 IEEE International Workshop on Haptic Audio Visual Environments and their Applications*, November, pp. 54-59
- [247] Brown, L. M., Brewster, S. A., Purchase, H. C. 2005. A first investigation into the effectiveness of tactons. In *Proceedings of the First Joint Eurohaptics Conference and Symposium on Haptic Interfaces for Virtual Environment and Teleoperator Systems*. Los Alamitos, CA: IEEE Computer Society, pp. 167-176
- [248] Goble, A.K., A.A. Collins and R.W. Cholewiak, 1996. Vibrotactile threshold in young and old observers: The effect of spatial summation and the presence of a rigid surround, *Journal of the Acoustical Society of America*, Vol. 99 (4-1), pp. 2256-2269
- [249] Blanka, Z., 2008. Application Of Fuzzy Sets In Employees ' Evaluation, *Journal of Applied Mathematics*, Vol. 1 (1), pp. 475-484
- [250] Ino, S., Homma, T., Izumi, T., 2008. Psychophysical Measurement of Multiple Tactile Sensations Using a Broadband Vibrotactile Display, *2008 Second International Symposium on Universal Communication* pp. 274-280
- [251] Zong, G., Deng, L., & Wang, W. 2006. A Method for Robustness Improvement of Robot Obstacle Avoidance Algorithm. *2006 IEEE International Conference on Robotics and Biomimetics* , pp. 115-119
- [252] Borenstein J, Koren Y. 1991. The vector field histogram fast obstacle avoidance for mobile robots, *IEEE Int. Conf. Robotics and Automation*, pp. 278-288
- [253] Deng, M., Inoue, a, Sekiguchi, K., & Jiang, L. 2010. Two-wheeled mobile robot motion control in dynamic environments. *Robotics and Computer-Integrated Manufacturing*, Vol. 26(3), pp. 268-272
- [254] Baltés J., Hildreth N, 2001. Adaptive path planner for highly dynamic environments, *RoboCup-2000: Robot Soccer World Cup iv*. Berlin: Springer Verlag, p. 76-85
- [255] Ku, A. L., C.-heng, Tsai, W.-hsiang, & Member, S. 2001. Obstacle Avoidance in Person Following for Guidance Using Vehicle Location Estimation and Quadratic Pattern Classifier. *System*, Vol. 48(1), pp. 205-215.
- [256] Toibero, J. M., Roberti, F., Carelli, R., & Fiorini, P. 2010. Switching control approach for stable navigation of mobile robots in unknown environments. *Robotics and Computer-Integrated Manufacturing*, Vol. 27(3), 558-568.

- [257] Ray, K.A., Behera, L., Jamshidi, M., 2009. Sonar Based Rover Navigation for Single or Multiple Platforms : Forward Safe Path and Target Switching Approach, *IEEE Systems Journal*, Vol. 2, no. 2, ,pp 258-272
- [258] Ray, A. K., Gupta, M., Behera, L., & Jamshidi, M. 2008. Sonar based Autonomous Automatic Guided Vehicle (AGV) navigation. *IEEE International Conference on System of Systems Engineering*, pp. 1-6
- [259] Marques, Carlos, Lima, P. 2004. Multisensor Navigation for Nonholonomic Robots in Cluttered Environments. *IEEE Robotics & Automation Magazine*, September, pp. 70-82.
- [260] Yi, J., Zhang, X., Ning, Z., & Huang, Q. 2009. Intelligent Robot Obstacle Avoidance System Based on Fuzzy Control. *First International Conference on Information Science and Engineering*, pp. 3812-3815
- [261] Chen, Y.-sheng, & Juang, J.-gau. 2009. Intelligent Obstacle Avoidance Control Strategy for Wheeled Mobile Robot. *ICROS-SICE 2009*, Japan, pp. 3199-3204.
- [262] Raguraman, S. M., Tamilselvi, D., & Shivakumar, N. 2009. Mobile Robot Navigation Using Fuzzy logic Controller. *Control Automation, Communication and Energy Conservation*, pp. 3-7.
- [263] Guo, H., Cao, C., Yang, J., & Zhang, Q. 2009. Research on Obstacle-Avoidance Control Algorithm of Lower Limbs Rehabilitation Robot Based on Fuzzy Control. *Sixth International Conference on Fuzzy Systems and Knowledge Discovery*, pp. 151-155
- [264] Pradhan, S., Parhi, D. Panda, A, 2009. Fuzzy Logic techniques for several mobile robots, *Applied Soft Computing*, Vol. 9, pp. 290-304
- [265] Park, K., & Zhang, N. 2007. Behavior-Based Autonomous Robot Navigation on Challenging Terrain: A Dual Fuzzy Logic Approach. *IEEE Symposium on Foundations of Computational Intelligence*, pp. 239-244.
- [266] Farooq, U., Hasan, K. M., Amar, M., Khan, S., & Javaid, S. 2010. A Low Cost Microcontroller Implementation of Fuzzy Logic Based Hurdle Avoidance Controller for a Mobile Robot. *Electrical Engineering*, pp. 480-485.
- [267] Maaref, H., & Barret, C. 2000. Sensor-based fuzzy navigation of an autonomous mobile robot in an indoor environment. *Control Engineering Practice*, Vol. 8(7), pp. 757-768.
- [268] Thongchai, S., & Kawamura, K. 2000. Application of fuzzy control to a sonar-based obstacle avoidance mobile robot. *IEEE International Conference on Control Applications. Conference Proceedings*, pp. 425-430
- [269] Liata, J.R, Sarabia, E.G., Arce J., Oria, J.P., 1998. Fuzzy controller for obstacle avoidance in robotic manipulators using ultrasonic sensors, AMC-98 Coimbra, pp. 647-652
- [270] Gharieb, W., Nagib, G. 2000. Fuzzy Guidance Control For a Mobile robot, *Current Advances in Mechanical Design and Production, MDP-7*, Cairo, pp. 67-74

- [271] Li, W. 1994. Fuzzy logic based robot navigation in uncertain environments by multisensor integration. *IEEE International Conference Multisensor Fusion and Integration for Intelligent Systems*, pp. 259-264
- [272] Choi, J. W., Kwon, S. H., Lee, H. Y., & Lee, S. G. 1998. Navigation strategy of an intelligent mobile robot using fuzzy logic. *International Conference on Fuzzy Systems Proceedings*, pp. 602-605
- [273] Kim, B. N., Kwon, O. S., Kim, K. H., Lee, E. H., & Hong, S. H. 1999. A study on path planning for mobile robot based on fuzzy logic controller. *Proceedings Multimedia Technology for Asia-Pacific Information Infrastructure*, pp. 1002-1005
- [274] Hui, NB, Pratihari DK, 2005. Mobile robot navigation: potential field approach vs. genetic-fuzzy system, 10th online world conference on soft computing
- [275] Liu, Q., Lu, Y, Xie C., 2006. Optimal Genetic fuzzy obstacle avoidance controller of autonomous mobile robot based on ultrasonic sensors, *Int. Conf. on Robotics and Biomimetics*, China, pp. 125-129
- [276] Liu, Q. 2006. Fuzzy Obstacle-avoiding Controller of Autonomous Mobile Robot Optimized by Genetic Algorithm under Multi-obstacles Environment. *6th World Congress on Intelligent Control and Automation*, pp. 3255-3259
- [277] Szemes, P. T., Hashimoto, H., & Korondi, P. 2005. Pedestrian-Behavior-Based Mobile Agent Control in Intelligent Space. *IEEE Transactions on Instrumentation and Measurement*, Vol. 54(6), pp. 2250-2257
- [278] Mahyuddin, M. N., Wei, C. Z., & Arshad, M. R. 2009. Neuro-fuzzy algorithm implemented in Alteras FPGA for mobile robot's obstacle avoidance mission. *TENCON IEEE Region 10 Conference*, pp. 1-6
- [279] Nasiruddin Mahyuddin, M. 2009. Neuro-fuzzy algorithm for obstacle avoidance mission of a mobile robot using FPGA. *Innovative Technologies in Intelligent Systems and Industrial Applications*, pp. 305-310
- [280] He, K., Sun, H., & Cheng, W. 2008. Application of fuzzy neural network based on T-S model for mobile robot to avoid obstacles. *7th World Congress on Intelligent Control and Automation*, pp. 8282-8285
- [281] Ray, A. K., Behera, L., & Jamshidi, M. 2009. GPS and sonar based area mapping and navigation by mobile robots. *7th IEEE International Conference on Industrial Informatics*, pp. 801-806
- [282] Hui, N. B., & Pratihari, D. K. 2009. A comparative study on some navigation schemes of a real robot tackling moving obstacles. *Robotics and Computer-Integrated Manufacturing*, Vol. 25(4-5), pp. 810-828
- [283] Neural Network Notes, MATLAB® 2008 Version.
- [284] Fuzzy Inference System Notes, MATLAB® 2008 Version.

- [285] Gaweda A.E., Scherer R., 2004, Fuzzy Number-Based Hierchical Fuzzy Systems, *Artificial Intelligence and Soft Computing*, pp. 302-307
- [286] Url-6 http://www.atmel.com/dyn/resources/prod_documents/doc8271.pdf accessed on February 2011
- [287] Knoblauch,R.L, Pietrucha, M.T, And Nitzburg, M., 2006. Field Studies of Pedestrian Walking Speed and Start-Up Time, *Transportation Research Record*, Vol. 1538, pp. 27-38
- [288] Tim J. Gates, David A. Noyce, Andrea R. Bill, Nathanael V., 2006. Recommended Walking Speeds for Pedestrian Clearance Timing Based on Pedestrian Characteristics, *TRB 2006 Annual Meeting*, Paper No. 06-1826
- [289] Url-7 <http://arduino.cc/en/uploads/Main/LilyPad_schematic_v18.pdf , accessed on February 2011
- [290] Url-8<<http://www.robotshop.com/arduino-lilypad-button-board.html>>, accessed on March 2011
- [291] Url-9<<http://www.robotshop.com/PDF/arduino-lilypad-vibe-board-schematic.pdf>>, accessed on March 2011
- [292] ASHRAE STANDARD 55-2010 Thermal Environmental Conditions for Human Occupancy
- [293] AATCC Test Method 135-2004 Dimensional Changes of Fabrics after Home Laundering

Appendices

Appendix-A1

Ultrasonic Rangefinder Comparison

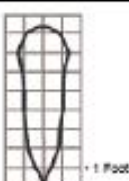
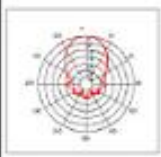
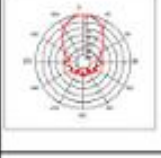
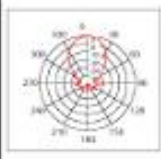
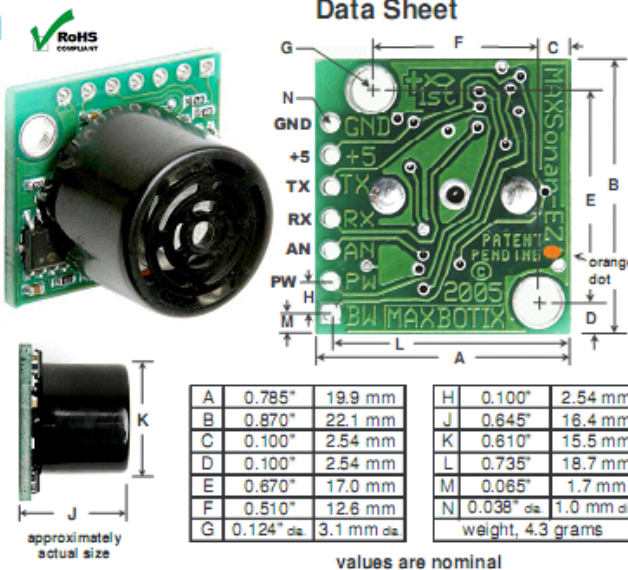
	Dimensions	Ranging Distance	Interface	Power Requirements	Approximate Beam Pattern
 Maxbotix MaxSonar-EZ1	19.9 mm Length 22.1 mm Width 16.4 mm Height	6 to 254 inches (6.45m)	Serial (0-5V), Analog Voltage or Pulse Width	Voltage: 5V Current: 3ma Typical.	
 Devantec SRF04	43 mm Length 20 mm Width 17 mm Height	3cm to 3m	<i>Positive TTL level signal, width proportional to range.</i>	Voltage: 5V Current: 30ma Typical, 50ma Max	
 Devantec SRF05	43 mm Length 20 mm Width 17 mm Height	1cm to 4m	<i>Positive TTL level signal, width proportional to range.</i>	Voltage: 5V Current: 4ma Typical	
 Devantec SRF08	43 mm Length 20 mm Width 17 mm Height	3cm to 6m	Standard I2C Bus	Voltage: 5V Current: 15ma Typical, 3ma Standby	
 Devantec SRF10	32 mm Length 15 mm Width 10 mm Height	3cm to 6m	Standard I2C Bus	Voltage: 5V Current: 15ma Typical, 3ma Standby	
 Devantec SRF235	34 mm Length 20 mm Width 19 mm Height	10cm to 1.2m	Standard I2C Bus	Voltage: 5V Current: 25ma Typical	
 Devantec SRF02	24 mm Length 20 mm Width 12 mm Height	15cm to 6m	Standard I2C Bus Serial (0-5V)	Voltage: 5V Current: 4ma Typical	

Fig. A.1 : Comparison of ultrasonic sensors

Appendix-A2

LV-MaxSonar®-EZ3™ High Performance Sonar Range Finder

With 2.5V - 5.5V power the LV-MaxSonar®-EZ3™ provides very short to long-range detection and ranging, in an incredibly small package. The LV-MaxSonar®-EZ3™ detects objects from 0-inches to 254-inches (6.45-meters) and provides sonar range information from 6-inches out to 254-inches with 1-inch resolution. Objects from 0-inches to 6-inches range as 6-inches. The interface output formats included are pulse width output, analog voltage output, and serial digital output.



Features

- Continuously variable gain for beam control and side lobe suppression
- Object detection includes zero range objects
- 2.5V to 5.5V supply with 2mA typical current draw
- Readings can occur up to every 50mS, (20-Hz rate)
- Free run operation can continually measure and output range information
- Triggered operation provides the range reading as desired
- All interfaces are active simultaneously
 - Serial, 0 to Vcc
 - 9600Baud, 81N
 - Analog, (Vcc/512) / inch
 - Pulse width, (147uS/inch)
- Learns ringdown pattern when commanded to start ranging
- Designed for protected indoor environments
- Sensor operates at 42KHz
- High output square wave sensor drive (double Vcc)

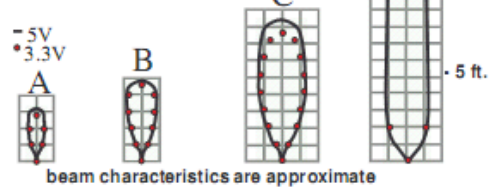
Benefits

- Very low cost sonar ranger
- Reliable and stable range data
- Sensor dead zone virtually gone
- Lowest power ranger
- Quality beam characteristics
- Mounting holes provided on the circuit board
- Very low power ranger, excellent for multiple sensor or battery based systems
- Can be triggered externally or internally
- Sensor reports the range reading directly, frees up user processor
- Fast measurement cycle
- User can choose any of the three sensor outputs

Beam Characteristics

Many applications require a narrower beam or lower sensitivity than the LV-MaxSonar®-EZ1™. Consequently, MaxBotix® Inc., is offering, the EZ2™, EZ3™, & EZ4™ with progressively narrower beam angles allowing the sensor to match the application. Sample results for the LV-MaxSonar®-EZ3™ measured beam patterns are shown below on a 12-inch grid. The detection pattern is shown for; (A) 0.25-inch diameter dowel, note the narrow beam for close small objects, (B) 1-inch diameter dowel, note the long narrow detection pattern, (C) 3.25-inch diameter rod, note the long controlled detection pattern, (D) 11-inch wide board moved left to right with the board parallel to the front sensor face and the sensor stationary. This shows the sensor's range capability.

Note: The displayed beam width of (D) is a function of the specular nature of sonar and the shape of the board (i.e. flat mirror like) and should never be confused with actual sensor beam width.



MaxBotix® Inc.

MaxBotix, MaxSonar, EZ2, EZ3 & EZ4 are trademarks of MaxBotix Inc.
LV-EZ3™ • v3.0c • 01/2007 • Copyright 2005 - 2007

8757 East Chimney Spring Drive, Tucson AZ, 85747 USA
4613 County Road 8, Brainerd, MN, 56401 USA

Email: info@maxbotix.com Web: www.maxbotix.com

Fig. A.2 : LV-MaxSonar® EZ3 Type ultrasonic sensor datasheet.

Appendix B.1

Table B.1 : Detection error calculations for scenario 1

Case No	Position of object (x,y)	Actual distance to obstacle from sensors (cm) [d]				If object is detected by sensor then measured average distance (cm) [\bar{x}]				Calculation for $MSE(\bar{X})$			
		Sensor 1	Sensor 2	Sensor 3	Sensor 4	Sensor 1	Sensor 2	Sensor 3	Sensor 4	Sensor 1	Sensor 2	Sensor 3	Sensor 4
1	(-40,40)	50.0	64.0	64.0	50.0	239.3	238.0	242.0	239.0	-	-	-	-
2	(-40,60)	67.1	78.1	78.1	67.1	239.0	238.0	242.0	239.0	-	-	-	-
3	(-40,80)	85.4	94.3	94.3	85.4	239.2	238.3	242.4	239.4	-	-	-	-
4	(-40,100)	104.4	111.8	111.8	104.4	239.3	238.4	242.4	239.5	-	-	-	-
5	(-40,120)	123.7	130.0	130.0	123.7	239.2	238.3	242.7	239.7	-	-	-	-
6	(-40,140)	143.2	148.7	148.7	143.2	239.2	238.2	242.6	239.6	197.5	-	-	-
7	(-40,160)	162.8	167.6	167.6	162.8	239.4	238.5	242.7	239.6	-	-	-	-
8	(-40,180)	182.5	186.8	186.8	182.5	239.2	238.2	242.5	239.7	-	-	-	-
9	(-40,200)	202.2	206.2	206.2	202.2	239.2	238.4	242.5	239.6	-	-	-	-
10	(-30,40)	44.7	56.6	56.6	44.7	239.2	238.2	242.6	239.6	-	-	-	-
11	(-30,60)	63.2	72.1	72.1	63.2	224.0	238.0	242.0	239.0	-	-	-	-
12	(-30,80)	82.5	89.4	89.4	82.5	78.5	238.3	242.6	239.7	15.7	-	-	-
13	(-30,100)	102.0	107.7	107.7	102.0	95.4	238.3	242.5	239.6	43.8	-	-	-
14	(-30,120)	121.7	126.5	126.5	121.7	112.3	238.4	242.5	239.5	87.8	-	-	-
15	(-30,140)	141.4	145.6	145.6	141.4	127.1	238.2	242.5	239.5	204.4	-	-	-
16	(-30,160)	161.2	164.9	164.9	161.2	146.2	238.4	241.8	239.4	227.2	-	-	-
17	(-30,180)	181.1	184.4	184.4	181.1	163.0	238.4	242.5	239.6	326.3	-	-	-
18	(-30,200)	201.0	204.0	204.0	201.0	179.8	238.1	242.6	239.9	447.3	-	-	-
19	(-20,40)	41.2	50.0	50.0	41.2	44.0	238.0	242.0	239.0	7.7	-	-	-
20	(-20,60)	60.8	67.1	67.1	60.8	59.0	238.0	242.0	239.0	3.3	-	-	-
21	(-20,80)	80.6	85.4	85.4	80.6	76.4	238.3	242.5	239.6	18.3	-	-	-
22	(-20,100)	100.5	104.4	104.4	100.5	93.4	238.3	242.4	239.4	50.5	-	-	-
23	(-20,120)	120.4	123.7	123.7	120.4	110.2	238.2	242.5	239.5	103.7	-	-	-
24	(-20,140)	140.4	143.2	143.2	140.4	124.8	129.1	242.7	239.6	242.7	199.6	-	-
25	(-20,160)	160.3	162.8	162.8	160.3	144.1	148.2	242.5	239.5	262.7	213.8	-	-
26	(-20,180)	180.3	182.5	182.5	180.3	161.1	164.9	242.7	239.6	366.8	308.3	-	-
27	(-20,200)	200.2	202.2	202.2	200.2	178.0	181.9	242.5	239.6	494.6	412.8	-	-
28	(-10,40)	40.0	44.7	44.7	40.0	42.0	238.0	242.0	239.0	4.0	-	-	-
29	(-10,60)	60.0	63.2	63.2	60.0	57.0	64.0	242.0	239.0	9.0	0.6	-	-
30	(-10,80)	80.0	82.5	82.5	80.0	74.0	78.0	242.0	239.0	36.0	19.9	-	-
31	(-10,100)	100.0	102.0	102.0	100.0	91.0	95.5	242.4	239.4	80.8	41.6	-	-
32	(-10,120)	120.0	121.7	121.7	120.0	110.2	114.1	242.7	113.5	95.4	57.7	-	42.8
33	(-10,140)	140.0	141.4	141.4	140.0	124.7	128.9	242.5	130.0	233.2	155.6	-	99.8
34	(-10,160)	160.0	161.2	161.2	160.0	143.9	145.9	242.7	147.7	259.5	236.3	-	151.3
35	(-10,180)	180.0	181.1	181.1	180.0	161.1	162.8	242.6	239.7	357.7	335.5	-	-
36	(-10,200)	200.0	201.0	201.0	200.0	175.6	179.6	242.6	239.6	593.2	458.0	-	-
37	(0--,40)	40.0	41.2	41.2	40.0	42.0	47.0	242.0	49.0	4.0	33.3	-	81.0
38	(0--,60)	60.0	60.8	60.8	60.0	57.0	60.0	242.0	62.0	9.0	0.7	-	4.0
39	(0--,80)	80.0	80.6	80.6	80.0	76.0	78.0	242.0	81.0	16.0	6.9	-	1.0
40	(0--,100)	100.0	100.5	100.5	100.0	91.2	93.6	242.5	96.3	77.1	47.8	-	13.8
41	(0--,120)	120.0	120.4	120.4	120.0	110.4	110.4	242.4	113.1	91.6	100.5	-	47.8
42	(0--,140)	140.0	140.4	140.4	140.0	127.1	127.1	242.4	130.1	166.8	175.9	-	97.8
43	(0--,160)	160.0	160.3	160.3	160.0	143.9	143.8	242.5	146.8	260.1	273.0	-	173.4
44	(0--,180)	180.0	180.3	180.3	180.0	158.8	160.8	242.4	163.7	449.2	380.1	-	265.9
45	(0--,200)	200.0	200.2	200.2	200.0	176.0	177.6	242.4	178.5	575.9	514.7	-	460.6
46	(0,40)	40.0	40.0	40.0	40.0	43.4	42.9	51.3	50.1	5.6	8.6	128.1	40.0
47	(0,60)	60.0	60.0	60.0	60.0	57.4	57.8	63.7	62.6	6.7	4.9	13.7	6.8
48	(0,80)	80.0	80.0	80.0	80.0	78.3	78.6	84.8	83.4	2.8	2.1	23.3	11.6
49	(0,100)	100.0	100.0	100.0	100.0	95.3	95.6	101.6	98.6	21.9	19.0	2.4	2.0
50	(0,120)	120.0	120.0	120.0	120.0	108.1	108.3	114.1	113.1	14.1	13.6	34.8	47.5
51	(0,140)	140.0	140.0	140.0	140.0	127.0	127.0	133.1	132.2	169.2	167.7	47.6	60.6
52	(0,160)	160.0	160.0	160.0	160.0	148.4	148.2	154.1	151.0	134.0	139.9	35.3	81.6
53	(0,180)	180.0	180.0	180.0	180.0	163.0	162.8	168.9	239.7	290.4	294.9	123.2	-
54	(0,200)	200.0	200.0	200.0	200.0	178.0	179.7	242.4	182.8	483.2	411.2	-	295.6
55	(0+,40)	41.2	40.0	40.0	42.4	46.8	45.0	51.7	239.7	30.9	24.6	136.2	-
56	(0+,60)	60.8	60.0	60.0	61.6	57.5	56.0	63.8	239.5	10.8	15.7	14.7	-
57	(0+,80)	80.6	80.0	80.0	81.2	78.5	76.8	84.7	239.5	4.5	10.4	22.5	-
58	(0+,100)	100.5	100.0	100.0	101.0	95.5	93.6	99.6	239.6	25.1	41.1	0.1	-
59	(0+,120)	120.4	120.0	120.0	120.8	112.2	110.2	116.4	239.5	68.1	95.7	13.3	-
60	(0+,140)	140.4	140.0	140.0	140.7	131.3	129.1	242.0	239.6	81.4	118.3	-	-
61	(0+,160)	160.3	160.0	160.0	160.6	148.1	147.8	242.6	239.7	148.7	148.3	-	-
62	(0+,180)	180.3	180.0	180.0	180.6	163.1	160.9	166.8	239.6	296.7	366.2	175.4	-
63	(0+,200)	200.2	200.0	200.0	200.5	178.0	177.4	242.4	239.6	494.6	510.7	-	-
64	(10,40)	44.7	40.0	40.0	44.7	239.2	45.0	240.4	239.7	-	25.2	-	-
65	(10,60)	63.2	60.0	60.0	63.2	63.7	57.8	66.1	239.6	0.2	4.8	37.3	-
66	(10,80)	82.5	80.0	80.0	82.5	80.7	76.8	82.7	239.3	3.1	10.4	7.1	-
67	(10,100)	102.0	100.0	100.0	102.0	95.4	93.6	99.5	239.4	42.9	40.4	0.3	-
68	(10,120)	121.7	120.0	120.0	121.7	239.1	110.2	240.0	239.4	-	95.4	-	-
69	(10,140)	141.4	140.0	140.0	141.4	239.3	127.3	241.4	239.6	-	160.6	-	-
70	(10,160)	161.2	160.0	160.0	161.2	239.3	150.3	242.2	239.5	119.5	198.7	-	-
71	(10,180)	181.1	180.0	180.0	181.1	219.3	162.8	242.6	239.7	-	295.8	-	-
72	(10,200)	201.0	200.0	200.0	201.0	182.0	179.5	242.6	239.6	359.2	420.7	-	-
73	(20,40)	50.0	41.2	41.2	50.0	239.2	44.9	240.3	239.6	-	13.7	-	-
74	(20,60)	67.1	60.8	60.8	67.1	239.1	57.7	240.9	239.5	-	9.8	-	-
75	(20,80)	85.4	80.6	80.6	85.4	239.3	78.8	240.4	239.5	-	3.2	-	-
76	(20,100)	104.4	100.5	100.5	104.4	239.3	93.6	242.2	239.5	-	47.0	-	-
77	(20,120)	123.7	120.4	120.4	123.7	239.0	110.2	240.5	239.7	-	104.8	-	-
78	(20,140)	143.2	140.4	140.4	143.2	239.1	130.2	242.5	239.6	-	102.5	-	-
79	(20,160)	162.8	160.3	160.3	162.8	239.2	148.2	241.5	239.4	-	147.3	-	-
80	(20,180)	182.5	180.3	180.3	182.5	239.2	164.9	242.5	239.5	-	236.0	-	-
81	(20,200)	202.2	200.2	200.2	202.2	239.4	179.6	242.6	239.6	-	427.6	-	-
82	(30,40)	56.6	44.7	44.7	56.6	239.4	238.4	240.4	239.6	-	-	-	-
83	(30,60)	72.1	63.2	63.2	72.1	239.2	61.9	240.4	239.5	-	1.8	-	-
84	(30,80)	89.4	82.5	82.5	89.4	239.2	81.1	240.3	239.6	-	2.0	-	-
85	(30,100)	107.7	102.0	102.0	107.7	239.2	97.8	240.3	239.6	-	17.3	-	-
86	(30,120)	126.5	121.7	121.7	126.5	239.0	114.4	240.3	239.6	-	52.7	-	-
87	(30,140)	145.6	141.4	141.4	145.6	239.2	238.4	240.7	239.4	-	-	-	-
88	(30,160)	164.9	161.2	161.2	164.9	239.1	148.0	241.1	239.5	-	176.5	-	-
89	(30,180)	184.4	181.1	181.1	184.4	239.1	164.8	242.5	239.5	-	267.4	-	-
90	(30,200)	204.0	201.0	201.0	204.0	239.2	182.0	242.6	239.8	-	359.9	-	-
91	(40,40)	64.0	50.0	50.0	64.0	239.0	238.2	240.4	239.6	-	-	-	-
92	(40,60)	78.1	67.1	67.1	78.1	239.2	238.2	240.3	239.6	-	-	-	-
93	(40,80)	94.3	85.4	85.4	94.3	239.2	238.2	240.2	239.5	-	-	-	-
94	(40,100)	111.8	104.4	104.4	111.8	239.3	238.5	240.2	239.5	-	-</		

Table B.2 : Detection error calculations for scenario 2

Case No	Position of object (x,y)	Actual distance to obstacle from sensors (cm) [a]				If object is detected by sensor then measured average distance (cm) [X̄]				Calculation for MSE(X̄)			
		Sensor 1	Sensor 2	Sensor 3	Sensor 4	Sensor 1	Sensor 2	Sensor 3	Sensor 4	Sensor 1	Sensor 2	Sensor 3	Sensor 4
1	(-40,40)	50.0	64.0	64.0	50.0	239.3	238.1	236.1	233.5	-	-	-	-
2	(-40,60)	67.1	78.1	78.1	67.1	239.1	238.2	240.3	234.3	-	-	-	-
3	(-40,80)	85.4	94.3	94.3	85.4	241.2	238.3	236.0	233.8	-	-	-	-
4	(-40,100)	104.4	111.8	111.8	104.4	239.3	238.4	236.1	233.5	-	-	-	-
5	(-40,120)	123.7	130.0	130.0	123.7	239.1	238.2	239.8	233.3	-	-	-	-
6	(-40,140)	143.2	148.7	148.7	143.2	242.3	238.5	236.2	233.6	-	-	-	-
7	(-40,160)	162.8	167.6	167.6	162.8	239.1	238.2	236.1	233.4	-	-	-	-
8	(-40,180)	182.5	186.8	186.8	182.5	241.3	238.1	236.1	233.5	-	-	-	-
9	(-40,200)	202.2	206.2	206.2	202.2	238.9	238.1	236.0	233.3	-	-	-	-
10	(-30,40)	44.7	56.6	56.6	44.7	239.3	238.4	236.0	233.3	-	-	-	-
11	(-30,60)	63.2	72.1	72.1	63.2	230.9	238.2	236.0	233.3	-	-	-	-
12	(-30,80)	82.5	89.4	89.4	82.5	240.4	238.1	235.9	233.5	-	-	-	-
13	(-30,100)	102.0	107.7	107.7	102.0	237.3	238.5	239.0	233.6	-	-	-	-
14	(-30,120)	121.7	126.5	126.5	121.7	239.0	238.3	236.8	234.1	-	-	-	-
15	(-30,140)	141.4	145.6	145.6	141.4	239.2	238.2	236.1	233.7	-	-	-	-
16	(-30,160)	161.2	164.9	164.9	161.2	198.3	237.7	236.2	233.4	-	-	-	-
17	(-30,180)	181.1	184.4	184.4	181.1	205.5	227.3	236.2	234.0	-	-	-	-
18	(-30,200)	201.0	204.0	204.0	201.0	228.0	237.2	238.0	233.4	-	-	-	-
19	(-20,40)	41.2	50.0	50.0	41.2	239.3	238.2	236.1	233.4	-	-	-	-
20	(-20,60)	60.8	67.1	67.1	60.8	239.3	238.1	237.4	233.3	0.2	-	-	-
21	(-20,80)	80.6	85.4	85.4	80.6	239.3	237.9	236.0	233.4	6.0	-	-	-
22	(-20,100)	100.5	104.4	104.4	100.5	239.3	238.3	246.7	235.4	26.4	-	-	-
23	(-20,120)	120.4	123.7	123.7	120.4	156.6	238.2	236.8	233.4	-	-	-	-
24	(-20,140)	140.4	143.2	143.2	140.4	157.0	217.6	236.1	233.4	178.8	-	-	-
25	(-20,160)	160.3	162.8	162.8	160.3	222.6	196.9	236.2	233.4	-	-	-	-
26	(-20,180)	180.3	182.5	182.5	180.3	236.3	238.1	236.1	233.4	-	-	-	-
27	(-20,200)	200.2	202.2	202.2	200.2	239.9	229.7	236.1	233.3	384.6	-	-	-
28	(-10,40)	40.0	44.7	44.7	40.0	40.1	238.1	236.2	43.5	0.0	-	-	12.5
29	(-10,60)	60.0	63.2	63.2	60.0	59.3	238.0	236.0	56.2	0.5	-	-	14.1
30	(-10,80)	80.0	82.5	82.5	80.0	76.2	237.8	236.9	228.5	14.2	-	-	-
31	(-10,100)	100.0	102.0	102.0	100.0	91.0	238.4	237.7	233.4	8.15	-	-	-
32	(-10,120)	120.0	121.7	121.7	120.0	107.9	204.0	236.1	106.9	145.6	-	-	171.1
33	(-10,140)	140.0	141.4	141.4	140.0	124.8	201.3	237.9	233.3	230.0	-	-	-
34	(-10,160)	160.0	161.2	161.2	160.0	140.2	233.3	236.1	233.6	390.8	-	-	-
35	(-10,180)	180.0	181.1	181.1	180.0	156.7	200.2	236.1	233.2	543.6	366.0	-	-
36	(-10,200)	200.0	201.0	201.0	200.0	175.4	223.5	236.0	233.3	602.9	507.2	-	-
37	(0-,40)	40.0	41.2	41.2	40.0	39.9	236.9	239.8	45.7	0.0	-	-	32.9
38	(0-,60)	60.0	60.8	60.8	60.0	57.3	122.7	245.1	54.1	7.6	-	-	35.0
39	(0-,80)	80.0	80.6	80.6	80.0	73.9	161.8	183.9	71.1	36.8	-	-	79.6
40	(0-,100)	100.0	100.5	100.5	100.0	91.8	188.9	238.7	90.0	66.7	-	-	100.3
41	(0-,120)	120.0	120.4	120.4	120.0	105.1	128.7	239.1	104.6	203.7	68.3	-	236.0
42	(0-,140)	140.0	140.4	140.4	140.0	124.8	172.4	236.2	132.4	229.8	-	-	57.6
43	(0-,160)	160.0	160.3	160.3	160.0	141.5	185.9	236.0	232.0	336.5	-	-	-
44	(0-,180)	180.0	180.3	180.3	180.0	158.7	159.8	238.6	163.4	544.1	419.2	-	274.7
45	(0-,200)	200.0	200.2	200.2	200.0	173.6	212.5	236.2	233.3	-	149.2	-	-
46	(0,40)	40.0	40.0	40.0	40.0	39.9	40.4	427.0	39.0	0.0	0.2	7.2	1.0
47	(0,60)	60.0	60.0	60.0	60.0	57.0	57.3	57.4	54.1	9.2	7.4	6.9	35.0
48	(0,80)	80.0	80.0	80.0	80.0	74.0	74.3	74.7	70.9	35.5	32.9	28.2	82.1
49	(0,100)	100.0	100.0	100.0	100.0	93.2	93.2	91.0	90.0	46.7	46.0	80.1	99.9
50	(0,120)	120.0	120.0	120.0	120.0	110.2	110.2	107.8	106.8	95.7	96.1	148.3	173.8
51	(0,140)	140.0	140.0	140.0	140.0	127.0	124.9	122.6	122.9	168.5	229.5	302.2	293.8
52	(0,160)	160.0	160.0	160.0	160.0	141.5	141.4	139.1	138.2	340.9	345.4	437.3	475.5
53	(0,180)	180.0	180.0	180.0	180.0	158.7	158.5	185.6	184.6	455.1	462.3	318	212
54	(0,200)	200.0	200.0	200.0	200.0	177.8	177.3	183.5	233.2	495.0	516.4	273.8	-
55	(0+,40)	41.2	40.0	40.0	42.4	247.7	40.7	42.6	236.8	-	0.5	6.5	-
56	(0+,60)	60.8	60.0	60.0	61.6	244.5	57.5	57.6	237.4	-	6.1	5.8	-
57	(0+,80)	80.6	80.0	80.0	81.2	247.8	74.4	74.3	247.5	-	31.9	32.3	-
58	(0+,100)	100.5	100.0	100.0	101.0	238.9	95.3	93.1	238.6	-	22.1	47.0	-
59	(0+,120)	120.4	120.0	120.0	120.8	247.6	110.2	108.0	235.2	-	95.5	144.4	-
60	(0+,140)	140.4	140.0	140.0	140.7	237.0	124.7	122.4	233.5	-	234.6	308.3	-
61	(0+,160)	160.3	160.0	160.0	160.6	247.6	144.6	234.1	233.2	-	237.8	-	-
62	(0+,180)	180.3	180.0	180.0	180.6	247.6	156.3	234.7	233.1	454.9	560.7	-	-
63	(0+,200)	200.2	200.0	200.0	200.5	238.8	175.0	234.9	233.3	-	623.3	-	-
64	(10,40)	44.7	40.0	40.0	44.7	247.3	42.7	233.9	233.2	-	7.5	-	-
65	(10,60)	63.2	60.0	60.0	63.2	247.2	57.5	57.7	233.3	-	6.3	5.4	-
66	(10,80)	82.5	80.0	80.0	82.5	247.1	76.4	76.4	229.7	234.8	-	13.0	-
67	(10,100)	102.0	100.0	100.0	102.0	247.4	91.0	90.5	235.2	-	80.1	28.7	-
68	(10,120)	121.7	120.0	120.0	121.7	247.1	113.7	110.2	233.2	-	40.0	96.6	-
69	(10,140)	141.4	140.0	140.0	141.4	241.2	168.8	243.7	236.6	-	-	-	-
70	(10,160)	161.2	160.0	160.0	161.2	247.0	185.7	234.5	233.4	-	-	-	-
71	(10,180)	181.1	180.0	180.0	181.1	239.6	200.2	242.5	234.0	-	409.2	-	-
72	(10,200)	201.0	200.0	200.0	201.0	238.9	177.3	234.3	233.5	-	516.4	-	-
73	(20,40)	50.0	41.2	41.2	50.0	239.8	63.8	235.7	233.0	-	508.0	-	-
74	(20,60)	67.1	60.8	60.8	67.1	247.6	73.4	237.8	241.1	-	157.8	-	-
75	(20,80)	85.4	80.6	80.6	85.4	244.3	238.2	233.8	240.2	-	-	-	-
76	(20,100)	104.4	100.5	100.5	104.4	239.2	238.2	244.1	236.2	-	-	-	-
77	(20,120)	123.7	120.4	120.4	123.7	247.6	158.2	242.3	233.4	-	-	-	-
78	(20,140)	143.2	140.4	140.4	143.2	243.3	171.1	234.1	233.3	-	-	-	-
79	(20,160)	162.8	160.3	160.3	162.8	238.8	183.7	236.0	233.4	-	547.5	-	-
80	(20,180)	182.5	180.3	180.3	182.5	239.2	200.6	236.1	233.3	-	411.9	-	-
81	(20,200)	202.2	200.2	200.2	202.2	239.1	213.0	236.1	233.5	-	162.9	-	-
82	(30,40)	56.6	44.7	44.7	56.6	247.5	236.2	241.9	233.2	-	-	-	-
83	(30,60)	72.1	63.2	63.2	72.1	243.5	236.9	245.7	233.3	-	-	-	-
84	(30,80)	89.4	82.5	82.5	89.4	247.6	238.1	250.9	233.6	-	-	-	-
85	(30,100)	107.7	102.0	102.0	107.7	243.8	236.7	239.3	232.9	-	-	-	-
86	(30,120)	126.5	121.7	121.7	126.5	247.5	160.5	236.0	233.4	-	-	-	-
87	(30,140)	145.6	141.4	141.4	145.6	241.4	171.0	233.9	234.7	-	-	-	-
88	(30,160)	164.9	161.2	161.2	164.9	239.0	185.7	236.2	233.3	-	-	-	-
89	(30,180)	184.4	181.1	181.1	184.4	239.2	201.2	236.2	233.6	-	405.1	-	-
90	(30,200)	204.0	201.0	201.0	204.0	239.2	215.3	236.1	233.3	-	203.5	-	-
91	(40,40)	64.0	50.0	50.0	64.0	246.7	236.1	244.7	236.5	-	-	-	-
92	(40,60)	78.1	67.1	67.1	78.1	247.5	238.0	242.5	245.6	-	-	-	-
93	(40,80)	94.3	85.4	85.4	94.3	247.5	237.8	233.9	237.6	-	-	-	-
94	(40,100)	111.8	104.4	104.4	111.8	244.6	238.2	234.9	233.1	-	-	-	-
95	(40,120)	130.0	123.7	123.7	130.0	239.3	160.8	234.0	238.7	-	-	-	-
96	(40,140)	148.7	143.2	143.2	148.7	239.1	173.1	235.5	235.2	-	-	-</	

Table B.3 : Detection error calculations for scenario 3

Case No	Position of object (x,y)	Actual distance to obstacle from sensors (cm) [d]				If object is detected by sensor then measured average distance (cm) [\bar{x}]				Calculation for MSE(\bar{x})			
		Sensor 1	Sensor 2	Sensor 3	Sensor 4	Sensor 1	Sensor 2	Sensor 3	Sensor 4	Sensor 1	Sensor 2	Sensor 3	Sensor 4
1	(-40,40)	50.0	64.0	64.0	50.0	247.5	246.6	244.3	243.6	-	-	-	-
2	(-40,60)	67.1	78.1	78.1	67.1	247.7	246.7	244.2	243.7	-	-	-	-
3	(-40,80)	85.4	94.3	94.3	85.4	247.3	246.5	244.3	243.9	-	-	-	-
4	(-40,100)	104.4	111.8	111.8	104.4	247.7	246.7	244.4	244.2	-	-	-	-
5	(-40,120)	123.7	130.0	130.0	123.7	247.5	246.6	244.3	243.7	-	-	-	-
6	(-40,140)	143.2	148.7	148.7	143.2	239.4	239.5	244.3	243.7	-	-	-	-
7	(-40,160)	162.8	167.6	167.6	162.8	238.6	238.3	245.9	243.7	-	-	-	-
8	(-40,180)	182.5	186.8	186.8	182.5	243.9	244.9	244.6	243.9	-	-	-	-
9	(-40,200)	202.2	206.2	206.2	202.2	247.4	246.6	244.4	243.9	-	-	-	-
10	(-30,40)	44.7	56.6	56.6	44.7	247.4	246.5	244.4	243.9	-	-	-	-
11	(-30,60)	63.2	72.1	72.1	63.2	244.8	245.7	244.0	242.6	-	-	-	-
12	(-30,80)	82.5	89.4	89.4	82.5	247.3	246.5	244.4	243.8	-	-	-	-
13	(-30,100)	102.0	107.7	107.7	102.0	247.5	246.7	244.4	243.7	-	-	-	-
14	(-30,120)	121.7	126.5	126.5	121.7	154.5	246.6	244.5	243.9	-	-	-	-
15	(-30,140)	141.4	145.6	145.6	141.4	221.5	231.7	244.5	243.8	-	-	-	-
16	(-30,160)	161.2	164.9	164.9	161.2	240.2	238.1	244.4	243.7	-	-	-	-
17	(-30,180)	181.1	184.4	184.4	181.1	246.0	245.9	244.3	243.8	-	-	-	-
18	(-30,200)	201.0	204.0	204.0	201.0	247.7	246.8	244.3	243.8	-	-	-	-
19	(-20,40)	41.2	50.0	50.0	41.2	247.4	246.4	244.5	247.2	-	-	-	-
20	(-20,60)	60.8	67.1	67.1	60.8	241.8	243.4	240.5	238.7	-	-	-	-
21	(-20,80)	80.6	85.4	85.4	80.6	247.5	246.6	244.7	243.4	-	-	-	-
22	(-20,100)	100.5	104.4	104.4	100.5	247.3	246.5	244.3	243.7	-	-	-	-
23	(-20,120)	120.4	123.7	123.7	120.4	247.7	246.7	244.3	243.5	-	-	-	-
24	(-20,140)	140.4	143.2	143.2	140.4	239.3	171.0	244.3	243.8	-	-	-	-
25	(-20,160)	160.3	162.8	162.8	160.3	240.7	240.5	244.4	243.7	-	-	-	-
26	(-20,180)	180.3	182.5	182.5	180.3	235.8	227.2	244.4	243.7	-	-	-	-
27	(-20,200)	200.2	202.2	202.2	200.2	247.5	246.6	245.3	243.7	-	-	-	-
28	(-10,40)	40.0	44.7	44.7	40.0	247.5	246.7	244.4	158.2	235.5	-	-	-
29	(-10,60)	60.0	63.2	63.2	60.0	137.2	246.1	244.4	180.6	-	-	-	-
30	(-10,80)	80.0	82.5	82.5	80.0	247.5	246.5	244.1	83.5	6.2	-	-	12.1
31	(-10,100)	100.0	102.0	102.0	100.0	247.5	246.7	244.3	329.0	644.5	-	-	-
32	(-10,120)	120.0	121.7	121.7	120.0	253.9	246.4	244.5	140.7	-	-	-	427.9
33	(-10,140)	140.0	141.4	141.4	140.0	339.4	171.1	244.5	392.0	-	-	-	-
34	(-10,160)	160.0	161.2	161.2	160.0	253.1	243.2	244.2	305.2	-	-	-	-
35	(-10,180)	180.0	181.1	181.1	180.0	240.9	241.6	244.8	255.7	-	-	-	-
36	(-10,200)	200.0	201.0	201.0	200.0	247.6	246.8	244.3	193.1	-	-	-	47.5
37	(0,-40)	40.0	41.2	41.2	40.0	247.5	244.5	243.3	77.0	408.8	-	-	-
38	(0,-60)	60.0	60.8	60.8	60.0	381.6	231.9	240.6	73.5	-	-	-	182.9
39	(0,-80)	80.0	80.6	80.6	80.0	247.5	246.3	244.3	81.6	2.3	-	-	2.7
40	(0,-100)	100.0	100.5	100.5	100.0	247.5	139.3	245.0	96.3	24.6	-	-	13.6
41	(0,-120)	120.0	120.4	120.4	120.0	354.7	167.7	244.4	111.1	-	-	-	78.3
42	(0,-140)	140.0	140.4	140.4	140.0	247.5	169.1	244.2	127.8	159.4	-	-	148.5
43	(0,-160)	160.0	160.3	160.3	160.0	247.5	164.9	244.1	140.4	9.9	20.9	-	385.2
44	(0,-180)	180.0	180.3	180.3	180.0	247.5	226.4	244.6	414.4	461.2	-	-	-
45	(0,-200)	200.0	200.2	200.2	200.0	247.6	246.7	244.2	245.2	-	-	-	-
46	(0,40)	40.0	40.0	40.0	40.0	247.5	49.5	65.9	75.1	231.7	89.4	-	-
47	(0,60)	60.0	60.0	60.0	60.0	99.4	62.5	74.7	52.3	-	6.3	216.2	58.7
48	(0,80)	80.0	80.0	80.0	80.0	114.3	79.1	87.1	112.0	-	0.8	50.9	-
49	(0,100)	100.0	100.0	100.0	100.0	345.2	95.7	131.1	121.2	-	18.7	-	448.5
50	(0,120)	120.0	120.0	120.0	120.0	116.1	141.6	253.6	295.8	279.6	465.8	-	-
51	(0,140)	140.0	140.0	140.0	140.0	327.4	168.3	393.9	384.3	-	-	-	-
52	(0,160)	160.0	160.0	160.0	160.0	306.5	145.9	265.1	512.9	-	-	-	-
53	(0,180)	180.0	180.0	180.0	180.0	249.1	182.2	183.5	182.7	-	5.0	12.0	7.3
54	(0,200)	200.0	200.0	200.0	200.0	208.4	223.8	246.5	240.6	79.6	-	-	-
55	(0+,40)	41.2	40.0	40.0	42.4	145.5	49.0	66.4	243.6	-	81.5	-	-
56	(0+,60)	60.8	60.0	60.0	61.6	249.2	62.6	72.1	243.7	-	6.6	146.2	-
57	(0+,80)	80.6	80.0	80.0	81.2	247.6	81.2	87.0	243.7	-	1.5	48.9	-
58	(0+,100)	100.5	100.0	100.0	101.0	229.2	95.6	99.7	243.9	-	19.2	0.1	-
59	(0+,120)	120.4	120.0	120.0	120.8	235.7	120.6	141.7	244.0	-	0.4	471.0	-
60	(0+,140)	140.4	140.0	140.0	140.7	247.4	161.3	133.3	243.9	-	453.6	44.8	-
61	(0+,160)	160.3	160.0	160.0	160.6	228.7	162.6	170.5	243.7	-	6.7	109.2	-
62	(0+,180)	180.3	180.0	180.0	180.6	247.3	181.5	514.3	243.9	-	2.2	-	-
63	(0+,200)	200.2	200.0	200.0	200.5	238.5	228.5	310.0	243.8	-	-	-	-
64	(10,40)	44.7	40.0	40.0	44.7	249.2	54.8	146.0	243.7	-	218.3	-	-
65	(10,60)	63.2	60.0	60.0	63.2	247.8	312.2	74.7	243.8	-	-	216.7	-
66	(10,80)	82.5	80.0	80.0	82.5	247.6	128.2	84.7	243.7	-	-	22.5	-
67	(10,100)	102.0	100.0	100.0	102.0	247.6	97.8	101.7	244.0	-	4.9	2.8	-
68	(10,120)	121.7	120.0	120.0	121.7	233.2	118.7	141.7	243.9	-	1.6	470.5	-
69	(10,140)	141.4	140.0	140.0	141.4	247.5	158.5	438.7	244.1	-	344.0	-	-
70	(10,160)	161.2	160.0	160.0	161.2	216.6	165.0	486.9	243.9	-	25.1	-	-
71	(10,180)	181.1	180.0	180.0	181.1	247.4	225.8	246.4	243.7	-	-	-	-
72	(10,200)	201.0	200.0	200.0	201.0	247.5	244.0	246.4	243.8	71.9	-	-	-
73	(20,40)	50.0	41.2	41.2	50.0	247.5	55.5	246.2	243.5	-	204.6	-	-
74	(20,60)	67.1	60.8	60.8	67.1	247.4	312.1	246.4	243.8	-	-	-	-
75	(20,80)	85.4	80.6	80.6	85.4	247.3	246.5	244.4	243.7	-	-	-	-
76	(20,100)	104.4	100.5	100.5	104.4	247.5	246.7	244.3	243.9	-	-	-	-
77	(20,120)	123.7	120.4	120.4	123.7	217.4	161.1	244.3	243.7	-	-	-	-
78	(20,140)	143.2	140.4	140.4	143.2	247.2	168.6	244.3	243.7	-	-	-	-
79	(20,160)	162.8	160.3	160.3	162.8	222.2	228.4	244.6	243.9	-	-	-	-
80	(20,180)	182.5	180.3	180.3	182.5	247.5	228.7	246.9	246.6	-	-	-	-
81	(20,200)	202.2	200.2	200.2	202.2	247.5	241.7	244.4	243.6	23.1	-	-	-
82	(30,40)	56.6	44.7	44.7	56.6	241.4	240.6	246.0	243.4	-	-	-	-
83	(30,60)	72.1	63.2	63.2	72.1	247.5	246.5	246.5	243.8	-	-	-	-
84	(30,80)	89.4	82.5	82.5	89.4	234.5	202.0	244.4	243.9	-	-	-	-
85	(30,100)	107.7	102.0	102.0	107.7	221.0	215.3	244.6	243.9	-	-	-	-
86	(30,120)	126.5	121.7	121.7	126.5	221.8	156.5	246.5	243.9	-	-	-	-
87	(30,140)	145.6	141.4	141.4	145.6	247.6	246.7	244.3	243.7	-	-	-	-
88	(30,160)	164.9	161.2	161.2	164.9	245.1	212.4	244.3	244.0	-	-	-	-
89	(30,180)	184.4	181.1	181.1	184.4	247.7	246.8	244.5	243.8	-	-	-	-
90	(30,200)	204.0	201.0	201.0	204.0	247.5	221.6	244.2	243.7	364.0	423.2	-	-
91	(40,40)	64.0	50.0	50.0	64.0	240.8	239.7	246.0	243.6	-	-	-	-
92	(40,60)	78.1	67.1	67.1	78.1	249.2	246.7	246.6	243.8	-	-	-	-
93	(40,80)	94.3	85.4	85.4	94.3	247.5	246.8	244.4	244.8	-	-	-	-
94	(40,100)	111.8	104.4	104.4	111.8	247.4	209.0	244.3	244.0	-	-	-	-
95	(40,120)	130.0	123.7	123.7	130.0	219.3	219.9	244.5	243.8	-	-	-	-
96	(40,140)	148.7	143.2	143.2	148.7	247.5	246.8	244.3	243.9	-	-	-	-
97	(40,160)	167.6	162.8	162.8	167.6	217.8	218.5	244.4	244.0	-	-	-	-
98	(40,180)	186.8	182.5										

Table B.4 : Detection error calculations for scenario 4

Case No	Position of object (x,y)	Actual distance to obsta from sensors (cm) [μ]				If object is detected by sensor then measured average distance (cm) [\bar{x}]				Calculation for $MSE(\bar{x})$			
		Sensor 1	Sensor 2	Sensor 3	Sensor 4	Sensor 1	Sensor 2	Sensor 3	Sensor 4	Sensor 1	Sensor 2	Sensor 3	Sensor 4
1	(-40,40)	50.0	64.0	64.0	50.0	238.6	237.5	239.3	238.6	-	-	-	-
2	(-40,60)	67.1	78.1	78.1	67.1	238.6	237.7	239.1	238.5	-	-	-	-
3	(-40,80)	85.4	94.3	94.3	85.4	238.5	237.6	239.2	238.6	-	-	-	-
4	(-40,100)	104.4	111.8	111.8	104.4	238.5	237.6	239.4	238.7	-	-	-	-
5	(-40,120)	123.7	130.0	130.0	123.7	238.6	237.6	239.2	238.2	-	-	-	-
6	(-40,140)	143.2	148.7	148.7	143.2	238.4	237.8	239.5	238.4	-	-	-	-
7	(-40,160)	162.8	167.6	167.6	162.8	238.7	237.9	239.3	238.4	-	-	-	-
8	(-40,180)	182.5	186.8	186.8	182.5	238.5	237.7	239.1	238.4	-	-	-	-
9	(-40,200)	202.2	206.2	206.2	202.2	238.5	236.1	239.1	238.4	-	-	-	-
10	(-30,40)	44.7	56.6	56.6	44.7	238.6	237.8	239.2	238.6	-	-	-	-
11	(-30,60)	63.2	72.1	72.1	63.2	236.2	237.7	239.0	238.3	-	-	-	-
12	(-30,80)	82.5	89.4	89.4	82.5	238.7	237.3	239.3	238.4	-	-	-	-
13	(-30,100)	102.0	107.7	107.7	102.0	237.2	237.3	239.3	238.4	93.5	-	-	-
14	(-30,120)	121.7	126.5	126.5	121.7	238.5	237.6	239.3	238.6	-	-	-	-
15	(-30,140)	141.4	145.6	145.6	141.4	238.8	237.8	239.0	238.2	-	-	-	-
16	(-30,160)	161.2	164.9	164.9	161.2	238.4	237.5	239.5	238.6	-	-	-	-
17	(-30,180)	181.1	184.4	184.4	181.1	228.1	237.6	239.2	238.5	-	-	-	-
18	(-30,200)	201.0	204.0	204.0	201.0	236.2	236.2	239.2	238.3	683.2	-	-	-
19	(-20,40)	41.2	50.0	50.0	41.2	238.7	237.6	239.3	238.6	-	-	-	-
20	(-20,60)	60.8	67.1	67.1	60.8	237.3	237.3	239.1	238.3	35.9	-	-	-
21	(-20,80)	80.6	85.4	85.4	80.6	237.4	237.4	239.1	238.3	51.9	28.9	-	-
22	(-20,100)	100.5	104.4	104.4	100.5	237.4	237.4	239.5	238.6	102.6	94.5	-	-
23	(-20,120)	120.4	123.7	123.7	120.4	237.2	237.2	239.2	238.4	231.9	200.4	-	-
24	(-20,140)	140.4	143.2	143.2	140.4	238.6	237.6	239.1	238.3	-	-	-	-
25	(-20,160)	160.3	162.8	162.8	160.3	219.0	237.3	239.2	238.4	-	-	-	-
26	(-20,180)	180.3	182.5	182.5	180.3	157.0	237.8	239.3	238.5	500.7	-	-	-
27	(-20,200)	200.2	202.2	202.2	200.2	175.1	233.6	239.0	238.3	633.5	-	-	-
28	(-10,40)	40.0	44.7	44.7	40.0	373.3	237.1	239.2	39.9	7.1	-	-	0.0
29	(-10,60)	60.0	63.2	63.2	60.0	54.5	59.3	239.3	57.1	30.8	15.9	-	8.7
30	(-10,80)	80.0	82.5	82.5	80.0	71.2	75.9	239.1	238.2	76.9	42.6	-	-
31	(-10,100)	100.0	102.0	102.0	100.0	38.3	92.6	239.0	238.2	137.3	88.2	-	-
32	(-10,120)	120.0	121.7	121.7	120.0	103.0	106.0	239.4	238.4	289.8	245.5	-	-
33	(-10,140)	140.0	141.4	141.4	140.0	109.7	237.5	239.2	205.5	403.8	-	-	-
34	(-10,160)	160.0	161.2	161.2	160.0	136.6	140.7	239.4	141.3	549.3	422.6	-	348.7
35	(-10,180)	180.0	181.1	181.1	180.0	156.3	157.9	239.2	200.0	563.3	536.4	-	400.2
36	(-10,200)	200.0	201.0	201.0	200.0	173.1	237.6	239.2	238.4	-	-	-	-
37	(0,-40)	40.0	41.2	41.2	40.0	373.3	40.8	239.1	39.9	7.2	0.2	-	0.0
38	(0,-60)	60.0	60.8	60.8	60.0	54.5	55.0	239.2	57.1	30.4	33.7	-	8.7
39	(0,-80)	80.0	80.6	80.6	80.0	71.5	71.9	239.3	73.9	72.6	76.0	-	36.6
40	(0,-100)	100.0	100.5	100.5	100.0	88.4	88.7	239.2	90.9	135.5	138.1	-	83.5
41	(0,-120)	120.0	120.4	120.4	120.0	103.0	105.4	239.3	107.6	289.3	226.4	-	153.1
42	(0,-140)	140.0	140.4	140.4	140.0	120.1	122.4	239.0	124.1	395.9	321.5	-	252.8
43	(0,-160)	160.0	160.3	160.3	160.0	135.4	138.8	239.5	139.2	604.5	463.9	-	431.2
44	(0,-180)	180.0	180.3	180.3	180.0	155.9	161.3	239.4	158.3	579.6	360.6	-	471.1
45	(0,-200)	200.0	200.2	200.2	200.0	173.0	237.4	239.5	210.6	-	-	-	113.1
46	(0,40)	40.0	40.0	40.0	40.0	39.8	40.3	458.8	42.2	0.1	0.1	34.2	4.8
47	(0,60)	60.0	60.0	60.0	60.0	41.8	42.4	45.7	44.2	331.6	310.3	204.5	250.3
48	(0,80)	80.0	80.0	80.0	80.0	73.9	67.1	78.6	70.0	37.1	167.3	2.1	99.3
49	(0,100)	100.0	100.0	100.0	100.0	90.6	90.7	94.4	92.9	87.8	85.9	34.2	50.9
50	(0,120)	120.0	120.0	120.0	120.0	103.4	103.5	108.6	107.6	274.6	273.5	130.0	153.6
51	(0,140)	140.0	140.0	140.0	140.0	124.4	124.3	127.7	126.8	242.2	247.9	151.5	174.9
52	(0,160)	160.0	160.0	160.0	160.0	134.1	133.3	146.5	145.5	673.1	710.7	182.2	210.6
53	(0,180)	180.0	180.0	180.0	180.0	158.4	158.3	161.3	160.8	467.6	471.4	351.5	367.2
54	(0,200)	200.0	200.0	200.0	200.0	175.3	175.1	178.3	177.2	609.8	620.0	470.2	520.1
55	(0+,40)	41.2	40.0	40.0	42.4	42.0	40.2	45.8	118.3	0.6	0.0	33.9	-
56	(0+,60)	60.8	60.0	60.0	61.6	42.0	40.3	45.8	224.8	352.6	388.1	200.9	-
57	(0+,80)	80.6	80.0	80.0	81.2	76.0	74.1	77.5	158.2	2.12	34.4	6.4	-
58	(0+,100)	100.5	100.0	100.0	101.0	93.0	90.8	94.0	238.4	56.6	84.2	35.4	-
59	(0+,120)	120.4	120.0	120.0	120.8	105.6	105.6	108.9	238.5	218.3	206.5	123.9	-
60	(0+,140)	140.4	140.0	140.0	140.7	124.5	122.4	125.6	228.7	252.3	308.6	208.3	-
61	(0+,160)	160.3	160.0	160.0	160.6	141.4	139.3	239.2	238.7	356.5	428.2	-	-
62	(0+,180)	180.3	180.0	180.0	180.6	220.8	156.2	239.2	238.7	-	566.2	-	-
63	(0+,200)	200.2	200.0	200.0	200.5	181.2	173.4	178.0	238.2	362.5	-	483.6	-
64	(10,40)	44.7	40.0	40.0	44.7	237.7	40.3	45.9	237.7	-	0.1	35.3	-
65	(10,60)	63.2	60.0	60.0	63.2	219.9	40.3	239.2	238.6	-	389.4	-	-
66	(10,80)	82.5	80.0	80.0	82.5	77.8	72.0	86.3	158.9	21.4	64.4	38.6	-
67	(10,100)	102.0	100.0	100.0	102.0	95.0	90.8	96.0	238.5	49.2	84.4	15.6	-
68	(10,120)	121.7	120.0	120.0	121.7	107.6	105.5	108.8	238.5	197.4	208.9	126.4	-
69	(10,140)	141.4	140.0	140.0	141.4	129.5	122.4	127.6	238.4	142.0	309.0	155.0	-
70	(10,160)	161.2	160.0	160.0	161.2	150.0	139.0	144.3	238.5	126.5	441.2	240.4	-
71	(10,180)	181.1	180.0	180.0	181.1	238.1	156.2	239.2	238.4	-	565.2	-	-
72	(10,200)	201.0	200.0	200.0	201.0	237.1	173.1	239.3	238.6	-	-	-	-
73	(20,40)	50.0	41.2	41.2	50.0	238.9	235.7	238.7	238.4	-	-	-	-
74	(20,60)	67.1	60.8	60.8	67.1	239.0	233.4	239.3	238.6	-	-	-	-
75	(20,80)	85.4	80.6	80.6	85.4	171.5	74.0	176.7	174.5	-	44.2	-	-
76	(20,100)	104.4	100.5	100.5	104.4	189.6	93.1	239.3	238.5	-	55.1	-	-
77	(20,120)	123.7	120.4	120.4	123.7	125.6	107.6	239.3	238.6	23.7	163.1	-	-
78	(20,140)	143.2	140.4	140.4	143.2	160.5	124.5	239.1	238.4	298.9	249.9	-	-
79	(20,160)	162.8	160.3	160.3	162.8	229.8	139.2	239.1	238.1	-	447.7	-	-
80	(20,180)	182.5	180.3	180.3	182.5	238.9	158.3	239.1	238.4	-	481.6	-	-
81	(20,200)	202.2	200.2	200.2	202.2	238.8	174.6	239.1	238.7	-	659.6	-	-
82	(30,40)	56.6	44.7	44.7	56.6	239.0	238.1	239.2	238.5	-	-	-	-
83	(30,60)	72.1	63.2	63.2	72.1	222.5	235.1	239.2	238.5	-	-	-	-
84	(30,80)	89.4	82.5	82.5	89.4	163.5	76.3	167.0	163.0	-	37.7	-	-
85	(30,100)	107.7	102.0	102.0	107.7	238.6	93.5	239.2	238.7	-	72.6	-	-
86	(30,120)	126.5	121.7	121.7	126.5	234.8	109.9	239.2	238.4	-	139.1	-	-
87	(30,140)	145.6	141.4	141.4	145.6	238.9	123.3	239.2	231.9	-	327.0	-	-
88	(30,160)	164.9	161.2	161.2	164.9	238.1	143.9	239.3	238.5	-	300.1	-	-
89	(30,180)	184.4	181.1	181.1	184.4	239.4	171.1	239.3	238.5	-	100.3	-	-
90	(30,200)	204.0	201.0	201.0	204.0	230.2	236.0	239.2	238.6	-	-	-	-
91	(40,40)	64.0	50.0	50.0	64.0	239.1	236.2	239.3	238.2	-	-	-	-
92	(40,60)	78.1	67.1	67.1	78.1	234.4	228.5	239.2	238.5	-	-	-	-
93	(40,80)	94.3	85.4	85.4	94.3	238.4	230.9	239.0	238.2	-	-	-	-
94	(40,100)	111.8	104.4	104.4	111.8	238.3	229.2	239.4	238.5	-	-	-	-
95	(40,120)	130											

Appendix-C1

<Rules for left obstacle avoidance>

Algorithm 1 (Rule-2): $Xd_{1i} < 2 \ \& \ Xd_{4i} < 2 \ \& \ (Xd_{2i} > 2 \ | \ Xd_{3i} > 2)$

- Rule 1:
If $Xd_{1i} = \text{Near} \ \& \ Xd_{2i} = \text{Near} \ \& \ Xd_{3i} = \text{VeryFar} \ \& \ Xd_{4i} = \text{Near} \Rightarrow \text{Turn Right VL}$
- Rule 2:
If $Xd_{1i} = \text{Near} \ \& \ Xd_{2i} = \text{Near} \ \& \ Xd_{3i} = \text{VeryFar} \ \& \ Xd_{4i} = \text{Far} \Rightarrow \text{Turn Right VL}$
- Rule 3:
If $Xd_{1i} = \text{Near} \ \& \ Xd_{2i} = \text{Far} \ \& \ Xd_{3i} = \text{VeryFar} \ \& \ Xd_{4i} = \text{Near} \Rightarrow \text{Turn Right VL}$
- Rule 4:
If $Xd_{1i} = \text{Near} \ \& \ Xd_{2i} = \text{Far} \ \& \ Xd_{3i} = \text{VeryFar} \ \& \ Xd_{4i} = \text{Far} \Rightarrow \text{Turn Right L}$
- Rule 5:
If $Xd_{1i} = \text{Far} \ \& \ Xd_{2i} = \text{Near} \ \& \ Xd_{3i} = \text{VeryFar} \ \& \ Xd_{4i} = \text{Near} \Rightarrow \text{Turn Right VL}$
- Rule 6:
If $Xd_{1i} = \text{Far} \ \& \ Xd_{2i} = \text{Near} \ \& \ Xd_{3i} = \text{VeryFar} \ \& \ Xd_{4i} = \text{Far} \Rightarrow \text{Turn Right L}$
- Rule 7:
If $Xd_{1i} = \text{Far} \ \& \ Xd_{2i} = \text{Far} \ \& \ Xd_{3i} = \text{VeryFar} \ \& \ Xd_{4i} = \text{Near} \Rightarrow \text{Turn Right L}$
- Rule 8:
If $Xd_{1i} = \text{Far} \ \& \ Xd_{2i} = \text{Far} \ \& \ Xd_{3i} = \text{VeryFar} \ \& \ Xd_{4i} = \text{Far} \Rightarrow \text{Turn Right L}$
- Rule 9:
If $Xd_{1i} = \text{Near} \ \& \ Xd_{2i} = \text{VeryFar} \ \& \ Xd_{3i} = \text{Near} \ \& \ Xd_{4i} = \text{Near} \Rightarrow \text{Turn Right VL}$
- Rule 10:
If $Xd_{1i} = \text{Near} \ \& \ Xd_{2i} = \text{VeryFar} \ \& \ Xd_{3i} = \text{Near} \ \& \ Xd_{4i} = \text{Far} \Rightarrow \text{Turn Right VL}$
- Rule 11:
If $Xd_{1i} = \text{Near} \ \& \ Xd_{2i} = \text{VeryFar} \ \& \ Xd_{3i} = \text{Far} \ \& \ Xd_{4i} = \text{Near} \Rightarrow \text{Turn Right VL}$
- Rule 12:
If $Xd_{1i} = \text{Near} \ \& \ Xd_{2i} = \text{VeryFar} \ \& \ Xd_{3i} = \text{Far} \ \& \ Xd_{4i} = \text{Far} \Rightarrow \text{Turn Right L}$
- Rule 13:
If $Xd_{1i} = \text{Far} \ \& \ Xd_{2i} = \text{VeryFar} \ \& \ Xd_{3i} = \text{Near} \ \& \ Xd_{4i} = \text{Near} \Rightarrow \text{Turn Right VL}$
- Rule 14:
If $Xd_{1i} = \text{Far} \ \& \ Xd_{2i} = \text{VeryFar} \ \& \ Xd_{3i} = \text{Near} \ \& \ Xd_{4i} = \text{Far} \Rightarrow \text{Turn Right L}$
- Rule 15:
If $Xd_{1i} = \text{Far} \ \& \ Xd_{2i} = \text{VeryFar} \ \& \ Xd_{3i} = \text{Far} \ \& \ Xd_{4i} = \text{Near} \Rightarrow \text{Turn Right L}$
- Rule 16:
If $Xd_{1i} = \text{Far} \ \& \ Xd_{2i} = \text{VeryFar} \ \& \ Xd_{3i} = \text{Far} \ \& \ Xd_{4i} = \text{Far} \Rightarrow \text{Turn Right L}$

Algorithm 1 (Rule-4): $(Xd_{1i} < 2 \ | \ Xd_{4i} < 2) \ \& \ Xd_{2i} > 2 \ \& \ Xd_{3i} > 2$

- Rule 17:
If $Xd_{1i} = \text{Near} \ \& \ Xd_{2i} = \text{VeryFar} \ \& \ Xd_{3i} = \text{VeryFar} \ \& \ Xd_{4i} = \text{VeryFar} \Rightarrow \text{Turn Right S}$
- Rule 18:
If $Xd_{1i} = \text{Far} \ \& \ Xd_{2i} = \text{VeryFar} \ \& \ Xd_{3i} = \text{VeryFar} \ \& \ Xd_{4i} = \text{VeryFar} \Rightarrow \text{Turn Right S}$
- Rule 19:

- If $Xd_{1i} = \text{VeryFar} \ \& \ Xd_{2i} = \text{VeryFar} \ \& \ Xd_{3i} = \text{VeryFar} \ \& \ Xd_{4i} = \text{Near} \Rightarrow \text{Turn Right S}$
- Rule 20:
If $Xd_{1i} = \text{VeryFar} \ \& \ Xd_{2i} = \text{VeryFar} \ \& \ Xd_{3i} = \text{VeryFar} \ \& \ Xd_{4i} = \text{Far} \Rightarrow \text{Turn Right S}$

Algorithm 1 (Rule-6): $Xd_{1i} < 2 \ \& \ Xd_{2i} < 2 \ \& \ Xd_{3i} > 2 \ \& \ Xd_{4i} > 2$

if $Xd_{1i} > Xd_{2i}$ obstacle at the right; else obstacle at the left

- Rule 21:
If $Xd_{1i} = \text{Near} \ \& \ Xd_{2i} = \text{Near} \ \& \ Xd_{3i} = \text{VeryFar} \ \& \ Xd_{4i} = \text{VeryFar} \Rightarrow \text{Turn Right L}$
- Rule 22:
If $Xd_{1i} = \text{Far} \ \& \ Xd_{2i} = \text{Far} \ \& \ Xd_{3i} = \text{VeryFar} \ \& \ Xd_{4i} = \text{VeryFar} \Rightarrow \text{Turn Right M}$
- Rule 23:
If $Xd_{1i} = \text{Near} \ \& \ Xd_{2i} = \text{Far} \ \& \ Xd_{3i} = \text{VeryFar} \ \& \ Xd_{4i} = \text{VeryFar} \Rightarrow \text{Turn Right S}$

Algorithm 1 (Rule-7): $Xd_{1i} > 2 \ \& \ Xd_{2i} > 2 \ \& \ Xd_{3i} < 2 \ \& \ Xd_{4i} < 2$

if $Xd_{4i} > Xd_{3i}$ obstacle at the right; else obstacle at the left

- Rule 24:
If $Xd_{1i} = \text{VeryFar} \ \& \ Xd_{2i} = \text{VeryFar} \ \& \ Xd_{3i} = \text{Near} \ \& \ Xd_{4i} = \text{Near} \Rightarrow \text{Turn Right L}$
- Rule 25:
If $Xd_{1i} = \text{VeryFar} \ \& \ Xd_{2i} = \text{VeryFar} \ \& \ Xd_{3i} = \text{Far} \ \& \ Xd_{4i} = \text{Far} \Rightarrow \text{Turn Right M}$
- Rule 26:
If $Xd_{1i} = \text{VeryFar} \ \& \ Xd_{2i} = \text{VeryFar} \ \& \ Xd_{3i} = \text{Far} \ \& \ Xd_{4i} = \text{Near} \Rightarrow \text{Turn Right S}$

Algorithm 1 (Rule-8): $Xd_{1i} < 2 \ \& \ Xd_{2i} > 2 \ \& \ Xd_{3i} > 2 \ \& \ Xd_{4i} < 2$

- Rule 27:
If $Xd_{1i} = \text{Near} \ \& \ Xd_{2i} = \text{VeryFar} \ \& \ Xd_{3i} = \text{VeryFar} \ \& \ Xd_{4i} = \text{Near} \Rightarrow \text{Turn Right S}$
- Rule 28:
If $Xd_{1i} = \text{Near} \ \& \ Xd_{2i} = \text{VeryFar} \ \& \ Xd_{3i} = \text{VeryFar} \ \& \ Xd_{4i} = \text{Far} \Rightarrow \text{Turn Right S}$
- Rule 29:
If $Xd_{1i} = \text{Far} \ \& \ Xd_{2i} = \text{VeryFar} \ \& \ Xd_{3i} = \text{VeryFar} \ \& \ Xd_{4i} = \text{Near} \Rightarrow \text{Turn Right S}$
- Rule 30:
If $Xd_{1i} = \text{Far} \ \& \ Xd_{2i} = \text{VeryFar} \ \& \ Xd_{3i} = \text{VeryFar} \ \& \ Xd_{4i} = \text{Far} \Rightarrow \text{Turn Right S}$

<Rules for right obstacle avoidance>

Algorithm 1 (Rule-3): $(Xd_{1i} > 2 \ | \ Xd_{4i} > 2) \ \& \ Xd_{2i} < 2 \ \& \ Xd_{3i} < 2$

- Rule 1:
If $Xd_{1i} = \text{Near} \ \& \ Xd_{2i} = \text{Near} \ \& \ Xd_{3i} = \text{Near} \ \& \ Xd_{4i} = \text{VeryFar} \Rightarrow \text{Turn Left VL}$
- Rule 2:
If $Xd_{1i} = \text{Near} \ \& \ Xd_{2i} = \text{Near} \ \& \ Xd_{3i} = \text{Far} \ \& \ Xd_{4i} = \text{VeryFar} \Rightarrow \text{Turn Left VL}$
- Rule 3:

-
- If $Xd_{1i} = \text{Near} \ \& \ Xd_{2i} = \text{Far} \ \& \ Xd_{3i} = \text{Near} \ \& \ Xd_{4i} = \text{VeryFar} \Rightarrow \text{Turn Left VL}$
 - Rule 4:
If $Xd_{1i} = \text{Near} \ \& \ Xd_{2i} = \text{Far} \ \& \ Xd_{3i} = \text{Far} \ \& \ Xd_{4i} = \text{VeryFar} \Rightarrow \text{Turn Left L}$
 - Rule 5:
If $Xd_{1i} = \text{Far} \ \& \ Xd_{2i} = \text{Near} \ \& \ Xd_{3i} = \text{Near} \ \& \ Xd_{4i} = \text{VeryFar} \Rightarrow \text{Turn Left VL}$
 - Rule 6:
If $Xd_{1i} = \text{Far} \ \& \ Xd_{2i} = \text{Near} \ \& \ Xd_{3i} = \text{Far} \ \& \ Xd_{4i} = \text{VeryFar} \Rightarrow \text{Turn Left L}$
 - Rule 7:
If $Xd_{1i} = \text{Far} \ \& \ Xd_{2i} = \text{Far} \ \& \ Xd_{3i} = \text{Near} \ \& \ Xd_{4i} = \text{VeryFar} \Rightarrow \text{Turn Left L}$
 - Rule 8:
If $Xd_{1i} = \text{Far} \ \& \ Xd_{2i} = \text{Far} \ \& \ Xd_{3i} = \text{Far} \ \& \ Xd_{4i} = \text{VeryFar} \Rightarrow \text{Turn Left L}$
 - Rule 9:
If $Xd_{1i} = \text{VeryFar} \ \& \ Xd_{2i} = \text{Near} \ \& \ Xd_{3i} = \text{Near} \ \& \ Xd_{4i} = \text{Near} \Rightarrow \text{Turn Left VL}$
 - Rule 10:
If $Xd_{1i} = \text{VeryFar} \ \& \ Xd_{2i} = \text{Near} \ \& \ Xd_{3i} = \text{Near} \ \& \ Xd_{4i} = \text{Far} \Rightarrow \text{Turn Left VL}$
 - Rule 11:
If $Xd_{1i} = \text{VeryFar} \ \& \ Xd_{2i} = \text{Near} \ \& \ Xd_{3i} = \text{Far} \ \& \ Xd_{4i} = \text{Near} \Rightarrow \text{Turn Left VL}$
 - Rule 12:
If $Xd_{1i} = \text{VeryFar} \ \& \ Xd_{2i} = \text{Near} \ \& \ Xd_{3i} = \text{Far} \ \& \ Xd_{4i} = \text{Far} \Rightarrow \text{Turn Left L}$
 - Rule 13:
If $Xd_{1i} = \text{VeryFar} \ \& \ Xd_{2i} = \text{Far} \ \& \ Xd_{3i} = \text{Near} \ \& \ Xd_{4i} = \text{Near} \Rightarrow \text{Turn Left VL}$
 - Rule 14:
If $Xd_{1i} = \text{VeryFar} \ \& \ Xd_{2i} = \text{Far} \ \& \ Xd_{3i} = \text{Near} \ \& \ Xd_{4i} = \text{Far} \Rightarrow \text{Turn Left L}$
 - Rule 15:
If $Xd_{1i} = \text{VeryFar} \ \& \ Xd_{2i} = \text{Far} \ \& \ Xd_{3i} = \text{Far} \ \& \ Xd_{4i} = \text{Near} \Rightarrow \text{Turn Left L}$
 - Rule 16:
If $Xd_{1i} = \text{VeryFar} \ \& \ Xd_{2i} = \text{Far} \ \& \ Xd_{3i} = \text{Far} \ \& \ Xd_{4i} = \text{Far} \Rightarrow \text{Turn Left L}$

Algorithm 1 (Rule-5): $Xd_{1i} > 2 \ \& \ Xd_{4i} > 2 \ \& \ (Xd_{2i} < 2 \ | \ Xd_{3i} < 2)$

- Rule 17:
If $Xd_{1i} = \text{VeryFar} \ \& \ Xd_{2i} = \text{Near} \ \& \ Xd_{3i} = \text{VeryFar} \ \& \ Xd_{4i} = \text{VeryFar} \Rightarrow \text{Turn Left S}$
- Rule 18:
If $Xd_{1i} = \text{VeryFar} \ \& \ Xd_{2i} = \text{Far} \ \& \ Xd_{3i} = \text{VeryFar} \ \& \ Xd_{4i} = \text{VeryFar} \Rightarrow \text{Turn Left S}$
- Rule 19:
If $Xd_{1i} = \text{VeryFar} \ \& \ Xd_{2i} = \text{VeryFar} \ \& \ Xd_{3i} = \text{Near} \ \& \ Xd_{4i} = \text{VeryFar} \Rightarrow \text{Turn Left S}$
- Rule 20:
If $Xd_{1i} = \text{VeryFar} \ \& \ Xd_{2i} = \text{VeryFar} \ \& \ Xd_{3i} = \text{Far} \ \& \ Xd_{4i} = \text{VeryFar} \Rightarrow \text{Turn Left S}$

Algorithm 1 (Rule-6): $Xd_{1i} < 2 \ \& \ Xd_{2i} < 2 \ \& \ Xd_{3i} > 2 \ \& \ Xd_{4i} > 2$

if $Xd_{1i} > Xd_{2i}$ obstacle at the right; else obstacle at the left

- Rule 21:
If $Xd_{1i} = \text{Near} \ \& \ Xd_{2i} = \text{Near} \ \& \ Xd_{3i} = \text{VeryFar} \ \& \ Xd_{4i} = \text{VeryFar} \Rightarrow \text{Turn Left L}$
- Rule 22:

- If $Xd_{1i} = \text{Far} \ \& \ Xd_{2i} = \text{Far} \ \& \ Xd_{3i} = \text{VeryFar} \ \& \ Xd_{4i} = \text{VeryFar} \Rightarrow \text{Turn Left M}$
- Rule 23:
If $Xd_{1i} = \text{Far} \ \& \ Xd_{2i} = \text{Near} \ \& \ Xd_{3i} = \text{VeryFar} \ \& \ Xd_{4i} = \text{VeryFar} \Rightarrow \text{Turn Left S}$

Algorithm 1 (Rule-7): $Xd_{1i} > 2 \ \& \ Xd_{2i} > 2 \ \& \ Xd_{3i} < 2 \ \& \ Xd_{4i} < 2$

if $Xd_{4i} > Xd_{3i}$ obstacle at the right; else obstacle at the left

- Rule 24:
If $Xd_{1i} = \text{VeryFar} \ \& \ Xd_{2i} = \text{VeryFar} \ \& \ Xd_{3i} = \text{Near} \ \& \ Xd_{4i} = \text{Near} \Rightarrow \text{Turn Left L}$
- Rule 25:
If $Xd_{1i} = \text{VeryFar} \ \& \ Xd_{2i} = \text{VeryFar} \ \& \ Xd_{3i} = \text{Far} \ \& \ Xd_{4i} = \text{Far} \Rightarrow \text{Turn Left M}$
- Rule 26:
If $Xd_{1i} = \text{VeryFar} \ \& \ Xd_{2i} = \text{VeryFar} \ \& \ Xd_{3i} = \text{Near} \ \& \ Xd_{4i} = \text{Far} \Rightarrow \text{Turn Left S}$

Algorithm 1 (Rule-9): $Xd_{1i} > 2 \ \& \ Xd_{2i} < 2 \ \& \ Xd_{3i} < 2 \ \& \ Xd_{4i} > 2$

- Rule 27:
If $Xd_{1i} = \text{VeryFar} \ \& \ Xd_{2i} = \text{Near} \ \& \ Xd_{3i} = \text{Near} \ \& \ Xd_{4i} = \text{VeryFar} \Rightarrow \text{Turn Left S}$
- Rule 28:
If $Xd_{1i} = \text{VeryFar} \ \& \ Xd_{2i} = \text{Near} \ \& \ Xd_{3i} = \text{Far} \ \& \ Xd_{4i} = \text{VeryFar} \Rightarrow \text{Turn Left S}$
- Rule 29:
If $Xd_{1i} = \text{VeryFar} \ \& \ Xd_{2i} = \text{Far} \ \& \ Xd_{3i} = \text{Near} \ \& \ Xd_{4i} = \text{VeryFar} \Rightarrow \text{Turn Left S}$
- Rule 30:
If $Xd_{1i} = \text{VeryFar} \ \& \ Xd_{2i} = \text{Far} \ \& \ Xd_{3i} = \text{Far} \ \& \ Xd_{4i} = \text{VeryFar} \Rightarrow \text{Turn Left S}$

<Rules for front obstacle avoidance>

Algorithm 1 (Rule-10): $Xd_{1i} < 2 \ \& \ Xd_{2i} < 2 \ \& \ Xd_{3i} < 2 \ \& \ Xd_{4i} < 2$

- Rule 1:
If $Xd_{1i} = \text{Near} \ \& \ Xd_{2i} = \text{Near} \ \& \ Xd_{3i} = \text{Near} \ \& \ Xd_{4i} = \text{Near} \Rightarrow \text{Turn Left/Right VL}$
- Rule 2:
If $Xd_{1i} = \text{Near} \ \& \ Xd_{2i} = \text{Near} \ \& \ Xd_{3i} = \text{Near} \ \& \ Xd_{4i} = \text{Far} \Rightarrow \text{Turn Left VL}$
- Rule 3:
If $Xd_{1i} = \text{Near} \ \& \ Xd_{2i} = \text{Near} \ \& \ Xd_{3i} = \text{Far} \ \& \ Xd_{4i} = \text{Near} \Rightarrow \text{Turn Right VL}$
- Rule 4:
If $Xd_{1i} = \text{Near} \ \& \ Xd_{2i} = \text{Near} \ \& \ Xd_{3i} = \text{Far} \ \& \ Xd_{4i} = \text{Far} \Rightarrow \text{Turn Left/Right VL}$
- Rule 5:
If $Xd_{1i} = \text{Near} \ \& \ Xd_{2i} = \text{Far} \ \& \ Xd_{3i} = \text{Near} \ \& \ Xd_{4i} = \text{Near} \Rightarrow \text{Turn Right VL}$
- Rule 6:
If $Xd_{1i} = \text{Near} \ \& \ Xd_{2i} = \text{Far} \ \& \ Xd_{3i} = \text{Near} \ \& \ Xd_{4i} = \text{Far} \Rightarrow \text{Turn Left/Right VL}$
- Rule 7:
If $Xd_{1i} = \text{Near} \ \& \ Xd_{2i} = \text{Far} \ \& \ Xd_{3i} = \text{Far} \ \& \ Xd_{4i} = \text{Near} \Rightarrow \text{Turn Right VL}$
- Rule 8:
If $Xd_{1i} = \text{Near} \ \& \ Xd_{2i} = \text{Far} \ \& \ Xd_{3i} = \text{Far} \ \& \ Xd_{4i} = \text{Far} \Rightarrow \text{Turn Right L}$
- Rule 9:

- If $Xd_{1i} = \text{Far} \ \& \ Xd_{2i} = \text{Near} \ \& \ Xd_{3i} = \text{Near} \ \& \ Xd_{4i} = \text{Near} \Rightarrow \text{Turn Left VL}$
- Rule 10:
If $Xd_{1i} = \text{Far} \ \& \ Xd_{2i} = \text{Near} \ \& \ Xd_{3i} = \text{Near} \ \& \ Xd_{4i} = \text{Far} \Rightarrow \text{Turn Left VL}$
 - Rule 11:
If $Xd_{1i} = \text{Far} \ \& \ Xd_{2i} = \text{Near} \ \& \ Xd_{3i} = \text{Far} \ \& \ Xd_{4i} = \text{Near} \Rightarrow \text{Turn Left/Right VL}$
 - Rule 12:
If $Xd_{1i} = \text{Far} \ \& \ Xd_{2i} = \text{Near} \ \& \ Xd_{3i} = \text{Far} \ \& \ Xd_{4i} = \text{Far} \Rightarrow \text{Turn Left L}$
 - Rule 13:
If $Xd_{1i} = \text{Far} \ \& \ Xd_{2i} = \text{Far} \ \& \ Xd_{3i} = \text{Near} \ \& \ Xd_{4i} = \text{Near} \Rightarrow \text{Turn Left/Right VL}$
 - Rule 14:
If $Xd_{1i} = \text{Far} \ \& \ Xd_{2i} = \text{Far} \ \& \ Xd_{3i} = \text{Near} \ \& \ Xd_{4i} = \text{Far} \Rightarrow \text{Turn Left L}$
 - Rule 15:
If $Xd_{1i} = \text{Far} \ \& \ Xd_{2i} = \text{Far} \ \& \ Xd_{3i} = \text{Far} \ \& \ Xd_{4i} = \text{Near} \Rightarrow \text{Turn Right L}$
 - Rule 16:
If $Xd_{1i} = \text{Far} \ \& \ Xd_{2i} = \text{Far} \ \& \ Xd_{3i} = \text{Far} \ \& \ Xd_{4i} = \text{Far} \Rightarrow \text{Turn Left/Right L}$

<Rule for there is no obstacle>

Algorithm 1(Rule 1): $Xd_{1i} > 2 \ \& \ Xd_{2i} > 2 \ \& \ Xd_{3i} > 2 \ \& \ Xd_{4i} > 2$

there is no obstacle (data filtration and pre-processing)

Algorithm 1(Rule-10): $Xd_{1i} < 2.5 \ \& \ Xd_{2i} < 2.5 \ \& \ Xd_{3i} < 2.5 \ \& \ Xd_{4i} < 2.5$

there is no obstacle when:

- Rule 77:
If $Xd_{1i} = \text{VeryFar} \ \& \ Xd_{2i} = \text{VeryFar} \ \& \ Xd_{3i} = \text{VeryFar} \ \& \ Xd_{4i} = \text{VeryFar} \Rightarrow \text{Go straight (Zero)}$

Appendix-D1

Table D.1 : AATCC Test Method 135-2004 Tables [293]

Table I—Alternative Washing and Drying Conditions (see 7.1)

Machine Cycle	Washing Temperature	Drying Procedure
(1) Normal/Cotton Sturdy	(II) 27 ± 3°C (80 ± 5°F)	(A) Tumble
(2) Delicate	(III) 41 ± 3°C (105 ± 5°F)	i. Cotton Sturdy
(3) Permanent Press	(IV) 49 ± 3°C (120 ± 5°F)	ii. Delicate
	(V) 60 ± 3°C (140 ± 5°F)	iii. Permanent Press
		(B) Line
		(C) Drip
		(D) Screen

Table II—Washing Machine Conditions Without Load (see 7.1)

	Normal	Delicate	Permanent Press
(A) Water Level	18 ± 1 gal	18 ± 1 gal	18 ± 1 gal
(B) Agitator Speed	179 ± 2 spm	119 ± 2 spm	179 ± 2 spm
(C) Washing Time	12 min	8 min	10 min
(D) Spin Speed	645 ± 15 rpm	430 ± 15 rpm	430 ± 15 rpm
(E) Final Spin Time	6 min	4 min	4 min

Table III—Dryer Setting Conditions (see 7.1)

	Cotton Sturdy	Delicate	Permanent Press
Exhaust Temperature	High 66 ± 5°C (150 ± 10°F)	Low < 60°C (140°F)	High 66 ± 5°C (150 ± 10°F)
Cool Down Time	10 min	10 min	10 min

Abbreviations

A	: Ampere, SI unit of electric current
AD	: Axiomatic Design
ADC	: Analog to Digital Converter
AHP	: Analytic Hierarchy Process
ANOVA	: Analysis of Variance
App	: Appendix
CCF	: Carbon Coated Fibers (CCF)
CLR/MLR	: Carbon or Metal Loaded Rubber
CNTs	: Carbon Nanotubes
CPCs	: Conductive Polymer Composites
DAQ	: Data Acquisition
DC	: Direct Current
dtex	: Decitex-measuring unit for yarn count: weight in grams per 10,000m
ECG	: Electrocardiograph
ETA	: Electronic Travel Aid
FIS	: Fuzzy Inference System
FLC	: Fluorescent Light Communication
FNN	: Fuzzy Neural Networks
GHz	: Gigahertz (10^9 Hz)
GIS	: Geographic Information System
GPS	: Global Positioning Systems
Hz	: Hertz (SI unit of frequency; the number of cycles per second)
I/O	: Input/Output
IR	: Infrared
kHz	: Kilohertz (10^3 Hz)
LCD	: Liquid Crystal Display
mA	: mili-ampere
MEMS	: Microelectromechanical Systems
NiMH	: Nickel-Metal Hydride Cell
PCBs	: Printed Circuit Boards
PDA	: Personal Digital Assistant
PET	: Polyethylene Terephthalate
PFM	: Potential Field Method
PIC	: Peripheral Interface Controller
POF	: Plastic Optical Fibers
PP	: Polypropylene
PVA	: Polyvinyl Alcohol
RBFN	: Radial Basis Function Network
RF	: Radio Frequency
RFID	: Radio Frequency Identification
RTA	: Robotic Travel Aids
SI	: International System of Units
SNR	: Signal to Noise Ratio
Tex	: Measuring unit for yarn count; weight in grams per 1 km of yarn
TFN	: Trapezoidal Fuzzy Numbers
TOF	: Time of Flight
TOPSIS	: Technique for Order Preference by Similarity to Ideal Solution
USB	: Universal Serial Bus
V	: Voltage

Wearable obstacle avoidance system integrated with conductive yarns for visually impaired people

Abstract: In this study, an innovative wearable obstacle avoidance system fully integrated to textile structures, enabling detection of obstacles, for visually impaired people has been developed. Electronic system components of the proposed smart clothing system were determined using an algorithm based on fuzzy AHP and fuzzy information axiom. Adaptation of sensor and actuator methodology to textile structures and their performances in terms of signal quality and accuracy have been analyzed. In order to find out optimal number of sensors as well as develop suitable obstacle avoidance algorithm, various scenarios have been developed and compared by chaining different number of sensors together at different angles. Vibrotactile perception level has been investigated in terms of fuzzy relations. In this manner, the kind of fabric structure, the area where smart clothing system actuators should be fixed, the kind of actuation signal waveform and its frequency level that should be applied to actuators, have been determined. An algorithm based on neuro-fuzzy controller for obstacle avoidance has also been developed by using neural network and fuzzy logic in order to guide visually impaired people with smart clothing system. Based on neuro-fuzzy control algorithm, microcontroller programming has been done. Finally, smart clothing prototype that combines garment with sensors, actuators, power supplies and a data processing unit has been developed. This system is easily worn as a garment and is able to detect and identify obstacle's position accurately. The proposed smart clothing system would become united part of visually impaired people's lifestyle without imposing upon them any physical or aesthetical load.

Système portable autonome d'évitement d'obstacles intégré avec des fils conducteurs pour les personnes malvoyantes

Résumé : Dans cette étude, un système portable d'évitement d'obstacles, novateur, totalement intégré aux structures de textile, permettant la détection d'obstacles pour les personnes malvoyantes, a été développé. Les composants du dispositif électronique du système de vêtement intelligent proposé ont été déterminés en utilisant un algorithme basé sur un système d'inférence hiérarchique. L'adaptation de la méthodologie des capteurs et actionneurs aux structures textiles et leurs performances en termes de qualité de signal et d'exactitude ont été analysés. Afin de trouver le nombre optimal de capteurs ainsi que de développer l'algorithme d'évitement d'obstacles adapté, différents scénarii ont été développés et comparés par enchaînement de plusieurs ensembles de capteurs à différents angles. Le niveau de perception vibrotactile a été quantifié par des relations floues. De cette manière, le type de structure du tissu, la zone où le système d'actionneurs du vêtement intelligent, doivent être fixés ; le type de signal de déclenchement d'onde et de son niveau de fréquence qui devrait être appliqué aux actionneurs ont été déterminés. Afin de guider les personnes malvoyantes avec le système de vêtement intelligent, un algorithme basé sur un contrôleur neuro-flou pour l'évitement d'obstacle a également été développé et implanté au microcontrôleur. Enfin, un prototype de vêtement intelligent avec des capteurs, des actionneurs, des alimentations et une unité de traitement des données intégrés aux structures textiles a été développé. Ce prototype est facilement portable comme un vêtement et est capable de détecter et de localiser les obstacles avec précision et en temps réel. Le système de vêtement intelligent proposé pourrait faire partie intégrante de la vie quotidienne des personnes ayant une déficience visuelle, sans toutefois leurs imposer une contrainte physique et esthétique.

Keywords: E-textiles, smart clothing, intelligent textiles, visually impaired people, fuzzy logic, neuro-fuzzy controller
